Characteristics of Rain at Microwave and Millimetric Bands for Terrestrial and Satellite Links Attenuation in South Africa and Surrounding Islands

SUBMITTED BY

Pius Adewale Owolawi

IN FULLFILMENT OF THE DEGREE OF

Doctor of Philosophy in Electronic Engineering from the University of KwaZulu-Natal

DATE OF SUBMISSION

JULY 2010

SUPERVISED BY

Prof. T. J. Afullo

&

CO-SUPERVISED

Dr. S.B. Malinga

Preface

The research presented in this thesis was done by Mr. Pius Adewale Owolawi, under the supervision of Prof. T. J. Afullo and co-supervision of Dr. S.B. Malinga in the School of Electrical, Electronic and Computer Engineering at the University of KwaZulu-Natal and Durban, and Hermanus Observatory Centre, Cape Town, South Africa, respectively. This work has been partially supported by and Telkom South Africa through the Centre of Excellence programme in the school and National Research Fund (NRF) South Africa.

Certain aspects of this thesis have been presented and published by the author at various fora: the Southern Africa Telecommunication Networks and Applications Conference (SATNAC) in 2007, and 2008 in Mauritius, and Eastern Cape respectively; the Eleventh URSI Commission F Triennial Open Symposium on Radiowave Propagation and Remote Sensing, Rio de Janeiro, Brazil in 2007; IEEE AFRICON Conference, Namibia in 2007. Part of this thesis has also been published in Radio Science journal in 2007, PIERS online journal in 2009, and one is under review in the American Geophysical Union of the Radio Science Journal.

The whole thesis, unless specifically indicated to the contrary in the text, is the author's original work, and has not been submitted in part, or in whole to any other University.

Acknowledgments

Firstly, I express my gratitude to Professor Thomas J. Afullo and Dr. Sandile B. Malinga for their total commitment to this research. I thank them for their time, encouragement, guidance, financial support, and valuable inputs which have aided my thorough understanding of the study and steered me towards the right path to achieve the research objectives.

I express my gratitude to the Head of School of Electrical, Electronic and Computer Engineering, University of Kwazulu Natal, Durban, South Africa, Professor Stanley Mneney for encouraging me to complete this work.

I thank my friends, especially Mr. and Mrs. Odedina, Mr. A. Owolabi, Mr. and Mrs. Oyerinde, Mr. C. Mulangu, Mr. G. Aiyetoro, Mr. I. Olufemi, Mr. and Mrs. Bakere, Mr. Adeaga, Mr. and Mrs. Adeoye, late Prof. A. Ogulu and his family as well as Mr. and Mrs. Durodola, for their encouragement.

I owe my deepest gratitude to my parents, brothers and sisters for their prayers and moral support. My heartfelt gratitude goes to my girlfriend, Miss. N. Meseko, who showed great consideration and understanding towards my work schedule. Her presence and support contributed to the timely completion of this thesis.

My appreciation goes to my colleagues from the institute. My special gratitude goes to Mrs. O. Ogunsanya for typing and proof-reading my work and all others who reviewed this thesis and suggested substantial improvements.

Finally, I thank God and my spiritual fathers, Pastor A. Moses and Pastor K. Nair, for their prayers and support during the course of my studies.

Dedication

This thesis is dedicated to my mother, the late Idowu Owolawi,
and my grandmother, the late Sabitiyu Adeyeye.
I would not be who I am today without their genuine love and support.
To God be the Glory.

Abstract

The emergence of a vast range of communication devices running on different types of technology has made convergence of technology become the order of the day. This revolution observed in communications technology has resulted in a pressing need for larger bandwidth, higher data rate and better spectrum availability, and it has become important that these factors be addressed. As such, this has resulted in the current resurgence of interest to investigate higher electromagnetic spectrum space that can take care of these needs. For the past decade, microwave (3 GHz-30 GHz) and millimeter waves (30 GHz-300 GHz) have been used as the appropriate frequency ranges for applications with properties such as wide bandwidth, smaller components size, narrow beamwidths, frequency re-use, small antenna, and short deployment time. To optimize the use of these frequency ranges by communication systems, the three tiers of communication system elements - receiver, transmitter and transmission channel or medium must be properly designed and configured. However, if the transmitter and receiver meet the necessary requirements, the medium in which signals are transmitted often becomes an issue at this range of frequencies. The most significant factor that affects the transmission of signals at these bands is attenuation and scattering by rain, snow, water vapour and other gases in the atmosphere. Scattering and absorption by rain at microwave and millimeter bands is thus a main concern for system designers.

This study presents results of research into the interaction of rainfall with microwave and millimeter wave propagation as a medium. The study of rainfall characteristics allows estimation of its scattered and attenuated effects in the presence of microwave and millimeter waves. The components of this work encompass rainfall rate integration time, cumulative distribution and modelling of rainfall rate and characteristics of rain drop size and its modelling. The effects of rain on microwave and millimeter wave signals, which result in rain attenuation, are based on rainfall rate variables such as rainfall rate cumulative distribution, raindrop size distribution, total scattering cross sections, rain drop shape, and rain drop terminal velocity. A regional rainfall rate

conversion factor from five-minute rainfall data to one-minute integration time is developed using the existing conversion method and a newly developed hybrid method. Based on these conversion factor results from the hybrid method, the rainfall at five-minute integration time was converted to a one-minute equivalent to estimate its cumulative distributions. In addition, new rain zones based on ITU-R and Crane designations are suggested for the entire region of South Africa and the surrounding Islands. The results are compared with past research work done in the other regions.

Rain attenuation is acutely influenced by rain drop size distribution (DSD). This study thus also investigates DSD models from previous research work. There are several DSD models commonly used to estimate rain attenuation. They are models which have their root from exponential, gamma, lognormal and Weibull distributions. Since DSD is dynamic and location-dependent, a simple raindrop size distribution model is developed for Durban using maximum likelihood estimation (MLE) method. The MLE method is applied to the three-parameter lognormal distribution in order to model DSD for Durban. Rain drop size depends on rainfall rate, drop diameter and rain drop velocity. Semi-empirical models of terminal velocity from previous studies are investigated in this work and proposed for the estimation of specific rain attenuation.

Table of Contents

Chapter Two

Literature Review

Chapter Four

Rainfall Rate Modeling and Its Characteristics in Southern Africa and Surrounding Islands

Chapter Five

Characteristics of Rain Dropsize Distribution

List of Tables

List of Figures

List of Acronyms

APR	Average Probability Ratio
AWM	Average Worst Month
AY	Average Year
CCIR	Consultative Committee for International Radio Communication (now ITU-R)
CD	Cumulative Distribution
Cdf	Theoretical Distribution Function
CDF	Cumulative Distribution Function
CHI	Chi-Square Statistic
C-R	Crane Global Model
DSD	Raindrop Size Distributions
Ecdf	Empirical Distribution Function
GIS	Geographic Information Systems
HDMI	High Definition Multimedia Interface
IDW	Inverse Distance Weighting
ITU-R	International Telecommunication Union
JWD	Joss-Waldvogel Distrometer
KIT	Kitami Institute of Technology
K-test	Kolmogrov-Smirnov Test
LMDS	Local Multipoint Distribution Services
LOS	Line-Of-Sight
MLE	Maximum Likelihood Estimation
M-ST	Moupfouma and Martin for Tropical/Sub-Tropic
M-TE	Temperate
MVDS	Microwave Video Distribution Services
NRF	National Research Foundation

Pdf	Probability Density Function
R-H	Rice-Holmberg
RME	Root Mean Square Error
RMS	Root Mean Square
SAC&W	South Africa Climate and Weather
SAWS	South Africa Weather Service
STD	Standard Deviation
SC	Self Consistency
UHF	Ultra High Frequency
VHF	Very High Frequency
WMO	World Meteorological Organization

Chapter One

General Introduction

1.0 Introduction

The development of complex radio access networks has resulted in increasing spectrum occupancy and demand for higher bandwidths; hence it is imperative to employ the advantages of higher frequencies, which are capable of supporting these demands. The obvious candidates are microwave and millimeter bands. The advantages offered by microwave and millimeter waves have attracted immense interest from academia and the communications industry. The main characteristics of both waves include short wavelength (hence small components), large bandwidth, and frequency re-use. The interaction of the waves with atmospheric constituents, especially with hydrometeors, results in serious impairment of the signal at these frequencies: these impairments include attenuation, scattering and depolarization.

This work thus presents the result of a theoretical and experimental assessment of hydrometeors' interaction with microwave and millimeter waves propagating in the medium containing the hydrometeors. The term "hydrometeor" refers to products of condensed water vapour in the atmosphere, usually observed as rain, hail, ice, fog, cloud and snow. The most important of these hydrometeors for radio propagation is rain, and as such, the study is concerned with the effect of rain on microwave and millimeter waves at frequencies of 1-300 GHz as shown in Table 1.1. The table shows the classification of a part of the electromagnetic spectrum particularly relevant to radio propagation (Hall, 1991).

In satellite and terrestrial links, signals transmitted at these frequencies interact with raindrops because it covers a substantial path of the links. An electromagnetic wave propagating through a region containing raindrops suffers two attenuating effects: one is absorption through which part of its energy is absorbed by the raindrops and transformed into heat; and the other is scattering where part of the energy is scattered in all directions.

Table 1.1 Parts of the electromagnetic spectrum

Frequency Band	Wavelength	Descriptive Designation
30-300 *Hz*	10000-1000 *km*	- ELF
3-30 *kHz*	100-10 *km*	Myriametric waves VLF
30-300 *kHz*	10-1 *km*	Kilometric waves LF
300-3000 *kHz*	1000-100 *m*	Hectometric waves MF
3-30 *MHz*	100-10 *m*	Decametric waves HF
30-300 *MHz*	10-1 *m*	Metric waves VHF
300-3000 *MHz*	100-10 *cm*	Decimetric waves UHF
3-30 *GHz*	10-1 *cm*	Centrimetric waves SHF
30-300 *GHz*	10-1 *mm*	Millimetric waves EHF
300-3000 *GHz*	1-0.1 *mm*	Sub-millimetric waves -

The comprehensive study of these two attenuating mechanisms is based on understanding the characteristics of raindrops. The characteristics of raindrops are examined in light of integration time of rainfall rate, cumulative distribution of rainfall rate and its modelling, worst-month statistics of rainfall rate, raindrop size distribution, and its pattern modelling at different categorization classes. All the mentioned rain attenuation mechanisms are presented in this thesis for easy determination of rain attenuation of radio frequency signals in the microwave and millimeteric bands.

1.1 Brief review of Existing Work

Several factors have necessitated the migration to higher operating frequency bands in communication systems. These factors include, among others, congestion at lower frequency spectrums, growing demand for larger bandwidth, a significant rise in the use of digital techniques, and insufficient orbital positions or slots in the geostationary orbit to handle new services (Ippolito, 1981). Unfortunately, the main problem in the use of microwave and millimeter wave bands for communication in terrestrial and satellite systems lies in the occurrence of strong interactions between radio waves and rain as the wavelength approaches raindrop sizes. This interaction tends to degrade the quality of

transmitted and received signals, and is primarily caused by two effects (Reddy, 1982). The first effect is that the electric field associated with the radio wave induces displacement currents in the water drops, and these currents are heavy, especially at high frequencies, because water has a higher dielectric constant than air. Secondly, the displacement currents act as a source of secondary radiation (scattering) in all directions, thereby weakening the strength of the radio wave in the direction of interest.

Therefore, to fully understand the magnitude of such interactions, detailed microphysical properties and scattering processes of raindrops must be known, in order for the degrading effects such as signal attenuation due to rain, rain-induced depolarization and so on can be evaluated quantitatively. Unfortunately, much of the extensive work done to date on this subject has been in the temperate and tropical regions. There appears to be a general lack of data with respect to measurement of shape effect, falling terminal velocity, rain rate and rain drop size distribution models and so on, in Southern Africa. Availability of statistical data for the quantitative evaluation of rainfall properties is also a major challenge.

Due to the spatial and dynamic variability of rainfall rate, the peak count of raindrops is important for the estimation of signal outage due to rain; thus the integration time of rainfall rate needs to be studied. In addition, longer integration intervals remove the higher rain rates and shift the distribution to a low rate (Crane, 1996). By International Telecommunication Union recommendations, one-minute rainfall rate integration time is the acceptable standard for the estimation of rain attenuation (ITU-R P.837-5, 2007). However, because data for one-minute rainfall rates is not common and not available for global coverage, many researchers have resorted to developing models that can convert the integration time of available data to a one-minute rate equivalent (Segal, 1986; Rice-Holmberg, 1973; Ajayi and Ofoche, 1984; Singh et al., 2007; Chebil-Rahman, 1999; Ito-Hosoya, 2006; Dutton and Dougherty, 1979; Karasawa-Matsudo, 1990; Emiliani, Luini and Capsoni, 2008).

Another component required to estimate rain attenuation is the cumulative distribution of rainfall rate in a particular region, especially where communication links are to be established. The prediction of rain rate patterns over a long period of time is essential for system designers and link-budget planners. Extensive research has been conducted in this area of prediction and researchers have come up with mathematical expressions and models to determine the rainfall rate value at given percentages of exceedence. The most widely known are Crane's Global Climatic model (Crane, 1980) and the ITU-R P-837 recommendation (ITU-R P.837, 2001) which was originally developed under International Radio Consultative Committee (CCIR) in 1974 and is now in its fifth revision under ITU-R (ITU-R P.837, 2007). Other rainfall rate distribution models commonly referred to are Rice-Holmberg's model (Rice and Holmberg, 1973), Moupfouma and Martin model (Moupfouma et al., 1995). In West Africa, the contribution of Ajayi and Ofoche (Ajayi et al., 1984) has added an African perspective to the global map, while, in Southern Africa, Owolawi et al. (2009; 2007 and 2006) have conducted similar research. Seeber's (1995) contribution for rainfall modelling for South Africa and surrounding islands was based on 1 five-minute integration time and few sample points. This seemingly laudable effort, however, is not adequate for use in radio planning.

As far as the measurement of shape effect, dropsize distribution and terminal velocity of rain drop are concerned, there also appears to be a general lack of data on these very important parameters for rain attenuation estimation for terrestrial and satellite links in Southern Africa. However, measurement of the distribution of raindrop sizes has been carried out in some parts of the world. Such measurements have been reported by Ajayi and Olsen (1985) and Adimula and Ajayi (1996) for Ile-Ife, South-West Nigeria; Moupfouma and Tiffon (1982) for equatorial Congo; Maciel and Assis (1990) for Brazil; Maitra et al (1995) for the tropical region of India; and Therek and Din (1992) for Malaysia. There seems to be a fair understanding of the distribution of raindrop sizes in the tropics as most of the studies suggest the lognormal distribution, rather than conventional models such as the Marshall and Palmer (1948), and Laws and Parsons model (1943), both of which are inclined to over estimate the lower drop sizes. In

Southern Africa, different distributions such as exponential, Weibull, Gamma and lognormal may be applicable-but these are all subjected to confirmation in this work. The microphysical properties of rain such as drop shape, size, and size distribution, contribute immensely to the computation of scattering (magnitude and orientation) and attenuation of the electromagnetic wave in the presence of rain. These properties depend on the wavelength of the propagating electromagnetic waves and the diameter distribution of the incident rain drop. However, scattering has been studied by Mulangu and Afullo (Mulangu et al, 2009), and will not be of our consern here.

1.2 Problem Formulation

The past decade has witnessed an explosive increase in broadband communication applications, which has imposed immense pressure on link capacity in terms of bandwidth requirements. The exploitation of higher frequencies (especially millimetric bands) has provided a possible solution to the above challenges, although it has been tempered by the presence of hydrometeors. Characteristics of radio wave propagation in space are described using statistical knowledge of space constituents through modelling of its inherent physical mechanisms. Rain is a special space constituent, especially at these bands. The non-uniformity of rain along the propagation path is taken into account via statistical models which depend on the accuracy of the rain rate measurement and measurement tools. Results of the models are incorporated into radio planning software to imitate the transmission chain and effect prediction of the link performance prior to deployment of the radio system.

The estimation of the extent of signal loss as a result of the interaction between electromagnetic waves with rain needs to be investigated. The problem is therefore split into two parts in order to provide a detailed description of characteristics of rain that result in signal impairment: firstly, the statistical characteristics of rain rate distribution and, secondly, microphysical studies of raindrops and dropsize distribution.

1.3 Scope of Work

The scope of this research work and its contribution to the body of knowledge are as follows:

- To investigate the existing rainfall rate integration time-conversion methods and develop a hybrid method that is based on a combination of the existing methods. The results are used to generate integration conversation constants maps for South Africa and surrounding islands. The results are compared with the existing ones, notably the ITU-R maps.
- To develop rainfall rate distribution models and maps for South Africa and surrounding islands. Using the method of maximum likelihood, distribution parameters such as Gamma, Weibull, and log-normal, the results are estimated and are compared with two common global rain climatic zones - Crane global and ITU-R rain climatic zones.
- To model raindrop size distribution, investigating three-parameter statistical distributions such as Weibull, Gamma, and Lognormal. Using the method of maximum likelihood estimation, and distributions such as gamma, Weibull and log-normal, the estimation results are compared with those of two common global rain climatic zones-the Crane global and ITU-R rain climatic zones.

1.4 Overview and Structure of Thesis

Chapter one is an introduction to the study which this thesis presents. The areas covered are: the research objectives; motivation for the study; a review of existing work on the research area; the problem statement; and the scope of the work are outlined. Chapter two focuses on the literature review. Rainfall rate modelling is an important component of estimating rain attenuation along a communication link. The models covered include physical models, analytical models, and empirical models. A good methodology is required to estimate all necessary parameters that will optimally describe the distribution patterns of rainfall rate. This section also explores different rain rate conversion techniques.

Chapter three deals with rain measurement and conversion methods from higher integration times to a lower (one-minute) equivalent. Several conversion methods are discussed and new hybrid methods together with their conversion factors maps are generated for South Africa and surrounding Islands. The results are compared with other models from different regions in the world. A classification of Rain climatic regions based on the Koppen classification is undertaken. Chapter four discusses various statistical rain distributions and their estimator methods. A comparison of the developed model and existing models, especially ITU-R and Crane Global models, is carried out since rain climatic zone maps are developed based on ITU-R and Crane designations. Chapter four further focuses on rainfall variability and its worst month. A mathematical model is proposed to show the relationship between annual rainfall rate distribution and its worst-month equivalent.

Chapter five provides details of different existing models of raindrops and their distributions. Knowledge of the distribution of raindrops with their sizes are important in calculating the amount of rain impairment along the signal path. A new raindrop size distribution model is developed based on the maximum likelihood estimator method for South Africa, and results are compared with similar work from West Africa and other parts of the world. Chapter six is the conclusion of the study. In this chapter, concise descriptions of the study's achievements are presented and the chapter further recommends future work in order to improve the proposed model and contributions.

1.5 Own Contribution

Certain aspects of this thesis have been published in journals and conference proceedings, and are shown below:

- M. O. Fashuyi, **P. A. Owolawi and** T. J. Afullo (2006), Rainfall Rate Modelling for LOS Radio Systems in South Africa, *Transactions of South African Institute of Electrical Engineers (SAIEE), Vol. 97 (1):* pp. 74 - 81 [Journal article].

- C.T. Mulangu, P.A. **Owolawi** and T.J. Afullo (2007), Rainfall Rate Distribution for LOS Radio Systems in Botswana In: *SATNAC 2007 Conference*, ISBN 978-0-620-39351-5, Port Louis, Mauritius [Conference Proceedings].

- **P.A. Owolawi and** T.J. Afullo (2007), Rainfall Rate Modelling and Worst Month Statistics for Millimetric Line-of-Sight Radio Links in South Africa. *Radio Science Vol. 42* [Journal article].

- **P.A. Owolawi and** T.J. Afullo**.** (2007), Rainfall Rate and Worst-Month Determination and Application for Radio Link Design in South Africa In: *IEEE Africon 2007 Conference*, ISBN No. 0-7803-8606-X, Windhoek, Namibia [Conference Proceedings].

- **P.A. Owolawi,** T.J. Afullo and S. Malinga (2008), Rainfall Rate Characteristics for the Design of Terrestrial Links in South Africa, Wild Coast, Eastern Cape, South Africa

- **P.A. Owolawi,** T.J. Afullo and S. Malinga (2009), Effect of Rainfall on Millimeter Wavelength Radio in Gough and Marion Islands. *PIERS Online Vol. 5 No. 4: pp 328-335* [Journal article].

- **P.A. Owolawi,** T.J. Afullo and S.B. Malinga (2007), Effect of Worst-Month Distribution on Radio Link Design in South Africa In: *Proceedings of the Eleventh URSI Commission F Triennial Open Symposium on Radiowave Propagation and Remote Sensing*, ISBN No. 978-85-87926-26-5, Rio de Janeiro, Brazil [Conference Proceedings].

- **P.A. Owolawi**, T.J. Afullo and S.B. Malinga (2009), One-minute Integration Time Map for the Estimation of rain Attenuation in South Africa and surrounding Islands (Submitted for review, *Radio Science*, 2009).

Chapter Two

Literature Review

2.0 Introduction

Rain attenuation is estimated from the mathematical combination of cumulative distribution of rain rate, which is a function of the sampling time, called integration time, and microphysics of rain primarily known as raindrop size distribution. This chapter will review some contributions of many researchers in the area of integration time, rain rate modelling, mapping, and is concluded with a discussion of raindrop size distribution characteristics and its models.

2.1 Review of Rain Rate Integration Time

This section provides an overview of different methods of converting rain rate from higher integration time to a one-minute equivalent which is the acceptable threshold of the ITU-R recommendations. The sub-sections covered here are: the effects of integration time on rain rate distribution, as well as classes of different existing integration time conversion methods.

In order to achieve an accurate measurement of rain rate distribution, the distribution ought to be based on long-term data approximately ten years and measured at a one-minute integration time or less. This is in accordance with ITU-R Recommendation P.618-6 or P.530-8. Though hourly and 5 to 30 minutes data are recorded by many weather services, one-minute rain data are rarely available (Crane, 1996). It is confirmed, as shown in **Figure 2.1**, that longer integration intervals remove the higher rate data and shift the distribution (Crane, 1996) , a fact which has encouraged researchers to develop methods to solve the problem of conversion from higher integration times to lower equivalents. The established conversion methods are grouped into different classes based on their functional principles as defined by Capsoni *et al* (2008):

- **Physical method**: This method uses climatic information such as annual rain rate, average rain rate, monthly and yearly accumulation. The most acknowledged

models are the Rice-Holmberg model (Rice-Holmberg, 1973), Dutton-Dougherty model (Dutton *et al*, 1974), Crane model (Crane, 1980), ITU-R (ITU-R P.837-5, 2007), EXCELL method (Capsoni *et al*, 2008) and the physical-stochastic method (Lavergnat and Golé, 1998).

- **Analytical method**: This is a process of shifting the cumulative distribution (CDF) of rain rate at integration time to its one-minute equivalent. Established works using this method include those of Moupfouma (Moupfouma *et al*, 1995), Karasawa (Karasawa *et al*, 1991) and Ito-Hosaya (Ito *et al*, 2006).
- **Empirical method**: This method provides conversion from one integration time to another at equal probability state. The most prominent authors are Segal (Segal, 1986), Burgueno (Burgueno *et al*, 1988), Watson (Watson *et al*, 1982), and Chebil-Rahman (Chebil *et al*, 1999).

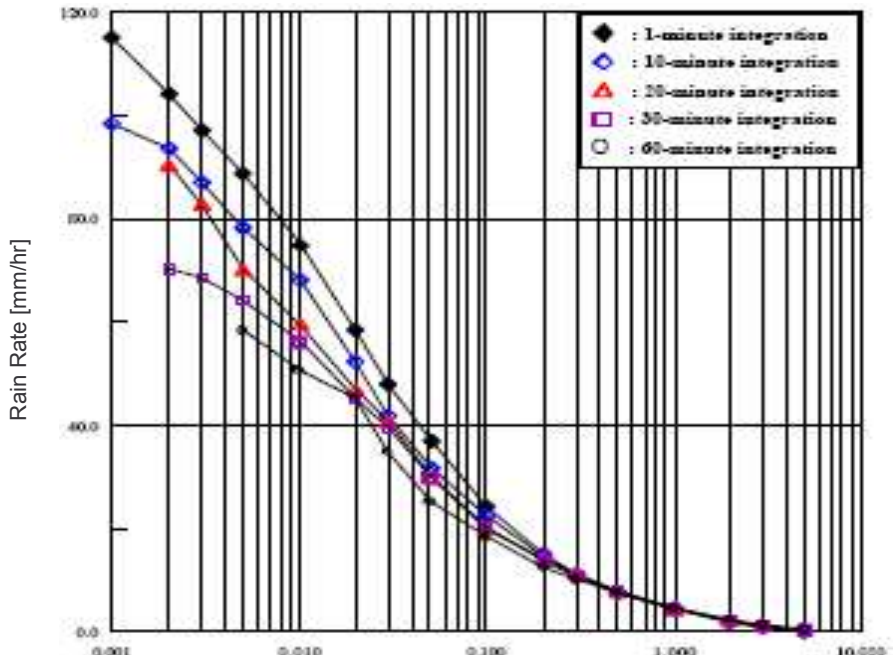

Figure 2.1: Total Statistics of rainfall rate data for various integration times (Joo *et al*, 2002)

2.2 The Physical Method

The physical modelling of rain rate gives the process of rain distribution a unique pattern with its mathematical representation. The physical input parameters of rain are required in describing its distribution patterns as a function of measuring time. Since many researchers have used climatic information in modelling the time series measurement of rain, it is ideal to define such conversion methods by using the physical method.

2.2.1 Rice-Holmberg and Dutton-Dougherty-Martin Models

The Rice-Holmberg model is based on the cumulative distribution of rain rate. There are two modes in their method: mode 1 deals with convective type of rain (M_1) while mode 2 deals with other types of rain (M_2). The total average accumulation is given by:

$$M = M_1 + M_2 \quad \text{(mm)} \tag{2.1}$$

A coefficient β is the ratio of convective rain or thunderstorm to the total average rainfall accumulation (M) and is given by:

$$\beta = M_1 / M \tag{2.2}$$

Their work was further improved by Dutton *et al* (1974). They combined the number of thunderstorm days (D_{th}) expressed in an average year, and the highest monthly precipitation (M_m) observed, where M is the average annual accumulation given in millimeters. The resulting expression proposed is the probabilistic state of rain rate with a one-minute integration time given as (Emiliani *et al*, 2004):

$$\begin{aligned} P(r > R) &= \frac{M}{87.66}\left\{0.03\beta^{-0.03R} + 0.2(1-\beta)\left[e^{-0.258R} + 1.8e^{-1.63R}\right]\right\} \\ \beta_0 &= 0.03 + 0.97e^{-5\exp(-0.004M_m)} \\ \beta &= \beta_0\left[0.25 + 2e^{-0.35(1+0.125M)/D_{th}}\right] \end{aligned} \tag{2.3}$$

2.2.2 Physical-Stochastic Model: EXCELL and Lavergnat-Golé Models

The physical-stochastic method is an up-grade of the physical method but with statistical properties. It takes advantage of the physical attributes of synthetic rain cells in order to simulate the actual counting process of a rain gauge operating at a given integration time (Capsoni *et al*, 2008). The EXCELL model describes the spatial profile of rain. Although the original formulation of the model was made for an elliptical rain cell, the model proposed by Capsoni *et al* (1987) is characterized by R profile within the CELL as shown in Figure 2.2. The refined version of the model by Paraboni *et al* (1998) extends the inclusion of rain rate up to zero rain rate. The rain rate time series R is given by:

$$R = (R_M + R_{low}) \exp(-\rho / \rho_o) - R_{low} \tag{2.4}$$

where R_M is peak rain rate, ρ is a distance from the peak, ρ_o is a cell radius (at R_M / e) and

$$\rho_{\max} = \rho_o \ln[(R_M + R_{low}) / R_{low}] \tag{2.5}$$

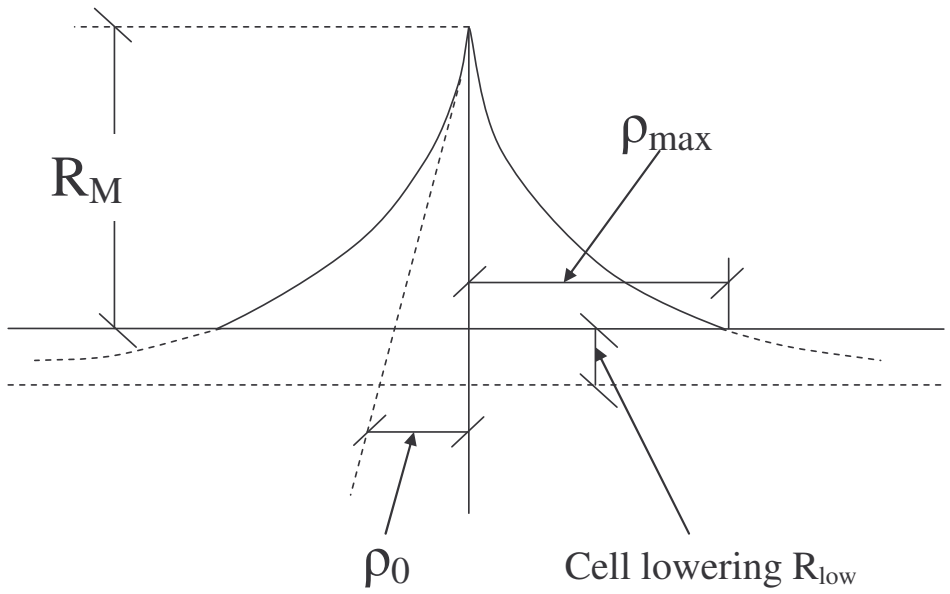

Figure 2.2: EXCELL model of rain cell (Paraboni *et al*, 1998)

The Lavergnat and Golé model (1998) can be grouped under the physical-stochastic category which builds on the sum of Pareto distributions with an exponentially decreasing term. Its simplicity, reliability and theoretical background make the Lavergnat-Golé model a good choice for many researchers. The conversion of cumulative distribution from an integration time t_1 to a target t_2 is given by the Lavergnat-Gole expression:

$$P_2(R_2) = k^a P_1(R_1) \tag{2.6}$$

$$R_2 = R_1 / k^a \,,\; k \equiv t_2 / t_1 \tag{2.7}$$

This method was confirmed to have better conversion accuracy than the method proposed by Ito and Hosoya (2000). The parameter a is proposed for the world using Kitami Institute of Technology (KIT) database. The expression is given by Ito and Hosoya (2001):

$$\begin{aligned} a = {} & 0.00219126|\phi| - 0.000205094|\lambda| - 0.001165957R_{0.01C} \\ & + 0.000869955R_{0.001C} + 0.0000492772M + 0.001336088D_{th} \\ & - 0.173738515\beta + 0.035580308 \end{aligned} \tag{2.8}$$

$$R_{0.001C} = 23.50390M^{\,0.27896}\beta^{0.34162} \tag{2.9a}$$

$$R_{0.01C} = 3.69786M^{\,0.46613}\beta^{0.43482} \tag{2.9b}$$

where ϕ is the latitude in degrees, λ is the longitude in degrees, $R_{0.01C}$ and $R_{0.001C}$ (mm/hr) are the calculated one-minute rain rates for 0.01% and 0.001% of a year, respectively.

2.3. The Analytical Method

The analytical method for rain rate modelling, as defined by Emiliani *et al* (2009), is considered when the shape of cumulative distribution of rain rate is maintained while parameters that determine the shape depend on the rain rate integration time. Universally acknowledged research in this method include those of Moupfouma and Martin (1995), Karasawa and Matsudo (1991) and Ito and Hosaya (2006).

2.3.1 Moupfouma-Martin Model

The Moupfouma-Martin rain rate model is a popular method because it includes local climatic parameters. Since climatic parameters are the key inputs that uniquely describe the distribution patterns of rain rate in any location, the incorporation of such parameters are needed to define the rain rate model expression. The Moupfouma-Martin expressions describe cumulative distribution of rain rate as:

$$P(R \geq r) = 100\left(\frac{R_{0.01}+1}{r+1}\right)^{b} e^{u(R_{0.01}-r)-\log_e(10^4)} \tag{2.10}$$

where:

$$b = \left(\frac{r}{R_{0.01}} - 1\right)\log_e\left(1 + \frac{r}{R_{0.01}}\right) \tag{2.11}$$

The climatic parameter u depends on the integration time and climatic location.
The expressions for temperate, tropic and sub-tropic locations are given by:

(a) For temperate localities

$$u(r) = \frac{\log_e(10^4)}{R_{0.01}} \frac{1}{1+\eta\left(\frac{r}{R_{0.01}}\right)^{\beta}} \tag{2.12}$$

where $\eta = 4.56$ and $\beta = 1.03$

(b) For tropical and sub-tropical localities

$$u(r) = \frac{\log_e(10^4)}{R_{0.01}} \exp\left(-\lambda\left(\frac{r}{R_{0.01}}\right)^{\gamma}\right) \tag{2.13}$$

where $\lambda = 1.066$ and $\gamma = 0.214$

Rain rate integration time that is less than one-hour can be converted to one-minute equivalent by the expression:

$$R(1\min)_{0.01} = (R(\tau\min)_{0.01})^{\alpha} \tag{2.14}$$

$$\alpha = 0.987(\tau(\min))^{0.061} \tag{2.15}$$

Provided $1\min \le \tau \le 1 hour$

2.3.2 Karasawa-Matsudo Model

The Karasawa-Matsudo model (Karasawa and Matsudo 1990, 1991) is based on Moupfouma's (1982) proposed probabilistic distribution expression:

$$f(R \mid r,u) = \frac{r}{R}\exp(-uR)\left\{\frac{1}{R} + u\right\} \tag{2.16}$$

$$F(R \mid r,u) = \int_R^{\infty} f(R)dR = \frac{r}{R}\exp(-uR)$$
$$(p = F \times 100\%) \tag{2.17}$$

Based on equations 2.16 and 2.17, climatic parameters defined by the Moupfouma distribution model for one-minute rain rate are re-defined by the Karasawa-Matsudo model(1990 , 1991), and given as:

$$r_m = 7.24\times10^{-4} R_{m.,0.01}, \quad U_m = 1.98 / R_{m.,0.01} \tag{2.18}$$

On the other hand, for one-hour rain rate, the expression is given by:

$$r_h = 1.52\times10^{-3} R_{h.,0.01}, \quad U_m = 2.72 / R_{h.,0.01} \tag{2.19}$$

In this model, the average of the five highest one-hour rain rates per year (m_{1-5h}), the one-minute rain rate $R_{m,0.01}$ exceeded for 0.01% of the time, is expressed in the following equation:

$$R_{m,0.01} = a_{1-5h}.m_{1-5h} \quad (a_{1-5h} = 2.3) \tag{2.20}$$

Using equations 2.18, 2.19 and 2.20, the one-minute rain rate distribution is expressed as:

$$F(R_m) = 7.24\times10^{-4} \frac{R_{m,0.01}}{R_m} \exp\left(\frac{-1.98R_m}{R_{m,0.01}}\right) \tag{2.21}$$

2.3.3 Ito-Hosoya Model

Out of all aforementioned rain rate integration time methods, the Ito-Hosoya model is the only model that proposes a global conversion method. There are two main reasons for the worldwide applicability: firstly, the model incorporates thunderstorm ratio β as a local climatic parameter and secondly, it is based on the Dutton-Dougherty model (Dutton *et al*, 1974). The Ito-Hosoya model is tagged KIT model (Ito and Hosoya, 1999), and its general expression is given by:

$$R_p = a_p M^{b_p} \beta^{c_p} \tag{2.22}$$

where a_p, b_p and a_p are coefficients determined by the following expressions:

$$\log(a_p) = 0.1574155x^4 + 1.348171x^3 + 3.528175x^2 + 1.479566x - 2.302276 \quad (2.23)$$

$$b_p = -4.583266\times10^{-2}x^4 - 0.4098161x^3 - 1.162387x^2 - 0.8261178x + 0.911857 \quad (2.24)$$

$$c_p = 2.574688\times10^{-2}x^4 + 0.1549031x^3 + 0.1747827x^2 - 0.2846313x + 1.255081\times10^{-2} \quad (2.25)$$

where x is $\log(p)$.

The climatic parameters β and M have a strong influence on the rain rate distribution patterns. This characteristic makes the Ito-Hosoya model a good choice when converting rain rate from any integration time to its one-minute equivalent.

2.4 The Empirical Method

The empirical method is extensively used in converting higher integration time to the required one-minute rain rate. Its popularity lies in a functional principle that compares rain rates of two different integration times at equiprobable state. Studies which have applied this method in different regions include Ajayi and Ofoche (1984) for Nigeria, Burgueno *et al* (1988) for Spain, Flavin (1982) for Australia, Ong and Zhu (1997) for Singapore, Watson *et al* (1982) for Europe, Xiao *et al* (1987) for China, Chebil and Rahman (1999) for Malaysia, and Segal (1986) for Canada.

In principle, the two main laws commonly used in empirical methods are the power law and the power-exponential law. In Emilian *et al* (2009), the laws are expressed as follows:

$$R_1(P) = aR_T(P)^b \tag{2.26}$$

where $R_1(P)$ and $R_T(P)$ are, respectively, the rain rate for a one-minute integration time and any integration time (T), at equal percentage of exceedence (P). Table 2.1 shows the constant values for parameters *a* and *b* with their respective rain rate integration times, τ.

Table 2.1: a and b values for various integration times ITU-R 837-5 (ITU-R 837-5, 2007)

τ	a	b
5 min	0.986	1.038
10 min	0.919	1.088
20 min	0.680	1.189
30 min	0.564	1.288

Table 2.2: a and b values for equation 2.26 for various integration times in Emilian *et al* (2009)

τ	**New proposed**		**ITU-R P.837-5**	
	a	b	a	b
5 to 1 min	0.924	1.044	0.986	1.038
10 to 1 min	0.829	1.097	0.919	1.088
20 to 1 min	0.736	1.169	0.680	1.189
30 to 1 min	0.583	1.265	0.564	1.288
60 to 1 min	0.509	1.394	-	-

The other law is expressed as:

$$CF(P) = \frac{R_1(P)}{R_T(P)}, CF(P) = aP^b, \quad 0 < P < 1, \tag{2.27}$$

$$CF(P) = \frac{R_1(P)}{R_T(P)}, CF(P) = aP^b + ce^{dp}, \quad 0 < P < 1, \tag{2.28}$$

where $CF(P)$ is conversion factor at a particular percentage of exceedence (P).

2.4.1 ITU-R Rain Rate Integration Time Contributions

The contribution of ITU-R study 3 which led to the revised ITU-R 837-5 (ITU-R 837-5, 2007) has given a good direction in resolving the issues around integration time, although the approach is based on the empirical method with limited climatological data from few regions in the world. In their proposal, power law was considered for four different integration times which are 5 min, 10 min, 20 min and 30 min as shown in Table 2.1.

In recent times, the group has put forward a revised recommendation with more data and analysis from many other regions in the world as detailed in ITU-R Document 3J/29-E (ITU-R Document 3J/29-E 2008). Mathematically, two expressions are proposed to determine the global coefficients for the power laws (equation 2.26) as shown in the expressions below:

$$\begin{aligned} a &= 0.0002t^2 - 0.0189t + 1.0136 \quad R^2 = 0.987 \\ b &= 0.0063t + 1.0366 \qquad\qquad\quad R^2 = 0.97 \end{aligned} \tag{2.29}$$

Emiliani *et al*'s (2008) contribution proposed new global coefficients for the application of the ITU-R P.837-5 power law conversion method. These new proposed coefficients extend its application to rain rate statistic conversion method in temperate, tropical and cold climate. Their work extends the ITU-R P.837-5 integration time from 5-, 10-, 20-, 30-minute to 60-minute interval as shown in Table 2.2.

2.5 Review of Existing Rain Rate Models

It is necessary to have prior knowledge of the probability at which rain rate is exceeding in order to estimate rain attenuation and thus, fade margin for a specified geographical

region. Rain rate modelling is an important component that makes the prediction of rain attenuation possible. Rain rate models can be classified into two categories according to the mode of applications. These classes are global and localized rain rate models.

2.5.1 Global Rain Rate Models

In global rain rate models, the mechanism used primarily depends on climatic parameters and geographical locations. Here, regional maps are useful for representing rain rate distribution at a chosen threshold of percentage of exceedence especially for a location where observing station is not sited. In the development of a global rain rate climatic model for communication systems, the earth was initially zoned into four designations or latitude bands namely arctic, mid-latitude, sub-tropics and tropics. The designations were later extended to eight to improve the variations with latitude and longitude. There are several global rain rate models available but the focus of this study is on Crane's and ITU-R global models. These two models are common in most radio planning software such as pathloss version 4 as documented in Pathloss version 4 user manual: Rain Section pp.1-4.

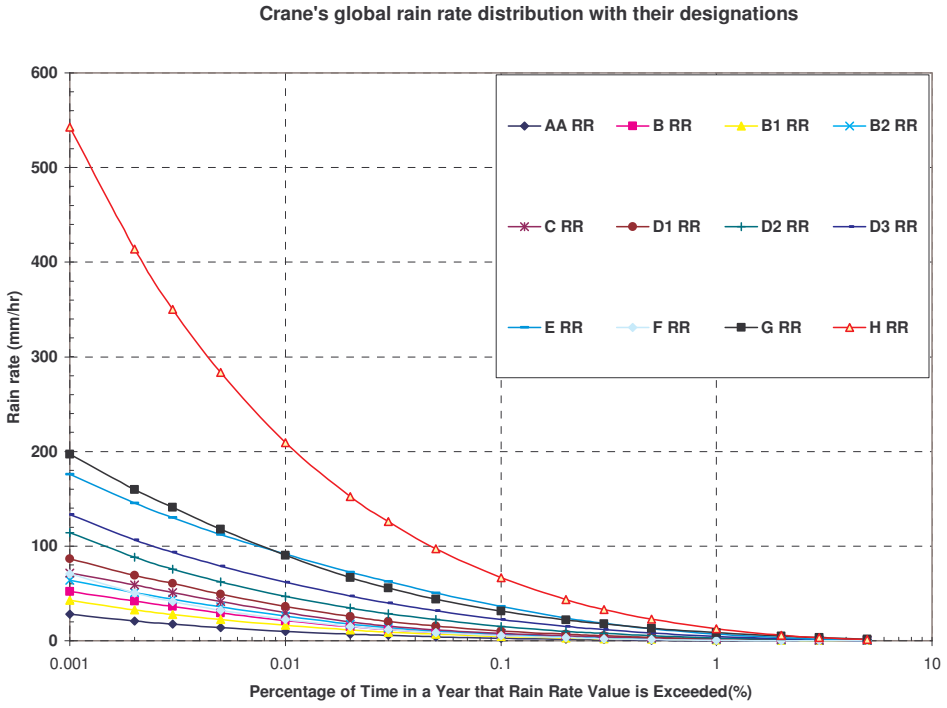

Figure 2.3: Global rain climatic zone using Crane's classification method

2.5.2 Crane's Global Rain Rate Model

The work done by Crane (1980) classified the globe into eight regions; each labelled **A** through **H** with varying degrees of dryness to wetness. Designation **A** connotes arctic dry while **H** is the tropical wet; and in the sub-tropics, **H** region is sub-divided into **E wet** and **E dry**. From available data points, there was a variation in rain rate at a smaller percentage of exceedence which led to creation of more designations. D region was further sub-divided into $D_1 - D_3$, with D_1 driest and D_3 wettest. Further review of the world map introduced additional designations of B region such as B_1 and B_2 added to the map.

Figure 2.3 shows rain climatic model cumulative distribution using Crane's designations which can be employed to estimate rain attenuation especially for areas where local rain data is scarce. In accumulating these distributions, a total of three station years of data were used for region G, 178 stations years of data were made available for region D_2 while other regions have their stations at the mid of the G and D_2. The regional rain climatic map is divided into three zones: America, Asia and Europe, and Africa.

Figure 2.4 represents Crane's global rain climatic map for Africa and Europe. It is observed on the map that South Africa can be grouped to 5 different climatic regions with designations C, D_1, D_2, D_3 and F while Marion and Gough Islands are represented by Crane designations A and C respectively.

2.5.3 ITU-R Global Rain Rate Model

The ITU-R provides another competent global rain rate climatic model termed characteristics of precipitation for propagation modelling as shown in Figure 2.5. The model was originally developed under CCIR in 1974 and several revisions have been made from ITU-R P837-1 (ITU-R P.837-1, 1994) to recently revised ITU-R P.837-5 (ITU-R –P.837-5, 2007). These recommendations are used to estimate rain attenuation at

terrestrial and satellite communication systems, thus their fade margin for defined probability of exceedence can be estimated. The ITU-R has divided the globe into 15 climatic zones with light rain rate denoted by letter **A** and profound rain rate represented by letter **Q**.

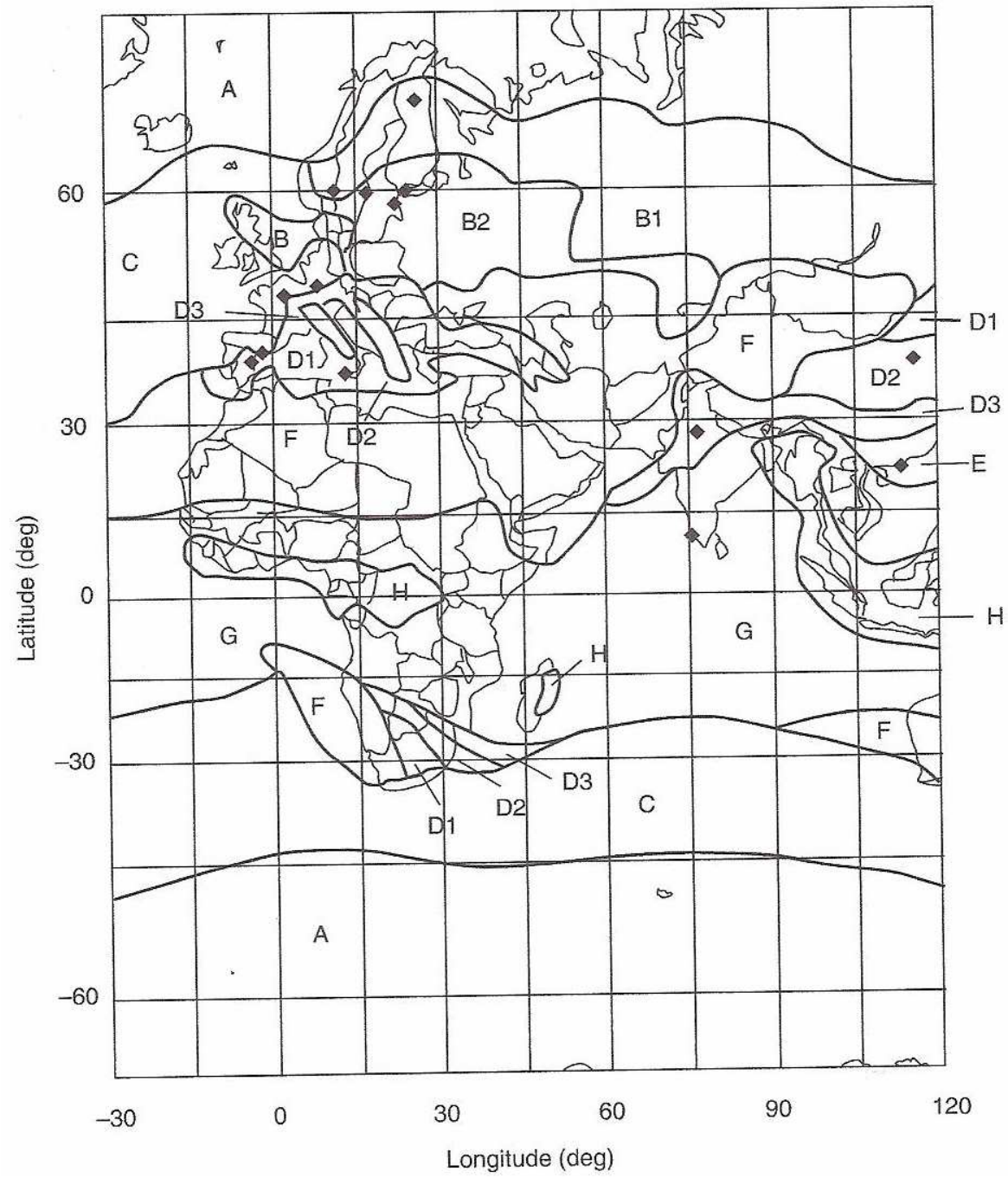

Figure 2.4: Global Crane rain climatic regions for Europe and Africa (Crane, 1996)

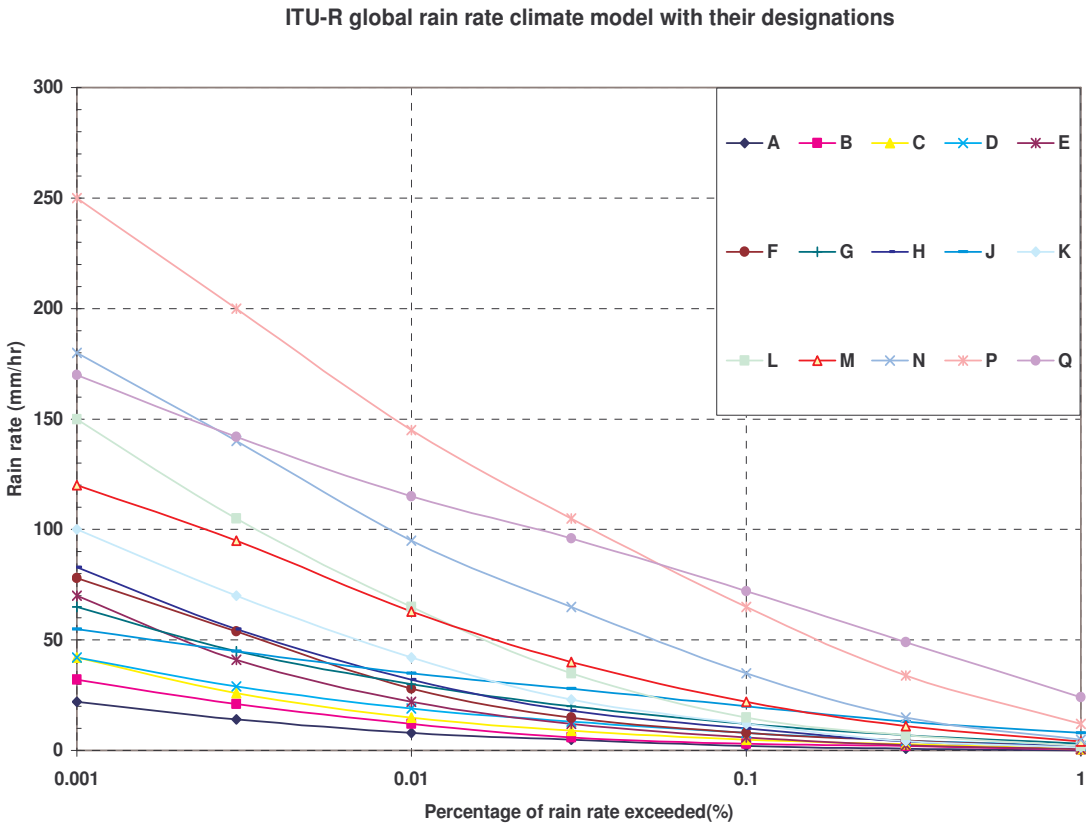

Figure 2.5: Global rain climatic zone using ITU-R's classification method

This model is based on measurements from different regions in the world with regular updates; this reduces the discrepancy commonly observed in using the model locally. The rain rate distribution for the ITU-R rain climatic map is applicable at percentage of exceedence ranging from 1% to 0.001%. The method used customized database parameters such as P_{r6}, M_c, M_s latitude and longitude of location of interest. The parameters P_{r6}, M_c, and M_s represent probability of a rainy 6 hour period, the annual rainfall amount of convective-type of rains, and the annual rainfall amount of stratiform-type rains respectively. The only parameters needed to determine rain rate at any percentage of exceedence are latitude and longitude of the location of interest. Figure 2.6 shows climatic region boundary for Africa and their designation letters. Figure 2.6 is extracted from ITU-R P.873-1, the first ITU-R recommendation; while Figure 2.7 is ITU-R P.873-5 updated in May 2008 and currently these standards are enforced. It provides

the global rain climatic map at 0.01% percentage of exceedence of rain rate which is one of the principal components required in estimating rain attenuation. The use of this simple model is hampered by the limitation of rain rate data at specified integration time for many parts of the world. Considering the recommendation ITU-R P.873-1 Fashuyi *et al* (2006) found that Southern Africa has six rain climatic zones, namely C, D, E, J, K and N of which South Africa has five. These are C, D, E, K and N. In their work, it was also confirmed that there is variation in the ITU-R P.873-1 and P.873-4 for many selected sites in South Africa. Marion island is found on the ITU-R rain climatic Zone A and Gough Island is found in the D rain rate zone.

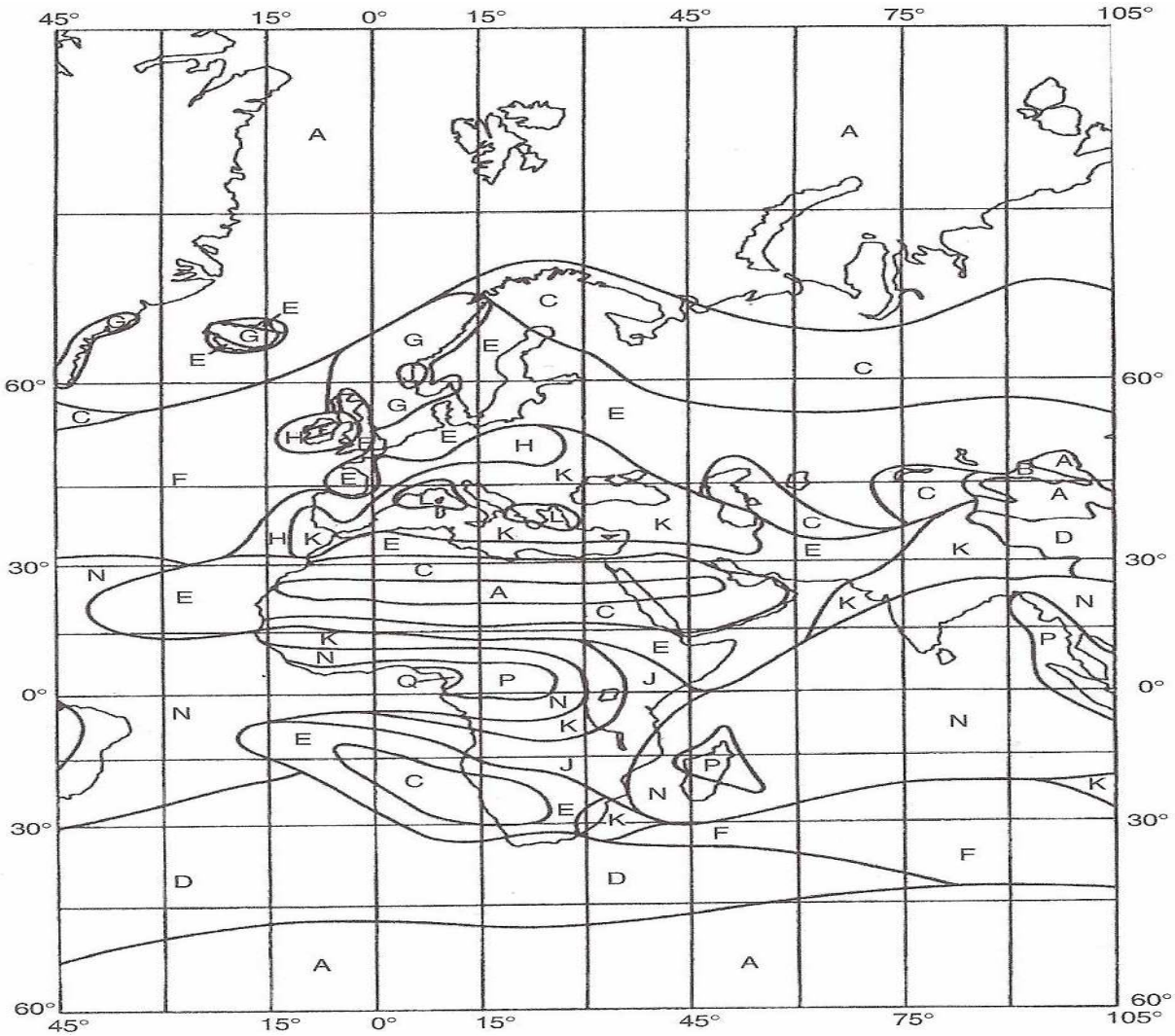

Figure 2.6: ITU-R rain map for Europe and Africa. (ITU-R P.837-3, 2001)

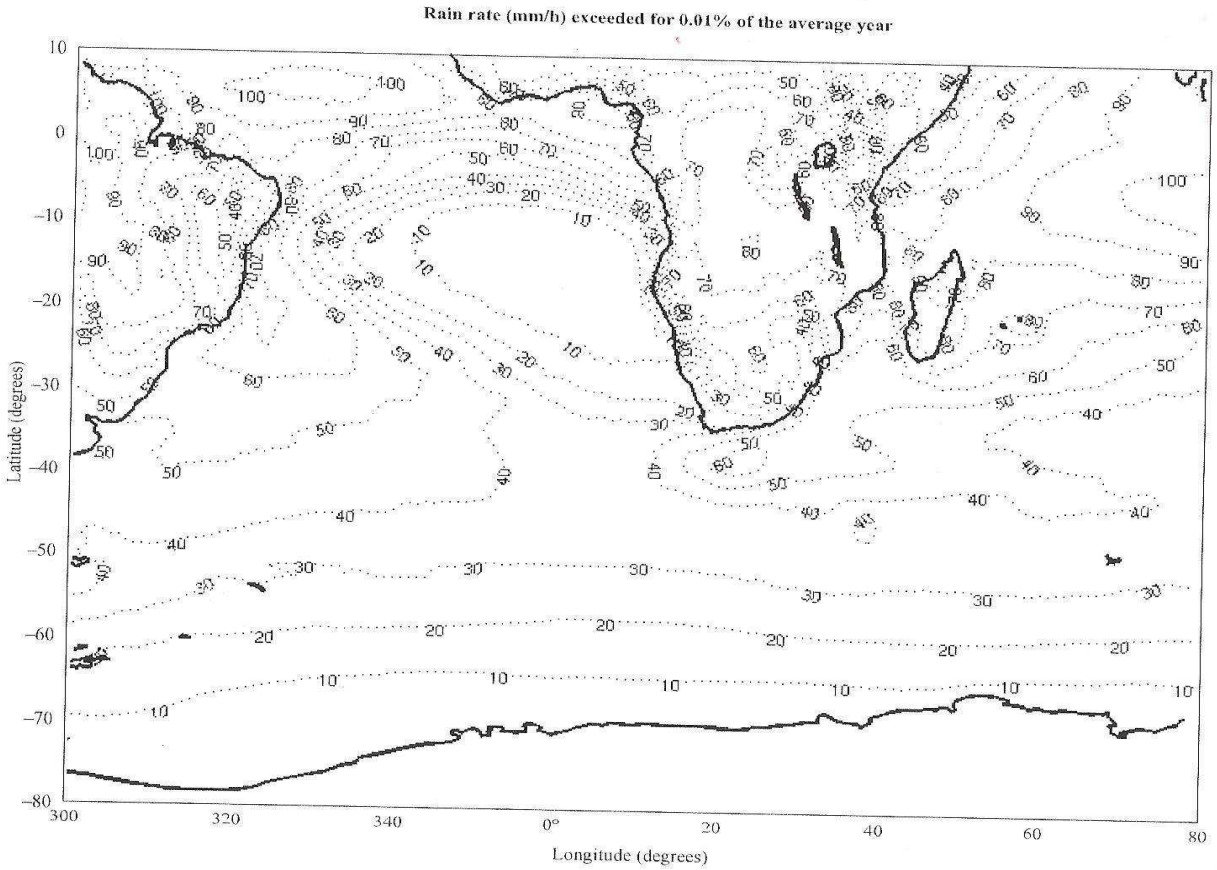

Figure 2.7: ITU-R rain map for Southern Africa. (ITU-R P.837-5, 2007)

2.5.4 Comparisons of Crane's and ITU-R's Global Rain Rate Model

Although both Crane and ITU-R global climatic models are widely known and adopted by many telecommunication companies to estimate their link budget, they are not adequate to account for seasonal, yearly or location-based variation. This dynamic variation is observed in South Africa's climatic zones as confirmed by other researchers in their localities. For example, in South America's tropical section, a large area which Crane's global model classified to be zone H, that is, it has 209.7 mm/hr rain rate at 0.01% percentage of exceedence (Crane, 1996); was classified by the ITU-R with three different rain zones of 80mm/hr, 100mm/hr and 120mm/hr (ITU-R P.837-2, 1999). This means that the difference between the rain rate estimated by the two models is about 100%.

In the case of South Africa and surrounding Islands, as shown in Figure 2.8, a similar trend of large variation is observed. In Durban, the ITU-R P.837-1 mapped rain rate to be 22 mm/hr at 0.01%, the ITU-R P.837-5 suggested 50mm/hr while Crane represented the rain rate by 46.8 mm/hr. The trend of variation between P.837-1 to P.837-5 is about 39% difference. The percentage difference between P.837-1 and Crane's suggested rain rate is 36%. In the recent enforced ITU-R P.837-5 the difference between ITU-R and Crane is 3.3% for Durban. This latter result shows a better improvement in the ITU-R global climatic rain rate model. In summary, the prime advantage of global rain rate is that even in the absence of lofty spatial resolution of point rain rate information, estimation of rain rate can be determined at a given percentage of exceedence using universal climatic information to characterize each of the regions of the globe. The disadvantages of this method are,

i) Discontinuity is observed at the boarder of the map, making them not quite useful at that point when planning link budget;

ii) They are not automatically updated and thus require human intervention.

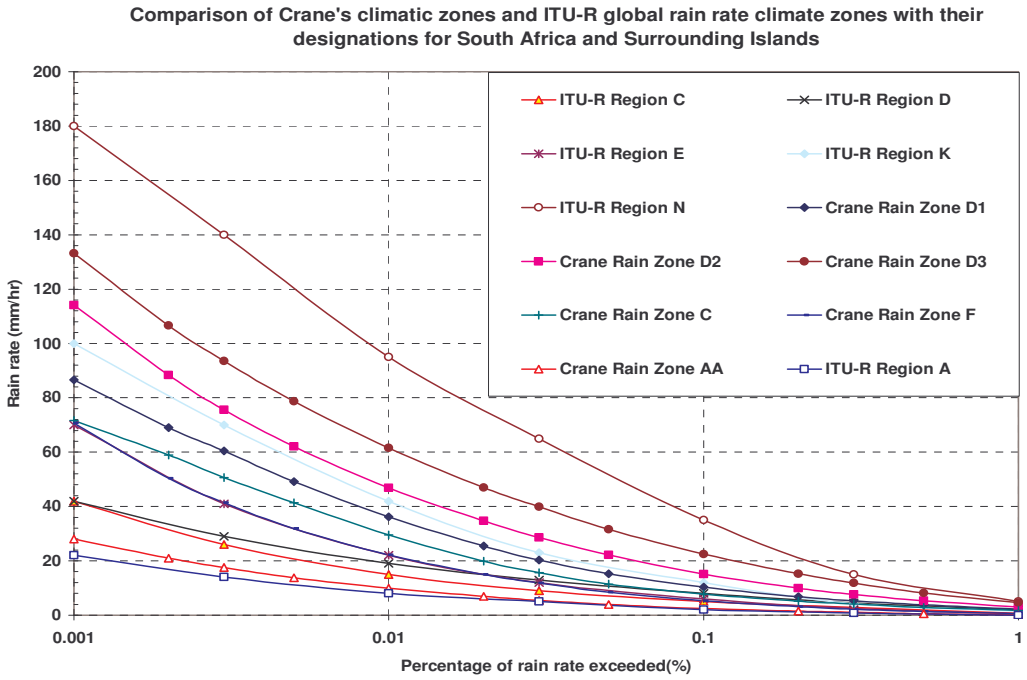

Figure 2.8: Comparison of Crane and ITU-R global climatic rain zones for South Africa and surrounding islands

2.6 Local Rain Rate Models

These rain rate models are developed from empirical equations using results of field measurements collected over a long period of time. Rain rate climatic models in this category which deserve mention include Rice-Holmberg model (Rice-Holmberg, 1973), Dutton-Dougherty model (Dutton-Dougherty, 1979 and 1984), Crane two-component model (Crane, 1996 and 2003), Moupfouma-Dereffye model (Moupfouma and Dereffye, 1982), Moupfouma model (Moupfouma, 1985), Moupfouma-Martin model (Moupfouma and Martin, 1993 and 1995), and Seeber rain rate model (Seeber,1995). In this section, the contribution made by Crane in the two-component rain rate model, Moupfouma, Moupfouma *et al*., and Seeber are considered.

2.6.1 Crane Two-Component Rain Rate Model

The Crane two-component rain rate model is a local model which provides both annual and monthly rain rate distribution predictions. The initial versions of this model discussed in Crane (1996) used five parameters determined from nonlinear fit to Crane climatic rain zones. The model combines two statistical distributions to model the rain data: exponential distribution to model small but relatively intense volume cells and lognormal distribution to model rain rate produced in debris regions surrounding the volume cells. The expression for the two-component distribution is given by (Crane 2003):

$$P(r \geq R) = P_V(r \geq R) + P_W(r \geq R) - P_{VW}(r \geq R) \tag{2.30}$$

$$P_V(r \geq R) = P_C^{e^{\frac{-R}{R_C}}} \tag{2.31}$$

$$\begin{aligned} P_W(r \geq R) &= P_D Q\left(\frac{\ln R - \ln R_D}{S_D}\right) \\ &= \frac{P_D}{\sqrt{2\pi} S_D} \int_R^\infty \exp\left[\frac{1}{2}\left(\frac{\ln(r/R_D)}{S_D}\right)^2\right]\frac{dr}{r} \end{aligned} \tag{2.32}$$

$$P_{VW}(r \geq R) = P_V(r \geq R) P_W(r \geq R) \approx 0 \tag{2.33}$$

where:

$P(r \geq R)$ = Probability that observed rain rate r exceeds specified rain rate R

$P_V(r \geq R)$ =Cumulative distribution function for volume cells

$P_W(r \geq R)$ = Cumulative distribution function for widespread rain debris

$P_{VW}(r \geq R)$ = Joint cumulative distribution function for cells and debris

r, R = Rain rates

P_C = Probability of cell

R_C = Average rain rate in cell

Q = Normal distribution function

P_D = Probability of debris

R_D = Median rain rate in debris (calculated from average of natural logarithm of rain rate)

S_D = Standard deviation of natural logarithm of rain rate

Table 2.3 gives input parameters needed to estimate both the annual and monthly rain rate distribution for any defined Crane global climatic rain rate Zone (Crane, 1996).

Table 2.3: Parameters for Crane's Two-Component Model (Crane, 1996, pp.121)

Zone	P_C	R_D	P_D	R_D	S_D
A	0.000088	3.45	2.27	0.205	1.49
B	0.023	14.3	10.8	0.178	1.44
B1	0.009	11.1	12	0.092	1.61
B2	0.023	17.5	12	0.181	1.48
C	0.03	19.8	12	0.293	1.31
D1	0.026	23.2	8.19	0.463	1.34
D2	0.031	14.3	9.27	0.475	1.48
D3	0.048	17.0	4	1.97	1.21
E	0.22	23.2	5.25	2.02	1.25
F	0.0048	8.29	6.95	0.0994	1.81
G	0.028	50.5	9.82	1.82	1.20
H	0.048	35.4	7	2.47	1.49

2.6.2 Moupfouma and Moupfouma et al Rain Rate Model

In early research by Moupfouma and Dereffye (1982), a semi-empirical model was developed based on measurements taken in the Congo with a mix of tropical and equatorial climates. The model uses three parameter inputs to estimate the cumulative distribution of rain rate. The major task achieved was to represent rainfall rate distribution by a single function for the whole range of relevant values leading to a general probability expression of the following structure:

$$P(R \geq r) = a\frac{e^{-ur}}{r^{b}} \tag{2.34}$$

Note, r has to be greater than 2mm/hr, where the parameters a, b and u are constants that depend on integration time and climate type. The constants were determined using the linear regression fitting method.

Moupfouma (Moupfouma, 1985), proposes a semi-empirical and very simple global cumulative distribution of rain rate which depends on a single parameter $R_{0.01}$. Parameter $R_{0.01}$, which is rain rate that is exceeded for 0.01% of the time in 15 different locations in the world, was used and linearly regressed with parameters a and b. The relationships are summarized in equations 2.35 and 2.36 as follows:

$$b = 8.22R_{0.01}^{-0.584} \tag{2.35}$$

Substitute equation 2.35 into 2.34 and a new general probability of cumulative distribution of rain rate is formulated as:

$$P(R \geq R_{0.01}) = a\frac{e^{-uR_{0.01}}}{R_{0.01}^{b}} = 0.01\% \tag{2.36}$$

$$a = 10^{-4} \times R_{0.01}^{b} e^{uR_{0.01}} \tag{2.37}$$

$$u = 2.5\times10^{-2} \tag{2.38}$$

Here parameter a must range between 0 and 1, and b must be greater than 0.

The Moupfouma-Martin model (Moupfouma and Martin, 1993) made a new improvement on the previous models by reviewing parameters b and u with the elimination of parameter a. It was found that u cannot be a constant value as it given in equation 2.38. Their improvement utilized the advantage of shape of cumulative distribution of rain rate which depends on the local climatic condition and geographical feature of the point of interest. It found that tropical zones are characterized by a steeper slope of rain rate distributions with low values of parameter u. For temperate zones, it is less steep with high values of parameter u. The cumulative distribution of rain rate is given by:

$$P(R \geq r) = \left(\frac{R_{0.01} + 1}{r + 1} \right)^{b} \times e^{[u \times (R_{0.01} - r)] - \log_e (10^4)} \tag{2.39}$$

Where r (mm/hr) represents the rain rate exceeded for a fraction P of the time.
Taking into account the shape of cumulative distribution of rain rate, parameter b is given by:

$$b = \left(\frac{r - R_{0.01}}{R_{0.01}} \right) \times \log_e \left(1 + \frac{r}{R_{0.01}} \right) \tag{2.40}$$

To distinguish between rain rate climates of one location from another, parameter u is given for two major zones which are temperate and tropical zones:

(a) For temperate zone:

$$u = \frac{\log_e (10^4)}{R_{0.01}} \times \frac{1}{\left[1 + \eta \times \left(\frac{r}{R_{0.01}} \right)^{\beta} \right]} \tag{2.41}$$

where $\eta = 4.56$ and $\beta = 1.03$ are positive constants.

(b) For tropical localities:

$$u = \frac{\log_e(10^4)}{R_{0.01}} \times e^{-\lambda \times (r/R_{0.01})^{\gamma}} \tag{2.42}$$

with $\lambda = 1.066$ and $\gamma = 0.214$

Moupfouma and Martin (1993) conclude that equations 2.34 through 2.42 have the probability law behaviour.

Finally, the Moupfouma-Martin model (Moupfouma and Martin,1995) complemented their initial work in (Moupfouma and Martin, 1993) by introducing a relationship whereby rain rate at different integration times is converted to one-minute equivalent at 0.01% percentage of exceedence of rain rate. The expression is given as:

$$R(1\,\text{min})_{0.01} = (R(\tau\,\text{min})_{0.01})^{\alpha} \tag{2.43a}$$

with:

$$\alpha = 0.987(\tau(\text{min}))^{0.061} \tag{2.43b}$$

provided that:

$$1\,\text{min} \le \tau \le 1\,hr \tag{2.43c}$$

2.6.3 Seeber South Africa Rain Rate Model

Seeber (1995) proposed a rain rate model for South Africa and two surrounding islands using an extreme-value theory. In summary, the theory approximated rain rate cumulative distribution based on the approached used by Lin (1976 & 1978):

$$P(R \geq r) \approx \frac{1}{2} P_0 .erfc\left[\frac{\ln r - \ln R_m}{\sqrt{2}.S_R} \right] \tag{2.44}$$

where S_R denotes standard deviation of $\ln(R)$ during the rain event, while $R_m, R, P_0, erfc(\sim)$, and $\ln(\sim)$ are median values of R during a rain event, rain rate, probability that rain will occur, the complementary error function, and natural logarithm, respectively.

The distribution parameters S_R, R_m and P_0 are represented by the following expressions:

$$S_R = \frac{P_0 .N}{\alpha} .\phi\left[\Phi^{-1}\left(1 - \frac{1}{P_0 .N} \right) \right] \tag{2.45}$$

$$R_m = \exp\left[U - S_R .\Phi^{-1}\left(1 - \frac{1}{P_0 .N} \right) \right] \tag{2.46}$$

$$M = 8760.e^{\frac{S_R^2}{2}} .R_m .P_0 \tag{2.47}$$

where $\phi(\sim)$, and $\Phi^{-1}(\sim)$ denote the normal probability density function and the inverse of the standard unit for the normal probability density function, respectively. N is the number of rain gauge integration time intervals per year with the expression:

$$N = 8760 / D \tag{2.48}$$

D is the integration time in hours.

The limitations of this model are the higher integration time of 15 minutes in which the rain rate data is collected as well as the dependence on many variables for estimating the cumulative distribution of rain rate. Furthermore, the numbers of stations used to develop the map are not enough to describe its contour boundary. The need to improve on the mentioned inadequacies in order to develop a proper and accurate contour map for South Africa and surrounding islands becomes imperative.

2.7 Review of Raindrop Size Distributions (DSD)

The estimation of the degree of signal loss as a result of electromagnetic wave interacting with rain, needs the understanding of microstructure of rain in terms of raindrop size, fall velocity of the drop, shape of raindrop, canting angle, rain drop size distribution and finally statistical modelling of its distribution pattern at different rain rates. This section deals with the review of rain microstructure characteristics. Among the issues presented are the velocity of falling raindrops, raindrop size and its shape, measurement method and the available instruments, and preview of raindrop size distribution models.

2.7.1 Terminal Velocity of Rain Droplet

The terminal velocity of a droplet is the resultant velocity produced by two different forces acting on a droplet: the upward forces (aerodynamic drag force), and the downward forces (gravitation pull). Fluid density must be low relative to the droplet density for it to fall through the air. A terminal velocity is reached by the rain drop at this condition provided the drag force is equal to gravitational force. In précis, terminal velocity of raindrop depends on the drop size, gravitational pull, and drag force which enveloped the rain droplet. The larger the drop, the faster the falling speed of the rain drop.

There are many contributors who proposed expressions to determine the terminal velocity of raindrops. Among most acknowledged ones are Gunn and Kinzer (Gunn and Kinzer 1949), Atlas-Ulbrich (Atlas et al., 1977), Atlas-Srivastava-Sekhon (Atlas et al., 1973), Sekhon- Srivastava (Sekhon et al., 1971), Van Mook (Mook, 2002).

2.7.1.1 Falling Velocity in Stagnant Air

Characteristics of rain drops can be easily evaluated if the terminal velocity of the drop is accurately measured. Many authors have contributed to experimental measurement of terminal velocity of rain drops at standard atmospheric conditions. The work done by Gunn and Kinzer (Gunn, R, et al., 1949) and Beard (Beard, 1976) had taken the front lead in the laboratory measurement of falling rain drop. Accurate observation data of falling velocity of rain was given by Gun and Kinzer in Table 8.1 of a book written by Roger and Yau (Roger R.R and Yau , M.K., 1989) and the empirical fitting of the data was done by Beard (Beard, 1976) which can be adjusted for different temperatures and pressure thresholds. A more accurate expression was proposed by Van Mook (Van Mook, 2002) as:

$$v(D) = 9.40(1 - \exp(-1.57 \times 10^3 D^{1.15})) \tag{2.49}$$

with $v(D)$ being the terminal velocity (meter per second) and D the equivalent raindrop diameter (m). The relationship expressed in equation (2.49) holds under conditions of still air at pressure of 760 mm Hg, a temperature of $20^0 C$ and a relative humidity of 50%. In the contribution of Atlas-Srivastava-Sekhon (Atlas et al., 1973) involving fitting experimental data of Gunn and Kinzer, the expression is given as:

$$v(D) = 9.65 - 10.30 \exp(-0.6D) \tag{2.50}$$

Equation (2.50) is valid for the raindrop diameter ranges between 0.1 mm through 7 mm. In a simplified power law fit of Gunn and Kinzer experimental, Atlas-Ulbrich (Atlas et al., 1977) represents terminal velocity of a raindrop as:

$$v(D) = 17.67 \times (0.1.D)^{0.6} \tag{2.51}$$

Other investigators who also presented their analytical results using power fitting were Sekhon- Srivastava (Sekhon et al., 1971), with the equation:

$$v(D) = 14.20 \times (0.1.D)^{0.5} \tag{2.52}$$

Since the terminal velocity of the falling raindrop changes and reaches a constant at a higher diameter, there is need to determine a specific relation for each defined range of diameter. The contribution of Matzler (2002) provides a solution to the limitation of equation (2.49) to (2.52) emanated as a result of shape and size of the drop. The expressions are given as follows:

$$v(D) = \begin{cases} 0 & D \le 0.03\,mm \\ 4.233.(D - 0.03) & 0.03\,mm < D \le 0.6\,mm \\ 9.65 - 10.30.\exp(-0.6\,D) & D > 0.6mm \end{cases} \tag{2.53}$$

The third expression of equation (2.53) is valid when the diameter of the drop is less than 0.6 mm. This expression has been widely used by many workers and it is similar to the one proposed by Atlas-Srivastava-Sekhon (Atlas et al., 1973). At a very low diameter, i.e. when diameter is less than 0.03 mm, the expression results in a negative value. The second expression was developed to provide solution to the negativity given by the third expression. The second expression is a linear fit of Gunn and Kinzer measurement while the first expression avoids a negative value of the second expression by assuming a constant value zero for the terminal velocity that is less than or equal to 0.03 mm.

Figure 2.9 is a graphical representation of the different raindrop terminal velocity models. It shows the laboratory measurement of Gunn and Kinzer under the standard atmospheric condition at sea level. Van Mook, Atlas-Srivastava-Sekhon and Matzler matched the measured data of Gunn-Kinzer better than the others as shown in the figure. From this, one can deduce that starting from a small diameter, the terminal velocity increases

considerably with an increase in diameter. Above 4.0 mm for Gunn-Kinzer, Van Mook, Atlas-Srivastava-Sekhon and Matzler, the steepness of the slope decreases and tends to be constant at larger diameters. A wide divergence of terminal velocity value is noticed at a diameter greater than 4.0 mm for Atlas-Ulbrich and Sekhon- Srivastava models. This observation indicates that drop-shape is not the same in all ranges of diameter.

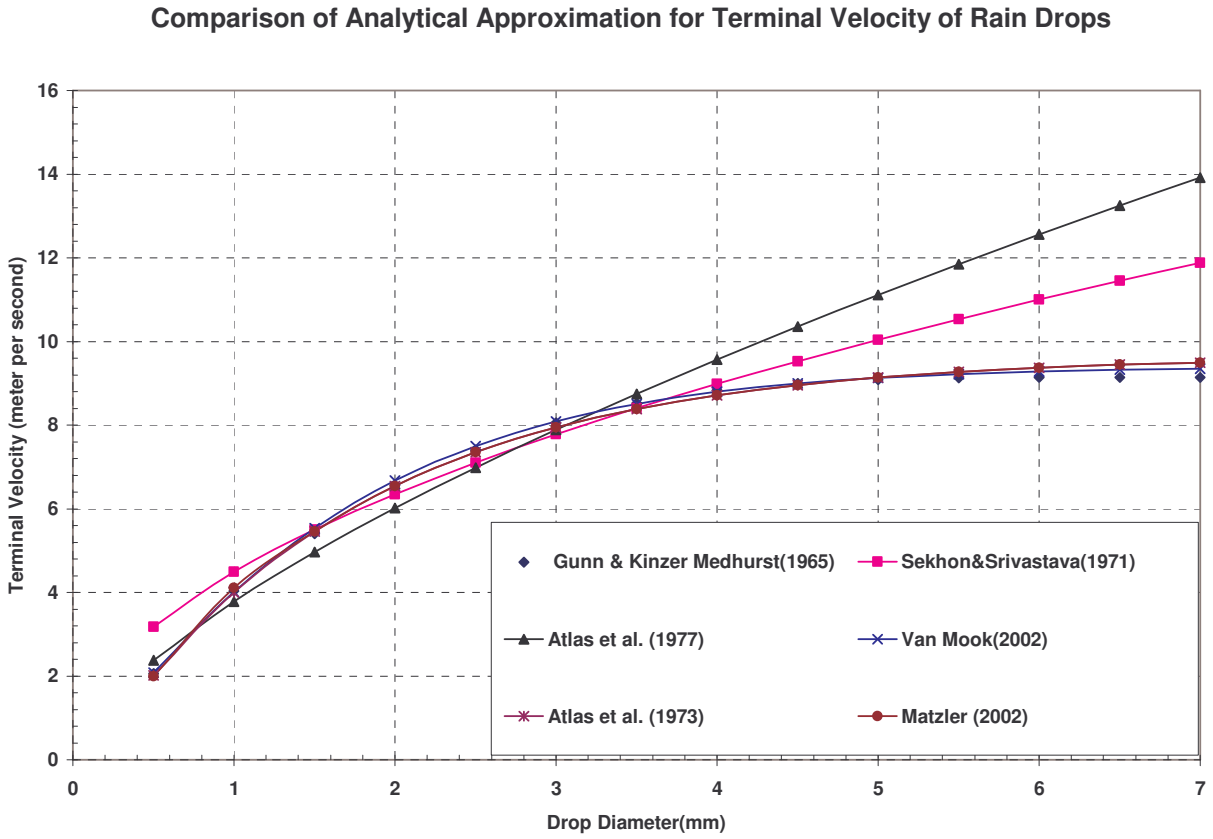

Figure 2.9: Comparison of raindrop terminal velocity models proposed by different authors.

2.7.1.2 Falling Velocity models in Non- Stagnant air

As mentioned earlier, terminal velocity of drops varies with air density and dynamic viscosity; that is why pressure, temperature and relative humidity are important. The classical Gunn-Kinzer measurement of the drop terminal velocity was conducted under the standard atmospheric conditions at sea level, with an air density of $1.23\,kg\,m^{-3}$. This

means that all the initially mentioned models are strictly valid under the same conditions as Gunn-Kinzer's. Many authors such as Foote-Toit (Foote et al., 1969), Best (Best, 1950) and Mitchell (Mitchell, 1996) made attempts to condition the Gunn-Kinzer measurements to other atmospheric conditions. In the contribution of Foote-Toit (Foote et al., 1969), the focus of their work was to determine terminal velocity at a condition other than the sea level condition. The experimental work was done with conditions of different air densities. In their efforts to arrive at a terminal velocity at arbitrary conditions, a general fit on the original data of Davies (Davies, 1969), resulted in the general terminal velocity expression:

$$V(D) = v(D)10^{Y}\left[1 + 0.0023\left(1.1 - \frac{\rho}{\rho_O}\right)(T - T_0)\right] \tag{2.54}$$

here:

$$Y = 0.43\log_{10}\left(\frac{\rho_0}{\rho}\right) - 0.4\left[\log_{10}\left(\frac{\rho_0}{\rho}\right)\right]^{2.5} \tag{2.55}$$

The parameters with subscript zero refer to $20^0 C$ and $1013\,mb$. Figure 2.10 shows several curves computed from the equations (2.54) and (2.55) at different pressure and temperature.

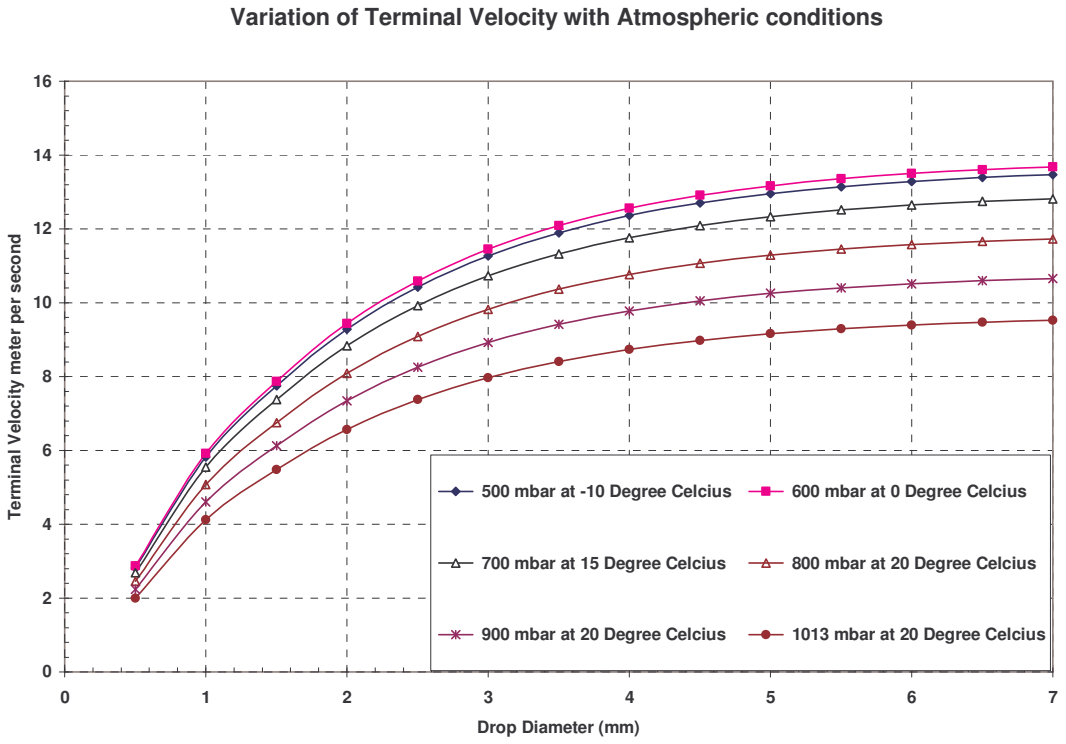

Figure 2.10: Falling velocities computed from equation (2.54 & 2.55) for indicated conditions.

Figure 2.10 shows that terminal velocity increases as the drop diameter increases. The bracket terms in equation (2.54) attempt to compensate for the dynamic of the viscosity of the fluid in space, which depends on temperature and pressure.

According to Best (Best, 1950), the contribution of C.N Davies (Davies, 1945) to the terminal velocity of a raindrop was done in two steps: by performing physical measurements of terminal velocity both at sea level and various atmospheric conditions. The general expression fitted from measurement is given by:

$$V(D,H) = A\exp bH\left(1-\exp\left[-(D/a)^n\right]\right) \qquad (2.56)$$

Equation (2.56) may be used to determine the terminal velocity of rain drops with larger diameter at any atmospheric conditions. $V(D,H)$ is a terminal velocity measured in

m/sec and it is a function of both drop diameter (D) measured in mm and height of falling drops (H) measured in km. Parameters A , b , a , and n are atmospheric dependent and are represented in Table 2.4.

Table 2.4: Designated values for Parameters A , b , a and n, taken from Best (Best,1950)

Range of D (mm)	**I.C.A.N atmosphere**				**Summer tropic atmosphere**			
	A	b	a	n	A	b	a	n
0.3 - 6.0	9.32	0.0405	1.77	1.147	9.58	0.0354	1.77	1.147
0.05-0.3	1.91	0.0290	0.316	1.754	1.88	0.0256	0.304	1.819

In Mitchell's (Mitchell, 1996) contribution, a mathematical expression was developed by combining the model of Abraham (Abraham, 1970) and Best coefficients. This model accounts for the effects of air density and mathematical concept that describes the physical process of the falling drops in a non-stagnant air. The Mitchell (Mitchell, 1996) expression to determine terminal velocity of rain drop is given as:

$$V(D) = v(D)\left(\frac{\rho}{\rho_0}\right)^{b-1} \tag{2.57}$$

where parameters ρ and ρ_0 are air density and air density at standard sea level, respectively. Coefficient $b = 0.638$ for $585 < X \le 1.56\times10^5$ and $b = 0.499$ for $1.56\times10^5 < X \le 10^8$.

2.7.2 Rain Drop Shape and Canting Angle

Raindrops are limited in size and their chance of breakup increases with an increase in the diameter. Raindrop sizes vary from a diameter 0.1 mm to 7 mm and tend to break up due to induced aerodynamic circulation of water in the drop. In the contribution of Komabayasi-Gonda-Isono (Komabayasi et al., 1964), based on their experiment, data was provided for the probability of spontaneous breakup as the raindrop diameter gets closer

to 3 mm, the ability of surface tension to hold the drop together becomes weaker, thus becoming unstable and breaks up.

Raindrop in freefall is not all spherical in shape, but changes with the diameter of the drop. At diameters less than 0.3 mm, the raindrop is assumed to be spherical in shape, while diameters ranging between 0.3 mm to 1.0 mm produce raindrop sizes that are oblate spheroid in shape. At diameters of 1.0 mm to 4.0 mm, the raindrop shape is asymmetric oblate spheroid, while beyond 4.0 mm, the bases of the drop become concave in shape and the breakup occurs.

In the contribution of Pruppacher-Beard (Pruppacher et al., 1970), a simple rain shape model was proposed for simple oblate spheroids with an equivalent radius ranging between 0.5 mm to 4.5 mm. The expression was given as:

$$r = (x / y) = 1.03 - 0.124 a_0 \quad (a_0 \text{ in mm}) \tag{2.58}$$

where $r = x / y$ is called the axis ratio, x and y are semi-minor and the semi-major axis lengths respectively. In the work of Pruppacher-Pitter (Pruppacher et al., 1971), a more realistic and universally accepted model for predicting the shape of raindrop was proposed. The model describes the shape of raindrop as a function of the angle:

$$r(\theta) = a_0 \left(1 + \sum_{n=1}^{10} c_n \cos(n\theta) \right) \tag{2.59}$$

where a_0 is the radius of the undistorted sphere, $c_0 \ldots c_9$ are deformation coefficients which depend on the radius of the drop, and θ is the elevation polar angle. The value of deformation coefficients are presented in Table 2.5.

Table 2.5: Computed deformation coefficients as a function of drop radii, from Pruppacher et al. (1971, Table 2)

Effective radius a_0 (mm)	**Deformation coefficients,** $c \times 10^5$								
	c_0	c_2	c_3	c_4	c_5	c_6	c_7	c_8	c_9
0.1711	-12	-36	-3	0	0	0	0	0	0
0.3505	-69	-208	-27	0	1	0	0	0	0
0.433	-181	-543	-97	-3	5	-2	0	0	0
0.532	-314	-939	-189	-12	10	-1	0	-1	0
0.62	-447	-1334	-300	-27	17	-2	1	-1	1
1.10	-1431	-4259	-1105	-173	632	25	3	-12	-4
1.40	-2344	-6977	-1843	-288	101	42	5	-19	-7
1.50	-2670	-7948	-2214	-330	115	48	5	-22	-8
1.80	-3659	-10889	-2963	-462	156	65	8	-30	-11
2.0	-4296	-12783	-3539	-551	182	77	9	-35	-13
2.50	-5734	-17053	-4959	-775	237	102	12	-47	-18
2.90	-6822	-20280	-6166	-971	274	122	14	-55	-21
3.00	-7089	-21070	-6482	-1023	283	127	15	-57	-22
3.50	-8380	-24888	-8151	-1310	318	149	18	-67	-25
4.0	-9763	-28966	-10143	-1677	346	173	21	-76	-29

Canting angle of raindrop is a consequence of non-spherical shape of raindrops. Non spherical raindrops have preferred axial orientation angles different from the vertical; as such they tend to cant away from the vertical direction. This is due to the various aerodynamic forces acting on them. Saunders (Saunders, 1971), made the first measurement of raindrop angle and shows that the distributions are almost normal, with a mean canting angle of $+7^0$. About 40% of the drops were found to have positive angle greater than 15^0 while 25% confirmed to have negative angle of less than -15^0.

Brussaard (Brussaard, 1976) proposed a physical model of drop canting in which it was assumed that the axes of symmetry of the raindrop are always parallel to the direction of air flow around the drop. The direction of air flow is determined by the vector addition of two orthogonal flow components which are vertical components due to the fall of

raindrops and the horizontal component due to vertical gradient of the horizontal wind speed. Knowledge of both raindrop shape and its canting angle are responsible for variations occurring in cross polarization of discrimination measurement. Another contribution to the knowledge of raindrops canting angle is observed as a crosstalk between two orthogonally polarized communication channels operating at the same frequency. Canting angles are either assumed to be constant for all the raindrops on a path, termed a deterministic model, or assumed to be uniformly distributed with a mean value and standard deviation, thus ensuring that the canting angles are the same in all raindrops at each location. This model is termed the stochastic model. The application of raindrop shape is not limited to the above propagation phenomenon only, but extends to the calculation of the scattering and extinction properties of rain in the presence of propagating electromagnetic wave.

2.7.3 Dropsize Distributions

In order to accurately estimate specific rain attenuation at a frequency above 10 GHz, it is necessary to know the raindrop size distribution for a given rain rate. Raindrop size distribution is a highly variable quantity, showing both spatial and temporal variations of microphysics of rain formation. It is observed that raindrop size distribution varies with respect to location, season, and year. Actual raindrops do not maintain actual drop shape and size, rather, a distribution of size and shapes which depends on the rate of at which rain is falling. However, theoretical calculation is often based on the best available measurements of the dropsize distribution. Many contributors have used different methods and principles to propose empirical relations to describe the best raindrop size distribution in different climatic regions. In this section we present a brief description of the methods used to obtaining dropsize distribution, as well as the mathematical fundamentals of raindrop size distributions, and raindrop size distribution models.

2.7.3.1 Review of existing raindrop approaches

The term Raindrop size distribution (DSD) is defined as the number of raindrops at a given diameter per unit volume. The best-known raindrop size distribution model is that of Laws and Parsons (Laws and Parsons, 1943), which was recommended by the

International Telecommunication Union (ITU-R) for the calculation of specific attenuation due to rain in the temperate region. This model was developed in an experiment using a pan containing fine flour which was exposed to rain, with the size of pellets produced by raindrops being measured, and corresponding size distributions were then inferred. Raindrop size distribution on the ground was represented from volume distribution, with a fall velocity, *v(a)*, as:

$$N(D)da = \frac{10^3 R\beta(m)da}{4.8\pi a^3 v(a)} m^{-3} \tag{2.60}$$

where $\beta(m)da$ represents the volume fraction percentage, a is the radius of the raindrop, and da represents the size interval from $a - \frac{da}{2}$ to $a + \frac{da}{2}$, and R stands for rain rate in mm/hr. Figure 2.11 shows further contributions, where a relationship was found between fractions of the total rain-water volume against the respective diameter of the drop at different rain rates. It also shows the volume fraction density $M(D)dD$ against drops diameter. The plot shows that the majority of volume fraction density falls within the small diameter and lower rain rate while at higher rain rate, lower volume fraction is recoded. Though volume fraction can be converted to dropsize distribution by the relation in equation (2.60), note $\beta(m)da$ is equivalent to $M(D)dD$ .This distribution has been found to be suitable for temperate regions.

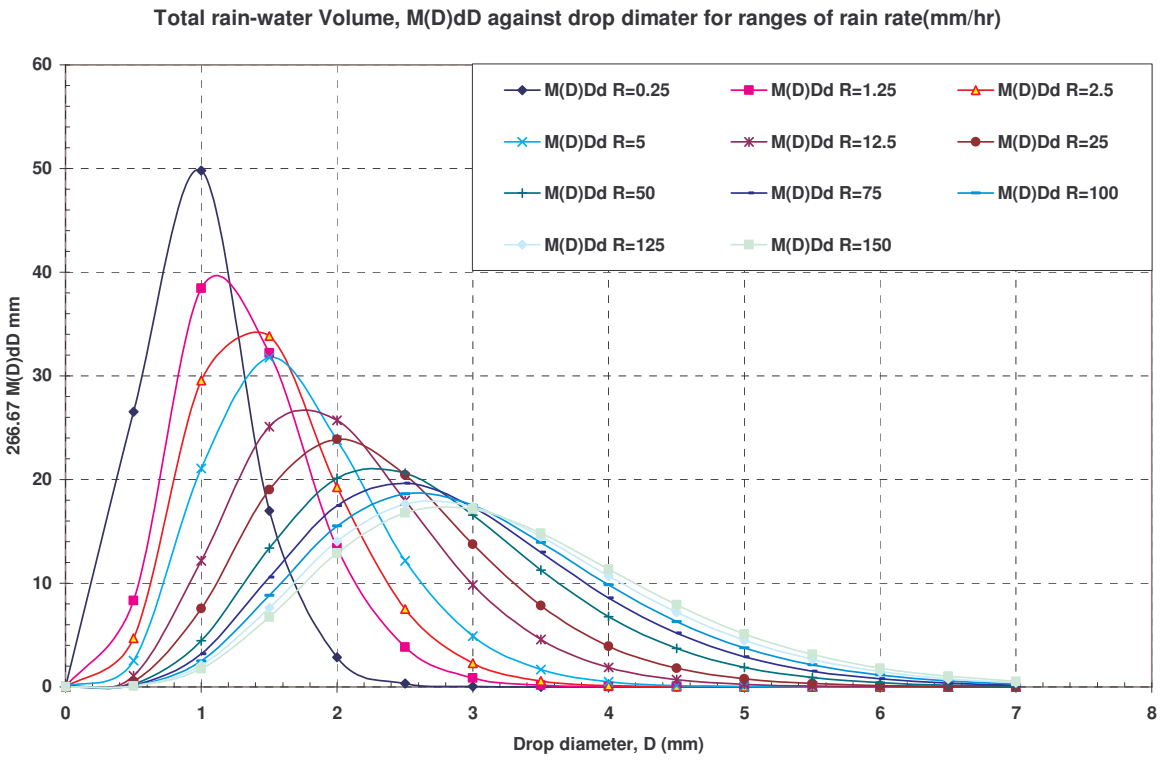

Figure 2.11: Total rain-water volume against its diameter.

In 1948, Marshall and Palmer (Marshall-Palmer, 1948) determined raindrop distribution density $N(D)$ by analytical method, and further improved it by extending the method to other types of rain as presented by Joss et al (Joss et al., 1969). Both suggested a negative exponential model given as expressed in equation 2.61:

$$N(D) = N_O \exp(-\Lambda D) \tag{2.61}$$

where N_O is a constant given as $8000\, mm^{-1} m^{-3}$; Λ is a constant that increases with an increase in rain rate, $\Lambda = 4.1R^{-0.21}\, mm^{-1}$. The Marshall and Palmer model is very close when compared with Law and Parsons Model, especially when applied to widespread type of rain in temperate region (Hall and Barclay, 1989). A noticeable disadvantage of this model is that it overestimates small raindrops below the diameter of about $1.5\, mm$ because of its exponential increase when D tends toward zero. Thus, the use of the

distribution will lead to higher attenuation value than the actual attenuation at frequencies higher than 30 GHz, especially outside the temperate region (Ajewole et al., 1999). Deirmendjian (Deirmendjian, 1969) modified the Marshall-Palmer's work by introducing a modified gamma distribution to describe raindrop size distribution. This model corrects the exponential increase of raindrop number density as D tends toward zero. It is commonly expressed as:

$$N(D) = N_O D^m \exp(-\Lambda D^\beta) \tag{2.62}$$

where N_O, m, β and Λ are constants which are positive and real. The greatest difficulty in the use of this distribution model is in obtaining experimentally the four constants involved in equation (2.62). In addition, the model has a tendency of cutting off both large and small ends of raindrop size distributions for values of m in the range 3 to 5 mm.

In recent years, the introduction of advanced measurement tools has improved modelling techniques and thus reliable models have been developed. In the work of Joss-Waldvogel (Joss et al., 1967), they used the distrometer, an electronic device employed to measure both size and fall velocity of a raindrop. It uses an electromechanical sensor that transforms the momentum of falling raindrops on a diaphragm into an electrical pulse. Joss et al (1967) measured raindrop size distributions with a distrometer at Lorcarno, Switzerland, and found that the distribution varied considerably for different types of rainfall. They obtained the parameters of the average exponential distributions for different types of rain. Their work represents the first attempt to model raindrop size distribution with respect to the variation of raindrop size within each rain storm (Joss et al., 1967). They then classified rainfall into three main classes: drizzle, widespread and thunderstorm. The "drizzle" distribution is allied with very light widespread rain composed mostly of small drops, while the "thunderstorm" distribution characterizes the drop-size distribution for convective rain with relatively high concentration of large drops. In their conclusion, they used Equation 2.62 with the constants values as shown in the Table 2.6 for different types of rain.

Table 2.6: Constant values for N_0 and Λ for different type of rain using equation 2.62

Type of rain	N_0	Λ
Drizzle(J-D)	30000	$5.7\,R^{-0.21}$
Widespread(J-W)	7000	$4.1\,R^{-0.21}$
Thunderstorm(J-T)	1400	$3.0\,R^{-0.21}$

2.7.3.2 Regional raindrop size distribution models

Due to the inadequacies of the negative exponential model as well as the modified gamma distribution in describing the small diameter drops, a number of investigators have studied the lognormal distribution, which is expressed as:

$$N(D) = \frac{N_T}{\sigma D\sqrt{2\pi}} \exp\left[-\frac{1}{2}\left\{ \frac{\ln(D) - \mu}{\sigma} \right\}^2 \right] \tag{2.63}$$

where $N(D)$ is the number of drops per unit volume per diameter interval, μ is the mean of $\ln(D)$, σ^2 is the standard deviation and N_T depends on climate, geographical location of measurement and rainfall type. Ajayi and Olsen (Ajayi et al., 1985) employed the lognormal distribution with a method of moment regression to produce a good theoretical fit to the measured data at Ile-Ife Nigeria. This was developed mainly for the tropical rainfall. The model is expressed by equation (2.63), with the three parameters related to rain rates as:

$$N_T = a_0 R^{b_0} \tag{2.64}$$

$$\mu = A_\mu + B_\mu \ln R \tag{2.65}$$

$$\sigma^2 = A_\sigma + B_\sigma \ln R \tag{2.66}$$

where a_o, b_o, A_μ, B_μ, A_σ, and B_σ are coefficients of moment regression (Ajayi et al., 1985).

Adimula and Ajayi (Adimula et al., 1996) extended the results further by making measurements for a period of three years at two more locations in Nigeria. The distributions obtained were confined within four classes of rain. The authors averaged their results and optimized them to obtain general lognormal distribution constants with respect to rain rate, namely: σ^2, μ, and N_T for the four rain types. The values of the coefficient of regression are given in Table 2.7 below.

Table 2.7: Coefficients of lognormal distribution for tropical region (Adimula et al., 1996)

Rain type	N_T		μ		σ^2	
	a_0	b_0	A_μ	B_μ	A_σ	B_σ
Drizzle	718	0.399	-0.505	0.128	0.038	0.013
Widespread	264	0.232	-0.473	0.174	0.161	0.018
Shower	137	0.370	-0.414	0.234	0.223	-0.034
Thunderstorm	63	0.491	-0.178	0.195	0.209	-0.030

In their contribution, Sekine and Lind (Sekine and Lind, 1982) proposed the Weibull raindrop size distribution model to estimate rain attenuation at centimeter, millimeter and sub-millimeter waves. Their expression is given as:

$$N(D) = N_0 \frac{\eta}{\sigma}\left(\frac{D}{\sigma}\right)^{\eta-1} \exp\left\{-\left(\frac{D}{\sigma}\right)^{\eta}\right\} \tag{2.67}$$

where D is the diameter in millimeters and η and σ are functions of the precipitation rate R in millimeters per hour. Jiang-Sano-Sekine (Jiang et al., 1997) used the Weibull distribution and arrived at constants $N_0 = 1000 m^{-3}$, $\eta = 0.95 R^{0.14}$ and $\sigma = 0.26 R^{0.42} mm.$ Considering the dependence of the relationship on the raindrop size distribution and the possible variability of the drop size distribution with climate, a comparison is done with other regions of the world and the expressions are summarized in Table 2.8 below.

Table 2.8: The raindrop size distribution models for different regions

Region	Model Type	Raindrop size distribution model
Japan (Manabe et al.,1987)	Exponential distribution	$N(D) = 17300R^{-0.16}\exp(-5.11R^{-0.253}D)$
Europe (Marshal-Palmer,1948)	Marshall and Palmer (exponential model)	$N(D) = N_0\exp(-\Lambda D)$ $\Lambda = 4.1R^{-0.21}$ $N = 8000$
Singapore (Timothy et al., 2002)	Gamma distribution	$N(D) = N_0 D^m \exp(-\Lambda D)$ $m = 3,$ $N_0 = 31444.3R^{0.244}$, $\Lambda = 5.753R^{0.032}$
Europe (Jiang et al., 1997)	Gamma distribution (Atlas and Ulbrich).	$N(D) = N_0 D^2 \exp(-\Lambda D)$ $N_0 = 64500R^{-0.5}$ $\Lambda = 7.09R^{-0.27}$

2.7.3.3 Mathematics of raindrop size distribution models

Specific rain attenuation γ measured in dB/km due to precipitation can be calculated using classical Mie scattering theory. This approach is based on the knowledge of the terminal velocity, refractive index of water, temperature and as well as drop size distribution. The expression is given as:

$$\gamma = 4.343\times10^3 \int_0^\infty Q_t(D)N_V(D)dD \quad (dB/km) \tag{2.68}$$

where $Q_t(D)$ is the extinction cross-section, determined theoretically from the classical scattering theory developed by Mie for frequencies above 3 GHz or the Raleigh approximation for frequencies between 1 and 3 GHz:

$$Q_T(D) = Q_s(D) + Q_A(D) \tag{2.69}$$

where Q_s and Q_A are the scattering and absorption cross-sections, respectively. $Q_t(D)$ is a function of drop size diameter, wavelength and complex refractive index *m* of the water

drops. $N_V(D)\,dD$ is the mean number density of raindrops with equivalent diameter D in the interval dD which is not measured by a distrometer but inferred from flux base measurement sof raindrop by distrometer. The parameter measured by the distrometer, denoted as $N_A(D)$, is related to desire mean number density of raindrops as:

$$N_A(D) = v(D)N_V(D) \tag{2.70}$$

where $v(D)$ is terminal velocity of the falling raindrop. The total number of raindrops per unit volume, $N_T(D)$, is given by the zero-order moment of the desired mean number of raindrops density $N_V(D)$. The expression is given by:

$$N_T(D,R) = \int_0^\infty N_V(D,R)dD \tag{2.71}$$

Considering the third-order moment of the desired mean number of raindrops density, $N_V(D)$ will result in the volume fraction $R_V(D)$ of rain-water in stagnant air. The expression is given as:

$$R_V(D) = \frac{\pi}{6}\int_0^\infty D^3 N_V(D,R)dD \tag{2.72}$$

To determine the total volume of rain-water $R_A(D)$ falling on the horizontal surface of unit area per unit time at third-order moment of $N_A(D)$ results in the expression:

$$R_A(D) = \frac{\pi}{6}\int_0^\infty D^3 N_V(D,R)v(D)dD \tag{2.73}$$

where $R_A(D)$ is measured in m/s and D in meters. To translate these units to the convectional unit of rain rate (mm/hr) and drop diameter (mm), equation 2.73 becomes:

$$R_N(D) = 6\pi \times 10^{-4} \int_0^{\infty} D^3 N_V(D,R) v(D) dD \tag{2.74a}$$

Equation 2.27 can be re-written as:

$$R_N \approx 6\pi \times 10^{-4} \sum D^3 N_V(D) V(D) \Delta D \tag{2.74b}$$

In order to present dropsize particle from different situation of rain rate, a process of normalization or self-consistency (SC) is employed. It can be summarized under the expression:

$$SC = R / R_N \tag{2.75}$$

When $SC = 1$, it is self-consistent, otherwise there is need of utilizing the scale factor of equation 2.75 with the mean number of raindrops with density $N_V(D)$ with the normalized dropsize distribution given as:

$$N_N(D) = SC \times N_V(D) \tag{2.76}$$

In the next chapter, the introduction of statistical distribution process starts with rain rate integration time. The term integration time is the sampling time of rain rate with measuring equipment. In order to estimate rain attenuation in terrestrial and satellite links, rain rate cumulative distribution must be calculated at one-minute integration time. Further, we need to investigate the existing physical, empirical and analytical conversion models and adapt them for South Africa and surrounding islands. Finally, we intend to propose a conversion method, since the initial rain rate models are based on the higher integration time. The proposed conversion models will allow the conversion of rain rate from five-minute integration time to one-minute equivalents.

Chapter Three

Rain Rate Integration Time

3.0 Introduction

The super and extremely high frequency communications are of great interest to service providers and system designers today because of the wide bandwidths available on these frequency ranges. Such wide bandwidths are valuable in supporting applications such as Local Multipoint Distribution Services (LMDS), Microwave Video Distribution Services (MVD), etc. However, signal transmission at these bands is impaired by various meteorological conditions, which impose severe limitations on the line-of-sight (LOS) radio systems. Absorption and scattering of signal energy by rain is a major problem at these bands.

This chapter is concerned with the investigation of the statistical rainfall data collected over 10 years with integration time of five minutes in nine provinces in South Africa and the surrounding islands of Marion Island and Gough Island, using automated rain gauges, and less than a year's data of one-minute rain rate data collected using a distrometer. The principal aim of the chapter is to investigate the best integration conversion methods, and hybrid them to come up with conversion expression. The results are then compared with the existing models such as the recommended International Telecommunication Union (ITU-R 837-5) standard, and others. The results are mapped into their respective geographical local using Köppen climatic region classification method.

3.1 Initial Attempts in Converting Rain rate from higher Integration Times to One-minute Integration

In a study published by Fashuyi et al (Fashuyi *et al*, 2006), the empirical method of power law was applied in converting rain rate from 60-minute integration time to one-minute integration time. While conversion factors a and b were determined based on the available one year one-minute rain rate data for Durban, the one-minute cumulative

distributions of rain rate of twelve locations were then presented using conversion factor coefficients of Durban.

3.1.1. Tropical Rain-Rate Campaigns

In a measurement campaign spearheaded by URSI, annual cumulative distribution of rain rate has been obtained at several locations in the tropical and sub-tropical regions in the world. In India, Sakar et al produced the reference data manual for rain rate distribution over the Indian sub-continent, making use of the heavy rainfall data of 5 minutes and 15 minutes available at 35 different geographical regions in India (Ajayi et al., 1996). The rapid response rain gauges with 10-second integration time were used to measure the rain rate in Delhi, Shillong, Calcutta, Bombay and Tirupati. The resulting rain rates at 0.01% probability (denoted as $R_{0.01}$) are 130 mm/h for Shillong, 128 mm/h for Calcutta, 130 mm/h for Bombay, 120mm/h for New Delhi, and 80 mm/h for Tirupati (Ajayi et al., 1996).

At the same time, a rain rate measurement campaign in Africa in 1994 covered Cameroun, Nigeria and Kenya. Although the total rain accumulation was highest in Doula (Cameroun), the rain rate exceeded 0.01% of the time were comparable at Doula and Ile-Ife in Nigeria. The rainfall cumulative distributions in Doula and Nairobi in Kenya showed that the rain climate was not well described by the ITU-R predictive distributions (Ajayi et al., 1996). Ajayi and Ezekpo used the Rice-Holmberg technique to predict short integration time (one-minute) rainfall rate from long-term precipitation data from 37 stations in Nigeria over a period of 30 years (Ajayi et al., 1996). Adimula et al compared the cumulative rainfall rate distribution obtained at Ilorin and Ile-Ife (Nigeria), Belem (Brazil), and Brazzaville (Congo) with the ITU-R rainfall rate distribution, while measurements in Brazil showed that ITU-R recommended distribution overestimate the measured distributions for all sites (Ajayi et al., 1996).

Segal has defined a conversion factor, $\rho_\tau(P)$ for converting data obtained with a gauge having an integration time of τ minutes to equivalent one-minute statistics, as follows (Segal, 1986):

$$\rho_\tau(P) = R_1(P) / R_\tau(P) \tag{3.1}$$

where R_1 and R_τ are the rainfall rate exceeded, with equal probability P, for the two integration times. The factor $\rho_\tau(P)$ is also given by the power law (Segal, 1986):

$$\rho_\tau(P) = a.P^b \tag{3.2}$$

over the range $0.001\% \le P \le 0.03\%$, with a and b being constants that depend on the climatic zone. Watson et al., (1981) considered the conversion factors C_R and C_e for rain gauge integration times in the range of 10 s to 60 min, where:

$$\begin{aligned} C_e(R) &= e_T / e_\tau \\ C_R(t) &= R_T / R_\tau \end{aligned} \tag{3.3}$$

and where C_e refers to the ratio of the exceedances (with the same probability P) for a given rain rate R measured using gauges with integration times T and τ; $C_R(t)$ refers to the ratio of rain rates exceeded for a given percentage of time t as measured by rain gauges with integration times T and τ. Here, $C_R(t)$ depends on the percentage of time considered (Ajayi et al., 1984, Watson et al., 1981). The conversion factors C_R and C_e obtained at Ile-Ife in Nigeria for the measurement period September 1979 to December 1981 using the rain rate data obtained from a fast response rain gauge with an integration time of 10 seconds are based on Watson's method (Watson et al., 1981). It has also been found that a power law relationship exists between the equiprobable rain rates of two integration times. The power law relationship is given by (Ajayi et al., 1984):

$$R_\tau = aR_T^b \tag{3.4}$$

where R is the rain rate, τ is the integration time at which the rain rate is required, and T the integration time at which the rain rate is available. Flavin (Flavin, 1981) also

sought a direct and universal expression between one-minute and five-minute rainfall rates by examining the cumulative distributions for four locations in Europe, four in North America and five in Australia. From a scatter plot of resulting data points a simple power-law fit was produced giving:

$$R_1 = u.R_5^v \tag{3.5}$$

where R_1 and R_5 are the one-minute and five-minute rainfall rates exceeded with equal probability, u and v are the regression coefficients[1] (Segal, 1986). The results obtained between one-minute and five-minute and 6-minute integration times at Ile-Ife have been compared with the results obtained by Flavin (Flavin, 1981), and the following relationships were established (Ajayi et al., 1984):

$$\begin{aligned} R_1 &= 0.991 R_5^{1.098} \\ R_1 &= 0.990 R_6^{1.054} \end{aligned} \tag{3.6}$$

where R_1 is the one-minute rain rate, R_5 is the equiprobable five-minute rain rate value, and R_6 is the equiprobable 6-minute value. The coefficient a may not be very dependent on climate, while the dependence of b on climate may require further investigation (Ajayi et al., 1983). From the 5-year rain rate data measured with an integration time of 60 minutes for 12 different locations in South Africa, the Segal and the Ajayi approaches were used to determine the conversion factor to convert from 60-minute integration time to an effective one-minute integration time. Therefore, the conversion factor obtained is based on the Segal power law relationship of equation (3.2). This results in a linear scatter plot of data points, in which a simple power law fits as shown in Figure 3.1 below:

[1] Although all of the data were merged into a single scatter plot, the integration time for the stations in Australia was actually 6 rather than 5 min. This discrepancy is believed to be negligible in comparison with the normal geographic and statistical variability [Segal, 1986]

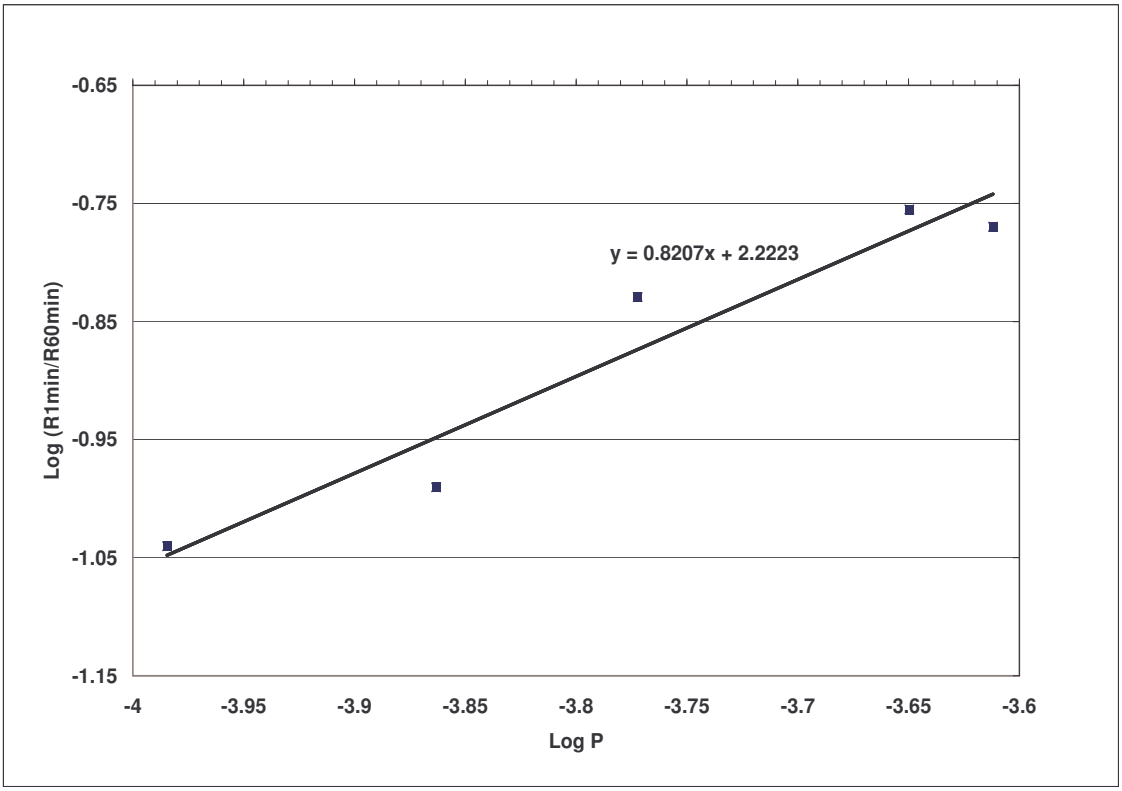

Figure 3.1. Determination of coefficients a and b for Durban, South Africa

$$R_{1\,\min} = 9.228 R_{60\,\min}^{0.8207} \tag{3.7}$$

Thus, the Durban coefficients of a and b in equation (3.7) are used to convert other 60-minute rain rate data from other locations in South Africa to an effective one-minute integration time (Ajayi et al., 1984). The results obtained between one-minute and 60-minute integration time rain rates in Durban from January 2000 to December 2004 were compared with those obtained by Ajayi and Ofoche (Ajayi et al., 1984). The latter examined the effective one-minute , 2-minute, five-minute , 10-minute, and 20-minute cumulative distributions of rain rate for Ile-Ife, Nigeria from September 1979 to December 1981. Table 3.1 above shows a comparison between the Durban coefficient of a and b and coefficients obtained for Ile-Ife in (Ajayi et al., 1984). In order to compare the values, linear extrapolation gives $a = 11.565$ for Ile-Ife for 60-minute integration time, while a logarithmic extrapolation gives $b = 0.7982$.

Table 3.1: Coefficients for $R_\tau = aR_T^b$ for $\tau = 1\text{min}$ (based on (Ajayi et al., 1984) and measurements)

Integration time T(min)		**Value of Coefficient**	
Station	**T**	*a*	*b*
Ile-Ife	2	0.872	1.055
Ile-Ife	5	0.991	1.098
Ile-Ife	10	1.797	1.016
Ile-Ife	20	4.311	0.853
Ile-Ife	60	11.565	0.798
Durban	60	9.228	0.8207

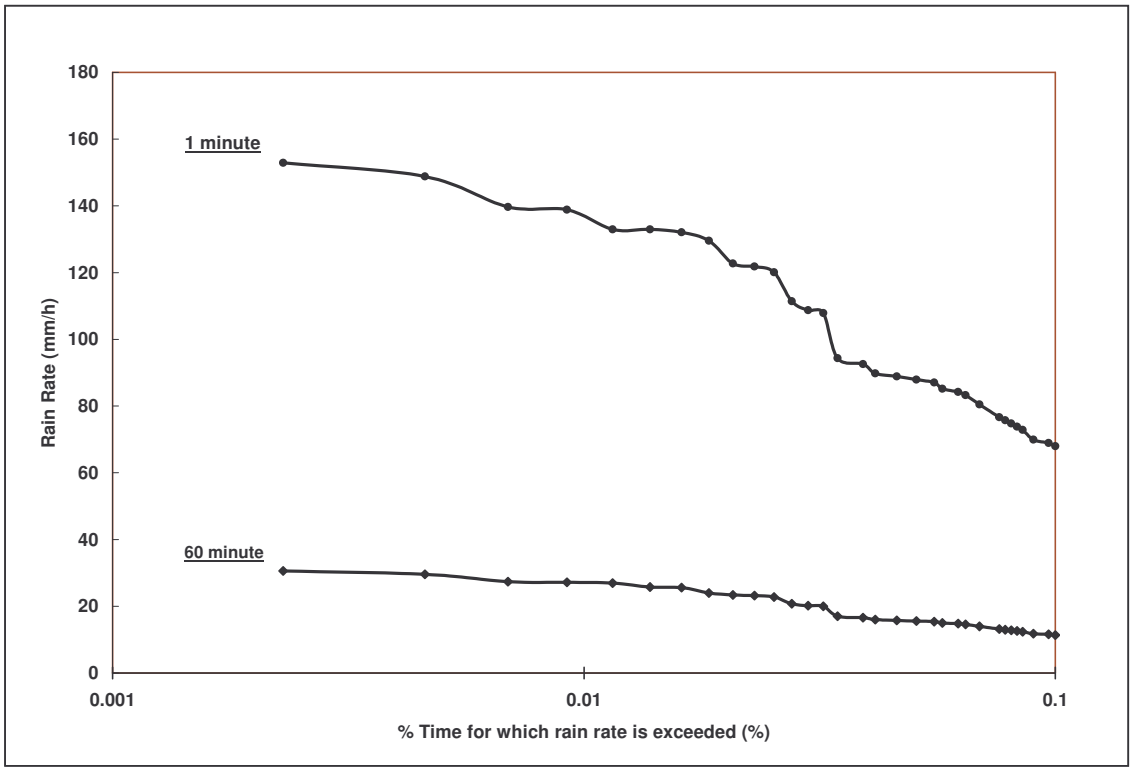

Figure 3.2. Cumulative Distribution of Rain-rate for Durban for one-minute and 60-minute integration times

These are quite close to the Durban values in (3.7). Figure 3.2 shows the values of equiprobable rain rate for integration time of 1 minute and 60 minutes for occurrence

probability of 0.1% or less. The figure confirms the power law relationship between equiprobable rain rates of two different integration times. It shows that the longer integration time hides the probable rainfall peaks, during which the highest outages take place. Therefore outage probabilities and fade margins would be inaccurately determined if the 60-minute integration data is used. In Mulangu, Owolawi and Afullo (2007), the cumulative distribution identity method was suggested by the authors in order to determine conversion factors for the available daily rainfall data for Botswana.

3.1.2 Conversion of five-minute to one-minute rain rate in Surrounding Islands

An improved approach was introduced by Owolawi, Afullo and Malinga (Owolawi et al, 2009) in which climatic parameters such as average annual total rainfall, highest monthly precipitation observed over thirty years, average number of thunderstorm days were used to determine an estimated cumulative distribution of one-minute for the studied sites. A linear relationship was proposed, and conversion coefficients were consequently determined. This sub-section presents the approach in a concise manner.

In order to convert rainfall rate from any higher available collecting time (>1 minute) to ITU-R accepted integration time of one minute, a simple equiprobable approach is employed. The equiprobable approach refers to rainfall rate or probability of exceedence at equal time probability or rainfall rate. The equiprobable approach can be employed in two ways:

i. By finding relationship of time probability between one-minute and known integration time distribution for the same rainfall rate (Lee et al, 2001),
ii. By obtaining the relationship between one-minute and unknown integration time rainfall rates for equal percentage of exceedence (Segal, 1986; Burgueno, 1988).

In this section, the latter method is used and the relationship between the rainfall rates at estimated one-minute with corresponding rainfall rate distribution at equal percentage of exceedence is given below:

Table 3.2: Coefficients of equation (2.22) and (3.8)

Site	M	M_m	D_{th}	φ	ψ	R^2
Gough Island	3163	600	7	1.3231	-0.4394	0.9335
Marion Island	2399	460	10	1.2333	-1.4414	0.9673
Durban	1015	401.6	40	2.6474	1.7811	0.9756
Cape Town	520	225	20	0.9796	5.3765	0.9666
Pretoria	673	490.1	20	1.9793	5.4599	0.9806

$$R_{1\,\min} = \varphi R_{\tau} + \psi \tag{3.8}$$

τ is the integration time at which rainfall rate data is collected, while the coefficients φ and ψ at five-minute integration time are shown in Table 3.2. In the case of none-rain event, the rainfall rate values should remain zero. Figures 3.3 to 3.4 show the graphical relationship between estimated one-minute and five-minute rainfall rate for the Islands.

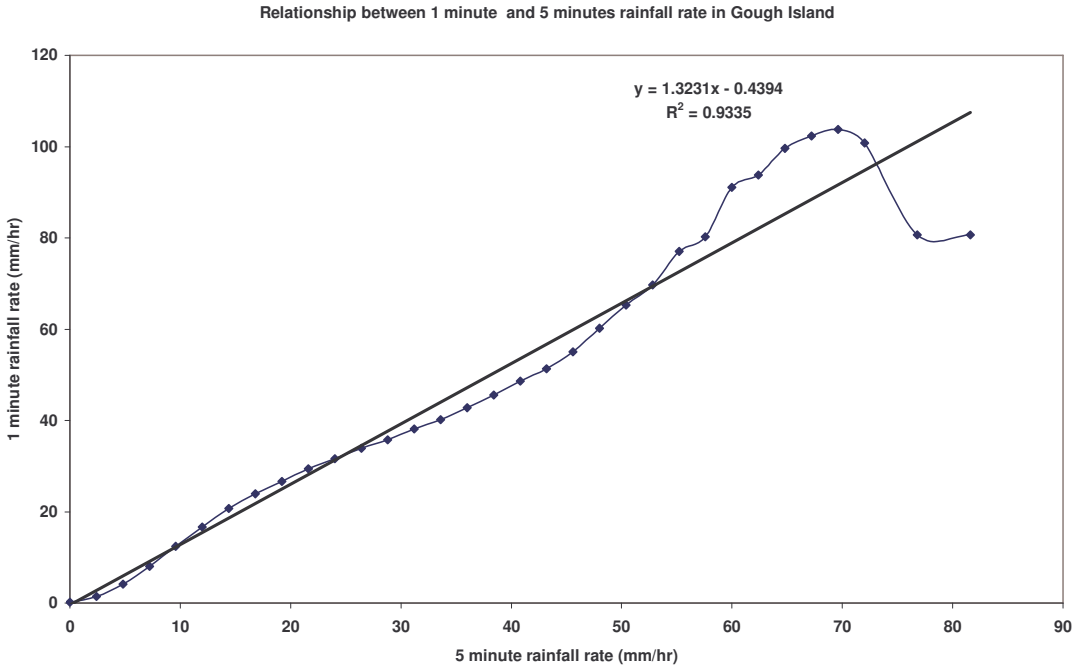

Figure 3.3: Relationship between 1-min and 5-min rainfall rate in Gough Island

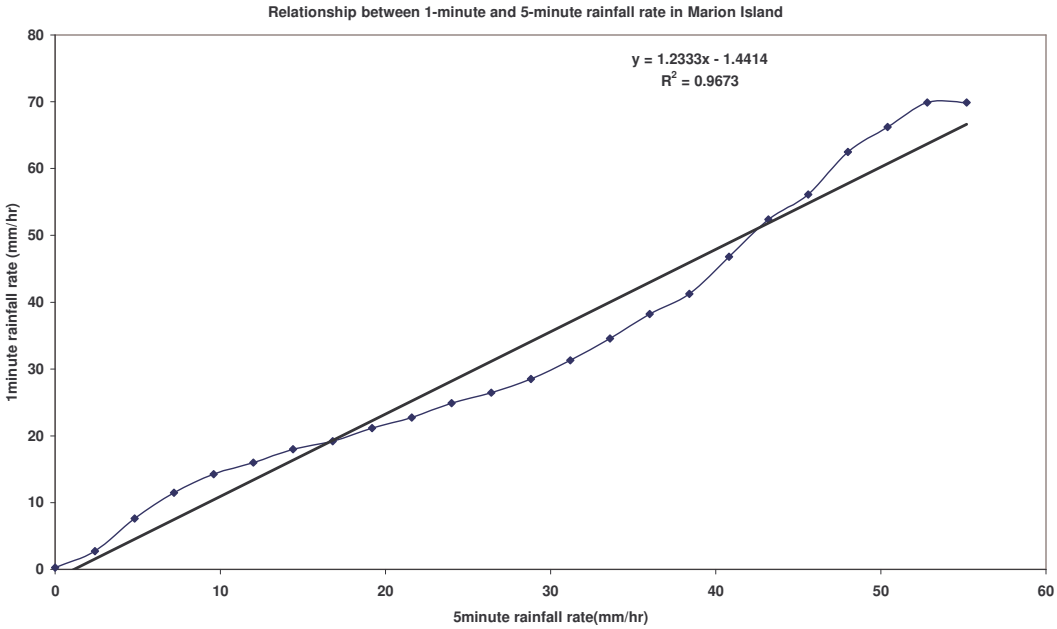

Figure 3.4: Relationship between 1-min and 5-min rainfall rate in Marion Island

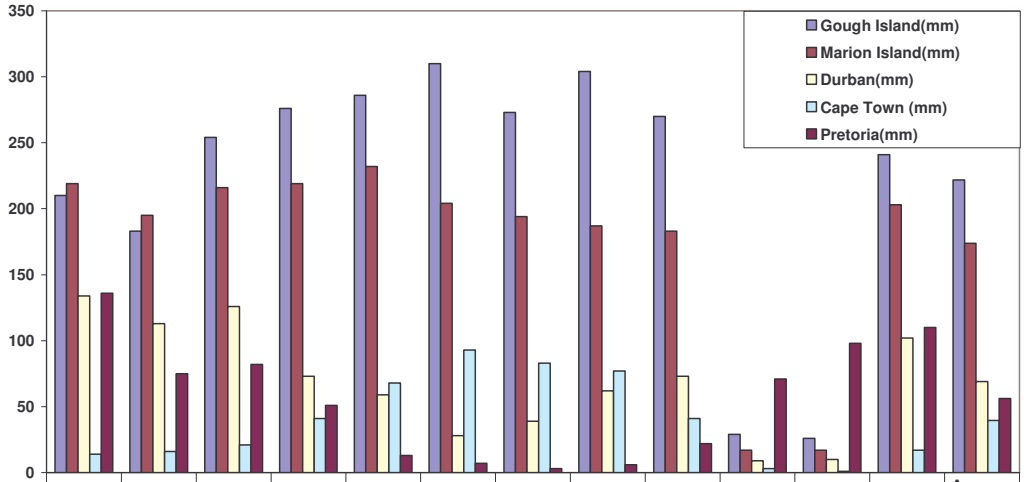

	January	February	March	April	May	June	July	August	September	October	November	December	Average month Accumul
Gough Island(mm)	210	183	254	276	286	310	273	304	270	29	26	241	222
Marion Island(mm)	219	195	216	219	232	204	194	187	183	17	17	203	174
Durban(mm)	134	113	126	73	59	28	39	62	73	9	10	102	69
Cape Town (mm)	14	16	21	41	68	93	83	77	41	3	1	17	40
Pretoria(mm)	136	75	82	51	13	7	3	6	22	71	98	110	56

Figure 3.5: Average annual total rainfall for 5 selected sites

Figure 3.3 shows more variations of rain rate above 65 mm/hr between the one-minute and five-minute data, while Figure 3.4 presents a variation that tends to be the same across all rainfall rates. Table 3.2, in addition, shows the values for average annual total rainfall $M\,(mm/yr)$, highest monthly precipitation observed over 30 years $M_m(mm/month)$ and the average number of thunderstorm day in a year D_{th} (day). Figure 3.5 gives graphical representation of accumulation averaged over 30 years. The large differences recorded between one-minute and five-minute rain rates in both Islands may be due to high average rainfall accumulation which leads to the negative value of β.

3.1.3 Contributions of the Present work – The Hybrid Method

The current work presented in this thesis further improves on the aforementioned studies because of the followings:

- Since physical, analytical and empirical models proposed by many studies may not perform very well in locations outside of the areas in which data was collected, the current work uses a combination of the good properties of the three classes of conversion methods and also intends to retain the integrity of rain rate distribution patterns for any location in South Africa and the surrounding Islands.
- In the ITU-R P837-5 (ITU-R P.837-5, 2007), ITU-R Document 3J/29, and ITU-R Document 3J/43, none of the African countries is included in the determination of the global average coefficients. The present work interpolates the proposed coefficients with its counterparts from other parts of the world. The work also includes the conversion coefficient for each defined Köppen climatic map for South Africa.

In the proposed hybrid rain rate integration time conversion method, the characteristics of the three classes of conversion methods discussed in section 2.1 to 2.4 are combined to give a better one-minute rain rate distribution. The key reason for this proposal is based on the facts stated above as well as the lack of one-minute rain rate data for South Africa and surrounding Islands. The three classes of conversion method and their selected models to be used are:

- Physical method
    - Rice-Holmberg and Dutton-Dougherty-Martin models
    - Lavergnat-Gole model with Ito-Hosoya constants
- Analytical method
    - Moupfouma-Martin model
    - Ito-Hosoya model
- Empirical method
    - Ajayi and Ofoche (Tropic) and Migliora, Pontes and Mello (Brazil)
    - ITU-R Document 3J/29-E (Temperate - Italy, USA, Canada, and Czech Republic (Prague).

3.2 Experimental Measurement Facilities

The rainfall data employed in this study has been collected by four different rain measuring equipment. Measurements have been obtained by means of Oregon Rain gauge, Vintage Pro Wireless weather station, and Joss-Waldvogel Distrometer (JWD). In addition, over ten years rainfall data with five-minute integration time has been provided by the South Africa Weather Service (SAWS).

3.2.1 Rain Gauge

The rain gauge is an instrument used to measure amount of rainfall, the most common type being a relatively cheap, easy-to-install tipping bucket. An Oregon rain gauge (RGR 382) was installed to measure the amount of rainfall. It is located at Latitude ($30^0 58^{'} E$) and Longitude ($29^0 52^{'} S$) at an altitude of 139.7 meters at the School of Electrical, Electronics and Computer Engineering in the University of KwaZulu-Natal, Howard College campus. The rain gauge collector has a diameter measuring 4 inches (101.6mm), and stands 5.75 inches high (146.05mm). The gauge contains a collecting bucket that tips after accumulation of 1 mm of rainfall. The measuring accuracy of the bucket with rain rate of 0 - 15 mm per hour is +/- 10 % while above 15 mm per hour is +/-15%. The gauge functioned for a period of one-year (2005-2006).

3.2.2 Wireless Vantage Pro2 (Complete Weather Station)

This is a complete weather station with good measuring resolution. The equipment is situated in the same site as the Oregon rain gauge. It measures rainfall and rain rate with a resolution of 0.2mm. The measuring accuracy of the equipment with rain rate starting from 1 mm/hr to 250 mm per hour is +/- 5%. The equipment is configured to sample data at 30 minutes interval.

3.2.3 Joss-Waldvogel Distrometer (JWD)

The Joss-Waldvogel distrometer is an instrument for measuring raindrop size distribution (DSD). This equipment is not limited to measuring raindrop distribution only, but is also incorporated into precipitation field measurement purposely to validate and complement the measurements of the rain gauge. The distrometer used in this study is capable of measuring rain rate, reflectivity, rain accumulation, raindrop size (diameter range 0.3-5.5 mm) at 30-second intervals with an accuracy of 5%. For the current study, the distrometer was installed in December 2008, and commenced operation in January 2009 with a sampling interval integrated over one minute. The equipments mentioned in section 3.2.2 and 3.3.3 are present at the master site (control site) and located approximately 2 meters from each other. The site is free of noise and shielded from abnormal winds.

3.2.4 South Africa Weather Services: Network of Rain Gauges

South Africa Weather Services (SAWS) provide rainfall data of five-minute integration time for over ten years for all the provinces in South Africa and the surrounding Islands. A SAW uses different means to collect their precipitation data. The most widely used method is via a network of rain gauges. Rain gauges used by SAWS are standard 127 mm in accordance with the World Meteorological Organization (WMO) standard. The 127 mm is the diameter of the rimmed circular funnel opening. The other type of rain gauge used by SAWS is the automated rain gauge, which is a tipping bucket rain gauge with a 200 mm funnel opening. The data used in this study is based on the specification and calibration of the two types of rain gauges mentioned.

3.3 Theory of the Hybrid Method - Extracting One-minute Rain Rate from Combined Rain Rate Model

Consider a hypothetical cumulative distribution of rain rate using different one-minute rain rate models. Let N be the number of models generating those one minute rain rate cumulative distributions e.g. rain rate distribution model 1 (N_1), rain rate distribution model 2 (N_2),……up to rain rate distribution model (N_n). Along the x-axis, let P represent the probability of rain rate exceedences using ITU-R's designations $P_{0.001}$, $P_{0.003}$, $P_{0.01}$, $P_{0.03}$, $P_{0.1}$, $P_{0.3}$, and P_1.

The conversion factors (CF) for each class of N is given by:

$$CF_{N=1,2,3...n} = \left(\frac{R_{1,1}(P_{0.001})}{R_{T,1}(P_{0.001}}\right) + \left(\frac{R_{1,2}(P_{0.001})}{R_{T,2}(P_{0.001})}\right) + ... \left(\frac{R_{1,n}(P_{0.001})}{R_{T,n}(P_{0.001})}\right)$$

$$CF_{N=1,2,3...n} = \left(\frac{R_{1,1}(P_{0.003})}{R_{T,1}(P_{0.003}}\right) + \left(\frac{R_{1,2}(P_{0.003})}{R_{T,2}(P_{0.003})}\right) + ... \left(\frac{R_{1,n}(P_{0.003})}{R_{T,n}(P_{0.003})}\right) \qquad (3.9a)$$

. .

. .

. .

$$CF_{N=1,2,3...n} = \left(\frac{R_{1,1}(P_1)}{R_{T,1}(P_1}\right) + \left(\frac{R_{1,2}(P_1)}{R_{T,2}(P_1)}\right) + ... \left(\frac{R_{1,n}(P_1)}{R_{T,n}(P_1)}\right)$$

where N is the designation number assigned to each model used, i.e $N = 1,2,3...n$

Suppose we assume $L_{i=0.001,0.003...1} = \frac{1}{N}\sum CF_{N=1,2,..n,0.001}$, and the hybrid conversion factors for each percentage of exceedences are $L_{0.001}$, $L_{0.003}$, $\ldots L_1$ respectively. Thus, the generalize expression for hybrid conversion factor is given as:

$$L_{i=0.001,0.003...1} = \frac{1}{N}\sum CF_{N=1,2,..n,0.001} \tag{3.9b}$$

where $\sum CF_{N=1,2,..n,0.001}$ is the sum of ratio of rain rates exceeded for a given percentage of time for rain gauges with integration times T minutes and one minute for each number of distributions N. Also, the principle can be repeated for a case of a set threshold of rain rate at unknown percentage of exceedence, as follows:

$$CF_{N=1,2,3...n} = \left(\frac{P_{1,1}(R_{0.001})}{P_{T,1}(R_{0.001}}\right) + \left(\frac{P_{1,2}(R_{0.001})}{P_{T,2}(R_{0.001})}\right) + ... \left(\frac{P_{1,n}(R_{0.001})}{P_{T,n}(R_{0.001})}\right)$$

$$CF_{N=1,2,3...n} = \left(\frac{P_{1,1}(R_{0.003})}{P_{T,1}(R_{0.003}}\right) + \left(\frac{P_{1,2}(R_{0.003})}{P_{T,2}(R_{0.003})}\right) + ... \left(\frac{P_{1,n}(R_{0.003})}{P_{T,n}(R_{0.003})}\right)$$

. .

. . (3.9c)

. .

$$CF_{N=1,2,3...n} = \left(\frac{P_{1,1}(R_1)}{P_{T,1}(R_1}\right) + \left(\frac{P_{1,2}(R_1)}{P_{T,2}(R_1)}\right) + ... \left(\frac{P_{1,n}(R_1)}{P_{T,n}(R_1)}\right)$$

Then equation (3.9b) can be assumed where $\sum CF_{N=1,2,..n,0.001}$ refers to the sum of ratio of exceedences for a given rain rate measured using gauges with T minute and one minute integration times for each number of distributions N.

3.3.1 Application of Hybrid method in Durban (Master Site)

For our purpose, the selected models for the hybrid conversion method are: the Moupfouma-Martin model (N_1); the Ito-Hosoya model (N_2); the Rice-Holmberg and Dutton-Dougherty-Martin models (N_3); the Lavergnat-Golé model with Ito-Hosoya constants (N_4); the Ajayi-Ofoche model (N_5); the Migliora, Pontes and Mello model (N6) (ITU-R Document 3J/29-E); the Italy model (N_7); the USA model (N_8); and the Canada model (N_9). The criteria for model selection for South Africa and surrounding

Islands are based on the fact that some model expressions involve location/region-based climatic parameters, as well as the incorporation of a few localized models in order to accommodate the mixed tropic and temperate climate which characterizes most of the South Africa region. The result of the mixed model approach is a hybrid method whose coefficients are used to convert the available five-minute data to one-minute equivalent.

There are two common relationships used in converting rain rate from one integration time to one-minute equivalents and is based on the equiprobable approach as demonstrated in sub-section 3.1.2. These are:

i. Finding the relationship between the time probabilities of one-minute integration time and the known integration time distribution for the same rainfall rate ,
ii. Obtaining the relationship between one-minute rainfall rate and unknown integration time rainfall rate for equal percentage of exceedence.

The latter approach is adopted for this study. Figure 3.6 shows the relationship between the estimated one-minute (hybrid method using nine rain rate models) and five-minute rain rate collected. Three different regression fits are applied; these are the second order polynomial fit, the linear fit and the power fit. These regression fits are used to estimate the distributions of rain rate at two different integration times but at equal percentage of exceedence. The regression curve is based on equal percentage of exceedence at which rain rate exceeded at a range between 0.001% and 1% with smaller unit intervals. The square value of correlation coefficients of the fits shows that the second order polynomial fit performs best, followed by linear fit, with the power fit performing worst. Figure 3.6 also reveals that at lower rain rate, the three fits' distributions give a good correlation with the minimum percentage deviation of 0.33%; however, at a higher rain rate, the power law fit diverges slightly by a maximum percentage deviation of 7.87%.

Another approach to present the conversion method expressions is to use conversion factors. This relates the ratio of rain rate at equal percentages of excceedence against its percentage of exceedence at each ratio of rain rate. Figure 3.7 is a graphic representation

of this method using rain rate data for Durban. It shows the relationship between rain rate conversion factor and percentage of exceedence for each individual rain rate ratio. Second order polynomial, logarithm and power law are the fit distributions applied. In Figure 3.7, the model rain rate conversion factor favours the second order polynomial fit using the square value correlation coefficient. It is noted that the square correlation coefficients were less than 0.5 and this poor correlation is common with other stations considered in this work.

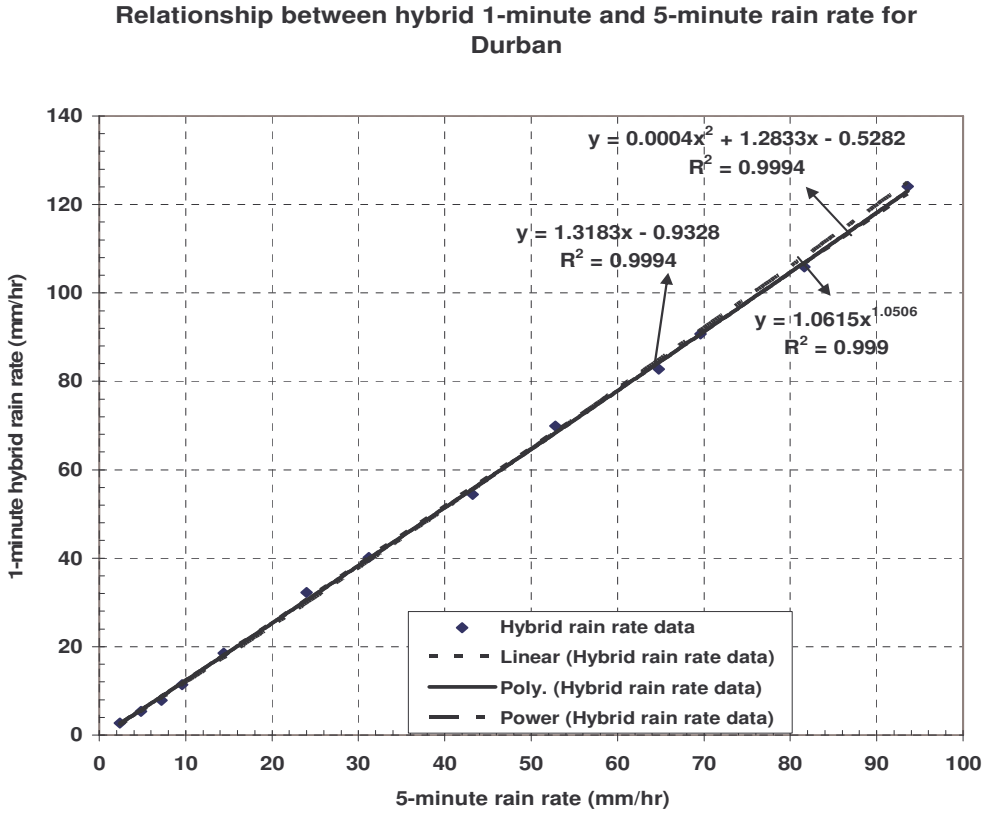

Figure 3.6: The hybrid one-minute rain rate against five-minute measured rain rate in Durban

As a result of the weak square correlation coefficient shown in Figure 3.7, the expressions (polynomial, power and linear fit) in Figure 3.6 are adopted to convert rain rate from five-minute integration time to one-minute equivalent. The results of converted five-minute cumulative distribution of rain rate using different fits are then

compared with each other as well as the one-minute measured data. The comparisons are also carried out with ITU-R Recommendation P837-5 conversion coefficients and the reviewed ITU-R P.837-5 results. The comparison is evaluated using a relative error method adopted by ITU-R and other authors. Figure 3.8 shows the comparison of measured one-minute rain rate with three different hybrid fits. The different distribution fits used are power fit, second order polynomial fit and linear fit. As seen in the diagram, the three chosen fits seem to describe one-minute measured rain rate distributions well with little degree of deviation at a higher rain rate for the power fit. The resulting one-minute rain rates estimated by the three distribution fits derived by hybrid method are tested against available eleven months one-minute rain rate data. The quantitative estimated errors are evaluated using one of the two common methods that are widely used by many workers. These methods are:

1. Logarithm error, recommended by ITU-R, where the ratio of predicted one-minute rain rate (using hybrid method) to measured one-minute rain rate is calculated for the range of rain rate data with the exceedence probability in the range 0.001% to 1%. The logarithm error expression is given by :

$$E_{Log,i} = \ln\left(\frac{R_{p,i}}{R_{m,i}}\right) \tag{3.10}$$

where R_p (mm/hr) and R_m (mm/hr) are predicted and measured one-minute rain rates, respectively. The average $E_{Log,i}$ is written as:

$$E_{mean} = \frac{\sum W_i E_{Log,i}}{\sum W_i} \tag{3.11}$$

where W_i is the weighting factor .

2. Relative error which is a widely used error evaluation method, and is given by :

$$E_{\mathrm{Re}l,i}(\%) = 100\left(\frac{R_{p,i} - R_{m,i}}{R_{m,i}}\right) \tag{3.12}$$

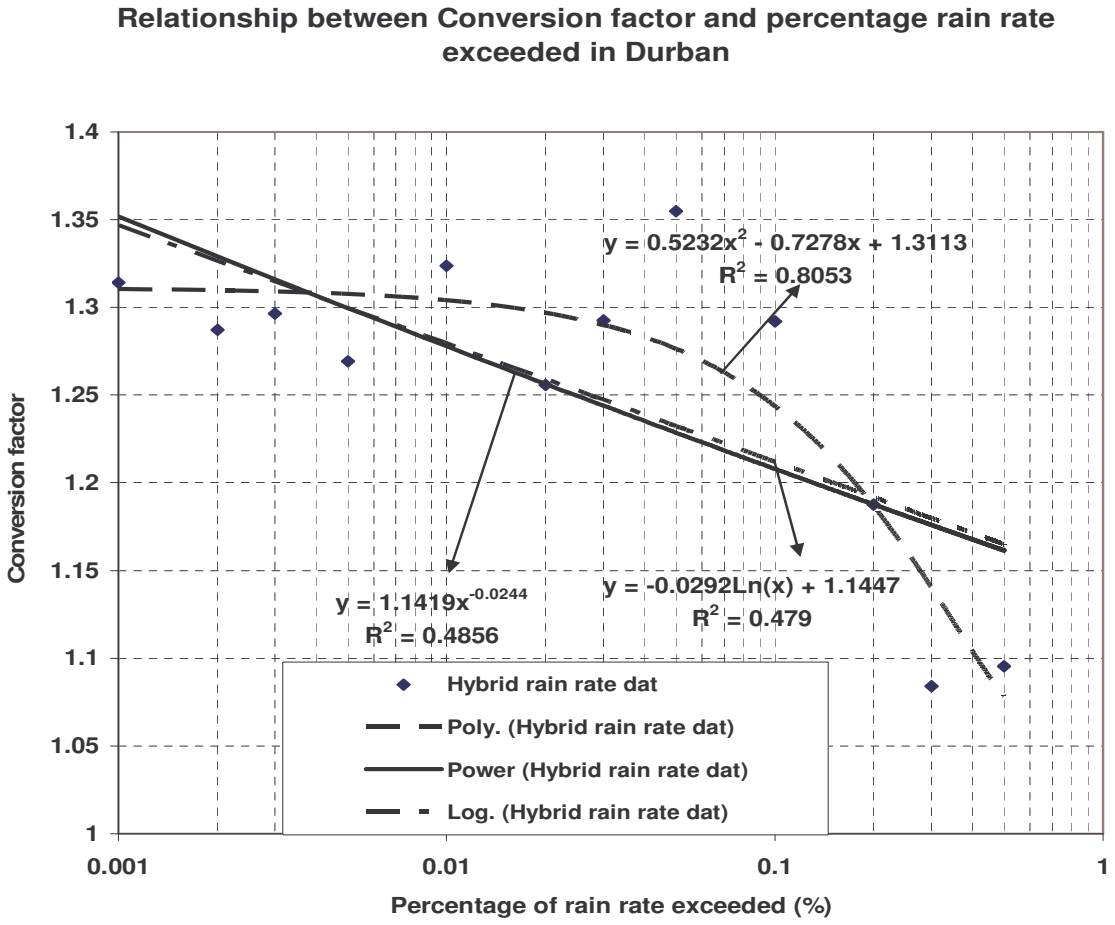

Figure 3.7: Relationship between conversion factor and percentage of time rain rate exceeded

It should be noted that the lower the values in equations 3.11 and 3.12, the better the proposed model. In this chapter, the relative error is chosen for comparing the proposed model with actual measured data. In order to confirm the most suitable fit distribution to best describe Durban, the average standard deviation (STD) of the absolute relative error and root mean square (RMS) of relative error are carried out as shown in Table 3.3. The table shows the best fit distribution that describes the proposed one-minute rain rate

(hybrid method) with measured one-minute rain rate. The average value of the absolute relative error is noted to be lowest when the polynomial fit of second order is used, while the maximum average error is observed with power law fit. The same trend is observed for the cases when STD and RMS of relative errors are used.

Table 3.3: Comparison between the different fit distributions for Durban using average, STD, and RMS values

Model	**Average value of absolute** $E_{\mathrm{Re}l,i}(\%)$	**STD value of absolute** $E_{\mathrm{Re}l,i}(\%)$	**RMS value of absolute** $E_{\mathrm{Re}l,i}(\%)$
Linear Fit	11.72	12.38	16.69
Polynomial fit (2nd order)	6.74	6.21	9.0
Power Fit	14.64	5.0	15.40
ITU-R P.837-5	10.85	7.05	12.80
New Proposed ITU-R	9.0	4.78	10.72

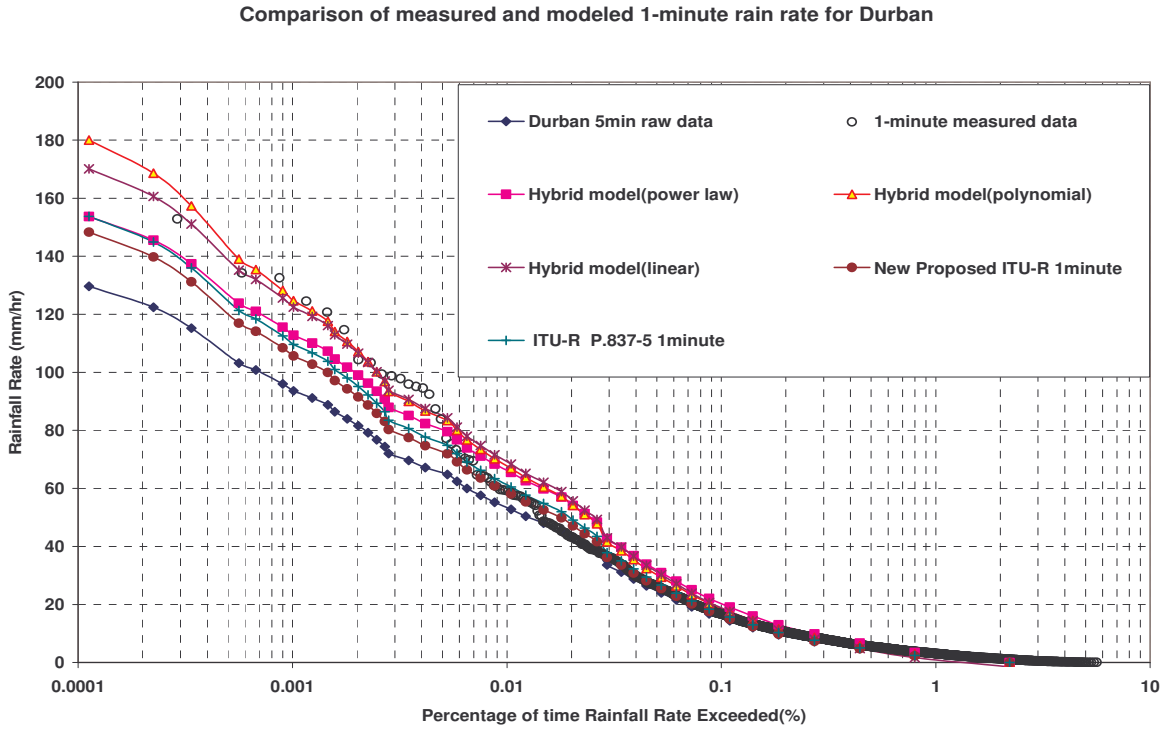

Figure 3.8: Comparison between one-minute measured rain rate and one-minute estimated using hybrid method.

At 0.01% percentage of exceedence, power fit seems to be considered as the best with 9.88% of relative error whereas linear and polynomial fits give 14.79% and 12.28% of relative error, respectively. This is confirmed by the RMS value where power fit records a value of 0.97%, while polynomial and linear fits record 1.5% and 2.1%, respectively. At 0.001% percentage of exceedence, the performance of polynomial fit is the best with 0.072% of relative error, while in the case of linear is 1.68% and highest relative error is observed in power fit. Comparisons between ITU-R P.837-5 and the suggested new global power model using Durban's data show that the percentage differences between the existing ITU-R and new global model in this study are 9.31% ,19.18% and 8.85%, when using average value of absolute error, standard deviation of absolute value of error and root mean square of absolute value of error, respectively. It is also noted from Table 3.3 and Figure 3.8 that both the ITU-R and suggested new ITU-R's global model describe the Durban cumulative distribution well at lower rain rate while at the higher rain rate there is greater deviation. The performance of the polynomial fit of second order is considered the best for conversion of rain rate from five-minute to one-minute equivalent because the average error evaluation confirmed the use of polynomial fit as overall best performing regression fit compared to its counterparts.

As a result, the polynomial model is proposed for conversion of rain rate from five-minute to one-minute equivalent for South Africa and surrounding islands with a simple general expression given as:

$$R_1(p_i) = aR_5(p_i)^2 + bR_5(p) + c \tag{3.13}$$

where a, b and c are constants. In the case of Durban, it is noted that a=0.0004, b=1.2833 and c=-0.5282.

The other expressions used in equiprobable method are the power fit and linear fit given as:

$$R_1(p_i) = d[R_5(p_i)]^e \tag{3.14a}$$

$$R_1(p_i) = f\,[R_5(p_i)] + g \tag{3.14b}$$

where d, e, f and g are constants with values for Durban given by 1.0615, 1.0506, 1.3183 and -0.9328, respectively.

The second part of the expression uses equal-rain rate method rather than the equiprobable approach, and is summarized as follows:

$$CF(R_i) = h\,(p(R_i))^2 + I\;p(R_i) + j \tag{3.15a}$$

$$CF(R_i) = k\,[p(R_i)]^l \tag{3.15b}$$

$$CF(R_i) = m \ln[p(R_i)] + n \tag{3.15c}$$

where $CF(R_i)$ and $p(R_i)$ are, respectively, the conversion factor and percentages of exceedence at equal chosen rain rate value. The parameters h, I, j, k, l, m and n are constants for Durban with values of 0.5232, -0.7278, 1.3113, 1.1419,-0.0244,-0.0292 and 1.1447, respectively.

Equations 3.15a to 3.15c are not adopted in this work because of the poor square correlation coefficient as shown in Figure 3.7 although the polynomial fit shows better square correlation value of 0.8053. The hybrid approach is adopted to estimate one-minute rain rate for other provinces in South Africa and the surrounding islands, and mapped using Koppen climatic classification method.

3.3.2 Köppen Climatic Classification of South Africa and Surrounding Islands

According to Peel *et al*. (2007), the Köppen classification system is widely used in the current approach to climate classification. It was first published in 1884 by the Russian climatologist Wladimir Köppen with several modifications by himself. This classification system divides the world climate into five main groups with several types and sub-types. The results of collaboration between Köppen and Geiger were based on the climate classification on native vegetation, annual and monthly precipitation, temperature and

seasonality of precipitation. Köppen method is applied to identify climatic trends that are based on vegetation and climatic phenomenon. According to Seeber (Seeber, 1985), South Africa is divided into 12 climatic regions using the Köppen climatic classification criteria. In the extension of classification to the present work, the study uses the same map but additional stations are added. Table 3.4 gives the description of each climatic zone as described by Seeber (Seeber, 1985), with added data points. The graphical representation shown in Figure 3.9 represents the location and climatic region of autographic rainfall stations where data was collected. The details of designations are explained in Table 3.4 with their respective Köppen climate classifications. The map also includes Gough Island (2500 km from Western Cape) and Marion Island (1500 km from Eastern Cape).

Table 3.4: South African Köppen climatic regions from Seeber (Seeber, 1995)

Climatic classification for South African(Köppen climatic system)		
Site Designation	***Köppen Classifications***	***Data points***
W	Northern Cape: Dessert climate.**(BW)**	Upington
M	South-Western Cape: Mediterranean climate with winter rain. **(Cs)**	Bethlehem, Cape Point
K	Karoo: Desert climate.(BW and BSk)	Beaufort
A	Southern coastal belt: Rain during all seasons.**(Cf)**	Port Alfred
SE	South-eastern coastal belt: Warm temperate with summer rain.**(Cfw)**	East London
E	Eastern coast and Zululand: Sub-tropical with summer rain. **(Cfw and Cfa)**	Durban, Richard Bay
D	Drekensberg and interior KwaZulu-Natal: Warm temperate with summer rain. **(Cwb)**	Ladysmith,Umtata Pietermaritzburg
L	Lowveld (Northern province): Hot steppe with summer rain. (BShw)	Skukuza
NT	Northern Province: Hot steppe with summer rain.(BShw)	Tshipise,Warmbad, Rustenburg, Pretoria
H	Highveld(Mpumalanga,Gauteng and Free state): Warm temperate with summer rain.**(Cwb)**	Spring, Bishop, Ermelo, Belfast
Sn	Northern Steppe (Free State and North-West): Steppe summer and autumn rain.(BSkw)	Klerksdorp, Kimberley
Ss	Southern Steppe (Eastern Cape and Free state):Cold Steppe with autumn rain.(BSkw)	Fort Beaufort

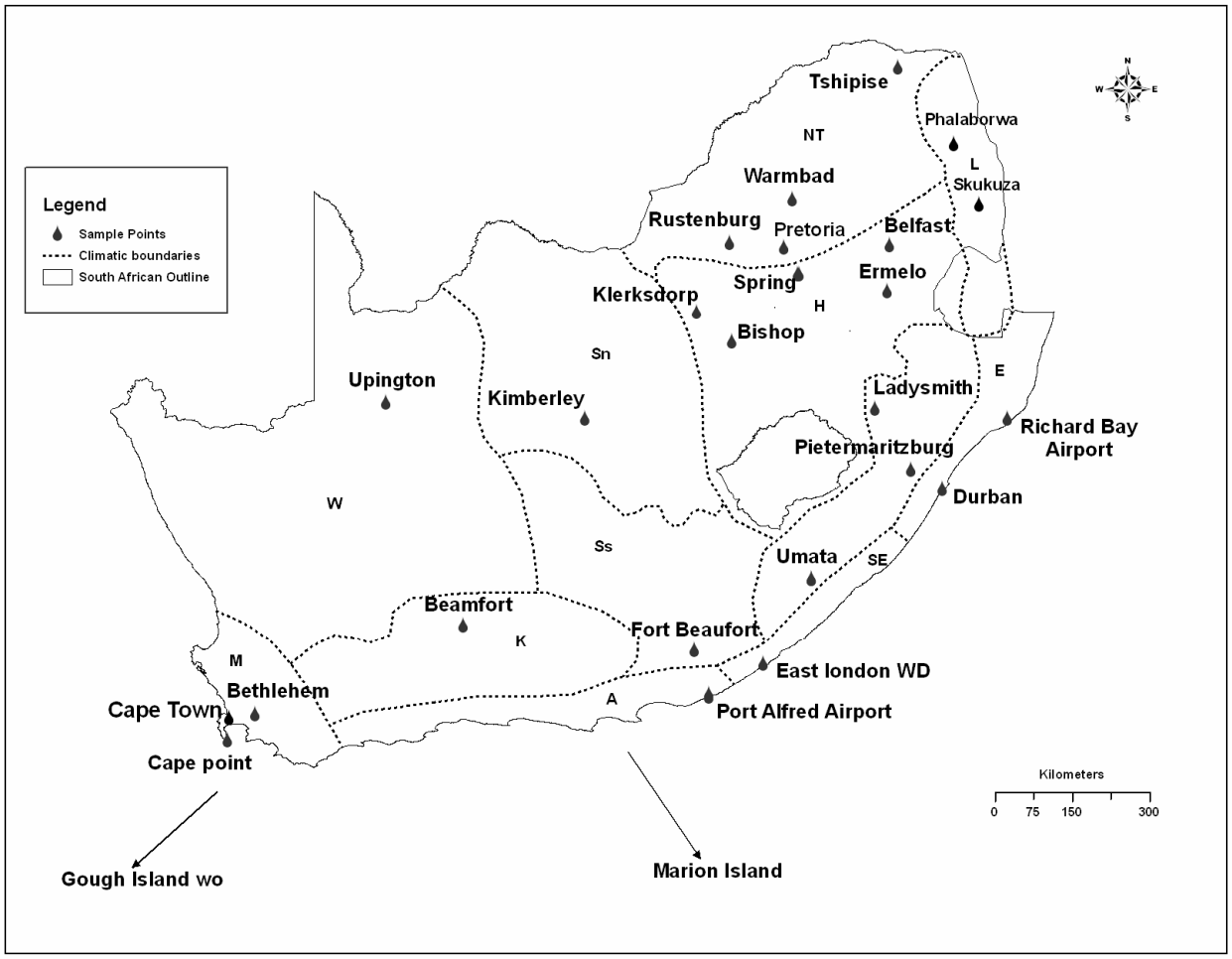

Figure 3.9: Climatic classification of South Africa and surrounding islands based on Köppen method.

3.3.3 Location-based Parameters used to estimate one-minute Rain Rate

Table 3.5 summarizes the parameters used in determining conversion constants for rain rate from five-minute integration time to the one-minute equivalent. The study area includes nine provinces with their respective Köppen climatic designations. The total number of studied sites is 25 with the inclusion of two surrounding islands. The parameters used are the highest monthly precipitation M_m (mm) obtained from SAWS data while the average annual rainfall, M (mm), and thunderstorm days, D^{th} (day), in a year were obtained from World Meteorological Organization (WMO) documents (WMO, 1953 and 1962). The parameters β is obtained from equation 2.3 in chapter two

and $R_{5\,\min}(0.01)$ is determined from the cumulative distribution of the five minute rainfall data over ten years as provided by SAWS. In this work, the models selected are those that have regional parameters, all of which have been applied in the chosen rain rate model to produce the hybrid model. The equations involved are equations 2.1 to 2.28 from chapter two.

Table 3.5: Regional parameters used in estimating one-minute rain rate by hybrid method

S ITE	**Lat.(deg)**	**Long.(deg)**	M **(mm)**	D^{th} **(day)**	M_m **(mm)**	β	$R_{5\,\min}(0.01)$ **(mm)**
Eastern Cape							
Port Alfred	-33.5	26.8	624	30	64	0.721	33.6
Bishop	-27.3	27.2	476	30	73	0.954	38.4
Fort Beaufort	-32.7	26.6	403	30	66	0.956	36.0
Umtata	-31.5	28.6	650	30	89	0.885	48.0
East London	-33.0	27.5	904	30	106		
Gauteng							
Spring	-26.2	28.4	713	30	125	0.918	40.8
Pretoria	-25.7	28.1	679	20	152	0.642	48.0
Free-State							
Bethlehem	-33.9	18.9	680	20	96	0.642	50.0
KZN							
Durban	-29.9	30.9	1009	30	134	0.688	55.2
Ladysmith	-28.5	29.7	749	30	145	0.899	57.6
Pietermaritzburg	-29.6	30.0	844	30	141	0.813	67.2
Mpumanlaga							
Ermelo	-26.4	29.9	711	30	146	0.938	52.2
Belfast	-25.6	30.0	878	30	170	0.795	43.2
Skukuza	-24.59	31.36	563	15	98		
Western-Cape							
Cape Point	-34.3	18.4	515	15	93	0.605	16.8
Beaufort	-32.3	22.6	236	15	35	0.885	31.2
Cape Town	-33.9	18.6	515	15	93	0.609	21.6
North West							
Rustenburg	-25.6	27.2	661	20	123	0.688	55.2
Klerksdorp	-26.8	26.6	482	10	92	0.429	54.0
Northern Cape							
Kimberley	-28.7	24.7	415	30	76	1.055	55.0
Upinton	-28.4	21.2	188	10	36	0.353	55.2
Limpopo							
Tshipise	-22.6	30.1	339	20	58	0.739	40.8
Warmbad	-24.9	28.3	634	15	124	0.538	31.2
Islands							
Gough Island	-40.3	9.8	3163	7.2	225.18	0.038	55.2
Marion Island	-46.8	37.5	2399	10	173.83	0.0275	31.2

3.3.4 Estimation of one-minute Rain Rate for South Africa and Surrounding Islands

Following the success of the principle used in sections 3.3 and sub-section 3.3.1 to determine the coefficients needed to convert rain rate from five-minute to one-minute equivalent, it is possible to generalize the approach to the rest of the sites in the region. The evidence of optimization method presented in Table 3.3 supports the approach, especially when one-minute rain rate data is scarce. However, it should be noted that before the method could be applied, at least some one-minute rain rate data is needed to optimize the selected models to the hybrid model.

Table 3.6a and 3.6b show the coefficients of equations 3.13 to 3.15 for South Africa with the square value of correlation coefficients. The values reflect variability from one Köppen class to another. In the case of the two Islands, the polynomial fit gives a positive value for c different from the trend shown in the South Africa region. Using the square correlation coefficient value, it is noted from the table that the polynomial and linear fits have a better performance than the power fit, though the result of the power fit distribution is acceptable because the square correlation coefficient records its least at 0.956. The implication of this is that using the equiprobable approach gives a better approximation than the conversion factor approach. Using the conversion factor method (at equal rain rate), the square correlation coefficient records its least value at 0.479 and best value at 0.990. The polynomial and logarithm fits give better approximations compared to the power fit. Gough and Marion islands are approximated using both equiprobable method and conversion factor approach. Polynomial, power and linear fits performed very well under the equiprobable method in the two islands. Although the polynomial and linear fits seem to do better than power fit especially in the case of Gough Island, all the three chosen fits do very well in Marion Island. Under conversion factor approach, none of the chosen fits seem to approximate the distribution well.

3.4 Conclusion

In this chapter, a review of models used to convert rain rate from any integration time to the required one-minute equivalent were applied, covering the classification of the conversion models into the three categories of physical, analytical and empirical models. A proposed hybrid method for the conversion of five-minute integration time to one-minute equivalent was discussed as well as comparison of the proposed model with two suggested global models.

In the proposed hybrid method, the strength of each category of model classes were combined to produce a hybrid model. The selected model consists of regional parameters in order to characterize the rain rate pattern for a defined area. The resulting one-minute cumulative distribution of rain rate is fitted with polynomial, power, linear and logarithm fits of distributions. The performances of these fits were optimized using standard deviation and root-mean square of absolute relative error at the control site of Durban. The optimizations were carried out over the equiprobable approach and conversion factor approach. The results show that the equiprobable approach gives better results than the conversion factor approach. In addition, the second order polynomial fit performed relatively better than its counterparts. The evidence of good performance by the second order polynomial fit makes it a good candidate for conversion of rain rate from five-minute to equivalent one-minute in South Africa and the surrounding Islands. The South African region was subsequently classified into 12 sub-climatic zones using the Köppen climatic classification. The coefficients of polynomial, power, linear and logarithm fits were given for each of the classes with their square correlation coefficients. Finally the polynomial fit of second order is adopted for South Africa and the two surrounding Islands.

Table 3.6 (a): Average coefficients for equations 3.13, 3.14 and 3.15 with their Köppen climate classifications for the South Africa Region

Site Designation/expression coefficients	W	M	K	A	SE	E
Polynomial Fit $R_1(p)/R_5(p)$	$\rho = 1.000$	$\rho = 0.997$	$\rho = 0.999$	$\rho = 0.999$	$\rho = 0.996$	$\rho = 0.999$
A	0.002	0.001	0.002	0.0005	0.0004	0.0004
B	1.023	1.231	1.255	1.273	1.257	1.283
C	-0.126	-0.503	-0.370	-0.646	-0.536	-0.528
Power Fit $R_1(p)/R_5(p)$	$\rho = 0.980$	$\rho = 0.971$	$\rho = 0.983$	$\rho = 0.999$	$\rho = 0.999$	$\rho = 0.999$
D	1.993	1.547	1.850	1.087	1.064	1.061
E	0.829	0.931	0.867	1.041	1.044	1.051
Linear Fit $R_1(p)/R_5(p)$	$\rho = 0.998$	$\rho = 0.997$	$\rho = 0.999$	$\rho = 0.999$	$\rho = 0.950$	$\rho = 0.999$
F	1.205	1.318	1.376	1.314	1.291	1.318
G	-2.007	-1.213	-1.331	-1.029	-0.839	-0.932
Polynomial Fit (cf)	$\rho = 0.797$	$\rho = 0.768$	$\rho = 0.750$	$\rho = 0.985$	$\rho = 0.766$	$\rho = 0.805$
H	1.284	1.042	1.912	1.820	1.789	0.523
I	-1.017	-0.885	-1.356	-1.257	-1.194	-0.727
J	1.134	1.284	1.328	1.286	1.265	1.311
Power Fit (cf)	$\rho = 0.990$	$\rho = 0.830$	$\rho = 0.730$	$\rho = 0.859$	$\rho = 0.721$	$\rho = 0.486$
K	0.930	1.064	1.084	1.085	1.080	1.142
L	-0.037	-0.035	-0.039	-0.030	-0.028	-0.024
Logarithm Fit (cf)	$\rho = 0.989$	$\rho = 0.839$	$\rho = 0.820$	$\rho = 0.868$	$\rho = 0.821$	$\rho = 0.479$
M	-0.038	-0.043	-0.048	-0.036	-0.033	-0.029
N	0.995	1.059	1.077	1.082	1.078	1.144

Table 3.6 (b): Average coefficients for equations 3.13, 3.14 and 3.15 with their Köppen climate classifications for the South Africa Region

Site Designation/expression coefficients	D	L	NT	H	Sn	Ss
Polynomial Fit $R_1(p)/R_5(p)$	$\rho = 0.999$	$\rho = 0.996$	$\rho = 0.997$	$\rho = 0.999$	$\rho = 0.999$	$\rho = 0.999$
A	0.0007	0.002	0.0025	0.0009	0.0014	0.0006
B	1.185	1.108	1.102	1.201	1.071	1.239
C	-0.483	-0.424	0.581	-0.252	-0.389	-0.615
Power Fit $R_1(p)/R_5(p)$	$\rho = 0.999$	$\rho = 0.998$	$\rho = 0.956$	$\rho = 0.980$	$\rho = 0.999$	$\rho = 0.999$
D	1.071	1.086	1.028	1.071	1.635	1.021
E	1.032	0.891	1.049	1.014	0.929	1.092
Linear Fit $R_1(p)/R_5(p)$	$\rho = 0.999$	$\rho = 0.998$	$\rho = 0.996$	$\rho = 0.999$	$\rho = 0.998$	$\rho = 0.999$
F	1.267	1.295	1.265	1.284	1.231	1.284
G	-1.322	-1.721	-1.405	-1.012	-1.645	-0.980
Polynomial Fit (cf)	$\rho = 0.809$	$\rho = 0.725$	$\rho = 0.584$	$\rho = 0.864$	$\rho = 0.824$	$\rho = 0.734$
H	1.123	1.383	1.014	1.259	1.606	2.686
I	-0.788	-0.716	-0.655	-0.956	-1.110	-1.548
J	1.224	1.218	1.204	1.289	1.187	1.247
Power Fit (cf)	$\rho = 0.698$	$\rho = 0.650$	$\rho = 0.506$	$\rho = 0.762$	$\rho = 0.979$	$\rho = 0.629$
K	1.086	1.383	1.083	1.103	0.993	1.044
L	-0.021	-0.016	-0.020	-0.023	-0.033	-0.031
Logarithm Fit (cf)	$\rho = 0.579$	$\rho = 0.782$	$\rho = 0.514$	$\rho = 0.772$	$\rho = 0.984$	$\rho = 0.659$
M	-0.025	-0.019	-0.023	-0.028	-0.037	-0.036
N	1.084	1.115	1.081	1.127	0.987	1.042

Table 3.5: Average coefficient for equations (3.13) to (3.15) for the two Islands

Location	Polynomial Fit $R_1(p)/R_5(p)$	a	b	c	Power Fit $R_1(p)/R_5(p)$	d	e	Linear Fit $R_1(p)/R_5(p)$	f	g
Gough Islands	$\rho = 0.997$	0.002	1.062	1.157	$\rho = 0.915$	4.567	0.667	$\rho = 0.998$	1.196	0.092
Marion Island	$\rho = 0.999$	0.001	1.110	0.524	$\rho = 0.999$	1.151	1.009	$\rho = 0.999$	1.199	-0.292
Location	Polynomial Fit (cf)	h	I	j	Power Fit (cf)	k	l	Logarithm Fit (cf)	m	n
Gough Islands	$\rho = 0.414$	0.301	0.351	1.191	$\rho = 0.012$	1.325	0.020	$\rho = 0.014$	0.026	1.329
Marion Island	$\rho = 0.115$	-0.617	0.330	1.158	$\rho = 0.0016$	1.199	0.008	$\rho = 0.0013$	0.007	1.119

Chapter Four

Rainfall Rate Modelling and Its Characteristics in Southern Africa and Surrounding Islands

4.0 Introduction

Rain attenuation has a serious impact on the availability and performance of radio communication services operating on frequencies above 10 GHz. In order to reliably predict rain attenuation for a given location, there is a need to study monthly and seasonal rainfall variability, worst month and average worst month statistics of rain, and rainfall rate distribution models for sites under study. This chapter presents the earlier contributions. Firstly, section 4.1 deals with early investigations of rain rate modelling, section 4.2 includes the rain characteristics in terms of variability, worst-month, seasonal changes, and dependence of the percentage of the average year (AY) on percentage of time of the average worst month (AWM) of rainfall rate, and obtained rainfall rate distribution models for eight regions in South Africa. In the second part of the chapter, section 4.3 deals with extension of the rain rate characteristics studies to the Southern Islands, and section 4.4, deals with the new proposed rate models with their new suggested designations based on the ITU-R and Crane designation alphabets.

4.1 Previous Investigation of Cumulative Distribution of Rain Rate in South Africa

In the initial attempt to model rain rate distribution for South Africa, a general conversion factor was used to convert hourly rainfall data to its one-minute equivalent. The conversion factor which was originally based on the available one-minute and hourly data, was used to propose the model. However, one-minute rain rate data is neither sampled at the same time nor in the same place as the hourly rain rate data. Fashuyi *et al*, (2006) employed the power law expression to convert the available 60-minute rain rate to

a one-minute equivalent for the twelve South African sites as presented in section 3.1 of chapter 2. This section deals with comparative studies of cumulative distribution of rain rate in South Africa.

4.1.1 Comparative Studies of Rain Rate Cumulative Distribution in South Africa

In this sub-section, comparisons of rain rate statistics for 12 locations in South Africa over a period of 5 years are carried out. It has been reported that the main factors that cause the differences in the annual rain rate in South Africa are the influence of the South Atlantic Ocean, the Indian Ocean, and the topography (Tyson et al., 1976). The combination of these effects causes the differences in the annual rain rate between the South Africa climatic regions. The rainfall is unreliable and unpredictable throughout the country. Large fluctuations around the regions are compared in Figures 4.1, 4.2 and 4.3.

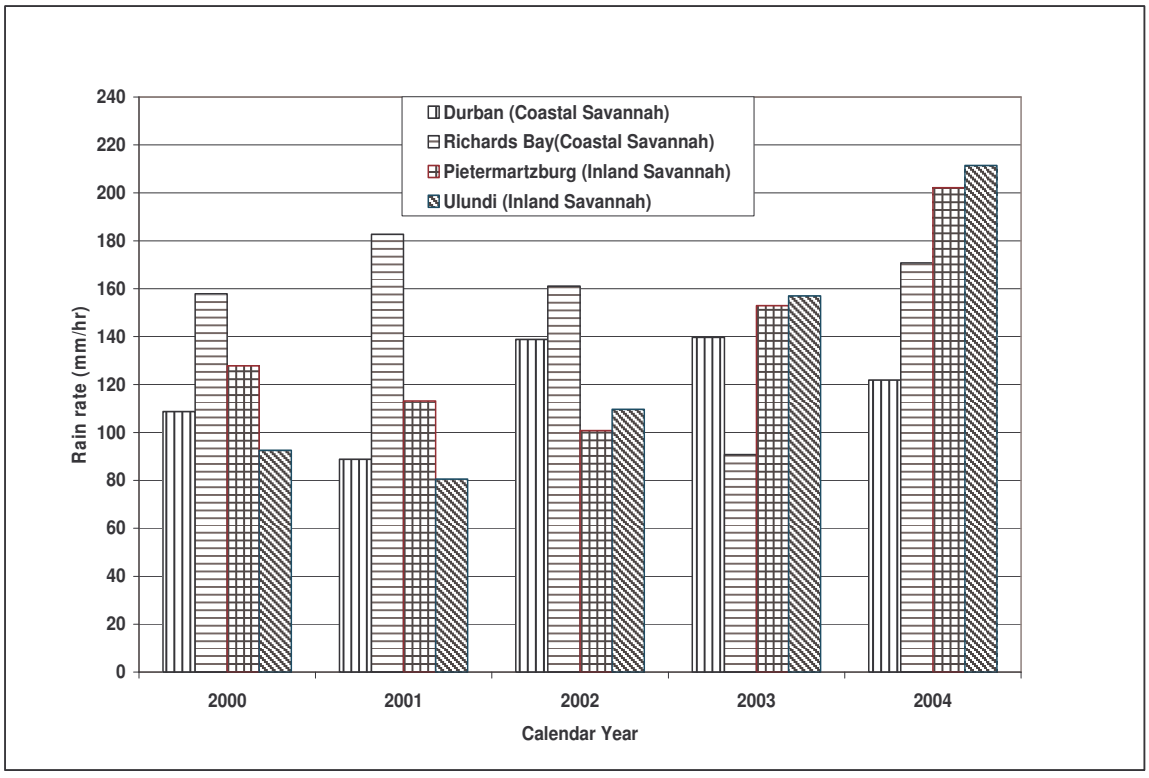

Figure 4.1: Variation in the Annual Rain Intensity (mm/h) Exceeded for 0.01% of the Time for South Africa (Coastal & Inland Savannah Regions)

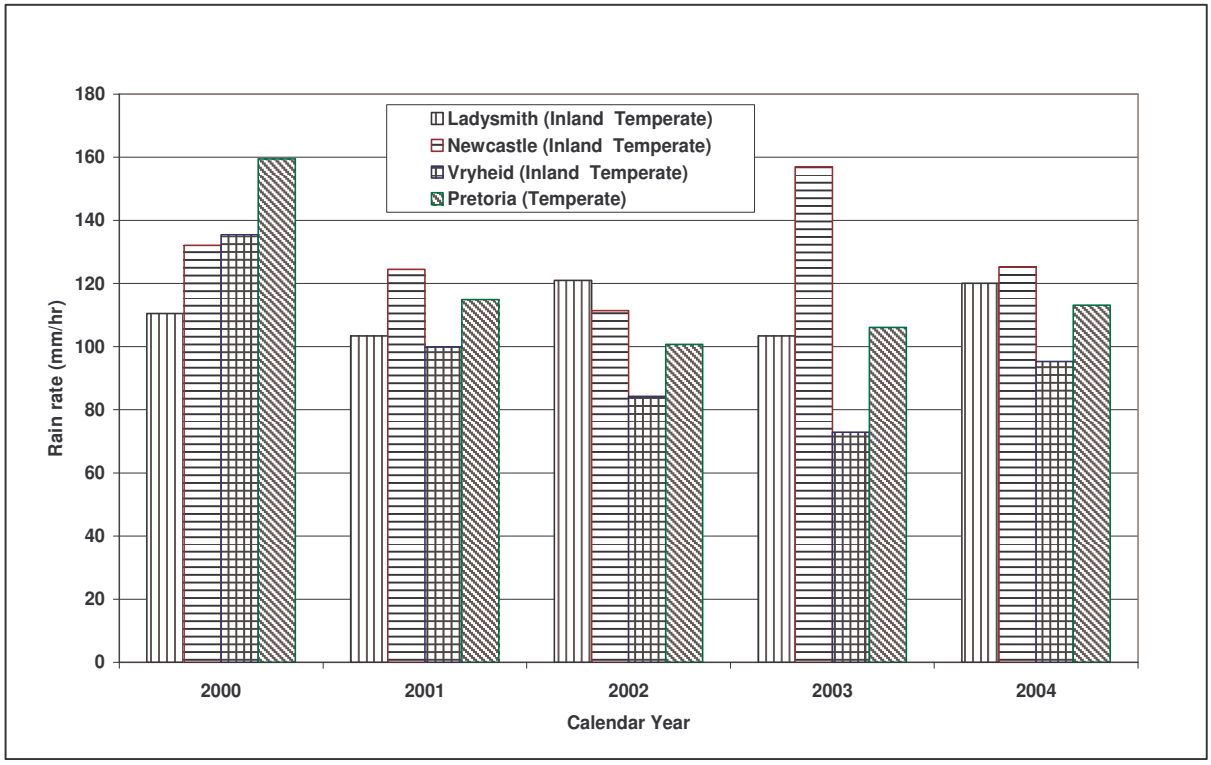

Figure 4.2: Variation in the Annual Rain Intensity (mm/h) Exceeded for 0.01% of the Time for South Africa (Temperate and Inland Temperate Regions)

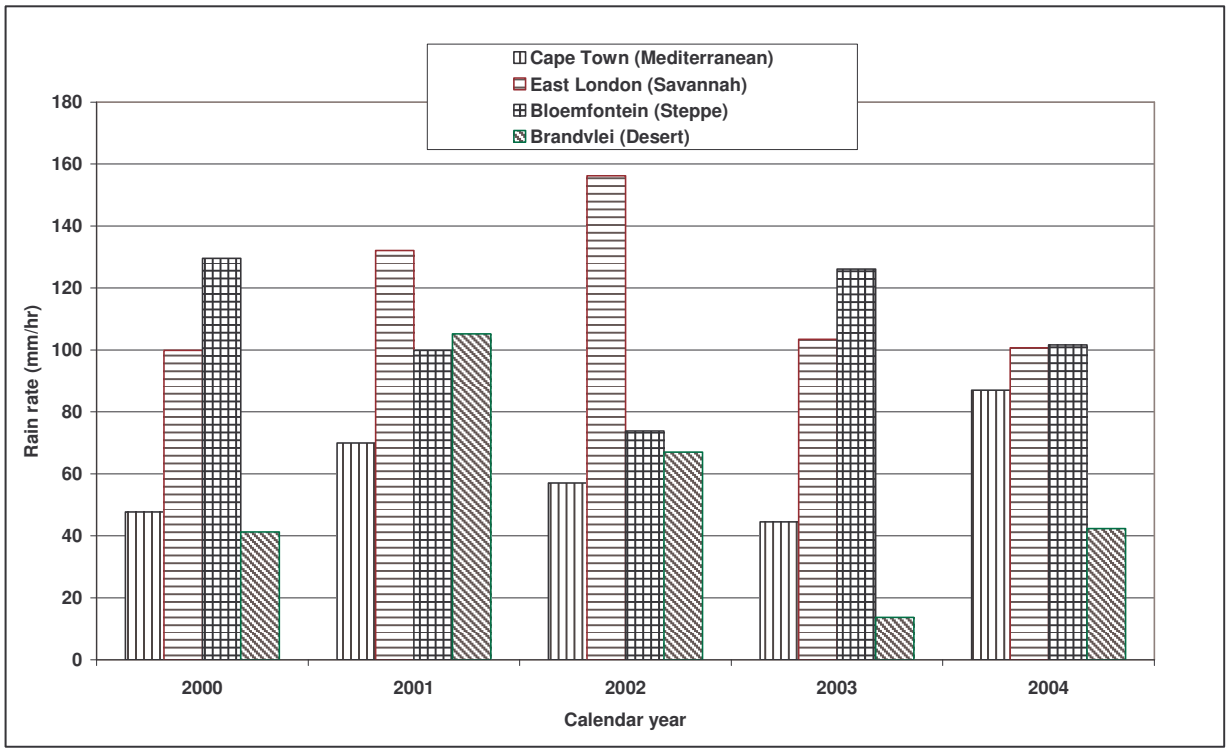

Figure 4.3: Variation in the Annual Rain Intensity (mm/h) Exceeded for 0.01% of the Time for South Africa (Mediterranean, Steppe, Savannah & Desert Regions)

The locations are then classified according to the South Africa climatic regions. Table 4.1 shows the locations where precipitation data was obtained from the South African Weather Service (SAWS), as well as the corresponding climatic categorization. The yearly one-minute integration time rain rate statistics at 0.01% exceedance for each location within the same climatic regions are compared. These give the variations in the annual rain intensity for the entire period of five years.

Table 4.1: Climatic Zone Classification in South Africa
(Source: South Africa Weather Service)

Locations	**Latitude South**	**Longitude East**	**Climatic Regions (SAWS)**
Durban	29°.97'	30°.95'	Coastal Savannah
Richards Bay	28°.78'	32°.02'	Coastal Savannah
Cape town	33°.97'	18°.60'	Mediterranean
Brandvlei	30°.47'	20°.48'	Desert
East London	33°.03'	27°.83'	Savannah
Ladysmith	28°.57'	29°.77'	Inland Temperate
Newcastle	27°.77'	29°.98'	Inland Temperate
Vryheid	27°.78'	30°.80'	Inland Temperate
Pretoria	25°.73'	28°.18'	Temperate
Bloemfontein	29°.10'	26°.30'	Steppe
Ulundi	28°.30'	31°.42'	Inland Savannah
Pietermaritzburg	29°.63'	30°.40'	Inland savannah

Tyson observed that over the period 1910-1972, much of the summer rainfall area of South Africa experienced a quasi 20-year oscillation rainfall cycle (Tyson et al., 1976). The rainfall spectrum shows a clear peak at about 20 years, as well as peaks in 2-3 and 3-4 year bands, as confirmed by South Africa climate. In Figure 4.1, Richards Bay consistently records the highest yearly rain rate in the initial three years (2000-2002), with a peak of 182.66 mm/h in 2001. Over these three years, Durban records the second highest of 139.66 mm/h in 2002, while Pietermaritzburg has a high value of 126 mm/h in

2000 and 115 mm/h in 2001. Despite the fact that Durban and Richards Bay lie in the same climatic region, there are differences in the rain intensity from year to year. The highest rain rate in the zone was recorded in the year 2004 with values of 211.38 mm/h and 202.16 mm/h for Ulundi and Pietermaritzburg, respectively. For three consecutive years, (2002 to 2004) Ulundi records a progressive increment in rain rate, as is also applicable to Pietermartzburg. And for two consecutive years, 2000 and 2001, a decrement in rain rate was recorded in both locations. A measure of differences is also noticed between the two locations in this climatic region, but the differences are not as large as that of the Coastal Savannah.

In Figure 4.2, we plot yearly rain rate variations for temperate and inland temperate regions. We observe that Newscastle and Pretoria record the two highest rates of 160 mm/h (in 2000) and 157 mm/h (in 2003), respectively. Vryheid records the lowest rates in this category, with a minimum rate of 76 mm/h in 2003. On the other hand, the rain intensity in Ladysmith appears to be roughly uniform over four years between 2001 and 2004, with a mean value of 103 mm/h. As already stated, Pretoria has a high rate of 160 mm/h in 2000, while the rain intensities for 2001 and 2004 are quite close (115 mm/h and 113 mm/h, respectively), with the corresponding values for 2002 and 2003 also remaining almost the same at 101 mm/h and 106 mm/h, respectively.

Finally, in Figure 4.3, we compare four different climatic zones, namely: Mediterranean, Savannah, Steppe and dessert. East London in the savannah zone records the highest two rates over the five years, namely, 133 mm/h in 2001 and 157 mm/h in 2002. This is followed by Bloemfontein in the Steppe zone, which records two similar highs in 2000 (130 mm/h) and 2003 (127 mm/h). Note that there is a discernible periodicity for Bloemfontein (with almost similar rates in 2000 and 2003, followed by similar ones in 2001 and 2004) and Cape Town. However, there is no obvious pattern for East London and Brandvlei (desert region). Cape Town, which lies in the Mediterranean region of South Africa, records its highest rain intensity of 87.04 mm/h in the year 2004, with rain intensities in the other years being relatively low. Rain rate in the year 2000 and the year 2003 are almost the same (47.7 mm/h and 44.5 mm/h respectively).

East London had its highest rain rate of 156.97 mm/h recorded in the year 2002, with years 2003 and 2004 having almost the same rain rates of 103.2 mm/h and 100.72 mm/h, respectively. The lowest rain rate was recorded in the year 2000 at 99.83 mm/h. Bloemfontein, which lies in the steppe region of South Africa, had its maximum rain rate of 129.54 mm/h recorded in the 2000. It is seen that the rain rate gradually decreases from 2002: in 2003, there is a rise in the rain rate to a value which is almost the same as that recorded for the year 2000, and for 2004 the rain rate value decreases again to a value close to one recorded for the 2001. Brandvlei, which lies in the desert region of South Africa, is seen to have an irregular and unpredictable type of rain intensity. On average, Brandvlei has low rain intensities as compared to other climatic regions in South Africa, with its highest peak of rain intensity of 105.2 mm/h recorded in 2001 and lowest rain rate of 13.67 mm/h recorded in 2003. It is also observed that years 2000 and 2004 have almost identical rain rate values of 41.25 mm/h and 42.34 mm/h, respectively. The 5-year rain statistics with one-minute integration time for the 12 locations in different climatic regions at 0.01% exceedance of the time are compared in Figure 4.4.

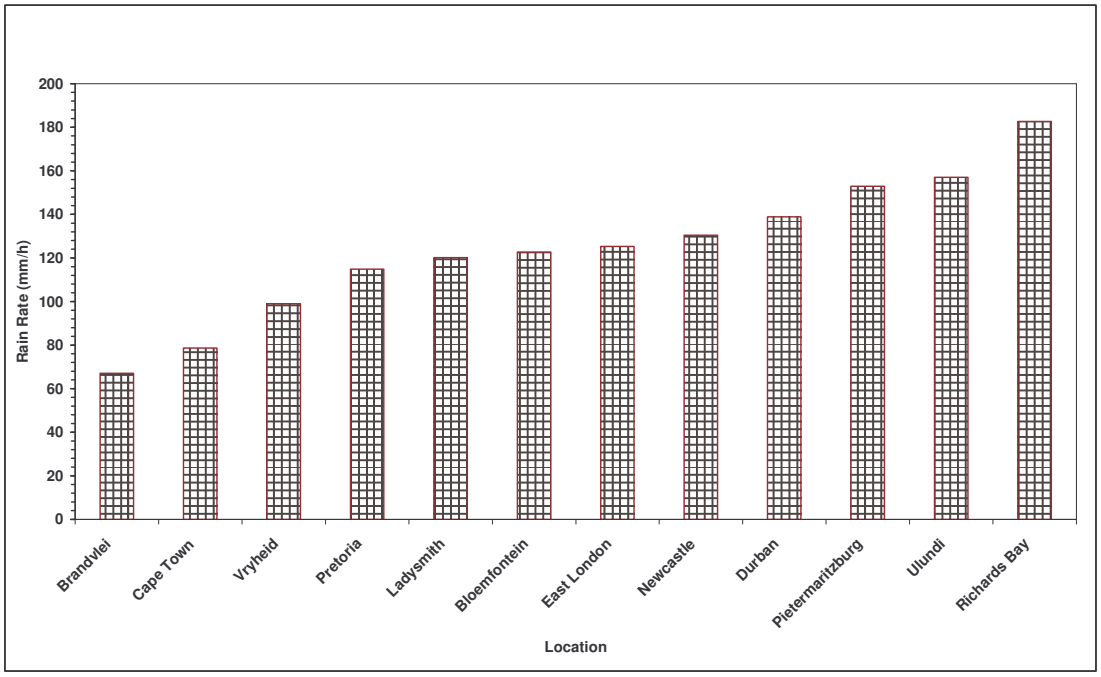

Figure 4.4. Comparison of the 5-year Rain Intensity (mm/h) for 12 locations in South Africa Exceeded for 0.01% of the Time

It is seen that Richards Bay, which lies in the coastal savannah, has the highest rain intensity, followed by Ulundi, Pietermaritzburg and Durban. Ulundi and Pietermaritzburg lie in the Inland area of the Coastal Savannah region. The high rain peaks that occur in these areas are mostly due to Indian Ocean influence in the region. The moist Indian ocean air masses which are the chief source of the rain over most of the countries gradually lose their moisture as they move towards western interior of the country. The very lowest rainfall occurs on the west coast, with Brandvlei which is found in the desert area showing the lowest rain intensity. Cape Town, which lies in the Mediterranean climate, is seen to have low rain rate, similar to that of Brandvlei which lies in the desert region of South Africa. This is because Cape Town is situated towards the western coast of South Africa, and its rainfall mostly occurs during winter (June through August), as opposed to other places in South Africa which have their rain fall during summer (November through March). One can therefore conclude that the north-eastern areas of South Africa (which has the coastal Savannah and Inland Savannah climate zones) have higher rain rates than the north-western parts (which have Mediterranean and desert climate zones).

4.1.2 Cumulative Distribution of Rain Intensities for South Africa

Cumulative distributions (CD's) of five-year one-minute rain intensities for each climatic region in South Africa are calculated based on conversion power law relation in equation 3.7 in sub-section 3.1.1 and plotted in Figure 4.5. The cumulative distribution is based on rain rate and percentages of time: the higher the rain rate the lower the corresponding percentage of time recorded, while the lower the rain intensity the higher the percentage of time. The analysis is done for single site in each of the eight climatic regions in South Africa. For Durban, at the higher time percentage of 0.1%, the rain rate recorded is 68.98 mm/h; while for the lower time percentage 0.01%, the rain rate is 138.83 mm/h. Therefore the rain intensity for time percentage differences between 0.1% to 0.01% is 69.85 mm/h. At higher time percentage of 0.1% for Pietermaritzburg, the observed rate is 79.55 mm/h, with the difference in rain intensities between 0.1% and 0.01% being 73.37 mm/h. Similarly for Newcastle, for 0.1% of time percentage the rain intensities is 63.07 mm/h and the lower time percentage the rain intensity is 130.39 mm/h. The rate

difference between 0.1% and 0.01% is 67.32 mm/h.

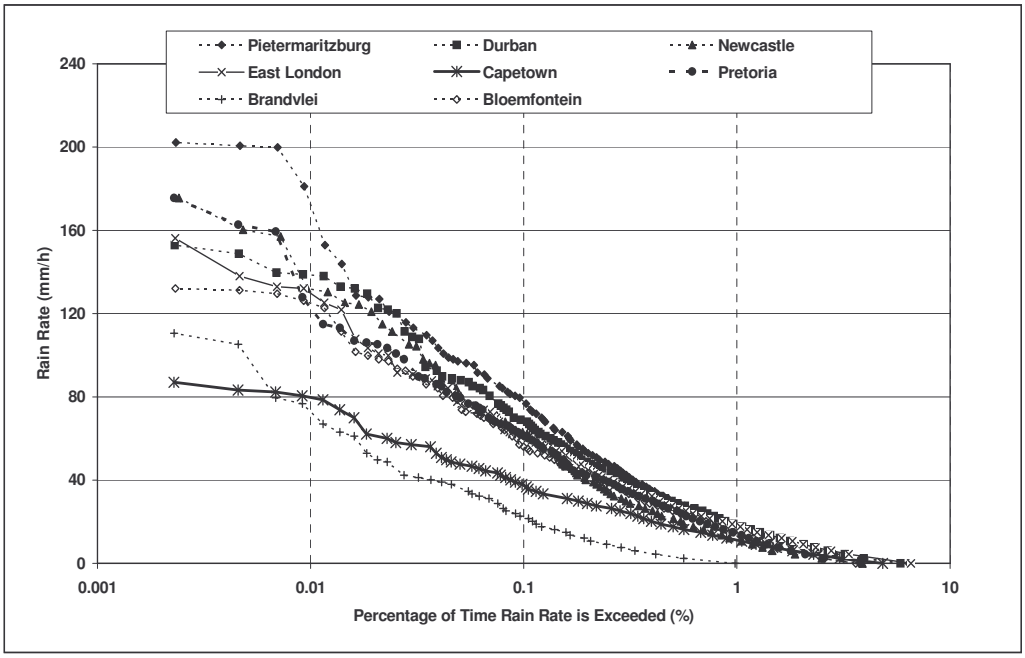

Figure 4.5: Cumulative Distribution of Rain Intensities for South Africa for an Average of 5 years

In the case of Pretoria, the distribution shows that at 0.1% the rain intensities is 61.07 mm/h and 0.01% has 114.90 mm/h. The rain rate difference between 0.1% and 0.01% of the time is 53.83mm/h. For Cape Town, we see that at the higher time percentage of 0.1% the rain intensity is 37.95 mm/h while at the lower time percentage of 0.01% the rain intensity is 78.60 mm/h. The rain intensity difference at higher and lower time percentage is 40.65 mm/h. This difference is close to that of Brandvlei. For East London, the time percentage of 0.1% has a rain intensity of 61.07% mm/h, while at 0.01% the rain intensity is 125.27 mm/h. The difference in rain intensity between 0.1% and 0.01% is 64.20 mm/h. At the higher time percentage of 0.1 % the rain intensity is similar to Pretoria. In Bloemfontein at higher percentage of 0.1%, the rain intensity is 56.01 mm/h, while at the lower time percentage of 0.01% the value is 122.70 mm/h. The difference between the higher and lower time percentage recorded gives an intensity of 66.69 mm/h. Finally, for Brandvlei, at higher percentage of 0.1% the rain intensity is 25.19 mm/h, while at the lower time percentage of 0.01%, the intensity is 67.02 mm/h. The rain intensity difference between the higher and lower time percentages is 41.83 mm/h, which is close to the difference in Cape Town.

4.2 Dynamic Rain Rate in Southern Africa using hourly rain data

In order to reliably predict rain attenuation for a given location, there is a need for studying monthly and seasonal rainfall variability, worst month and average worst month statistics of rain, and rainfall rate distribution models for site under study. In this section these are embarked upon by processing five-year rain rate data for selected sites in South Africa. The dependence of the percentage of the average year (AY) on percentage of time of the average worst month (AWM) of rainfall rate, and the obtained rainfall rate distribution models for eight regions in South Africa, are assessed by examining the root mean square (RMS), the average probability ratio (APR), and the chi-square statistic (CHI) based on measured data and the ITU-R estimations.

4.2.1 Variability of Rainfall rate distribution in South Africa

In a document posted on the website titled "South Africa Climate and Weather (SAC&W)" there are four major seasons in South Africa, namely, summer, autumn, winter and spring. The summer period (November-March) is characterized by higher rainfall rate than the other seasons. In the summer rainfall region, light orographic rains are common along the windward slope of the eastern escarpment of South Africa. Over most of the summer rainfall season, however, violent convection storms, accompanied by thunder, lightning, sudden squalls and often hail, are the source of most of the rainfall. The period between June and August (the winter period) is characterised by often long lasting and not very intense rains except along mountains, where the orographic effect may induce heavy showers according to the SAWS. Between the winter and summer rainfall regions lies a transitional area where rain comes in milder measures. Figure 4.6 shows four plots of seasonal variations of rainfall rate, while Table 4.2 displays the rainfall rate at 0.1% exceedence level for twelve stations with the four climatological seasons. The four stations were chosen based on vegetation classification and rainfall distribution behaviour. From Figure 4.6, it was observed that the seasonal variation of cumulative rain distribution for Durban, Bloemfontein, Ulundi, Pietermaritzburg, Vryheid and Brandvlei shows a maximum rainfall rate in summer and a minimum in winter. The opposite is the case for Cape Town. Newcastle, Ladysmith and Pretoria have

their maximum rainfall rate in spring (September-October) and minimum rainfall rate in winter. Finally, both East London and Richards Bay have their maximum rainfall rate in summer and their minima in spring and autumn, respectively.

4.2.2 Statistics of the worst month

Based on seasonal, month-to-month and year-to-year rain rate variability, the concept of the worst month comes in handy. This defines the worst conditions for which propagation engineers must design the radio link, which ultimately determines link availability. To address the issue of variability, ITU propagation working groups came up with the concept of worst month, as defined in Recommendation ITU-R P.581-2. Figure 4.7 shows samples of plots of cumulative distribution of month-to-month variability for four of the 12 sites discussed in Table 4.2. The month-to-month variability was observed for monthly cumulative distributions of one-minute rainfall rate. For the percentage of time at 0.1% exceedence level, the maximum difference between rainfall rates reaches 184.97 mm/h. The maximum average worst month rainfall rate observed is 211.38 mm/h for the month of February in Ulundi and the minimum average worst month rainfall rate is 7.69 mm/h for the month of June in Newcastle. The maximum average worst month spreads between January to March when summer is pronounced. The winter rainfall region is a relatively small area along the Cape's western and south-western coasts, and has a rainfall regime of Mediterranean type with a conspicuous winter maximum.

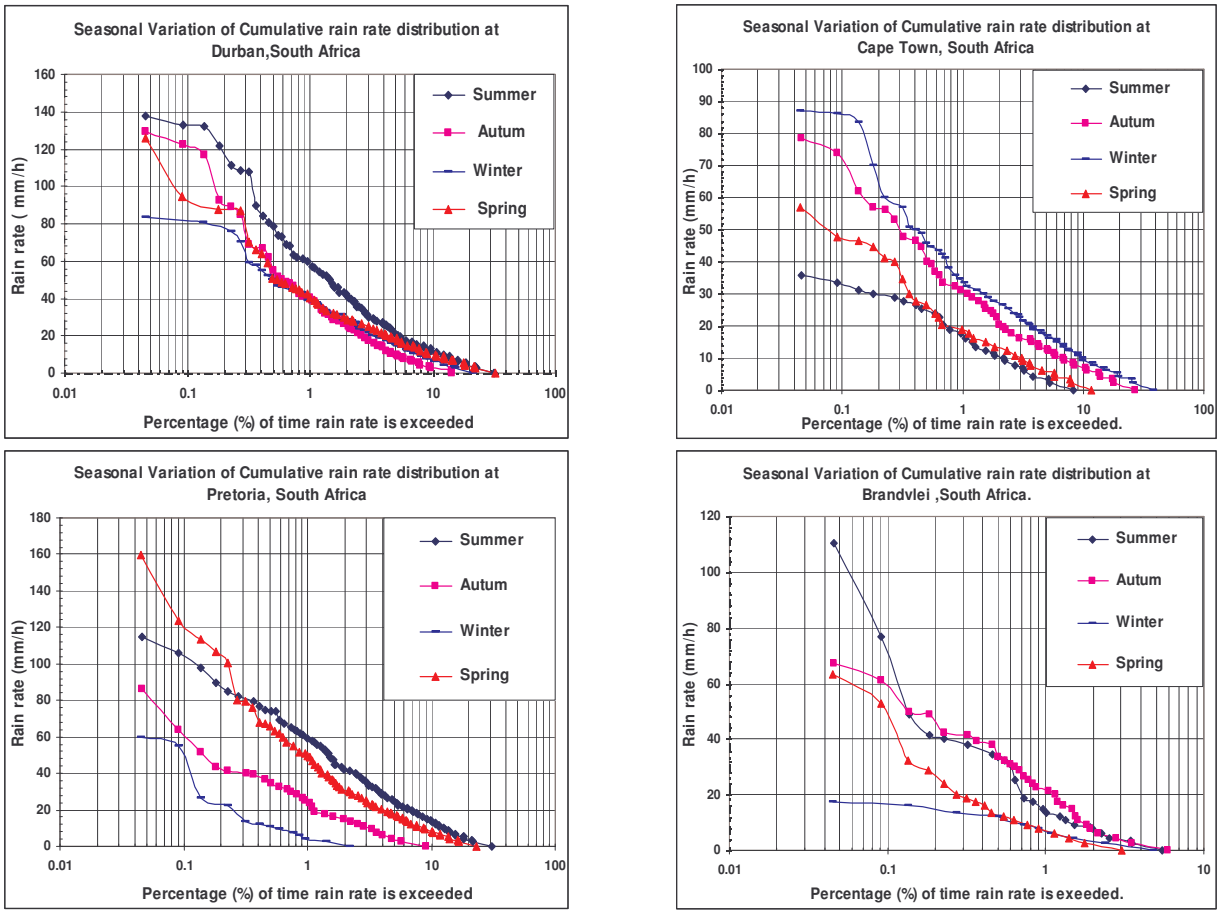

Figure 4.6: Seasonal Variation of Cumulative Distribution in SA.

Table 4.2: Seasonal variation of rain rate for 12 locations in South Africa at 0.1% exceedence

Locations	Summer	Autumn	Winter	Spring
Durban	132.94	122.7	82.32	94.4
Bloemfontein	129.54	60.07	48.76	93.49
East London	132.09	85.18	88.89	77.65
Ulundi	207.55	67.02	62.07	156.19
Richards Bay	182.66	74.80	80.49	148.8
Newcastle	124.42	60.07	48.76	175.53
Ladysmith	98.93	52.93	40.16	175.53
Pietermaritzburg	199.85	97.12	49.28	123.56
Pretoria	106.09	64.06	54.99	123.56
Vryheid	98.93	40.16	34.58	84.25
Cape Town	33.44	73.83	86.11	47.70
Brandvlei	76.7	61.07	17.2	52.93

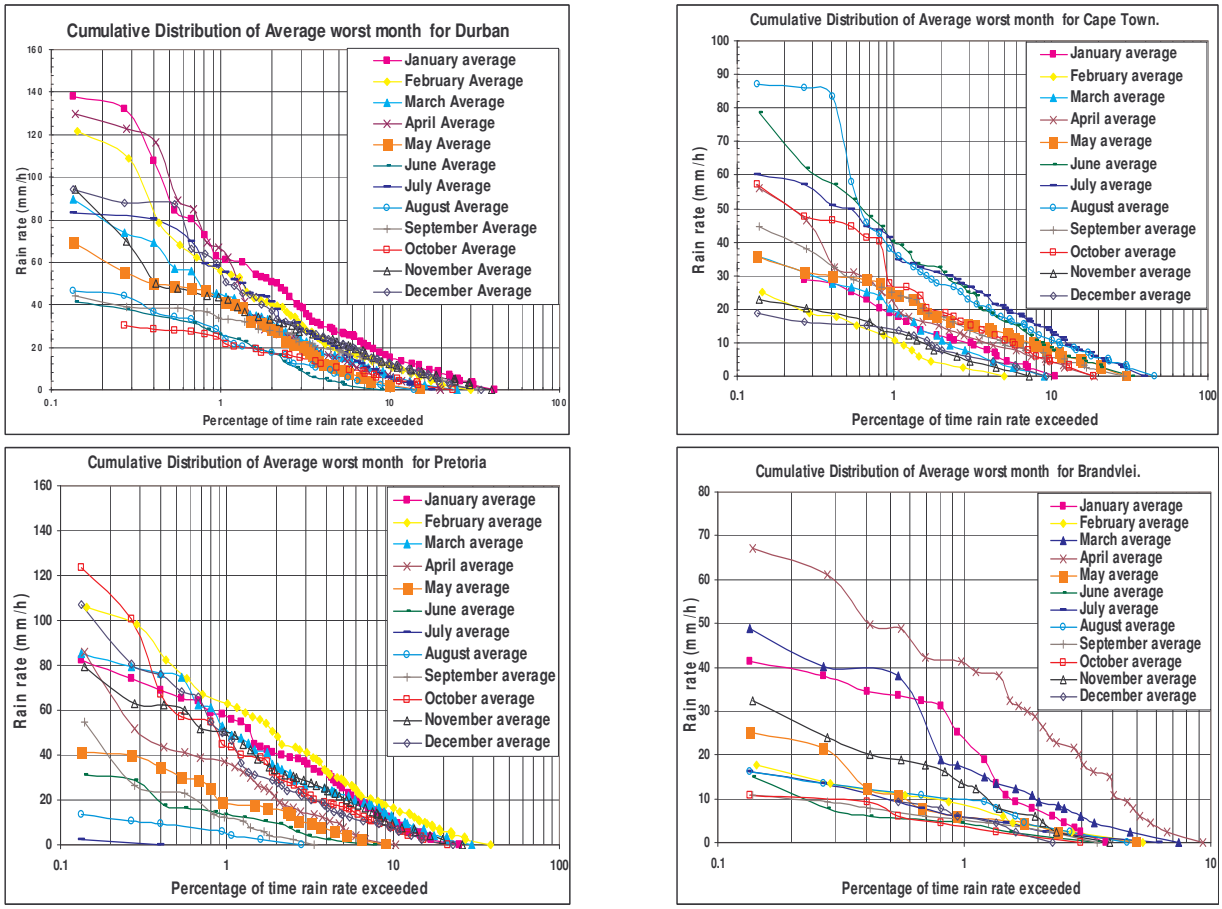

Figure 4.7: Cumulative distribution of average monthly rain rate for 4 Stations in SA

The exception is Cape Town which has its maximum average worst month rainfall rate in August and the minimum in December.

4.2.3 Relation between AY and AWM

Cumulative distributions of one-minute s rainfall rate for average year (AY) and average worst month (AWM) for the twelve stations are obtained by the statistical processing of rainfall rate data. The obtained dependence of percentage of time of the average year P_{AY} on percentage of time of the average worst month P_{AWM} for the same average one-minute rainfall rate are shown by equations (4.1) and (4.2) which is validated by using the correlation coefficient R^2.

$$P_{AY} = a\, P^{b}{}_{AWM}\ (\%) \tag{4.1}$$

$$P_{AWM} = \alpha\, P^{\beta}{}_{AY}\ (\%) \tag{4.2}$$

Here a, b, α, and β are coefficients of the equations (4.1) and (4.2). The values of the coefficients are shown in the Table 4.3. The relationship between the percentage of time of average year (P_{AY}) and average worst month (P_{AWM}) is optimized by using the root mean square (RMS) error, average probability ratio (APR), and the chi-square statistic (χ^2). The RMS error is defined by Timothy et al (2002):

$$RMS = \sqrt{1/N \sum_{i=1}^{N} (X_{est,i} - X_{mea,i})^2} \tag{4.3}$$

Here, N is the number of data points, and X_{est} and X_{mea} are the estimated and measured quantities, respectively. APR is given by Timothy et al (2002):

$$APR = \frac{1}{N} \sum_{i=1}^{N} \left(\frac{P_{est,i}}{P_{mea,i}} \right) \tag{4.4}$$

Here, P_{est} and P_{mea} denote the cumulative probabilities of estimated and measured quantities, respectively. Both RMS and APR enable us to optimize the proposed relations and models while the chi-square (CHI) statistic is used to confirm the acceptance or rejection of the null hypothesis of the relations/models in question. The statistic, χ^2, is defined as:

$$\chi^2 = \sum_{i=1}^{N} \frac{\left(X_{est,i} - X_{mea,i}\right)^2}{X_{est,i}} \tag{4.5}$$

The above measure specifies a probability, or "significance level", α. This probability defines, for a given application, what constitutes a significant enough deviation from expected or modeled behaviour to justify rejection of the hypothesis or model. A good model should give an APR close to unity and a minimum RMS error (ideally, close to 0.0). It should also give a χ^2 statistic that is lower than the threshold t_α for a defined probability value α for N-1 degrees of freedom (DF). Typically α is chosen to be 1% or 5%. In this work, $\alpha = 1\%$ is considered.

Table 4.3: Coefficients and correlation coefficients validity for approximation (4.1) and (4.2) for rain rate range $0.01 \leq R \leq 212$

Locations	a	b	α	β	R^2
Durban	0.2217	0.9593	4.7465	1.0353	0.9931
Bloemfontein	0.2188	0.9789	4.7097	1.0197	0.9981
East London	0.2542	0.9978	3.9358	1.0007	0.9985
Ulundi	0.2252	0.9969	4.0414	1.0016	0.9985
Richards Bay	0.2593	0.9631	4.0561	1.0373	0.999
Newcastle	0.2201	1.030	4.3085	0.9662	0.9958
Ladysmith	0.2448	0.8946	4.7797	1.1125	0.9952
Pietermaritzburg	0.2635	0.9484	4.0414	1.0481	0.9985
Pretoria	0.2298	0.9848	4.4291	1.0128	0.9974
Vryheid	0.2161	0.963	4.8787	1.0357	0.9973
Cape Town	0.2183	1.0197	4.4329	0.979	0.9983
Brandvlei	0.2016	1.0014	4.9488	0.9986	1.0000

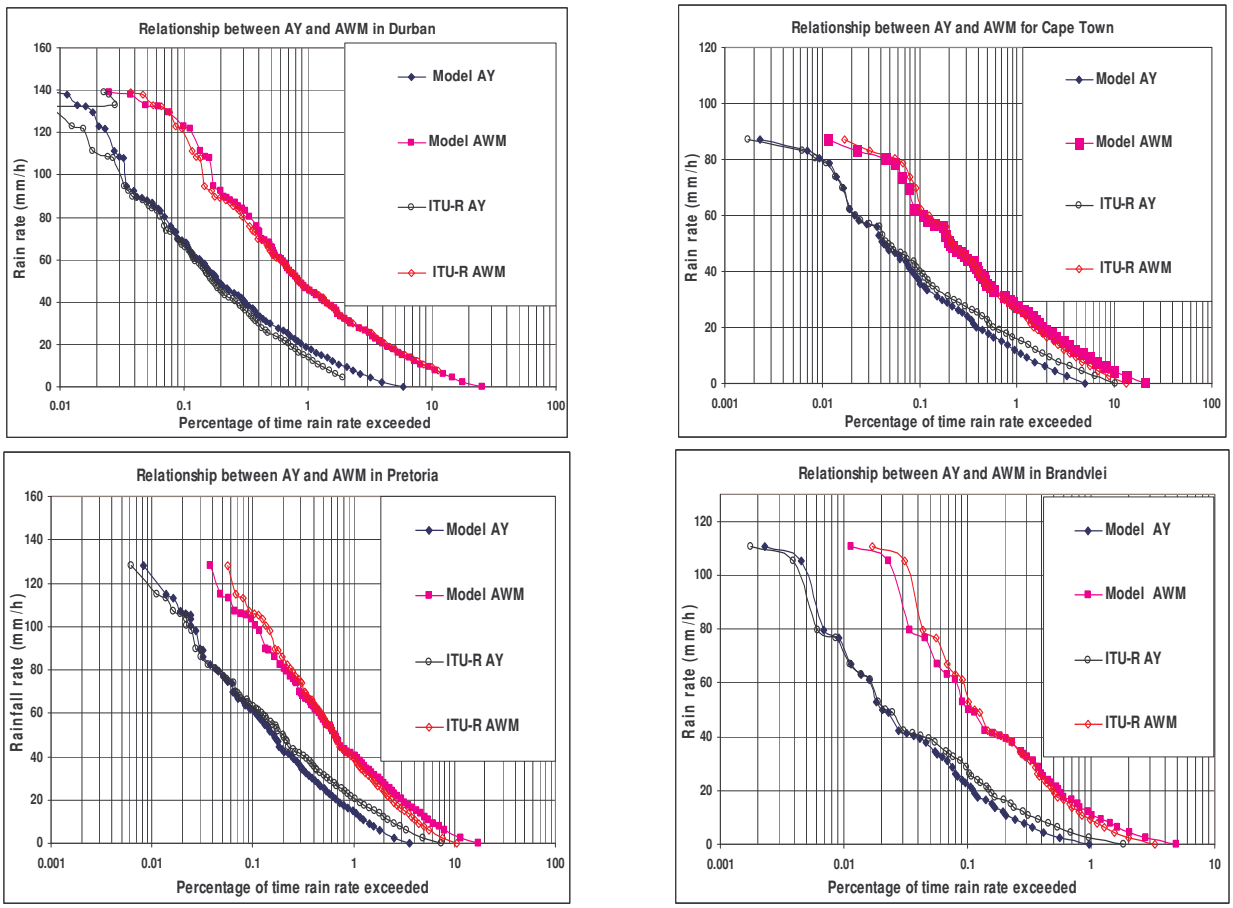

Fig.4.8: Modeled and ITU-R Cumulative Distributions of Rain rate for AY and AWM for four sites

Figure 4.8 shows samples of modelled and ITU-R cumulative distributions of rainfall rates for average year and average worst month for four stations. Table 4.4 shows a comparison between the derived model and ITU-R model percentage of time of AY and AWM. The RMS, APR and χ^2 values give the best value for the relations in all the sites. The RMS and APR show that the modelled relations are appropriate for obtaining relations between percentage of time of AY and AWM. Note that the threshold t_α for the chosen $\alpha = 1\%$ are as follows: t_α=112.3 for 80 DF, 100 for 70 DF, 76 for 50 DF, 63.7

Table 4.4: comparison between the models, measured data and ITU-R cumulative distributions of rain intensities for AY and AWM for 8 stations in South Africa

.

Sites		Model AY	Model AWM	ITU-R AY	ITU-R AWM
Durban	RMS	0.031	0.12	0.37	0.64
	APR	1.007	0.95	0.86	0.95
	CHI	0.24	3.75	8.35	8.82
Bloemfontein	RMS	0.005	0.028	0.28	0.48
	APR	1.029	1.034	1.041	0.885
	CHI	1.029	0.031	3.92	2.57
East London	RMS	0.055	0.23	1.015	1.52
	APR	1.01	1.024	1.15	1.088
	CHI	0.021	0.088	1.85	1.20
Newcastle	RMS	0.004	0.022	0.138	0.22
	APR	1.015	0.99	1.019	1.05
	CHI	0.0085	0.04	2.45	1.36
Pietermaritzburg	RMS	0.016	0.081	0.22	0.43
	APR	1.021	1.024	1.085	1.086
	CHI	0.059	0.29	3.91	4.07
Pretoria	RMS	0.0076	0.035	0.17	0.28
	APR	1.017	1.019	1.048	0.971
	CHI	0.021	0.095	3.066	1.92
Cape Town	RMS	0.0083	0.038	0.14	0.23
	APR	0.995	1.011	1.0124	1.242
	CHI	0.009	0.041	1.56	0.92
Brandvlei	RMS	0.0002	0.0008	0.029	0.045
	APR	1.034	1.033	1.066	1.091
	CHI	0.025	0.088	1.85	1.20

for 40DF, and t_α=50.9 for 30 DF. In Table 4.4, the value of N ranges between 30 and 80. As expected, from Table 4.4, it is observed that the AY and AWM models give a closer fit to the measured data than the ITU-R curves for AY and AWM. This is immediately apparent from the CHI and RMS values.

4.2.4 Initial Proposed rain rate model using Moupfouma approach

Designing line-of-sight (LOS) or satellite link systems needs yearly rainfall rate statistics for several percentages of time in the locations of interest. Thus it is necessary to estimate, within an average year, the time percentage during which attenuation due to rain is significant, and consequently the future link performance and availability. There are several rainfall rate climatological models for short integration-time and long integration-time statistics of precipitation as presented in sections 2.5 and 2.6 of chapter two.

Rainfall rate measurements obtained for eight regions in South Africa over a period of five years were processed to derive regional empirical models at one-minute integration time, as supported by ITU-R. The three parameters approach of equation (2.34) as found in the sub-section 2.6.2 was used to compute the distributions for the eight selected sites. The results provided in Table 4.5 are a good fit of the rainfall rate probability distribution function observed in various sites in South Africa. The values of constants $a, b,$ and u, shown in Table 4.5, were used in equation (2.34) of chapter two to plot cumulative distributions for the eight sites, as displayed in the Figure 4.9.

Table 4.5: Estimated values of a, b, and u for eight regions in South Africa (2000-2004)

Name	a	b	u	$R_{0.01}$
Pietermaritzburg	0.014	$5.2956\ R_{0.01}^{-0.4637}$	0.021	152.92
East London	0.017	$4.1113\ R_{0.01}^{-0.3675}$	0.021	125.27
Bloemfontein	0.81	$4.2935\ R_{0.01}^{-0.4004}$	0.02018	126.13
Brandvlei	0.016	$6.9709\ R_{0.01}^{-0.5422}$	0.022	73.0
Cape Town	0.013	$6.3322\ R_{0.01}^{-0.512}$	0.0276	80
Newcastle	0.85	$5.7062\ R_{0.01}^{-0.4848}$	0.017	130
Pretoria	0.0117	$6.0236\ R_{0.01}^{-0.4998}$	0.0246	114.9
Durban	0.0115	$5.555\ R_{0.01}^{-0.477}$	0.0247	137.99

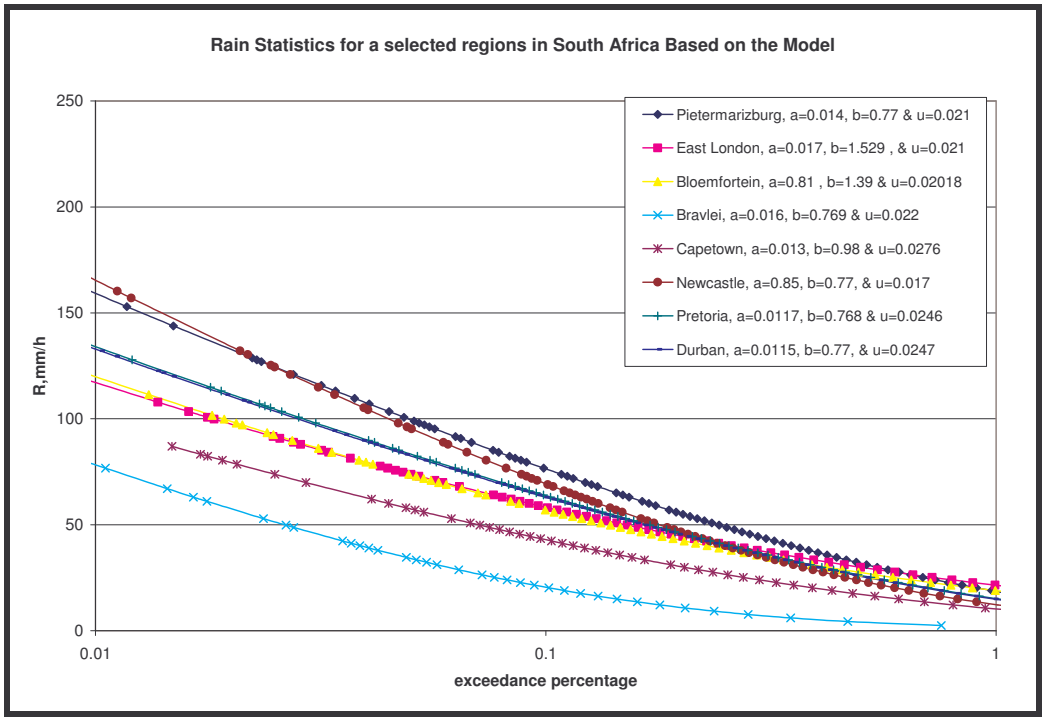

Figure 4.9: Rain Statistics for selected regions in South Africa based on the proposed model.

4.2.5 Evaluation of the *b* Parameters for All Regions

The parameter b is plotted against the value of rainfall rate exceeded 0.01% of time for each location; the corresponding points can be fitted by the relationships obtained for all the computed locations given in Table 4.5. By using linear regression for different $R_{0.01}(mm/h)$, the values of b for different locations are obtained for South Africa. The results show fairly good agreement with the ITU-R (Moupfouma) model in some locations that have high rain intensities, and very good agreement with location that have low rain intensities e.g. Brandvlei. It may also be seen that for higher rain rate (above 100 mm/h) there is a rather sizeable difference between the predicted results and experimental values. This is not surprising since the accuracy of the model proposed here depends on the conversion factor of the rain data, especially for the high rain rate for which measurement inaccuracies may occur [Chi-Huei et al; 2005].

4.3 Improvements on the new Proposed Rain Rate Model for South Africa

In the initial attempt to model rain rate distribution for South Africa, a general conversion factor was used. The conversion factor which was originally based on the available one-minute and hourly data was used to propose the model. Fashuyi *et al*, (2006) and Owolawi and Afullo (2007a) employed the power law expression to convert available 60-minute rain rate to a one-minute equivalent for the twelve South African sites. This modelling theory was based on the approach employed by Moupfouma and Dereffye (1982) in which the relative values were determined for eight sites in South Africa. However, these current studies improve on the limitations of that initial proposed rain rate model which may not be adequate in describing the rain rate due to the following reasons:

- Lack of one-minute rain rate to carry out conversion processes using power laws for the entire country and surrounding islands;
- Inadequate rain data to develop the model that is less than the ten years;

- Fitting of the rain rate data with other established rain rate models may lead to the concession of the model parameters.

In this new proposed approach, all these factors are taken into consideration and are properly and adequately addressed. The current proposal uses a maximum likelihood estimator to fit different statistical distributions. The work presented is based on five-minute rainfall data converted to a one-minute equivalent using a newly developed hybrid method discussed in chapter three. There are three major objectives of the new approach for which this section is presented. Firstly, to develop a rainfall rate model based on the maximum likelihood method (ML); secondly, to develop rainfall rate contour maps at 0.01% percentage of exceedence; and thirdly, to re-classify the ITU-R and Crane rain zones for the Southern Africa region.

The theoretical background of probability distribution of rainfall rate with their respective maximumu likelihood estimator methods are discussed in Appendix A of this thesis.

4.3.1. Application of Probability Model on Estimated One-minute Rainfall Rate

Figures 4.10a and 4.10b show sample histograms of one-minute integration time of rainfall rate estimated from its equivalent five-minute rainfall data for a period of ten years. This data was obtained from the South African Weather Services. As aforementioned, the three most commonly used distributions to describe the rain rate distribution patterns are Weibull, Lognormal and Gamma. The probability density functions plots of each distribution are superimposed on each histogram as shown in Figures 4.10a and 4.10b. This was done for twenty-one stations in South Africa and two surrounding Islands. The distributions are based on the maximum likelihood estimation method as described for each distribution in the appendix A of this thesis. Each of the distribution parameters for each site is estimated using MLE as presented in Table 4.6. The results of the table are based on equation (A.10) for Weibull distribution, equations (A.13) and (A.14) for lognormal distribution, and finally equations (A.19) to (A.21) for Gamma distribution. It is observed that the three distributions describe the rainfall rate patterns fairly well.

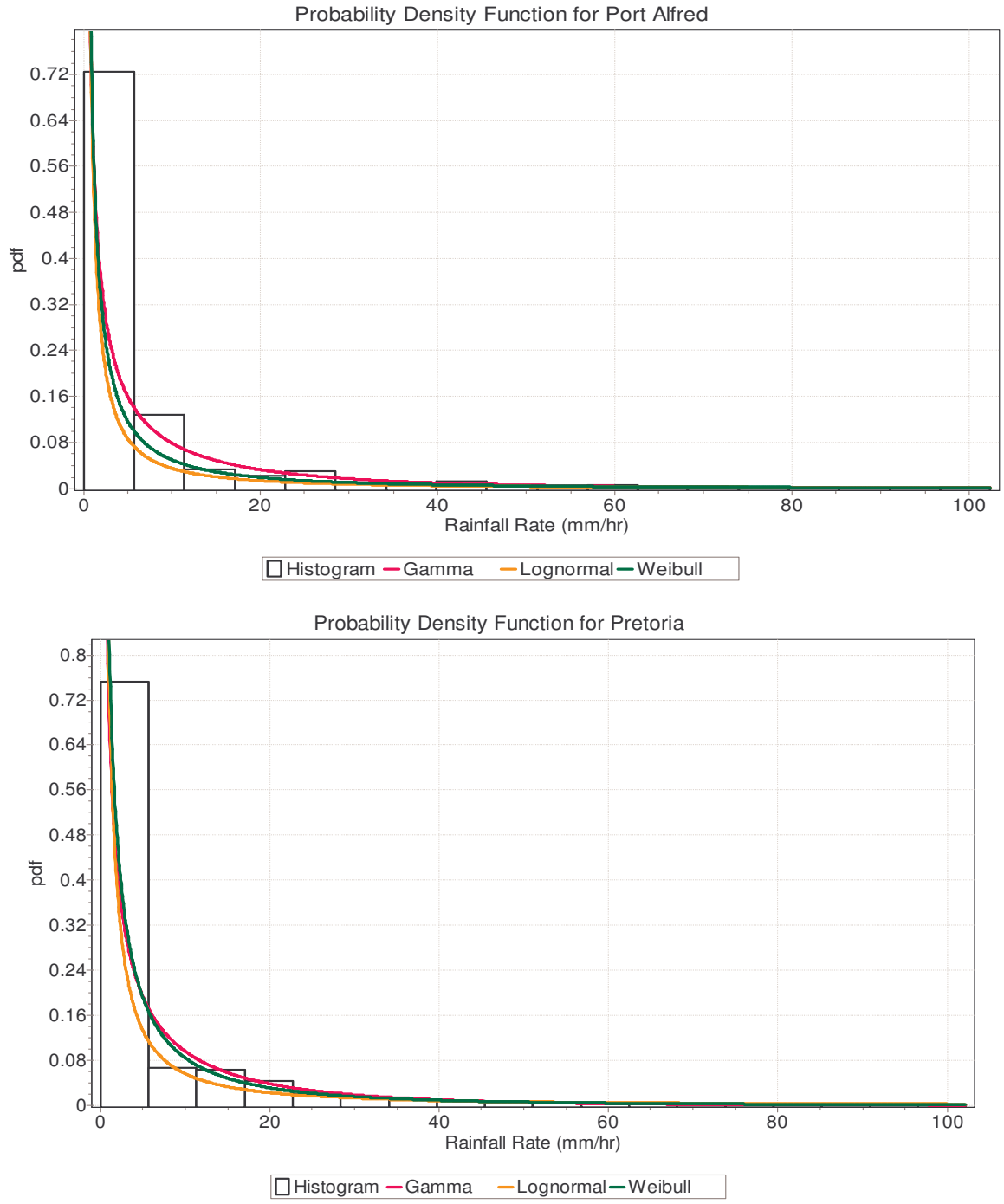

Figure 4.10a: Sample histograms with Gamma, Lognormal and Weibull probability density function for Port Alfred and Pretoria

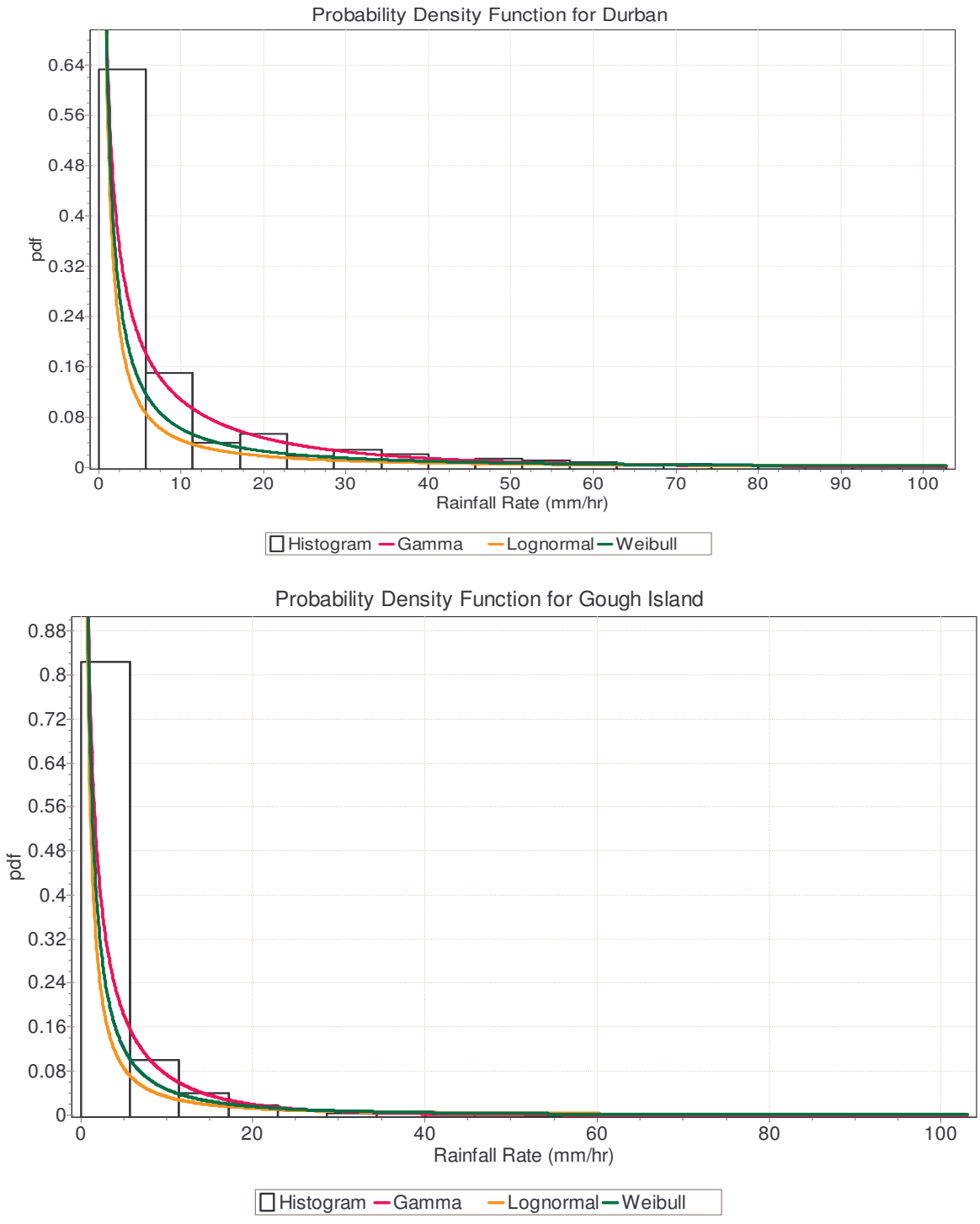

Figure 4.10b: Sample histograms with Gamma, Lognormal and Weibull probability density function for Durban and Gough Island

Table 4.6. Estimates of distribution parameters for the three distributions

Location	W-B Parameters	L-G Parameters	G-M Parameters
Port-Alfred	$\hat{\alpha}=0.31\ \hat{\beta}=1.26$	$\hat{\sigma}=1.03\ \hat{\mu}=1.52$	$\hat{\alpha}=0.18\ \hat{\beta}=39.87$
Bisho	$\hat{\alpha}=0.31\ \hat{\beta}=1.40$	$\hat{\sigma}=1.03\ \hat{\mu}=1.35$	$\hat{\alpha}=0.16\ \hat{\beta}=53.64$
Fort Beaufort	$\hat{\alpha}=0.38\ \hat{\beta}=1.77$	$\hat{\sigma}=1.03\ \hat{\mu}=0.90$	$\hat{\alpha}=0.14\ \hat{\beta}=41.58$
Umtata	$\hat{\alpha}=0.32\ \hat{\beta}=1.90$	$\hat{\sigma}=1.03\ \hat{\mu}=1.04$	$\hat{\alpha}=0.24\ \hat{\beta}=39.87$
Pretoria	$\hat{\alpha}=0.46\ \hat{\beta}=3.45$	$\hat{\sigma}=2.18\ \hat{\mu}=0.06$	$\hat{\alpha}=0.27\ \hat{\beta}=25.66$
Bethlehem	$\hat{\alpha}=0.34\ \hat{\beta}=3.25$	$\hat{\sigma}=2.63\ \hat{\mu}=0.56$	$\hat{\alpha}=0.29\ \hat{\beta}=37.46$
Durban	$\hat{\alpha}=0.71\ \hat{\beta}=9.40$	$\hat{\sigma}=1.31\ \hat{\mu}=1.54$	$\hat{\alpha}=0.34\ \hat{\beta}=35.56$
Spring	$\hat{\alpha}=0.37\ \hat{\beta}=4.61$	$\hat{\sigma}=2.15\ \hat{\mu}=0.03$	$\hat{\alpha}=0.24\ \hat{\beta}=39.87$
Ladysmith	$\hat{\alpha}=0.44\ \hat{\beta}=3.45$	$\hat{\sigma}=1.83\ \hat{\mu}=0.08$	$\hat{\alpha}=0.23\ \hat{\beta}=34.99$
Pietermaritzburg	$\hat{\alpha}=0.41\ \hat{\beta}=2.88$	$\hat{\sigma}=1.86\ \hat{\mu}=0.31$	$\hat{\alpha}=0.19\ \hat{\beta}=41.70$
Tshipise	$\hat{\alpha}=0.43\ \hat{\beta}=3.50$	$\hat{\sigma}=1.94\ \hat{\mu}=0.12$	$\hat{\alpha}=0.31\ \hat{\beta}=26.38$
Ermelo	$\hat{\alpha}=0.42\ \hat{\beta}=3.20$	$\hat{\sigma}=1.94\ \hat{\mu}=0.22$	$\hat{\alpha}=0.23\ \hat{\beta}=36.40$
Cape Town	$\hat{\alpha}=0.28\ \hat{\beta}=0.47$	$\hat{\sigma}=0.94\ \hat{\mu}=1.62$	$\hat{\alpha}=0.17\ \hat{\beta}=20.73$
Beaufort	$\hat{\alpha}=0.67\ \hat{\beta}=6.28$	$\hat{\sigma}=1.39\ \hat{\mu}=1.09$	$\hat{\alpha}=0.32\ \hat{\beta}=26.80$
Cape Point	$\hat{\alpha}=0.32\ \hat{\beta}=1.03$	$\hat{\sigma}=1.06\ \hat{\mu}=1.58$	$\hat{\alpha}=0.18\ \hat{\beta}=32.50$
Rustenburg	$\hat{\alpha}=0.35\ \hat{\beta}=1.71$	$\hat{\sigma}=1.53\ \hat{\mu}=0.27$	$\hat{\alpha}=0.31\ \hat{\beta}=28.11$
Klerksdorp	$\hat{\alpha}=0.79\ \hat{\beta}=5.27$	$\hat{\sigma}=1.09\ \hat{\mu}=1.06$	$\hat{\alpha}=0.31\ \hat{\beta}=19.85$
Kimberley	$\hat{\alpha}=0.30\ \hat{\beta}=1.61$	$\hat{\sigma}=1.08\ \hat{\mu}=1.48$	$\hat{\alpha}=0.24\ \hat{\beta}=30.78$
Upinton	$\hat{\alpha}=0.64\ \hat{\beta}=2.97$	$\hat{\sigma}=1.28\ \hat{\mu}=0.38$	$\hat{\alpha}=0.17\ \hat{\beta}=27.14$
Gough Island	$\hat{\alpha}=0.35\ \hat{\beta}=2.55$	$\hat{\sigma}=1.56\ \hat{\mu}=0.77$	$\hat{\alpha}=0.33\ \hat{\beta}=24.20$
Marion Island	$\hat{\alpha}=0.42\ \hat{\beta}=1.15$	$\hat{\sigma}=1.31\ \hat{\mu}=1.08$	$\hat{\alpha}=0.21\ \hat{\beta}=16.55$

4.4 Comparison and Goodness of Fit Test of the Distributions with Existing Models

In this section, the root mean square method is applied to test the goodness-of-fit and robustness of the proposed models (that are based on statistical distributions) with Weibull, lognormal and Gamma rainfall distribution models. In addition, a Chi-square test is carried out on all twenty-three sites to confirm acceptance or rejection of the hypothesis in both the distributions and existing models. Figures 4.11a and 4.11b show a comparison of the rainfall rate at equal percentage of exceedence for all selected stations. The percentage probability of exceedence chosen is based on the ITU-R specification range of 1% to 0.001%. Estimated rainfall rate is compared with distributions such as two-parameter Weibull (W-B), two-parameter lognormal (L-G), two-parameter Gamma (G-M). The estimated rainfall rate is also compared with existing models such as Rice-Holmberg (R-H), ITU-R P.837-1, P.837-5, Crane Global model (C-R), Moupfouma and Martin for tropical/sub-tropic (M-ST) and temperate (M-TE).

Figures 4.11a and 4.11b show that the estimated rainfall rate distribution patterns are similar in shape when compared with the described distributions and existing models except in the case of Rice-Holmberg whose distribution is almost linear in shape. The only sites that Rice-Holmberg distribution describes properly are Gough Island, Marion Island, Upington and Klerksdop. ITU-R recommendadtions P.837-1 and P.837-2 give the same pattern distribution of estimated rainfall but do not properly fit into the data (especially that of ITU-R P.837-1). The ITU-R P.837-5, that is currently implemented, gives a better description of sites such as Pretoria, Ermelo, Cape Town, and the two Islands. These mentioned locations may be sample sites for ITU-R as well as Crane Global for model classification of rain climatic zone for South Africa and the surrounding Islands. In this work, both Weibull and Gamma distributions show a better description of the estimated rainfall rate distribution for the majority of the selected sites; the Crane distribution model shows reasonably acceptable distribution in some sites such as Pretoria and Cape Town.

Tables 4.7 and 4.8 show the statistical analysis carried out on twenty-one stations using the two statistical optimization methods. Table 4.7 shows the numeric results of root mean square (RMS). The average RMS values indicate that the Gamma model has the best performance with about 4.23% of the total RMS, while Rice-Holmberg model has the least performance with 19.36% of the total RMS. W-B, M-TE, and M-ST have percentage values of less than 15% of total RMS values. The ITU-R 1, ITU-R 2 and C-R have percentage values of between 10% and 17% of total RMS values. Table 4.8 shows the comparison of the performance of the models through the Chi-square results for 40 degrees of freedom, the threshold for 1% significance is 63.7. A small Chi-square value corresponds to a better fit of the distribution or model.

Table 4.8 shows that the Gamma distribution gives the lowest χ^2 statistics for 76% of the stations (16 out of 21). For Pretoria, the best distribution is Weibull, followed closely by ITU-R (5) and Gamma. The only other serious exception is Beaufort, the only site at which the Gamma distribution hypothesis is rejected; instead, the preferred distribution is ITU-R (5), followed by the Crane model. Thus, the Gamma model best suits the Southern African region, with an average χ^2 statistic of 10.8 over the 21 stations. The next distribution model is the Weibull, with an average χ^2 statistic of 19.85. The other models give average χ^2 statistics of above 55, which is rather too close to the threshold of 63.7 to be acceptable.

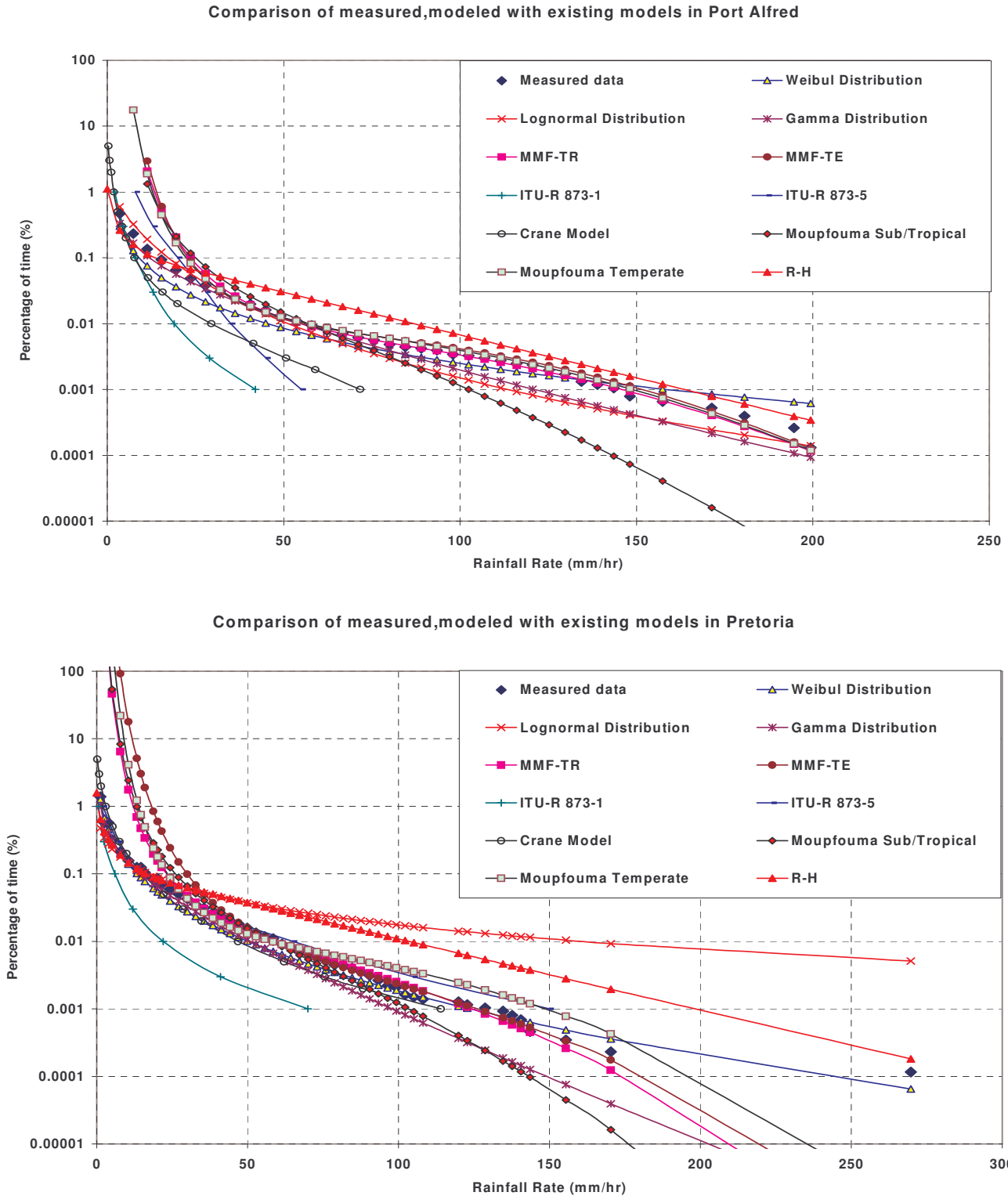

Figure 4.11a: Comparison samples of estimated one-minute rainfall rate with the distributions and existing models

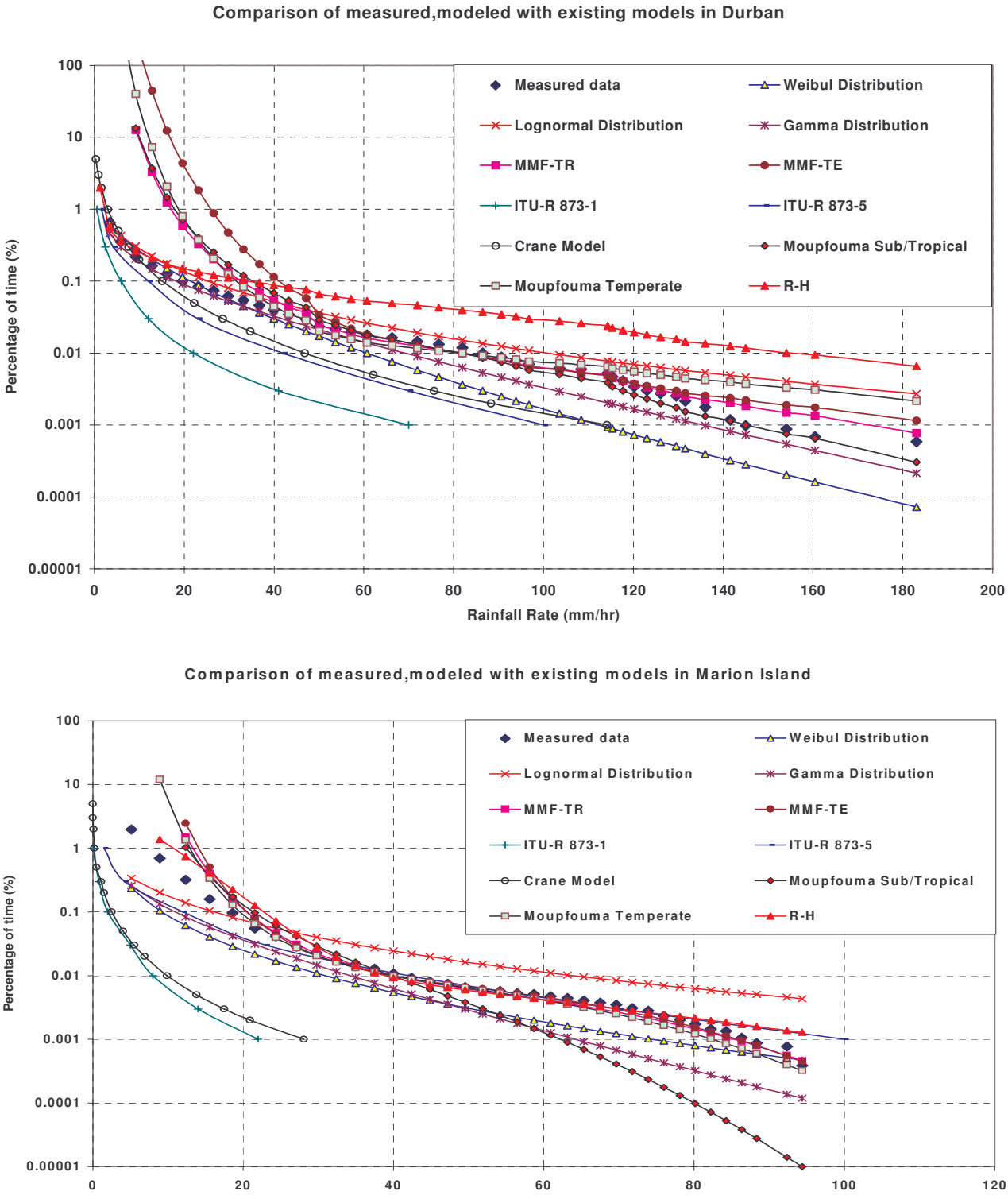

Figure 4.11b: Comparison samples of estimated one-minute rainfall rate with the distributions and existing models

Table 4.7 Comparison using Root Mean Square Error

Location	W-B	L-G	G-M	R-H	ITU-R 1	ITU-R5	C-R	M-ST	M-TE
Port-Alfred	8.366	16.273	11.239	17.04	53.83	44.00	38.78	11.43	6.13
Bisho	13.11	35.18	12.29	14.62	64.60	55.15	41.72	33.18	13.85
Fort Beaufort	14.54	42.48	13.09	15.89	34.71	40.38	37.23	20.07	10.57
Umtata	8.49	40.68	7.42	16.05	38.52	43.35	33.09	14.34	9.72
Pretoria	5.47	57.47	7.54	33.06	27.31	6.92	8.88	7.86	9.71
Bethlehem	29.80	92.62	8.60	45.80	61.49	15.11	46.99	11.69	32.77
Durban	22.34	64.50	10.14	85.26	54.28	34.85	29.30	11.31	24.04
Spring	19.33	81.49	11.76	88.98	15.96	40.64	16.22	16.22	13.81
Ladysmith	11.40	60.11	13.05	68.77	45.78	15.47	15.58	12.02	23.44
Pietermaritzburg	22.89	36.74	24.64	27.28	59.96	40.49	33.96	19.40	14.64
Tshipise	12.11	57.06	5.09	48.35	17.26	23.51	17.42	15.07	10.93
Ermelo	12.92	73.19	12.83	78.45	47.31	8.55	47.31	11.32	21.11
Cape Town	15.54	13.46	2.30	56.02	18.27	2.59	2.89	9.71	2.79
Beaufort	9.43	61.11	14.85	53.56	26.42	8.38	11.29	13.30	7.56
Cape Point	11.26	13.45	2.85	69.52	33.48	16.12	18.29	8.55	14.27
Rustenburg	11.93	48.67	2.58	50.63	32.50	16.89	20.09	7.44	14.05
Klerksdorp	17.32	6.15	5.14	20.01	18.38	28.87	6.20	15.06	7.71
Kimberley	22.84	5.0	4.83	73.59	32.13	16.72	19.82	17.33	9.60
Upinton	23.75	14.89	7.42	18.20	21.20	26.32	9.71	17.28	20.88
Gough Island	3.39	5.13	3.48	6.31	17.40	7.27	13.33	6.73	7.96
Marion Island	13.06	48.24	14.10	4.69	39.32	7.24	36.46	14.61	4.65

Table 4.8 Comparison using Chi-Square Statistics

Location	W-B	L-G	G-M	R-H	ITU-R 1	ITU-R5	C-R	M-ST	M-TE
Port-Alfred	10.73	18.42	7.30	28.37	164.21	129.99	90.14	60.36	50.27
Bisho	9.91	55.43	7.32	34.39	196.27	150.85	97.88	106.99	66.52
Fort Beaufort	12.70	97.83	8.77	30.42	71.93	92.90	79.02	102.32	80.86
Umtata	8.76	94.75	3.67	23.62	95.85	108.76	68.10	87.81	72.66
Pretoria	4.19	260.07	4.84	90.85	73.86	4.44	8.47	42.26	41.63
Bethlehem	11.07	347.0	4.83	110.62	143.09	17.12	99.49	19.09	52.95
Durban	26.47	179.63	6.02	384.15	176.51	73.60	53.66	103.92	104.60
Spring	19.34	323.37	8.10	490.58	21.66	490.58	21.66	100.69	79.06
Ladysmith	11.76	167.60	11.47	269.70	139.98	16.73	17.29	86.90	105.06
Pietermaritzburg	34.08	228.08	32.33	223.70	189.78	82.93	56.85	86.61	73.93
Tshipise	18.34	249.72	12.54	157.16	30.15	65.89	112.34	194.32	174.22
Ermelo	14.72	263.47	11.85	352.73	148.09	5.72	148.09	105.30	194.27
Cape Town	19.51	42.00	1.37	470.88	34.86	2.06	1.57	13.84	6.17
Beaufort	51.99	350.97	68.69	214.34	59.45	7.97	12.20	53.85	41.46
Cape Point	9.57	16.94	1.13	548.42	89.90	27.20	31.14	27.60	35.51
Rustenburg	17.98	132.29	0.65	156.08	92.69	16.14	35.18	30.99	36.43
Klerksdorp	33.36	4.48	6.92	31.72	35.54	75.52	4.78	22.84	11.43
Kimberley	31.15	9.58	2.05	409.10	82.64	19.36	30.49	33.25	22.06
Upinton	44.94	18.46	5.24	8.27	55.62	38.15	76.61	9.86	24.05
Gough Island	2.31	3.42	1.80	14.72	40.09	7.60	25.57	34.53	49.00
Marion Island	23.98	191.89	20.11	4.14	157.78	10.98	138.59	25.09	3.18

4.4.1 Rainfall Rate Re-Zoning for South Africa and Surrounding Islands

Many researchers have conducted comparative studies of rainfall rate distributions to improve existing models and determine the best-performing model (Emiliani *et al* , 2004). Reviews of some of the works show instances where the average difference between measured rainfall rates and estimated ITU-R predictions was as high as 73%. In Norway, approximately 50% difference was noted between ITU-R and the measured rainfall rate (Emiliani *et al*, 2004). The majority of researchers often conclude that ITU-R model either over-estimates or under-estimates the rainfall rate at a certain defined percentage of exceedence. Figures 4.12a and 4.12b compare the rainfall rate distributions with ITU-R rain climate zone designations. Both come up with re-definition of the rain zone for different sites in South Africa and surrounding islands. Figures 4.13a and 4.13b show the same process carried out with Crane's climatic rain zones. The reclassification is based on the chi-square optimization method.

In Figure 4.12a, Port Alfred shows that the currently enforced ITU-R P83-5 differs from the ITU-R P837-1 by 29.62%. The newly assigned designation of rain zone L with chi-square statistic of 7.16 at six degrees of freedom and at 5% confidence level, differs from ITU-R P837-5 by 26.31%. Its counterpart, the Crane rain zone, as shown in Figure 4.13a considered D_2 as the appropriate zone for the region and differs from the old designation of C by 22.67%. For the same degrees of freedom, the chi-square test confirmed Crane's D_1 and ITU-R L rain climatic zones for Bisho with 13.65% and 9.09% differences from the old designations respectively. Pietermaritzburg and most of the studied sites showed that ITU-R and Crane's rain climatic zone under-estimate rainfall rate at 0.01% except in the case of Tshipise and Kimberley where the ITU-R was over-estimated by 8.60% and 3.40% respectively. The results of these comparisons are shown in Table 4.9.

Table 4.9 consists of six columns: location, ITU-R 1 and ITU-R 5 with their respective rainfall rate values at 0.01% of exceedence. Other columns show suggested designations and remarks summing up the findings for both, the ITU-R and suggested designations. The table shows the new enforced ITU-R P.837-5 has drastically improved the classification of rain climatic zone. This is supported by research done in Singapore

where the percentage difference reduces from 24% to 8% using ITU-R P.837-4. (Emiliani *et al*, 2004; Ong and Zhu, 1997). In this study, a difference as low as 2.44% from ITU-R P.837-5 and the newly assigned designation is observed. These are noted in stations such as Rustenburg and Marion Island. 4.34% differences are observed in Pretoria and springs. A worse situation of high percentage differences is observed in Fort Beaufort with a value of 33.33%. Comparing the new designation with ITU-R P837-1, it is observed that there is a wide difference, from a high 68% for Marion Island to the low of 7.32% for Cape Town. In Crane's rain climatic zones, the percentage difference is as low as 0% for Pretoria, and Beaufort, and as high as 57.04% in the case of Marion Island. In general, most sites showed that both ITU-R P.837-1 and P.837-5 under-estimate the rainfall rate value at 0.01% except in a few locations such as Cape Town and Klerksdorp. The Crane zones climate show under-estimation for all the sites except in cases where the old designation is the same as proposed designations.

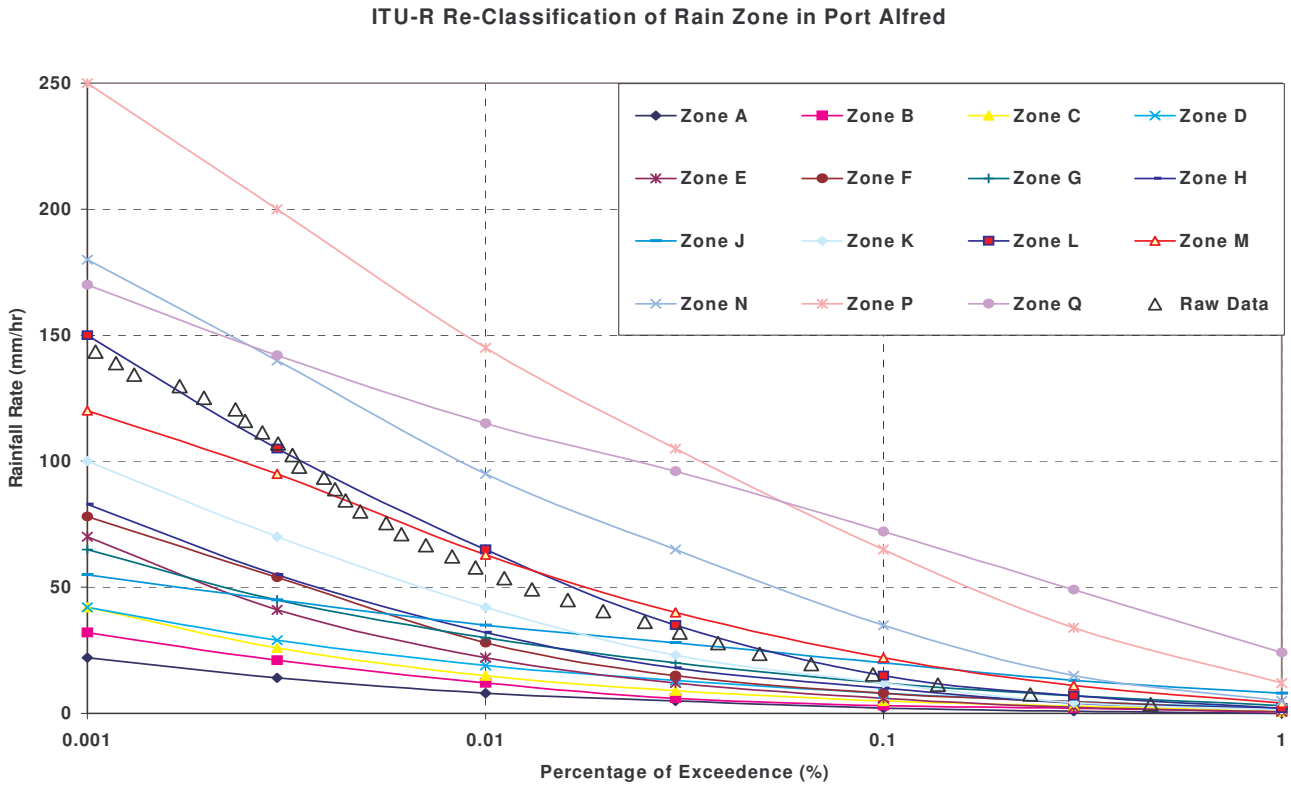

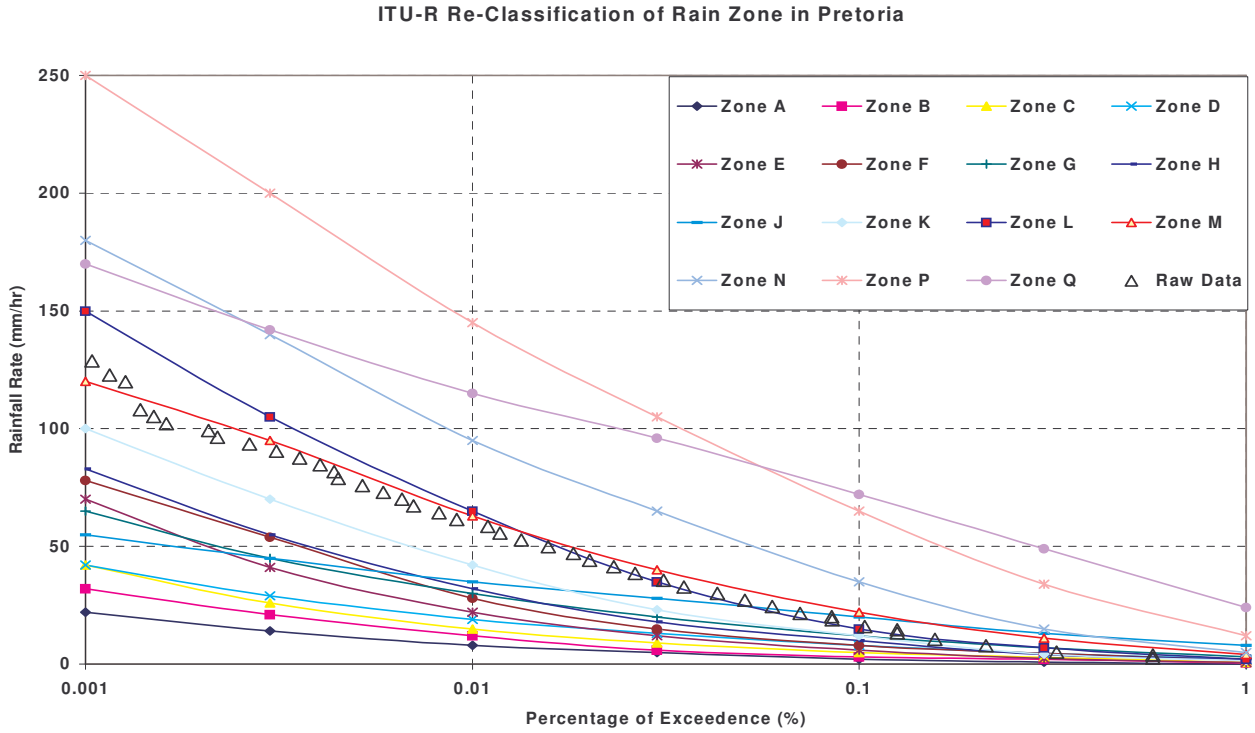

Figure 4.12a: ITU-R rain classification re-zoning for South Africa and surrounding islands

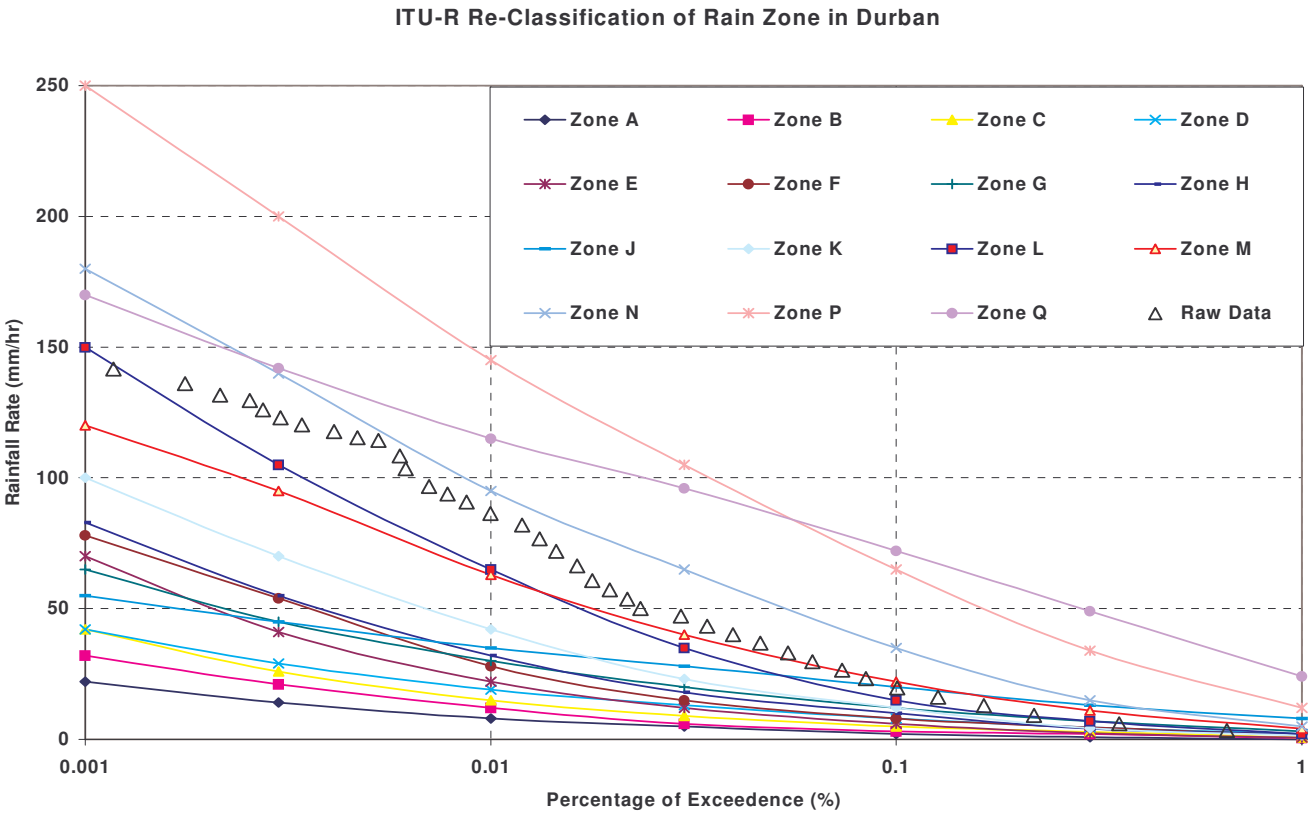

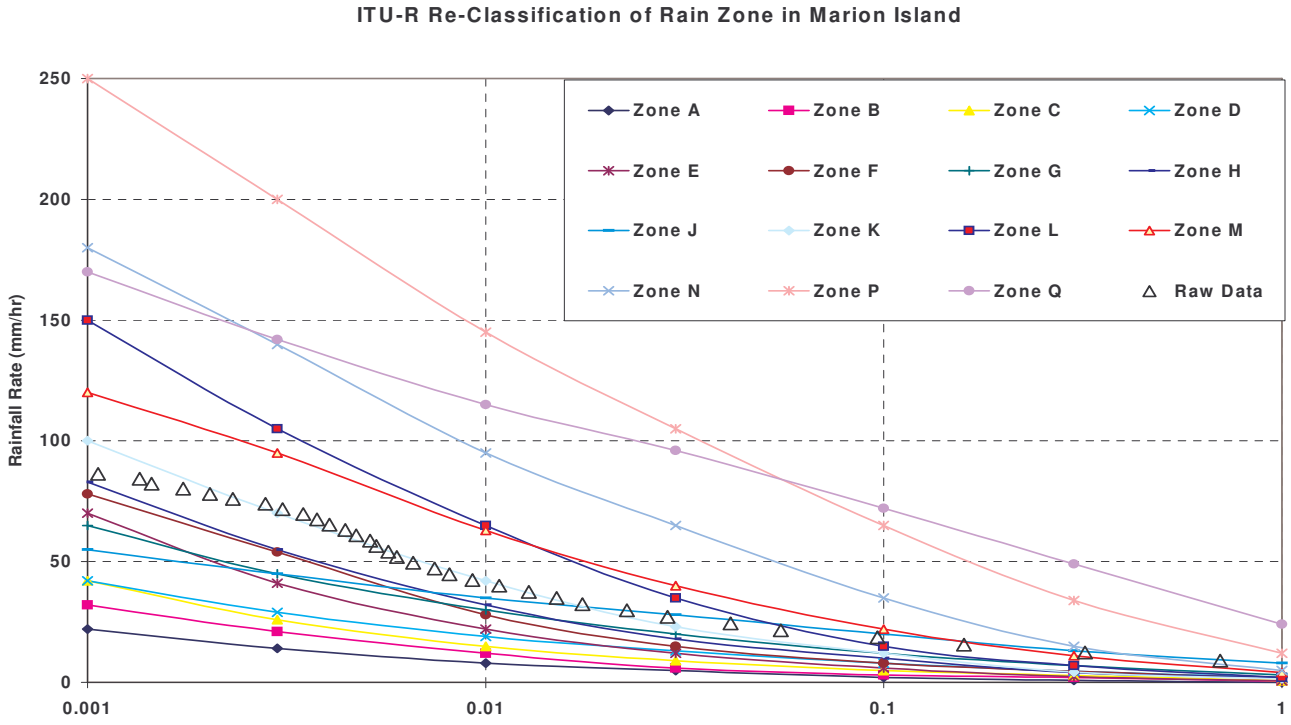

Figure 4.12b: ITU-R rain classification re-zoning for South Africa and surrounding islands

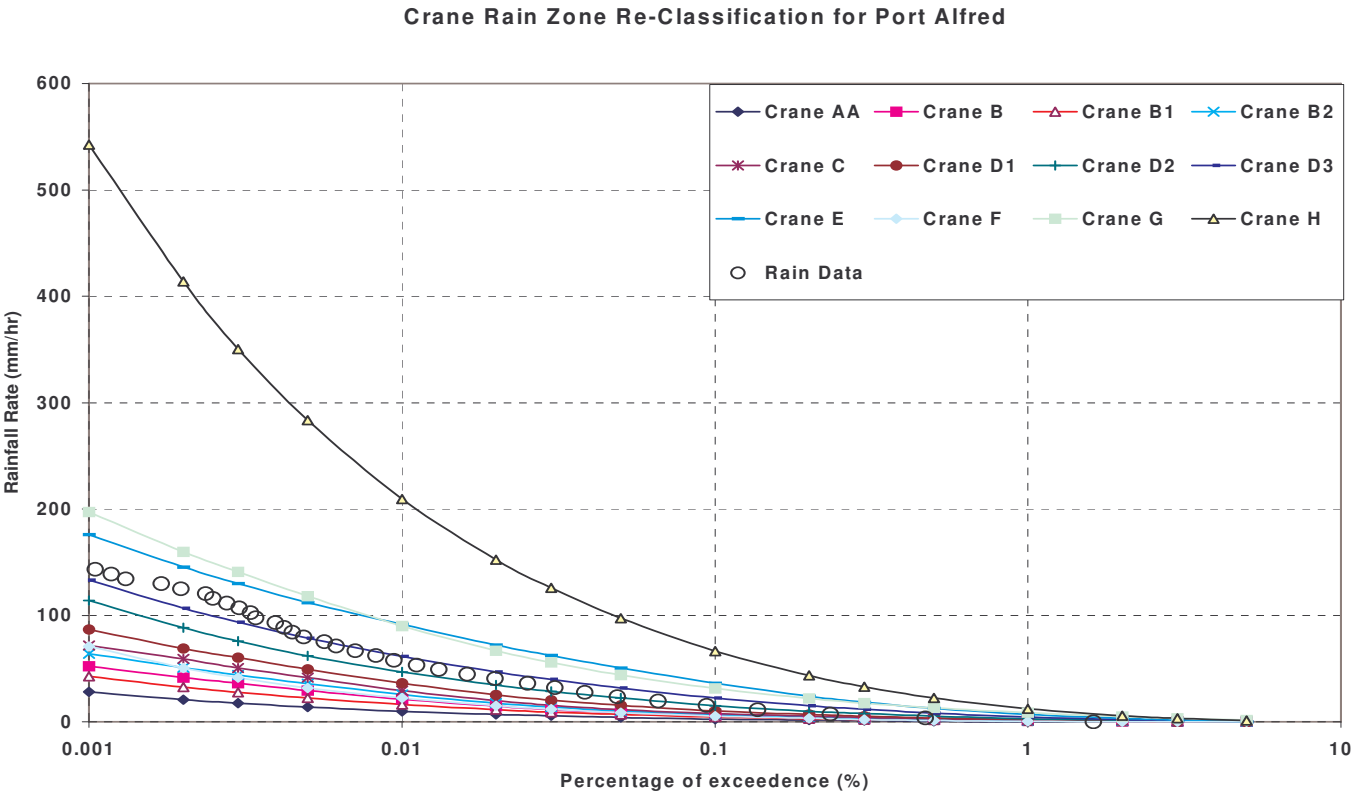

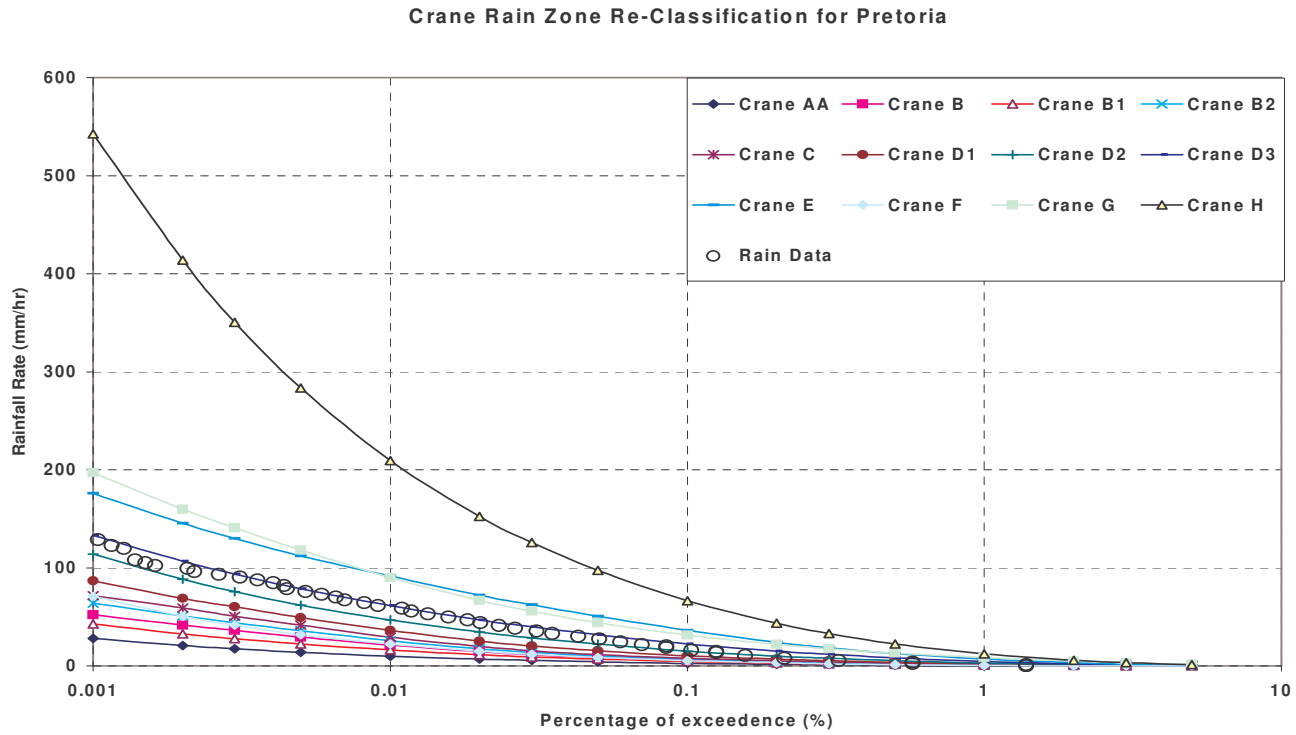

Figure 4.13a: Crane rain classification re-zoning for South Africa and surrounding islands

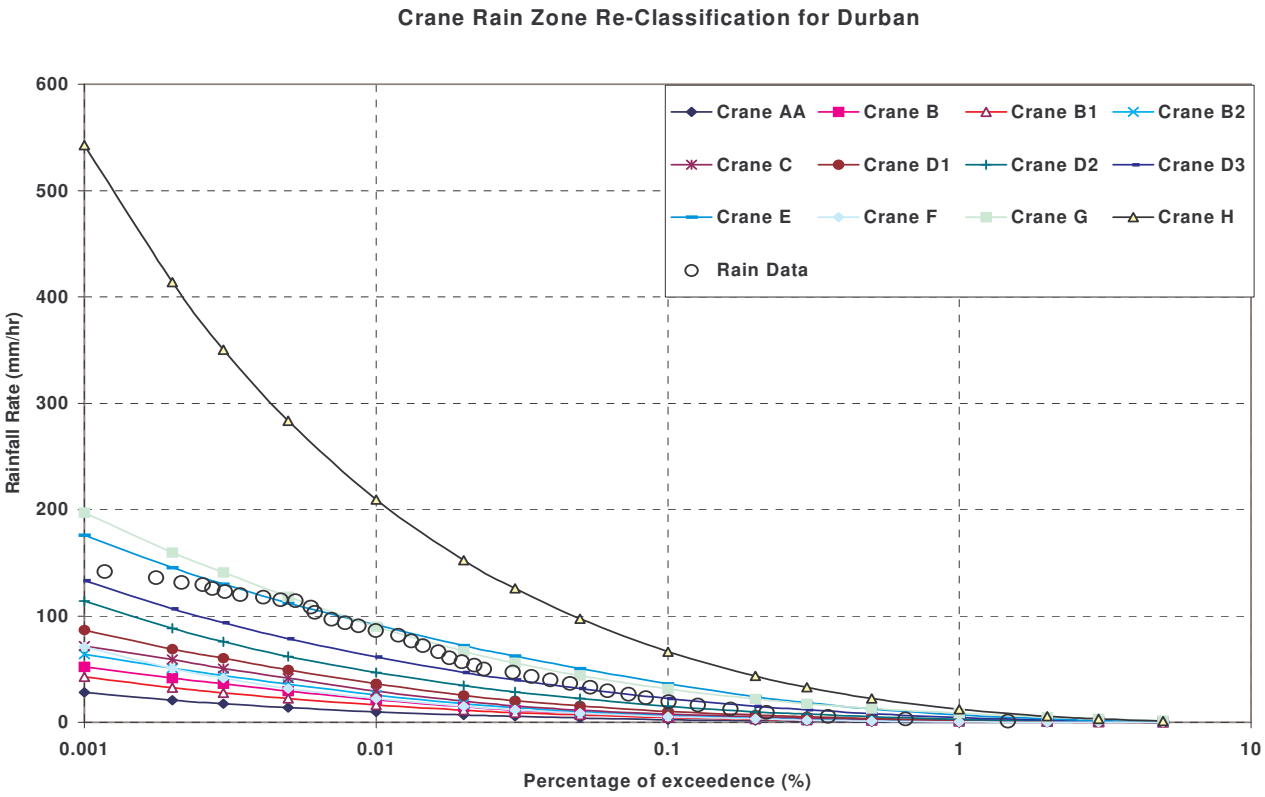

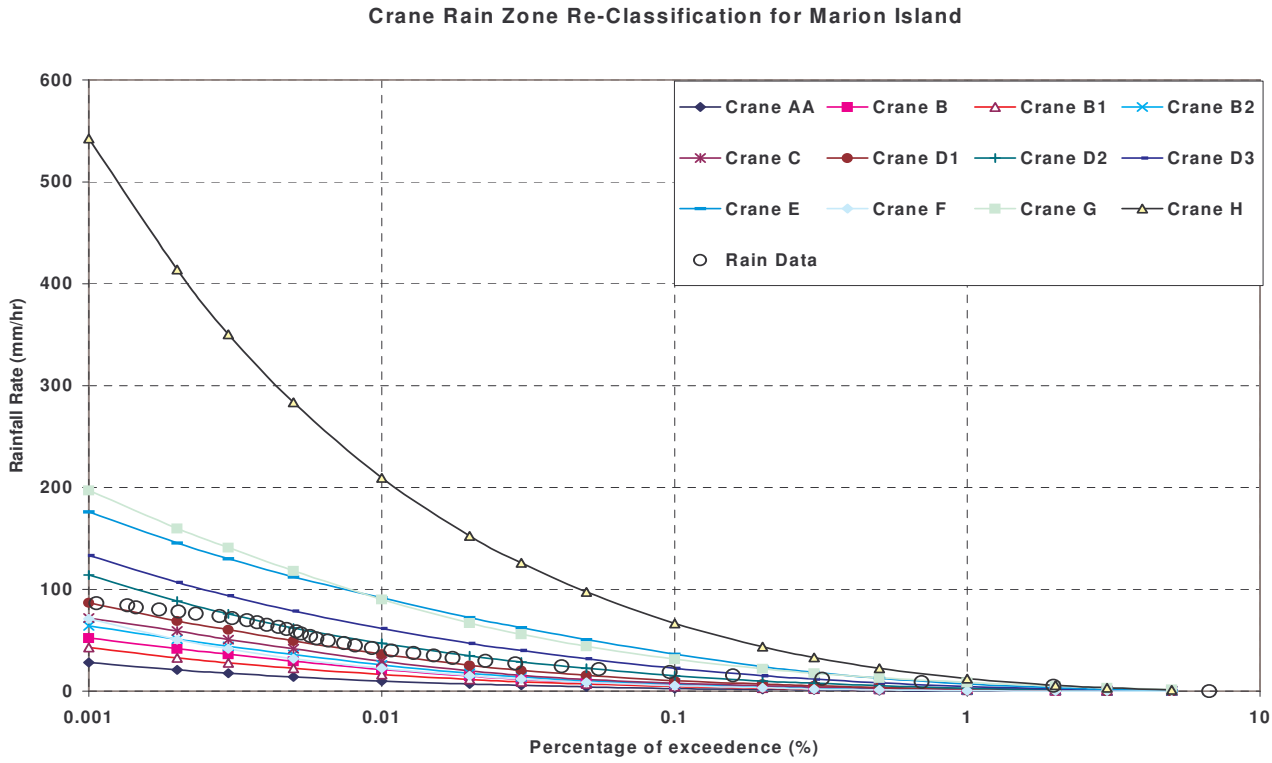

Figure 4.13b: Crane rain classification re-zoning for South Africa and surrounding islands

Table 4.9. Characteristic of rainfall rate climatic zone designation for both ITU-R and Crane's models at 0.01%

Location	ITU-R 1	ITU-R 5	Suggested ITU-R Designation	C-R Designation	Suggested C-R Designation
Port-Alfred	D-19	35	L-60	C-29.5	D_2 -46.8
Bisho	D-19	35	L-60	D_1 -36.2	D_2 -46.8
Fort Beaufort	F-28	30	L-60	C-29.5	D_2 -46.8
Umtata	F-28	30	L-60	D_1 -36.2	D_3 -61.6
Pretoria	E-22	55	L-60	D_2 -46.8	D_2 -46.8
Bethlehem	D-19	35	L-60	C-29.5	D_3 -61.6
Durban	E-22	50	L-60	D_2 -46.8	D_3 -61.6
Springs	E-22	55	L-60	D_1 -36.2	D_3 -61.6
Ladysmith	E-22	50	L-60	D_2 -46.8	D_3 -61.6
Pietermaritzburg	E-22	45	L-60	D_2 -46.8	D_3 -61.6
Tshipise	F-28	50	K-42	D_1 -36.2	D_1 -36.2
Ermelo	E-22	50	L-60	F-22.2	D_3 -61.6
Cape Town	D-19	35	E-22	C-29.5	C-29.5
Beaufort	D-19	25	F-28	C-29.5	C-29.5
Cape Point	D-19	25	K-35	C-29.5	D_1 -36.2
Rustenburg	E-22	60	M-63	D_1 -36.2	D_2 -46.8
Klerksdorp	E-22	60	K-42	D_1 -36.2	D_1 -36.2
Kimberley	E-22	45	K-42	D_1 -36.2	D_2 -46.8
Upinton	E-22	35	K-42	D_1 -36.2	D_1 -36.2
Gough Island	D-19	40	K-42	C-29.5	D_1 -36.2
Marion Island	A-8	40	K-42	A-9.9	D_1 -36.2

4.4.2 Rainfall Rate Contour Maps at 0.01% of Probability of Exceedence

In this section, the suggested rainfall climatic zone for South Africa and surrounding Islands are redefined based on results shown in Figures 4.12 and 4.13 as well as Table 4.9. Due to the number of stations used, there is a need to use interpolation to estimate the unknown points. For this study, a simple inverse distance weighting (IDW) model is used. The model uses the contributions of observed data points, summarizing their characteristics in the form of weighting to estimate the unknown points. The IDW expression is given by:

$$Z_j = K_j \sum_{i=1}^{n} \frac{1}{d_{ij}^{\alpha}} Z_i \tag{4.27}$$

where $K_j = \sum_{i=1}^{n} \frac{1}{d_{ij}}$ is the adjustment that optimizes the weighting to add up to 1 when the parameter $\alpha = 1$. Using this estimator, we are able to provide for the unknown data points and draw contour maps using both ITU-R and Crane designation alphabets for an easy application for radio planning engineers.

Figures 4.14 and 4.15 show the proposed rain climatic zones using ITU-R and Crane designations respectively. It is noted from both figures that the eastern section experiences a higher rainfall rate distribution than the western part, with the exception of Bethlehem. This is as a result of the eastern wind from the Indian Ocean that hits the great escarpment that extends down to the tip of Bethlehem. Figures 4.11 and 4.12 confirmed the effect of the extensive wall, causing an orographic type of rainfall. In Figure 4.11, the tip of Cape Town, Upington and the islands record the lowest rainfall rate while the highest rainfall rate is recorded in the areas surrounding the extensive coast of the ocean.

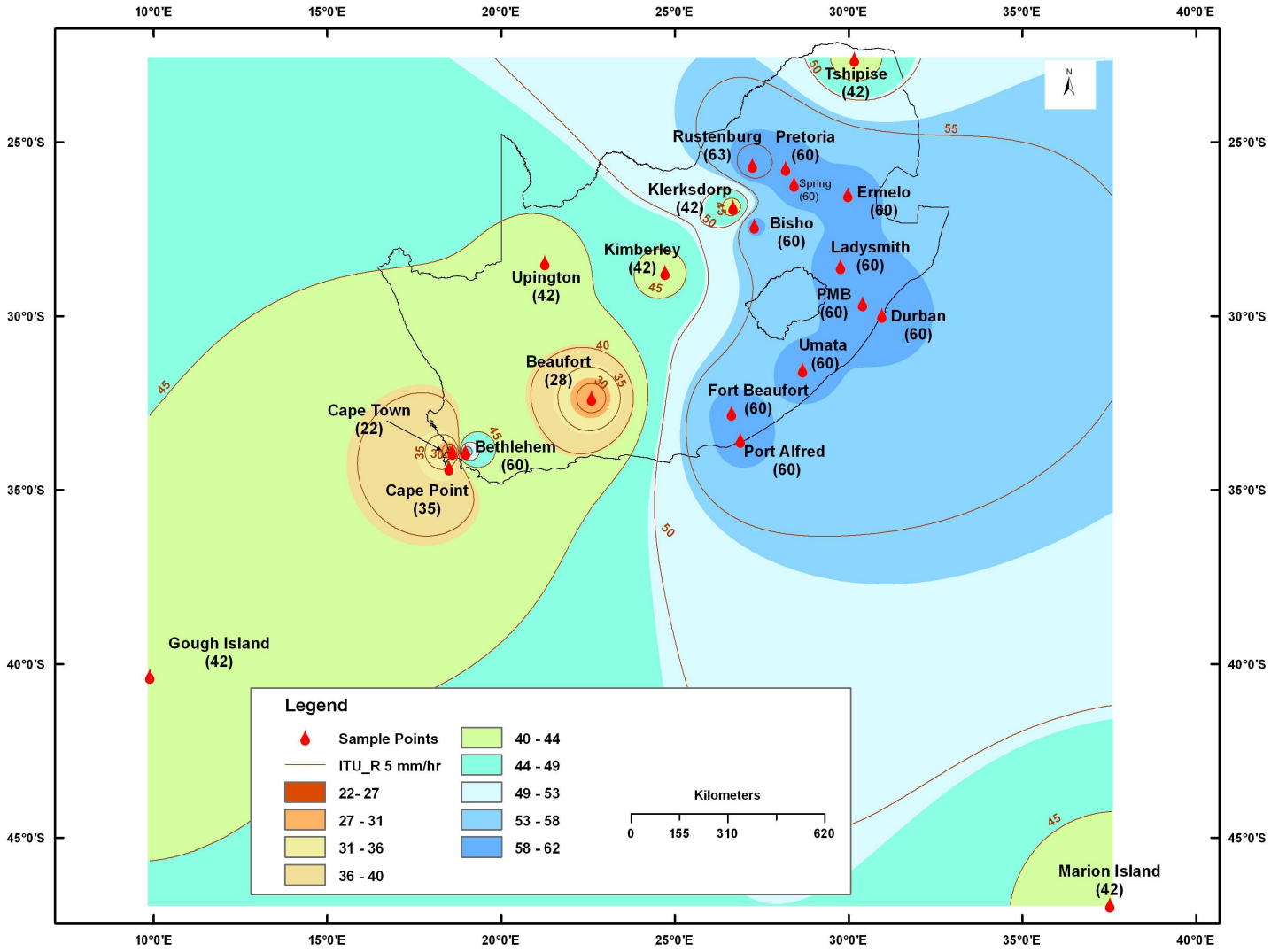

Figure 4.14: Contour plot using ITU-R designation for South Africa and surrounding islands

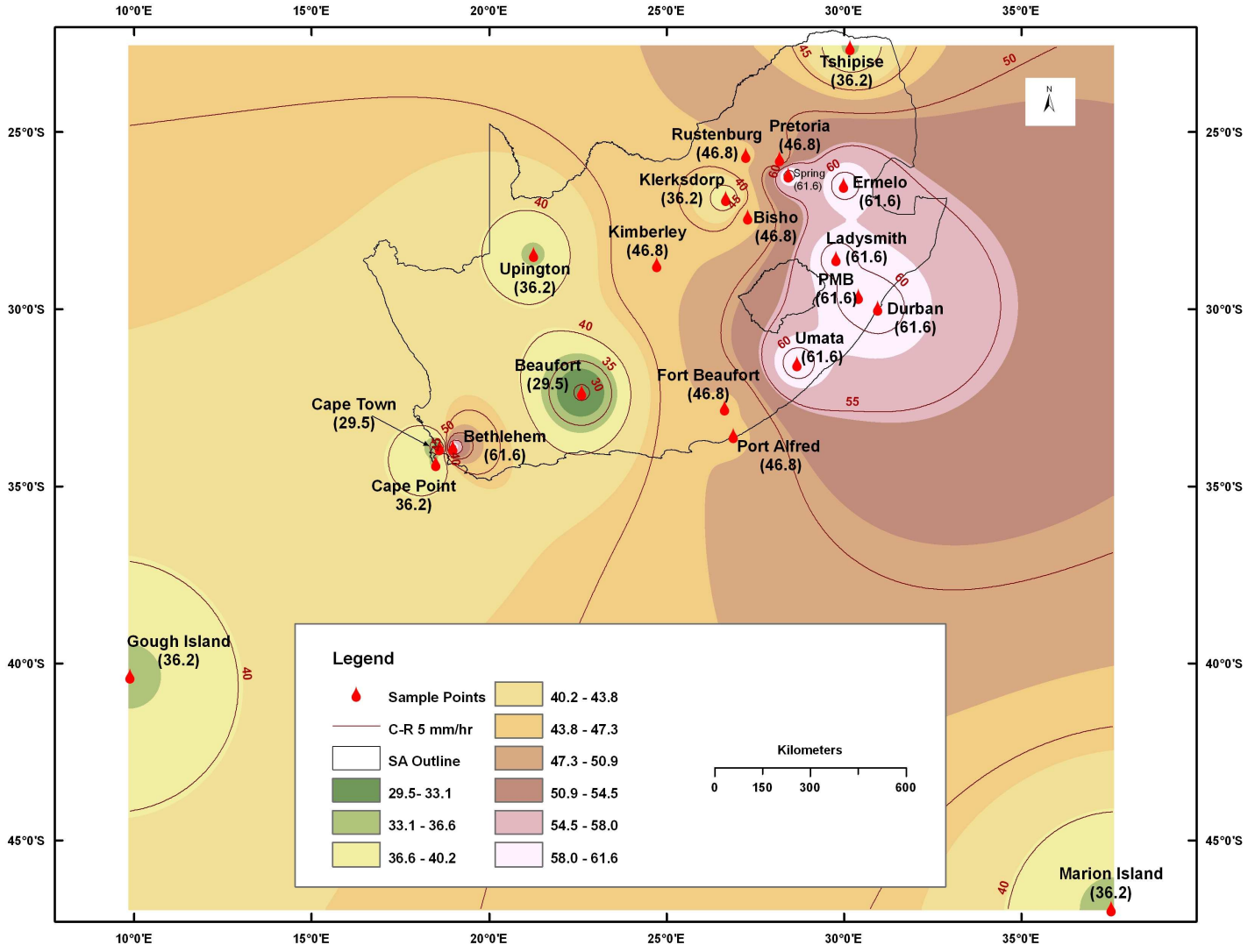

Figure 4.15: Contour plot using Crane designation for South Africa and surrounding islands

4.5 Conclusion

In this study, it is observed that the Western Cape region gets most of its rainfall in winter, while the rest of the country is generally a summer rainfall region. The additional factors that contribute to this variation is the striking contrast between temperatures on the country's east and west coasts, due to the warm Agulhas and cold Benguela currents that sweep the coastlines. Being in the Southern hemisphere, the seasons stand in opposition to those of Europe and North America.

The rainfall data for South Africa and the two islands used in this study was obtained from the South Africa Weather Service at a five-minute integration time, and then processed and converted to one-minute equivalent. The most widely used probability distributions were investigated using the maximum likelihood estimator to optimize the distributions. It was found that most of the studied areas were best defined by the Gamma distribution model, followed by Weibull distributions model, while lognomal did well in very few sites. For the 21 stations, the Gamma model had an average χ^2 statistic of 10.8, followed by the Weibull model with an average of 19.85. The rest of the models gave an average χ^2 statistic of above 55, which is too close to the threshold 63.7 for 40 degree of freedom. The average root mean square percentage also gives evidence to the fact that the Gamma model is the most appropriate to describe most sites in South Africa and surrounding islands. The proposed model will serve as a good tool for system designers because it is easy to use when rainfall distribution is needed for any site, and its parameters are easily understood.

The study proposes new rainfall climatic zones based on ITU-R and Crane rain climatic zone designations. It is found in some sites that the ITU-R model over-estimated, while in many others the ITU-R model under-estimated, rainfall rate values at defined probability of exceedences. It is observed that the widest percentage of differences between ITU-R P.837-1 and P.837-5 was 66.67% for Marion Island, and the least percentage was 13.63% observed in Beaufort and Cape Point. Crane rain climatic zone designations matches in

some sites as noted in Pretoria, Tshipise, Cape Town, Beaufort, Klerksdorp and Upington.

Rain contour maps have been identified as desirable tools for the objective of providing system designers, site engineers and network planners with estimated fade margins due to rain attenuation. The two plotted contour maps were tailored to satisfy accepted rainfall climatic zones defined by the ITU-R and Crane maps which are available in most radio planning tools. In this research, the contour map was developed using advanced Geographic Information Systems (GIS) tools with the adoption of IDW estimator to provide the contour map for rainfall rate at 0.01% of exceedence.

Chapter Five

Characteristics of Rain Dropsize Distribution

5.0 Introduction

The past decade has witnessed a rapid increase and sophisticated application of communications technology in transport systems, mobile telephone, data transfer, etc. This progress has put pressure on link capacity in terms of bandwidth and frequency congestion. The exploitation of higher frequency provides a solution to the above challenges, though it has been unattractive because of perceived technology limitations as a result of hydrometeors, especially rain. The generation and transmission of electromagnetic energy at higher frequency such as millimeter wavelength requires interaction with a medium, thus the scale wavelength factor is an important issue for consideration. For example, millimeter radio wave (1 mm - 10mm) has a comparable wavelength with raindrop size. To properly estimate the amount of signal that will be attenuated as a result of the presence of rain as a medium, both external distribution (statistical modelling of rain) and internal structure (rain microstructure) of rain must be understood. To estimate the degree of signal loss due to interaction of electromagnetic wave with rain, there is need to understand the microstructure of rain in terms of raindrop size, fall velocity of the drop, shape of raindrop, canting angle, rain drop size distribution and finally statistical modelling of its distribution pattern at different rain rates. In this chapter, rain microstructure characteristics are presented for Durban, South Africa. Among the issues to be discussed are the raindrop size distribution model (DSD), the statistical theory of DSD modelling using the maximum likelihood method, and comparison of the proposed model with existing DSD models.

5.1. Raindrop Size Distribution Model for Durban, South Africa

The physical processes leading to the formation of raindrop size distribution are complex and varying due to environmental factors and internal physics of the raindrops. DSD is a property of a rain event in the sense that it gives the physics of rain formation and it

shape. To describe the pattern of distribution of raindrops at different sizes, probability methods of statistical techniques are often employed. In this section, the focus is to describe the average raindrop size distribution measured in Durban, the coastal region of South Africa, using a conventional statistical approach with robust estimator method of maximum likelihood method (MLE).

5.1.1 Introduction to Raindrop Size Distribution Models

Raindrop size distribution models are required for the estimation of attenuation due to rain through scattering and absorption of microwave and millimeter wave signals. Several DSD models, as described in section 2.7, have been developed for the calculation of attenuation due to rain. However, most of these models were derived for Europe, Asia, and tropical regions of Africa. There is thus need for measurement and modeling of raindrop size data for Southern Africa, not for communication purposes only, but also to investigate the anomalous behaviour of climatic conditions of the Southern Africa. This study thus aims to put Southern Africa on the list of regions with raindrop size distribution measured data.

5.1.2 Raindrop Size Distribution Measurement

Raindrop size distribution data used in this study was collected with a Joss and Waldvogel (1968 and1969) distrometer (JWD), specifically RD-80 as shown in Figure 5.1. The figure comprises: a sensor, which is the outdoor unit, as well as a processor and computer unit which are indoor. RD-80 consists of electromechanical sensors which convert mechanical momentum of falling drops into electrical pulses. The distrometer has $50\,cm^2$ of sampling area with an accuracy of 5%. It collects raindrop sizes ranging between 0.3 mm to 5.3 mm in diameter with 20 bins or channels of diameter classes. The equipment is placed at latitude $30^0 58^{'} E$, longitude $29^0 52^{'} S$, and altitude of 139.7 m at the School of Electrical, Electronics and Computer Engineering in the University of KwaZulu-Natal, Howard College, Durban. In the present study the distrometer was installed in December 2008 and commenced full operation in January 2009 till now, with a sampling interval integrated over one minute.

In the analysis, the measured data is classified using drop diameter tabulation according to Waldvogel (1974), and rain rate regimes according to Timothy *et al*. (2002). The latter method of classification is adopted in this study. Table 5.1 summarizes the classifications using diameter as presented by Timothy *et al*. (2002).

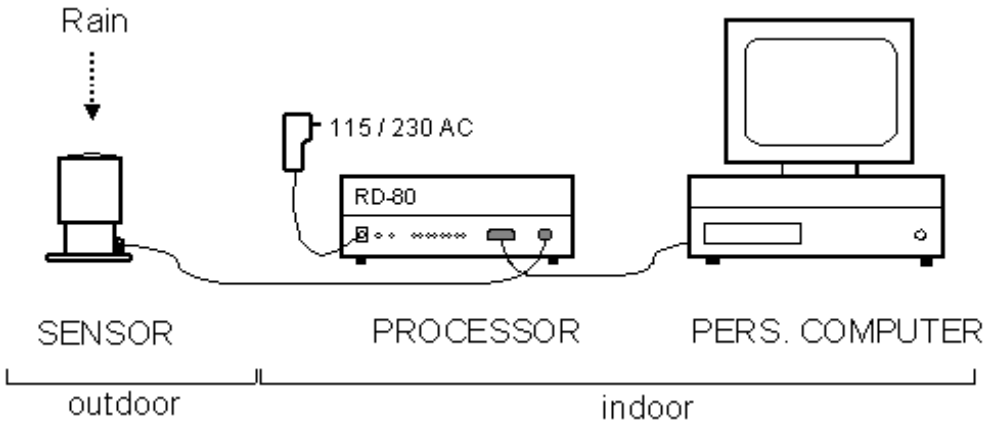

Figure 5.1a: Schematics diagram of configuration of distrometer with other accessories (RD-80 product description:http://www.distromet.com/1_index_e.htm)

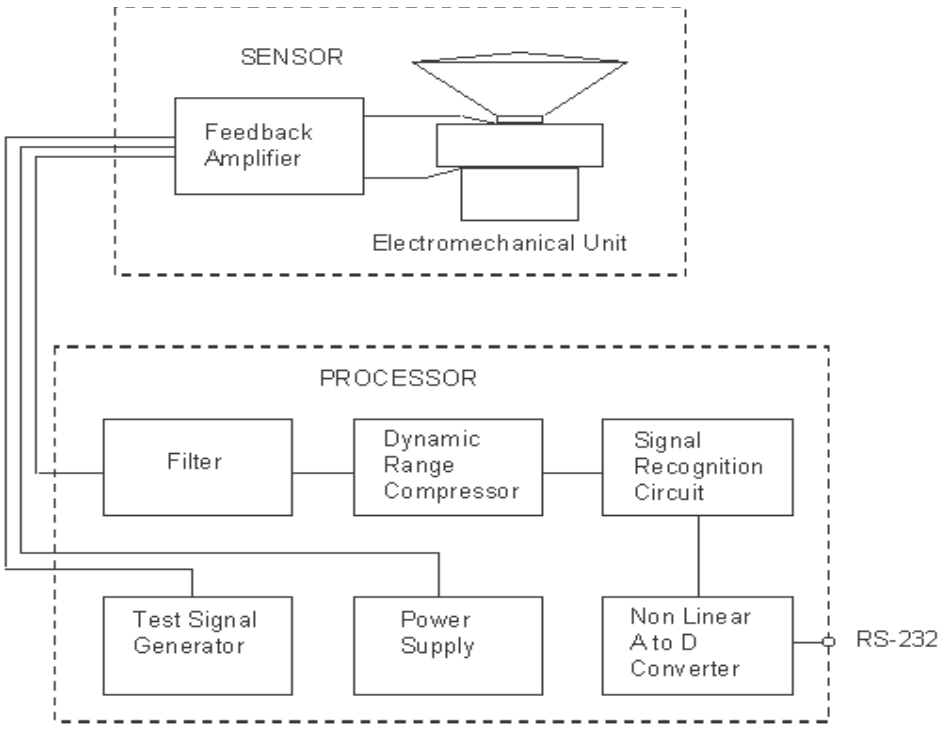

Figure 5.1b: Block diagram of the disdrometer RD-80

(RD-80 product description:http://www.distromet.com/1_index_e.htm)

Table 5.1: Classification of $N(D)$ based on rain rate regimes

Rain Type	Diameter Range(mm)
Regime one	$0 < R \leq 20$
Regime two	$20 < R \leq 100$

The database used in this study consists of a nine-month pool of data with 125 different rain events spread over 6,000 minutes of sampling time. The data sampling months are December 2008 to October 2009, although there were missing events in some months when samples were not recorded by the distrometer data logger. Figure 5.2a shows a sample profile of total $N_T(D)$ for all analyzed events at logarithmic scale. The peak of total $N_T(D)$ recorded was at profile of 2292 mm^{-3}.

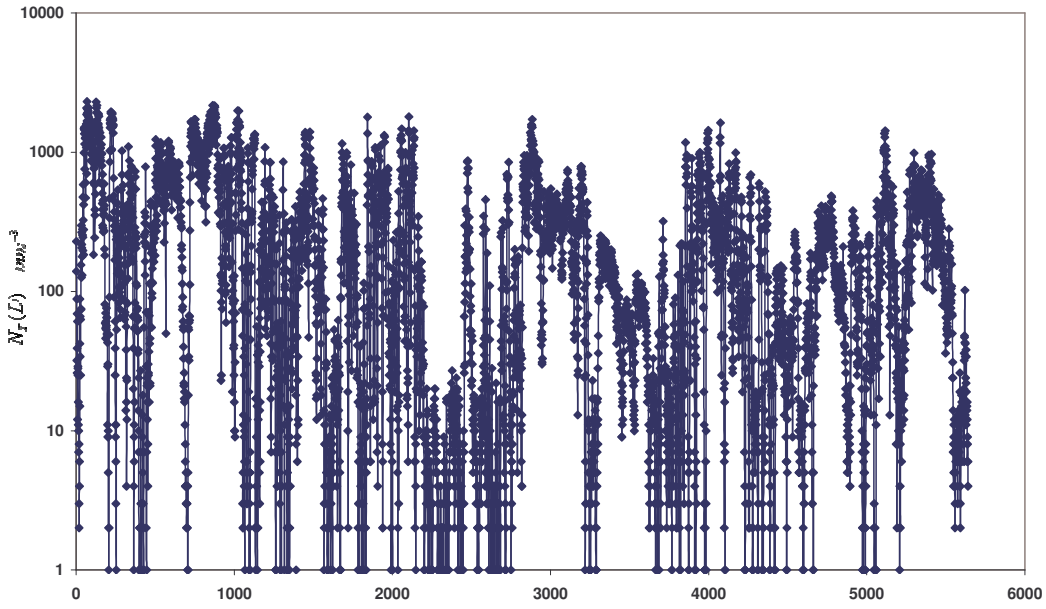

Figure 5.2a: Profile of total $N_T(D)$ against time (one-minute resolution for each event)

Figures 5.2b and 5.2c are profiles of average diameter and log of rain rate against time. The peak rain rate captured during these events was a record 84.76 mm/h and mean drop diameter was also observed at 5.3 mm.

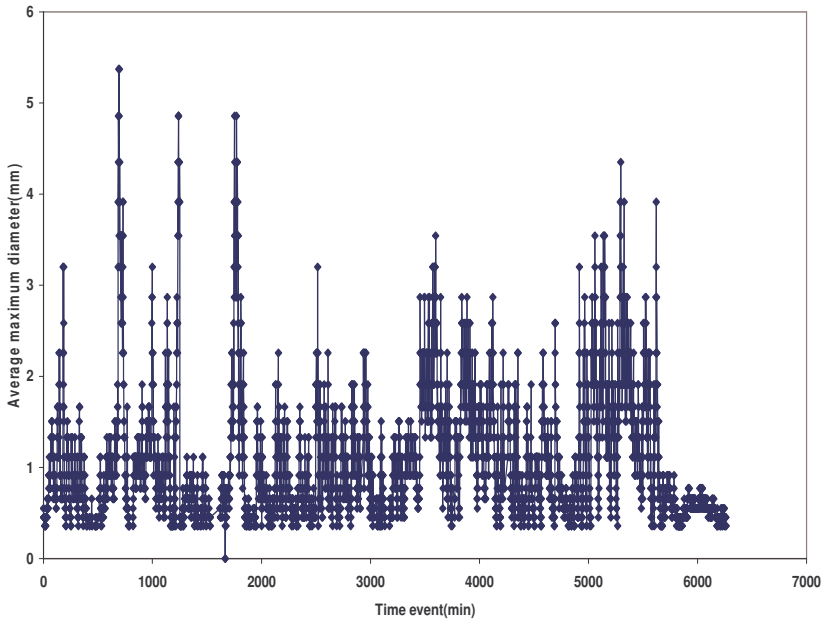

Figure 5.2b: Profile of average diameter against time (one-minute resolution for each event)

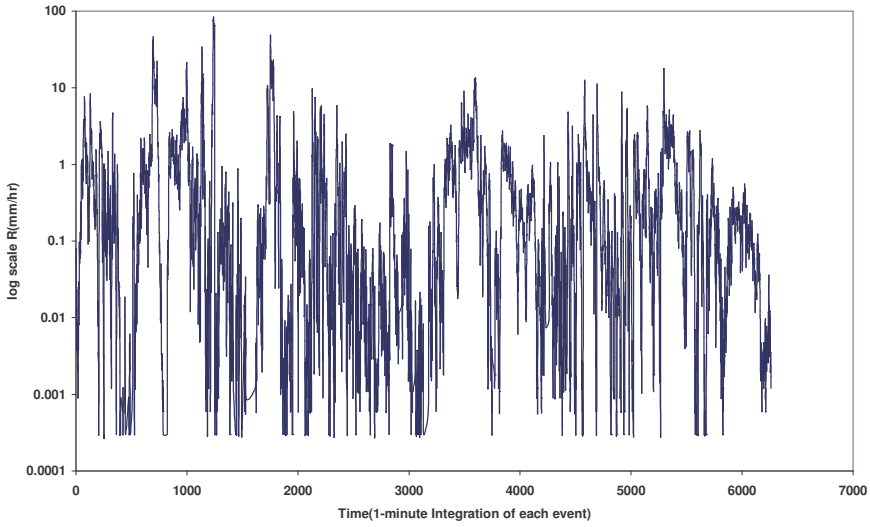

Figure5.2c: Profile log of rain rate against time (one-minute resolution for each event)

5.2. Statistical Theory of DSD Modelling for Durban

Earlier techniques used in modelling raindrop size distribution seem to have begun with fits to the average drop distributions measured at single rain rates. Most of these fits were

applied directly to the drop size distribution data such as the Marshall and Palmer where direct graphical fitting approach was used (Marshall and Palmer, 1948). In order to improve the modelling approach and results, there is need to employ a systematic method such as moment and maximum likelihood to estimate modelling parameters. Ajayi and Olsen (1985) used the method of moments to estimate modelling parameters for the tropical region of Africa while Barclay *et al*. (1978) considered the maximum likelihood method for Australia. In this section, the maximum likelihood approach is considered for Durban raindrop size distributions. The estimator method is then applied on the three-parameter lognormal distribution.

5.2.1 Maximum Likelihood Function for Three-Parameter Lognormal Distribution

Measured raindrop size distribution can be approximated as the product of total number of drops of all size $N_T(D)$ and probability density function of lognormal distribution. In this study, probability density function of three-parameter lognormal distribution is used and expressed as:

$$N(D) = N_T(D) \times pdf(D;\gamma,\mu,\sigma) \tag{5.1}$$

where random variable mean drop diameter D is said to have a three-parameter lognormal distribution if the random variable $Y = \ln(D-\gamma)$, where D is greater than γ, is normally distributed (μ,σ^2), and σ is considered to be greater than zero. The probability density function of three-parameter lognormal distribution is then given by Pan *et al*. (2005) as:

$$pdf(D;\gamma,\mu,\sigma) = \frac{1}{\sigma\sqrt{2\pi}(D-\gamma)}\exp\frac{-1}{2\sigma^2}\left[\ln(D-\gamma)-\mu\right]^2 \tag{5.2}$$
$$\gamma < D < \infty \qquad \sigma > 0$$

and equation 5.2 will be zero if the condition in the equation is not met. Parameter σ^2 is the variance of Y; it is the shape parameter of D and μ is the mean of Y.

Cohen *et al*. (1980) define the likelihood function for a random sample of drop size distribution as a function of diameter with size n with $pdf\,(D;\gamma,\mu,\sigma)$ (5.2) as:

$$L(D_1,..,D_n;\gamma,\mu,\sigma^2)=(2\pi\sigma^2)^{-n/2}.\exp\left\{-\sum_1^n\left[\ln(D_i-\gamma)-\mu\right]^2/2\sigma^2\right\}.\prod_1^n\left(D_i-\gamma\right)^{-1} \tag{5.3}$$

Adopting partial differential of logarithm of equation 5.3 and equating to zero, results in the following maximum likelihood estimation (MLE) equations:

$$\frac{\partial \ln L}{\partial \mu}=\frac{1}{\sigma^2}\sum_1^n\left[\ln(D_i-\gamma)-\mu\right]=0$$

$$\frac{\partial \ln L}{\partial \sigma}=\frac{n}{\sigma}+\frac{1}{\sigma^3}\sum_1^n\left[\ln(D_i-\gamma)-\mu\right]^2=0 \tag{5.4}$$

$$\frac{\partial \ln L}{\partial \gamma}=\frac{1}{\sigma^2}\sum_1^n\frac{\left[\ln(D_i-\gamma)-\mu\right]}{(D_i-\gamma)}+\sum_1^n(D_i-\gamma)^{-1}=0$$

By elimination, σ^2 and μ are eliminated from equation 5.4, the resulting residual part of the equation as a function of γ becomes:

$$\lambda(\gamma)=\left[\sum_1^n(D_i-\gamma)^{-1}\right]\left[\sum_1^n\ln(D_i-\gamma)-\sum_1^n\ln^2(D_i-\gamma)+(1/n)\left(\sum_1^n\ln(D_i-\gamma)\right)^2\right]$$
$$-n\sum_1^n\frac{\ln(D_i-\gamma)}{(D_i-\gamma)}=0 \tag{5.5}$$

From equation 5.4, $\hat{\mu}$ and $\hat{\sigma}^2$ are estimated as:

$$\hat{\mu} = (1/n)\sum_{1}^{n} \ln(D_i - \hat{\gamma}),$$

$$\hat{\sigma}^2 = (1/n)\sum_{1}^{n} \ln^2(D_i - \hat{\gamma}) - \left[(1/n)\sum_{1}^{n} \ln(D_i - \hat{\gamma}\right]^2 \tag{5.6}$$

In order to provide a solution for γ in equation 5.5, only admissible roots for which $\gamma < D_1$ are considered. A standard iterative method of Newton-Raphson approximation method is adopted for solving equation 5.5 and thus, $\hat{\gamma}$ is estimated.

5.2.2 Probability Density Function (pdf) of proposed DSD model on Durban Data

In this sub-section, the probability density and cumulative distribution functions for two different regimes of DSD as a function of rain rate are presented and discussed. In modelling DSD for Durban, two regimes of DSD evolution were used, which are based on rain rate above and below 20 mm/hr. Three-parameter lognormal probability density function and estimates of its parameters are obtained using MLE as explained in section 5.2.1. The MLE method is used to construct estimates of parameters that match the probability density function of lognormal distribution. Forty DSD samples are considered for this work, twenty-four for DSD regime of rain rate lower than 20 mm/hr and sixteen for rain rate above 20 mm/hr. In the first regime of DSD where rain rate is less than 20 mm/hr, the lower and upper rain rate samples are presented in Figures 5.3 to 5.4 while Figures 5.5 and 5.6 represent the second DSD regime where rain rate is greater than 20 mm/hr.

The "a" sections of Figures 5.3 to 5.6 represent probability density functions (pdf) of raindrops size distributions while "b" sections of the figures are cumulative distributions. The pdf section of regimes with less than 20 mm/hr rain rate show that over 67% of drops fall within diameter range of 0.5 mm and 0.9 mm, while the rain rate regime greater than 20 mm/hr shared 45% of peak drops between 0.5 mm and 0.8 mm, and 20% of remaining peaks were found between 0.9 mm and 2 mm.

In order to see the degree of description of the chosen estimator with respect to probability density function of the data, a goodness-of-fit test is carried out. Examples of such tests are Chi-square, Anderson-Darling, and Kolmogorov-Smirnov. In this work, Kolmogrov-Smirnov test (K-test) is chosen because the experimental sample size is small (20) and this is the strength of the test over Chi-square whose accuracy depends on large sample size. Press *et al*. (1992) and Massey (1951) explain the K-test as a comparison between vertical difference of empirical distribution function (ecdf) and theoretical distribution function (cdf). The empirical cdf is given as:

$$f_n(x_i) = \frac{1}{n}.[number\ of\ observations \leq x] \tag{5.7}$$

on the vertical difference between the theoretical and experimental cumulative distribution functions. The K-test is mathematically expressed as:

$$D = \max_{1 \leq i \leq n} absolute\left(F(x_i) - F_n(x_i)\right) \tag{5.8}$$

where $x_i \ldots x_n$ is a random sample cumulative distribution function for either ecdf or cdf.

The hypothesis regarding the distribution under test is rejected provided that test statistics D in equation (5.8) is greater than the critical value as shown in the Table 1-A in Appendix B. A significance level of 0.05 (5%) is chosen most of the time and sometimes in some other important industrial applications a lower significance level is considered. In this study, 5% significant level is used. Table 5.2 gives a summary of the K-test with remarks at their various classes of DSD regimes. The table confirms the suitability of lognormal distribution and MLE parameters to be appropriate for describing DSD modelling for Durban. It is noted that at all the chosen regimes, the entire hypotheses were accepted for the MLE estimators.

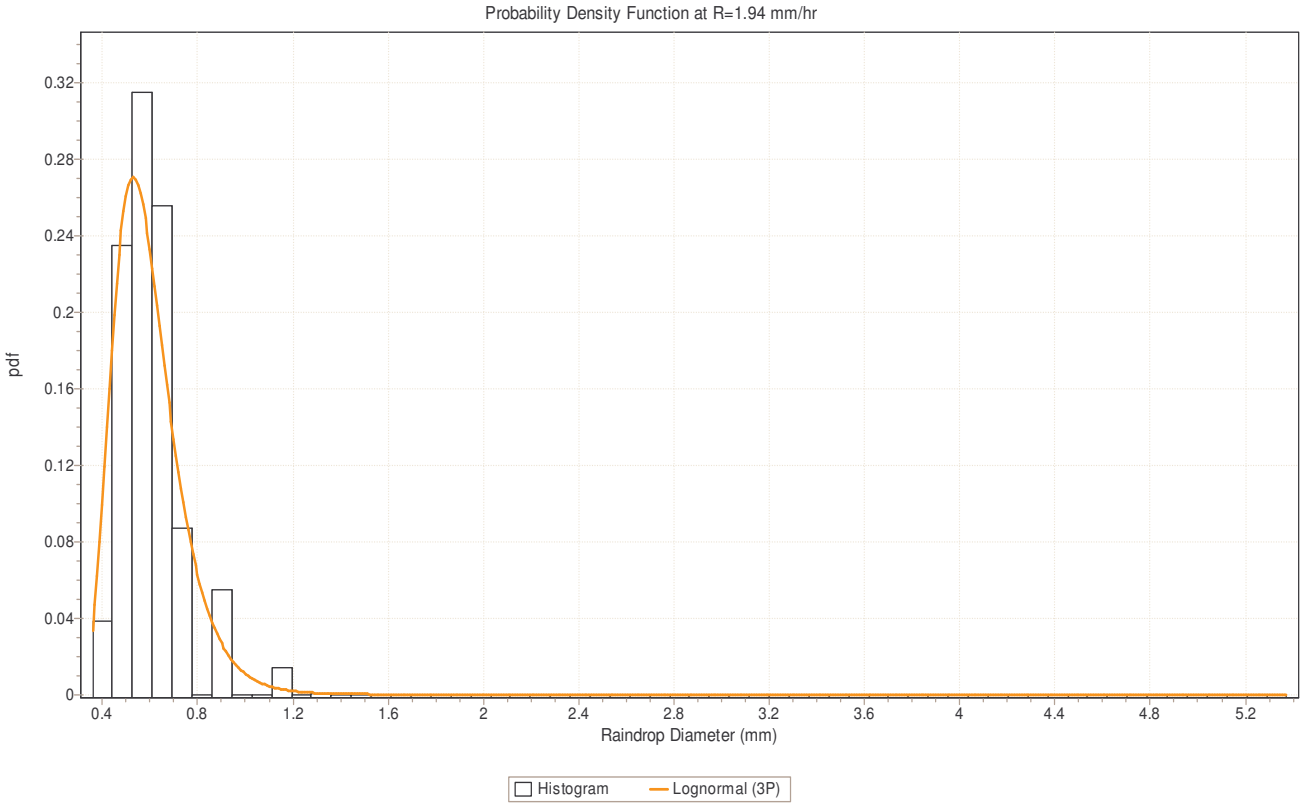

Figure 5.3a: Probability Density Function of N (D) at R=1.94 mm/hr

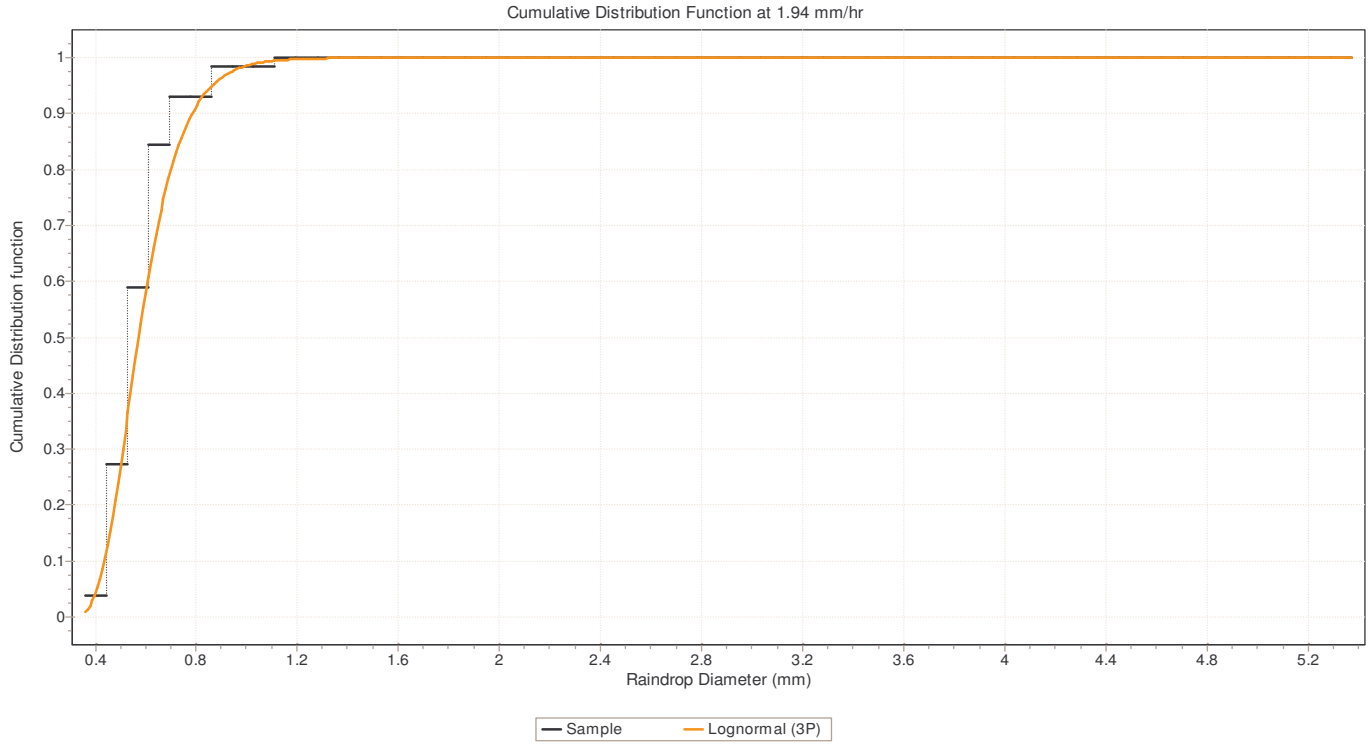

Figure 5.3b: Cumulative Distribution of N (D) at R=1.94 mm/hr

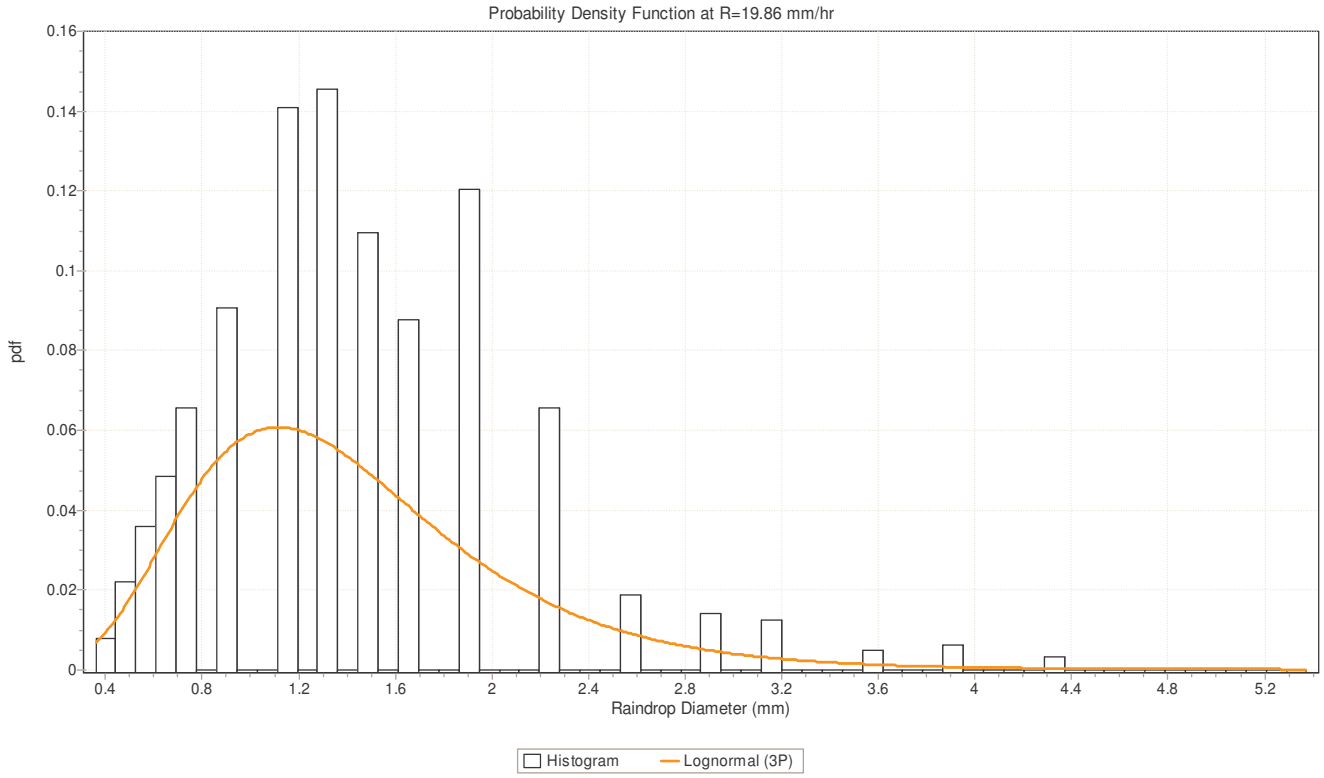

Figure 5.4a: Probability Density Function of N(D) at R=19.86 mm/hr

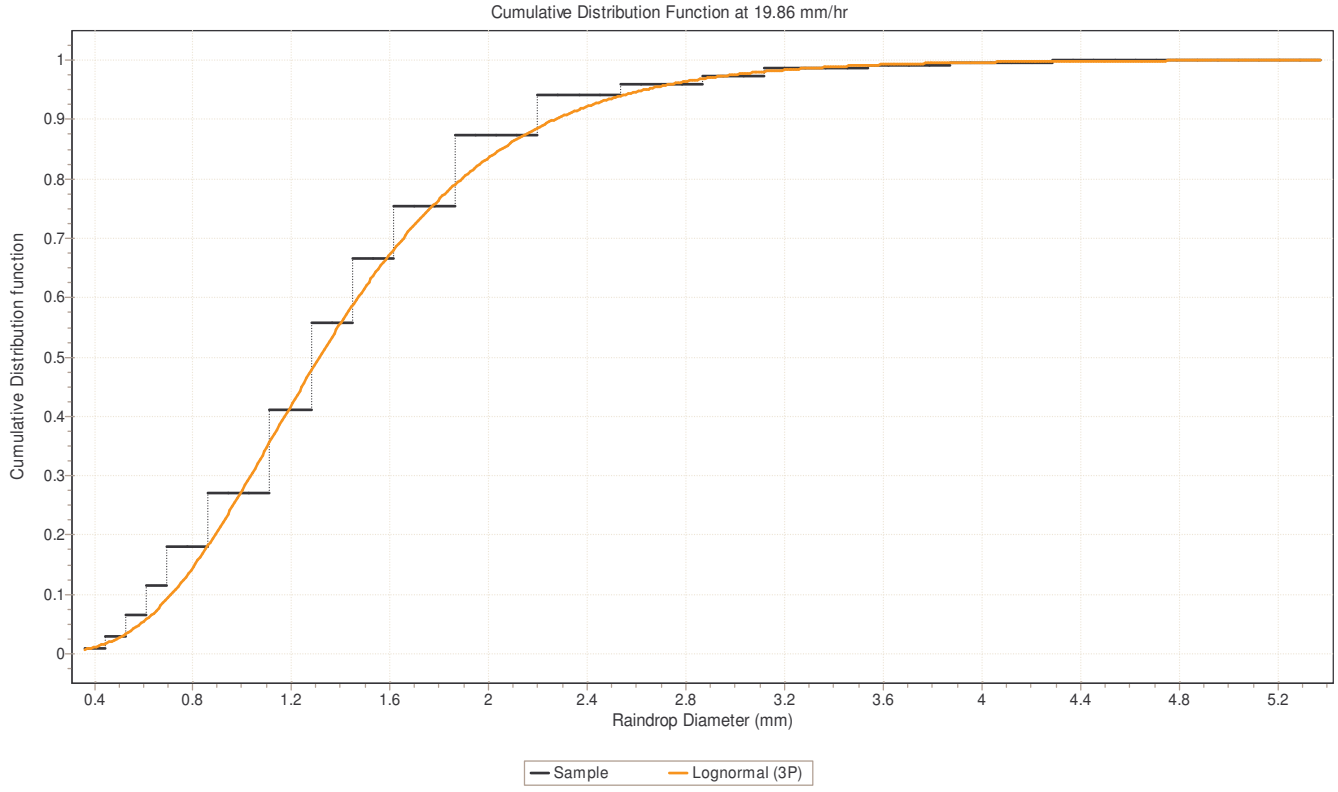

Figure 5.4b: Cumulative Distribution of N (D) at R=19.86 mm/hr

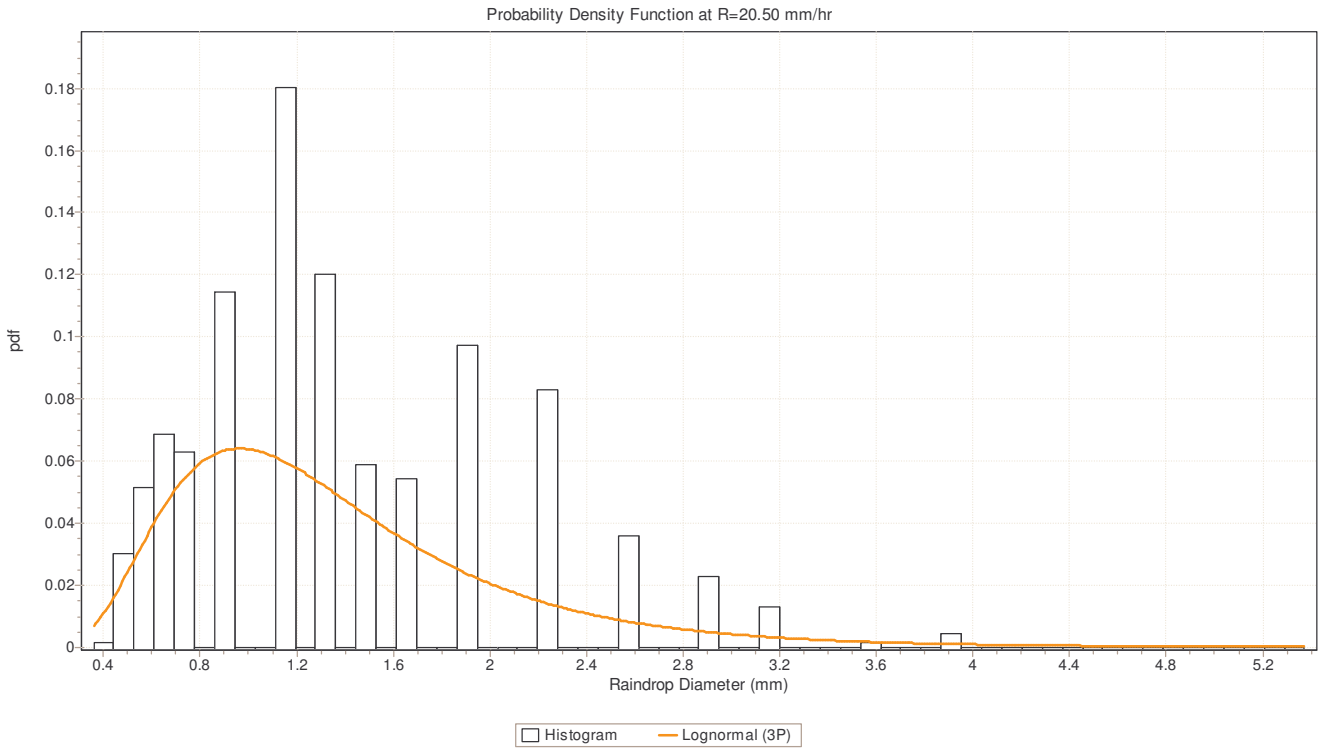

Figure 5.5a: Probability Density Function of N (D) at R=20.50 mm/hr

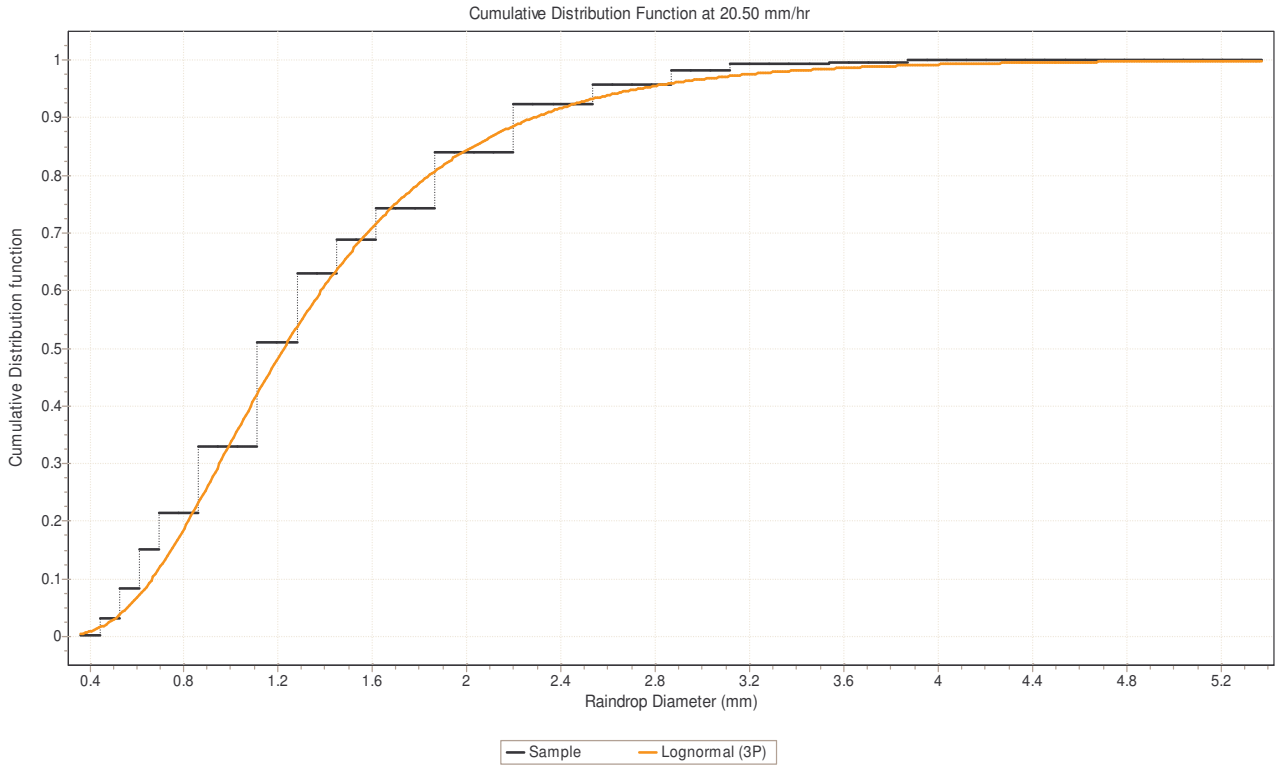

Figure 5.5b: Cumulative Distribution of N (D) at R=20.50 mm/hr

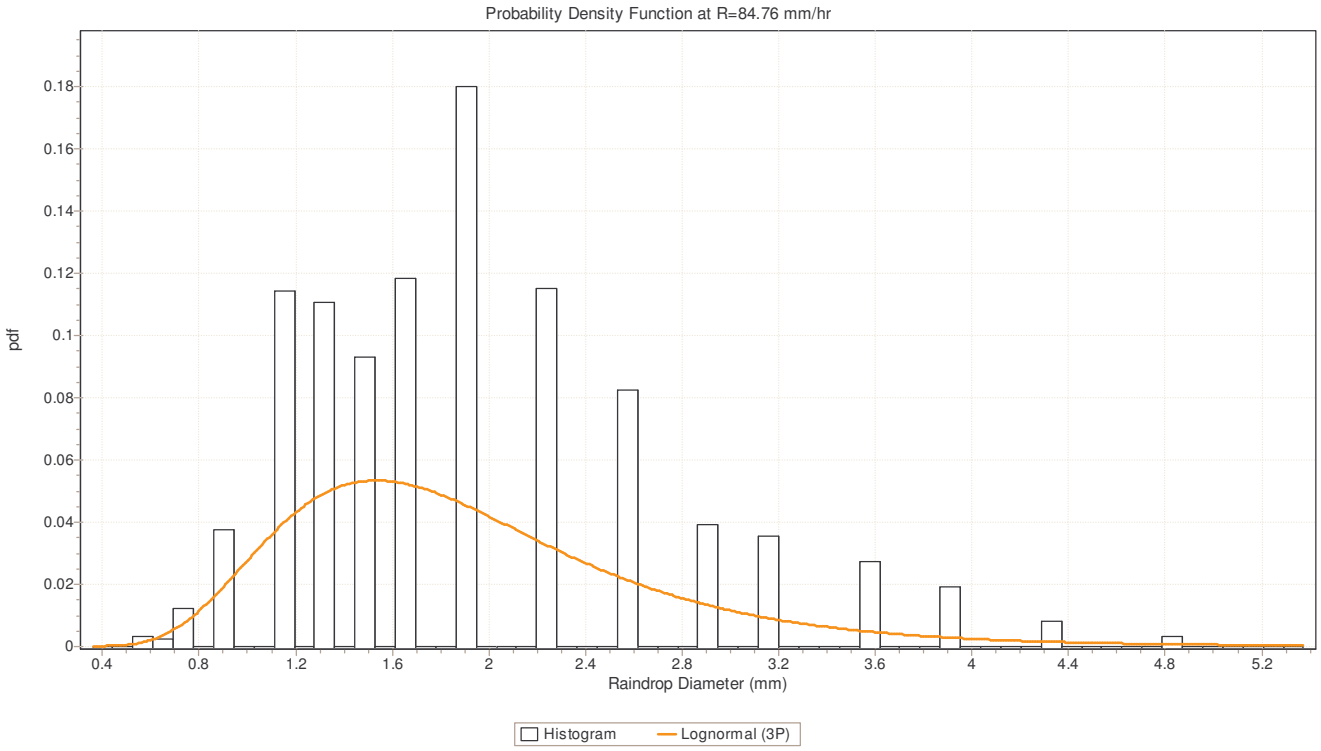

Figure 5.6a: Probability Density Function of N(D) at R=84.78 mm/hr

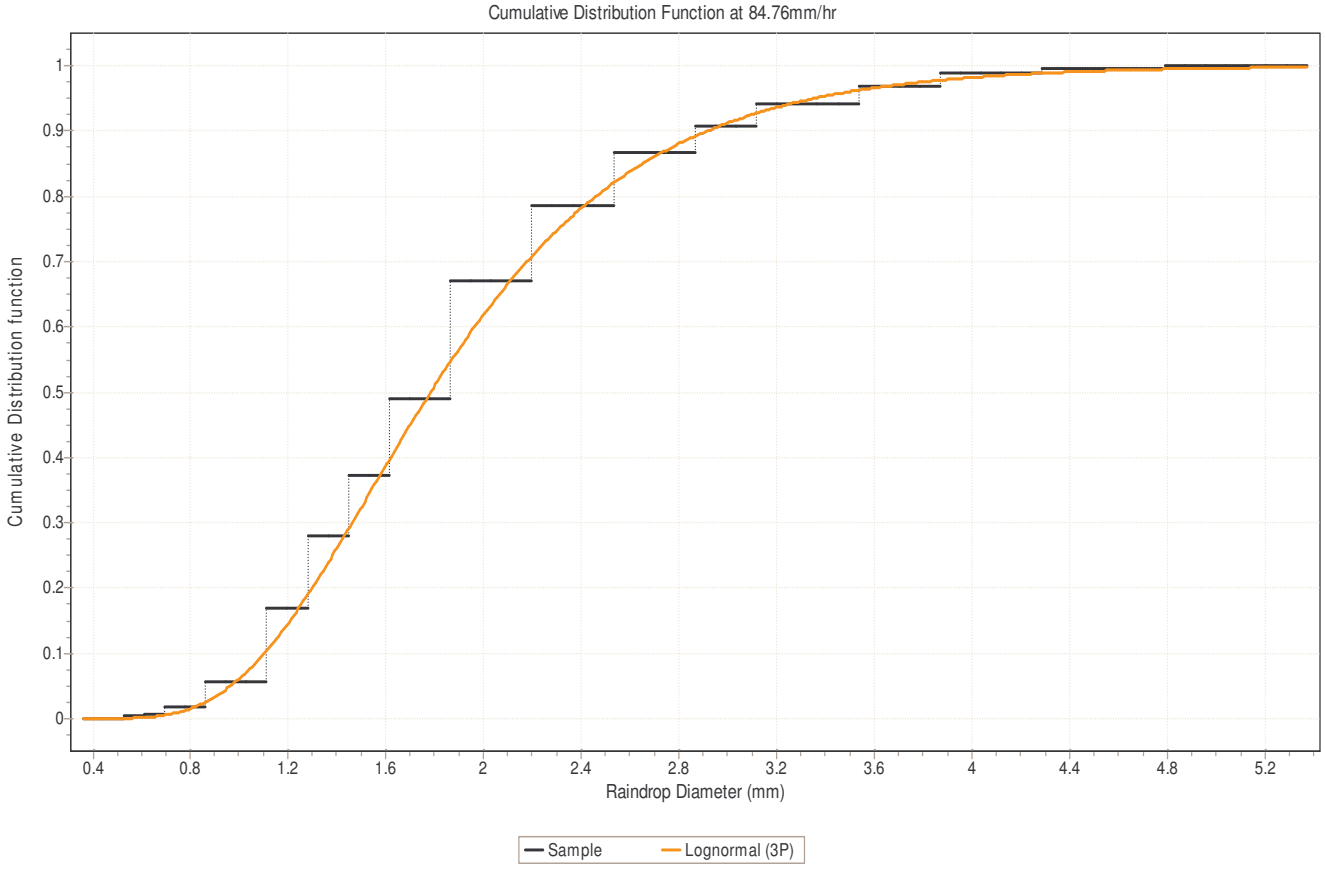

Figure 5.6b: Cumulative Distribution of N (D) at R=84.78 mm/hr

Table 5.2 Kolmogorov-Smirnov goodness-of-fit test for the DSD modelling

Classifications Based on two Regimes (mm/hr)	**Critical value at 5% significance level**	**Hypothesis Accepted**		**Classifications Based on two Regimes(mm/hr)**	**Critical value at 5% significance level**	**Hypothesis Accepted**
1.94	0.15896	Yes		20.50	0.09522	Yes
2	0.17526	Yes		25.32	0.10822	Yes
2.93	0.1362	Yes		34.02	0.0916	Yes
3.08	0.14981	Yes		35.24	0.0777	Yes
3.92	0.16883	Yes		41.90	0.10911	Yes
4.12	0.17859	Yes		46.32	0.08596	Yes
4.15	0.17859	Yes		57.17	0.10445	Yes
5.96	0.13681	Yes		59.33	0.12822	Yes
6.11	0.14734	Yes		61.74	0.10072	Yes
6.73	0.13527	Yes		62.42	0.11006	Yes
6.98	0.15192	Yes		64.65	0.10661	Yes
7.21	0.13527	Yes		64.79	0.10117	Yes
8.36	0.15134	Yes		69.08	0.12026	Yes
8.93	0.12391	Yes		71.07	0.0873	Yes
9.0	0.12078	Yes		77.70	0.08279	Yes
9.79	0.1448	Yes		84.76	0.09737	Yes
11.59	0.14949	Yes		**Sample Size=20 Channels**		
12.86	0.13451	Yes				
15.02	0.13035	Yes		**Significant level of 5%=0.29408**		
16.36	0.12693	Yes				
17.92	0.09455	Yes				
18.26	0.13073	Yes				
19.89	0.1002	Yes				

5. 3 Application of Proposed DSD model

Raindrop size distributions have been achieved using the three-parameter lognormal distributions. The parameter $N_T(D)$ is modeled primarily from the average raindrop data. The results presented in Figures 5.7a and 5.7b are variations of total $N_T(D)$, with rain rate obtained at Durban for the two rain rate ranges chosen. The least square regression technique is then applied and their respective power law coefficients are obtained as shown in equation 5.9.

$$N_T(D) = 284\,R^{0.744} \qquad 1.94mm/hr < R \le 20.0mm/hr$$

$$N_T(D) = 63\,R^{0.706} \qquad 20.0mm/hr < R \le 100.0mm/hr \tag{5.9}$$

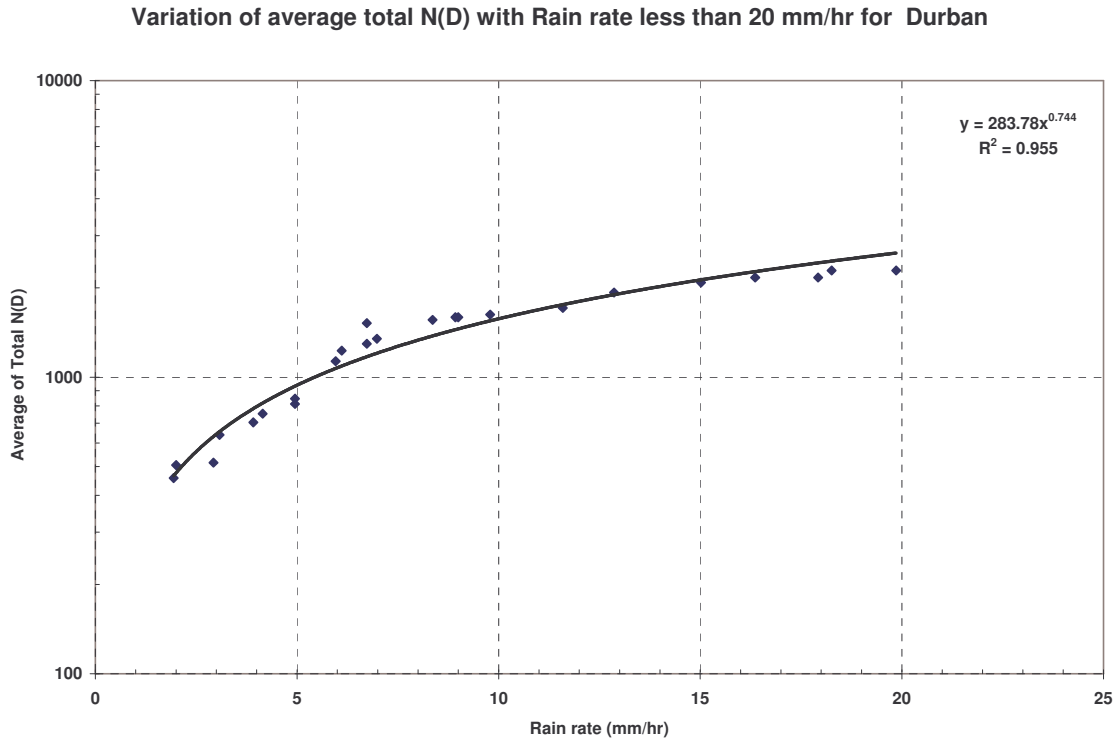

Figure 5.7a: Variation of $N_T(D)\,m^{-3}mm^{-1}$ with rain rate less than 20 mm/hr for Durban

In the sample for lower rain rate, it is observed that the power fit curve is most influenced by many data points. Rain rates higher than 20 mm/hr are noted to be faithfully represented by the power law; thus the classifications for this power law fit starts for point rain rate of 1.94 mm/hr. In the analysis, 24 selected lower rain rate data points were considered in order to get a reasonable power fit. The square of correlation coefficient for the lower rain rate samples is 0.955, which is reasonable for a good fit. In the case of higher rain rate, the power fit is reasonably accurate and this reflects in the square of correlation coefficient of 0.975.

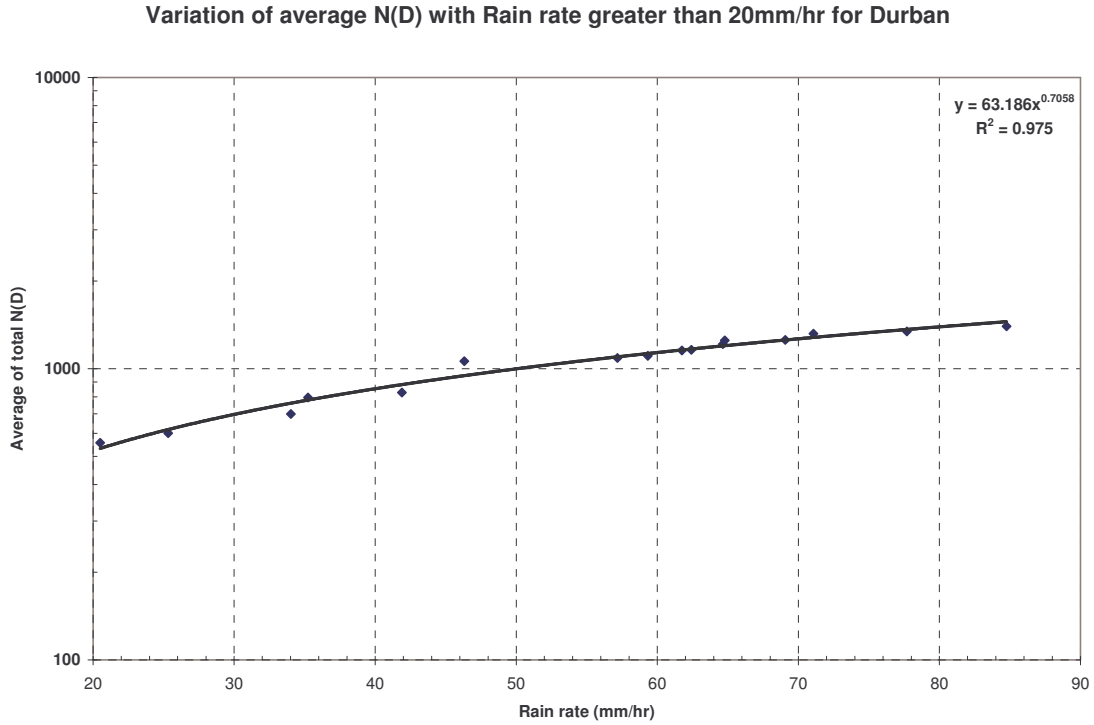

Figure 5.7b: Variation of $N_T(D)\,m^{-3}mm^{-1}$ with rain rate greater than 20 mm/hr for Durban

The maximum likelihood method, as explained before, is used to solve a set of non-linear equations associated with three-parameters of lognormal distribution from measurement of raindrop size distribution data. The resulting parameters μ, σ^2 and γ are plotted in Figures 5.8 to 5.10 for the two classes of rain rate ranges. Examining Figures 5.8a and

5.8b, the scatter data points are wider apart as rain rate increases. This may be as a result of an internal instability in the raindrops as variation of diameter increases. The square correlation coefficients testify to this: with the lower rain rate, the correlation is 0.4974, while at higher rain rate it gives 0.3426. The following relations are obtained for the mean of the two rain rate regimes:

$$\begin{aligned} \mu &= -1.3652 + 0.6531\ln(R) \qquad 1.94mm/hr \lhd R \lhd 20.0mm/hr \\ \mu &= -0.9663 + 0.4062\ln(R) \qquad 20.0mm/hr \lhd R \le 100.0mm/hr \end{aligned} \tag{5.10}$$

The two parameters σ^2 and γ also depend on rain rate and are given as follows for the two regimes of DSD:

$$\begin{aligned} \sigma^2 &= 0.0954 - 0.00121\ln(R) \qquad 1.94mm/hr < R \le 20.0mm/hr \\ \sigma^2 &= 0.9486 - 0.2035\ln(R) \qquad 20.0mm/hr < R \le 100.0mm/hr \end{aligned} \tag{5.11}$$

and,

$$\begin{aligned} \gamma &= 0.3345 - 0.2891\ln(R) \qquad 1.94mm/hr < R \le 20.0mm/hr \\ \gamma &= 0.1808 - 0.1283\ln(R) \qquad 20.0mm/hr < R \le 100.0mm/hr \end{aligned} \tag{5.12}$$

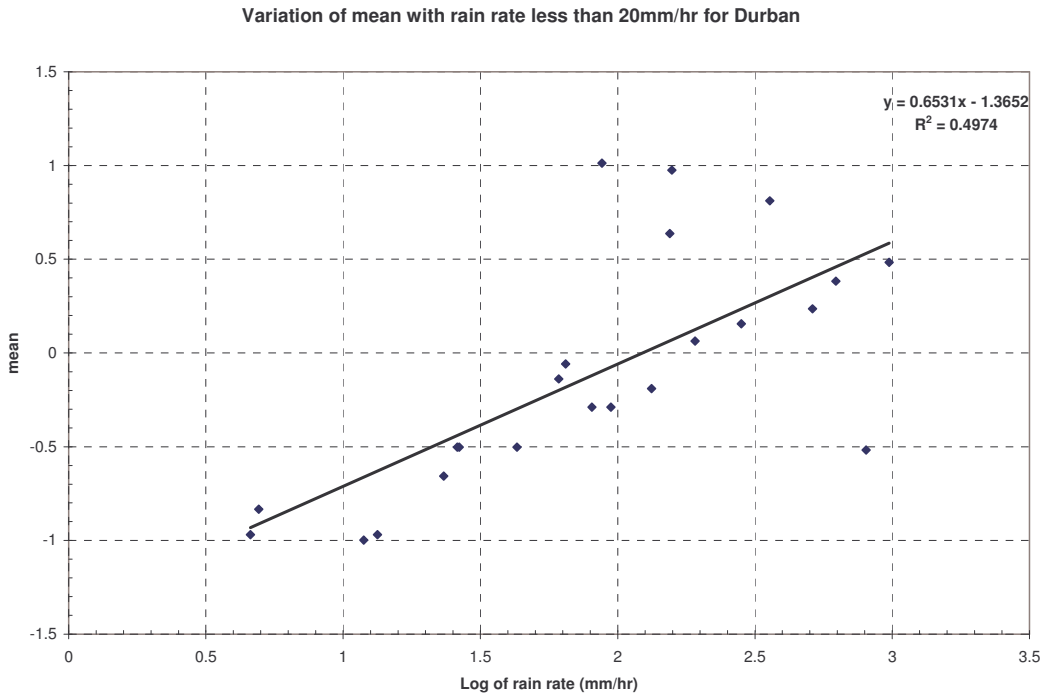

5.8a: Variation of mean $\mu\ mm$ with log of rain rate less than 20 mm/hr for Durban

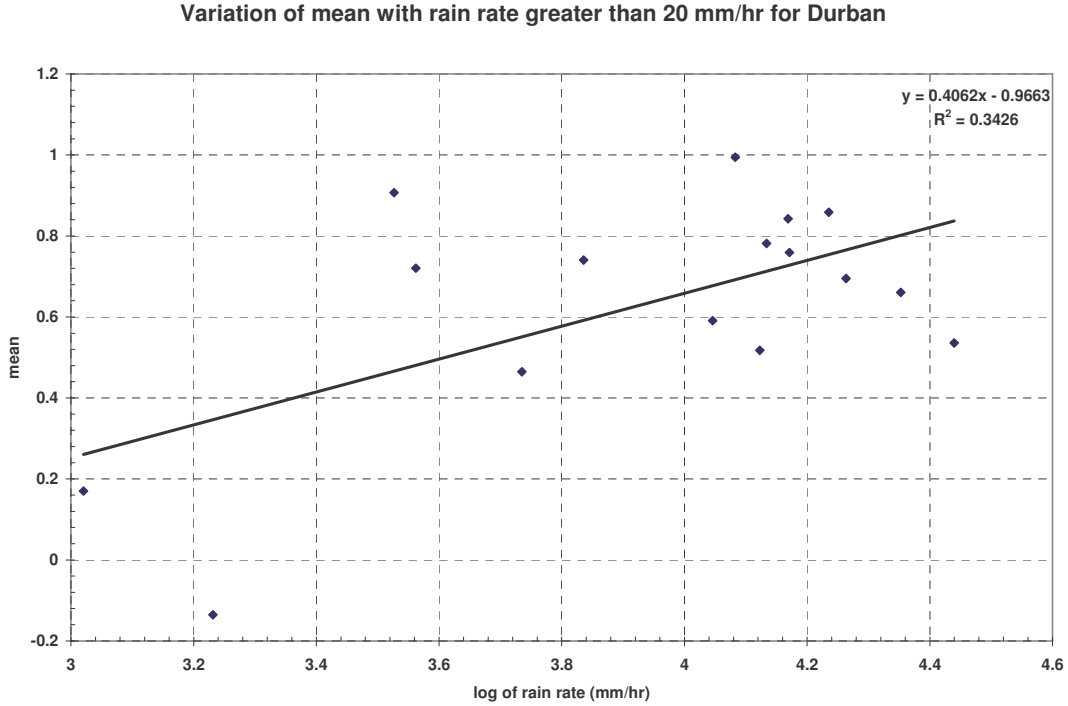

Figure 5.8b: Variation of mean $\mu\ mm$ with log of rain rate greater than 20 mm/hr for Durban

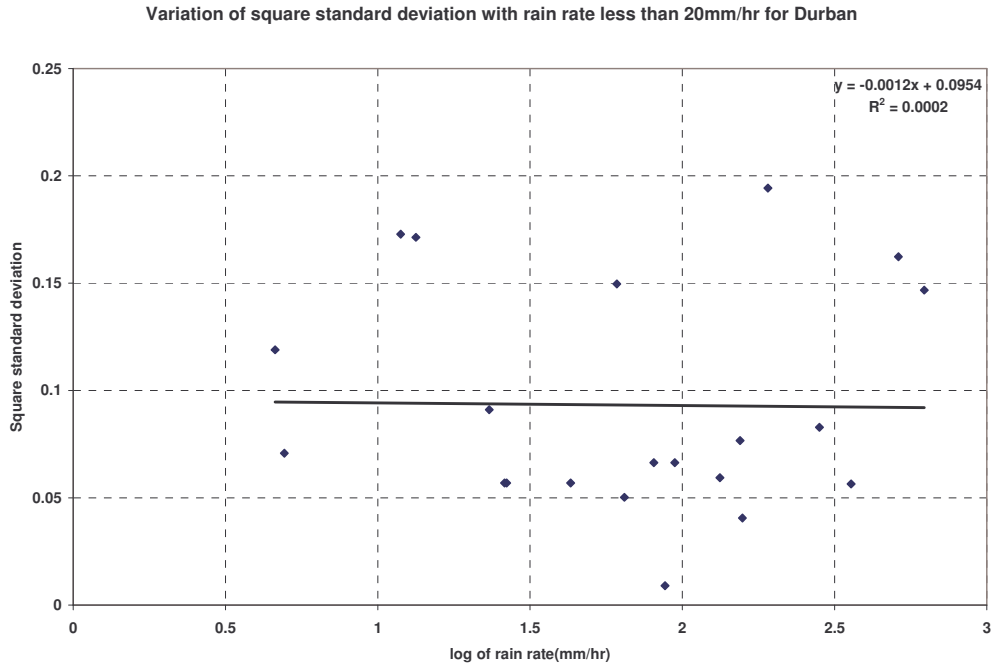

Figure 5.9a: Variation of mean σ^2 *mm* with log of rain rate greater than 20 mm/hr for Durban

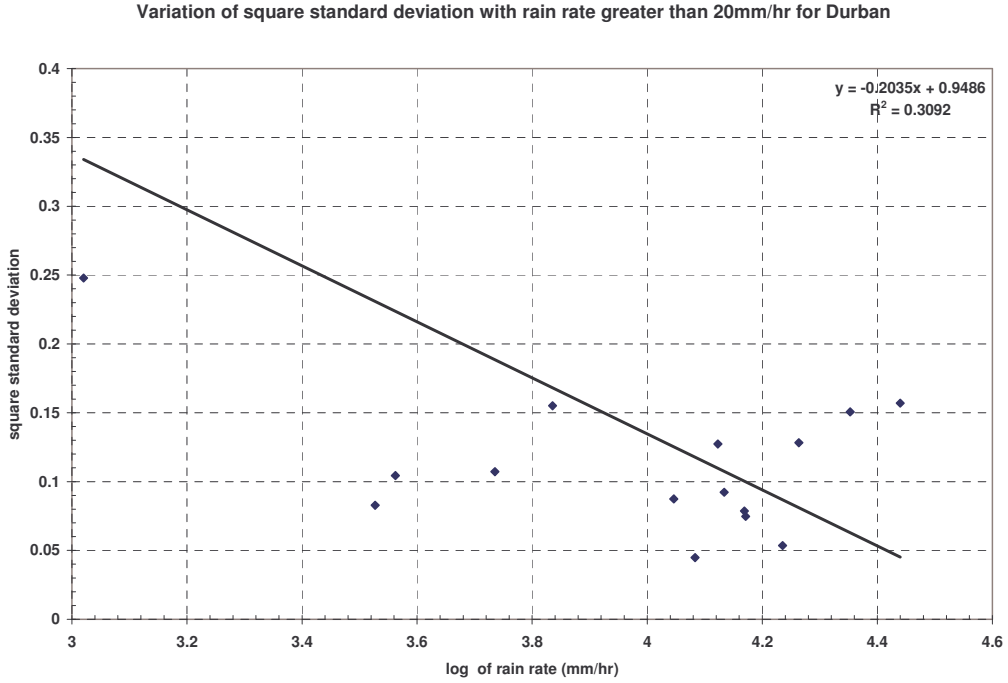

Figure 5.9b: Variation of mean σ^2 *mm* with log of rain rate greater than 20 mm/hr for Durban

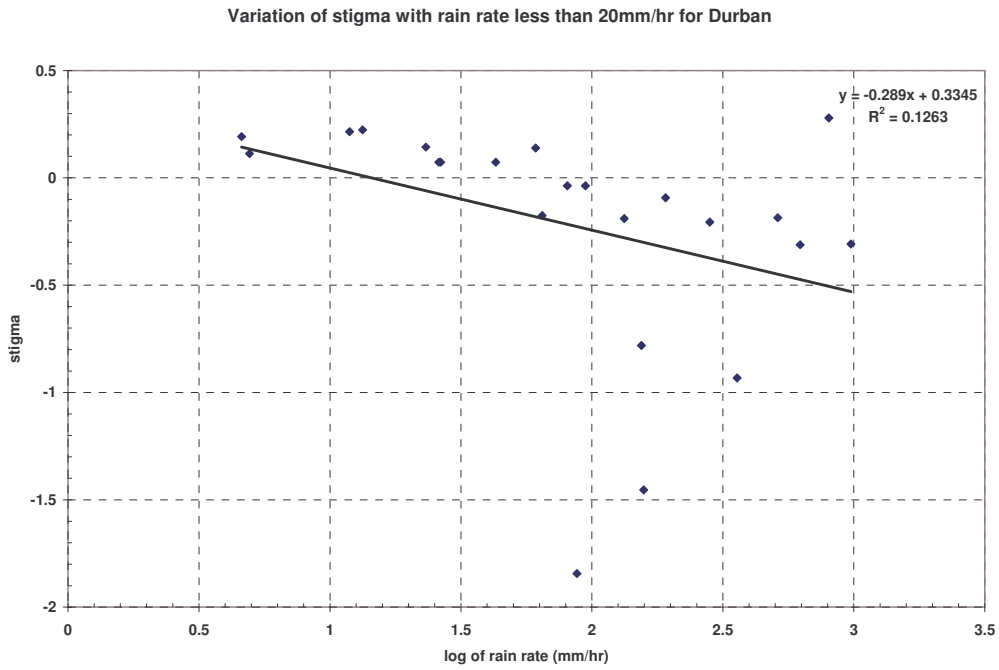

Figure 5.10a: Variation of mean $\gamma\ mm$ with log of rain rate greater than 20 mm/hr for Durban

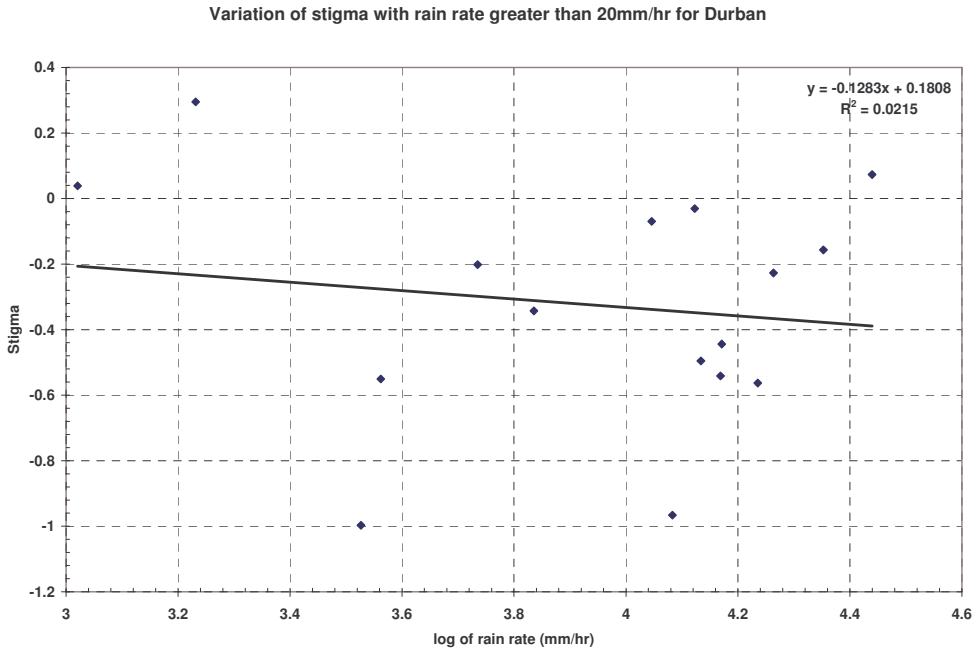

Figure 5.10b: Variation of mean $\gamma\ mm$ with log of rain rate greater than 20 mm/hr for Durban

5.3.1 Self-Consistency (SC) of Proposed DSD

The method proposed is validated by comparing the observed rain rates with computed ones using the DSD model, and Gunn and Kinnzer terminal velocity. Self-consistency of the model is determined by the degree of departure from unity of coefficient ratio of the observed to estimated rain rate. The coefficients of self-consistency (SC) is computed for all selected rain rates starting from 1.94 mm/hr to 84.76 mm/hr. The minimum coefficient of SC considered for regime of rain rate less than 20 mm/hr falls within 12% of unity, while for the regime greater than 20 mm/hr falls within 18% of unity. The expressions for self consistency for the two regimes of rain rate are derived using second order polynomials, and expressed as:

$$\begin{aligned} Normalized(R) &= 1.2853 - 0.2169X + 0.0082X^2 \qquad 0 < R \le 20 mm/hr \\ Normalized(R) &= 0.0345 - 3\times10^{-3}X + 3\times10^{-6}X^2 \qquad 20 < R \le 100 mm/hr \end{aligned} \tag{5.13}$$

Here $X = \ln(R)$. Table 5.3 shows samples of different DSD models for different regions with their determined self-consistence expressions.

5.3.2 Comparison of Proposed Model with Existing Models

Comparison of proposed models for South Africa is tested against its counterparts from other regions using the Root Mean Square Error (RME) method. Table 5.3 shows selected DSD models with their respective identification names. Figure 5.11 and Figure 5.12 show the comparisons between the proposed models and those described in Table 6.8, respectively. RMS error is calculated for all the compared models by using the following formula:.

$$RMSE = \sqrt{\sum_{i=1}^{n} \frac{[Measured\ N(D_i) - Modeled\ N(D_i)]^2}{n}} \tag{5.14}$$

Where, $N(D_i)$ is raindrop size distribution at different diameter sizes and n is the number of channels considered.

In the overall analysis, the RMSE differences are a bit large for the compared models but the proposed model shows lower values of RMSE between the proposed model and measured DSD. The performance analysis using RMSE at region of rain rate less than 20 mm/hr confirms that the proposed model performs better in all fifteen spectra of DSD samples. The average minimum RMSE is found with proposed model with value of 51.19 while the lowest RMSE is associated with the Marshall and Palmer model. The best performances based on RMSE are rated in ascending order as follows: Marshall and Palmer, Atlas *et al*., Timothy *et al*., Ajayi *et al*., and the proposed South Africa model.

In the case of regime of rain rate greater than 20 mm/hr, the average minimum RMSE is obtained in the proposed model with RMSE value of 27.23 and the least is found with Marshall and Palmer. The performance based on RMSE in ascending order is as followings: Marshall and Palmer, Atlas et.al, Timothy, Ajayi et al., and the proposed model.

5.4 Conclusion

The purpose of this chapter was to study the characteristics of raindrop size distribution. The raindrop size distribution spectra showed that the major part of the drop density falls within the 0.3 mm and 4.0 mm diameter range. Using the maximum likelihood regression method on the collected data, the three-parameter lognormal distributions are estimated for two rain rate regimes. The technique employed gives proper description of the DSD distribution curves very well even at lower rain rate. In this study, it was confirmed that Marshall and Palmer and other considered DSD models are not adequate to describe raindrop size distribution in the southern Africa region. A simple lognormal distribution model is proposed to describe the raindrop distribution for Durban using two rain rate regimes. Based on the comparisons carried out, it was found that the proposed model performs better than its counterparts, though at higher rain rates, the distribution patterns of Timothy *et al*. (2002) and Ajayi *et al*. (1985) seem to give similar shapes of distribution.

Table 5.3 Comparison of DSD models with their respective normalized rain rate

Model title	DSD model	Normalization X=Ln(R)
Marshall and Palmer	$N(D) = N_0 \times e^{-\Delta D}$ $N_0 = 8000(m^{-3}mm^{-1})$ $\Delta = 4.1 \times R^{-0.21}(mm^{-1})$	$0.8425 - 0.00889X + 0.00687X^2$
Atlas et al.	$N(D) = N_0 \times D^2 \times e^{-\Delta D}$ $N_0 = 64500 \times R^{-0.5}(m^{-3}mm^{-1})$ $\Delta = 7.09 \times R^{-0.27}(mm^{-1})$	$2.392 - 0.6364X + 0.05827X^2$
Jiang et al.	$N(D) = N_0 . \frac{\eta}{\sigma}\left(\frac{D}{\sigma}\right)^{\eta-1} \exp\left[-\left(\frac{D}{\sigma}\right)^{\eta}\right]$ $\eta = 0.95 \times R^{0.14}$ $\sigma = 0.26 \times R^{0.42}$ $N_0 = 1000$	$1.184 - 0.03466X + 0.02591X^2$
Timothy et al.	$N(D) = \frac{N_T}{\sigma D\sqrt{2\pi}} \exp\left[-\frac{1}{2}\left\{\frac{\ln(D)-\mu}{\sigma}\right\}^2\right]$ $N_T(D) = 203R^{0.241}$ $0mm/hr < R \le 20.0mm/hr$ $\mu = -0.313 + 0.2227\ln(R)$ $\sigma^2 = 0.108 - 0.0086\ln(R)$ $N_T(D) = 78.3R^{0.558}$ $20.0mm/hr < R \le 250mm/hr$ $\mu = -0.312 + 0.1175\ln(R)$ $\sigma^2 = 0.1184 + 0.0086\ln(R)$	$0.0961 - 0.0004X + 2\times10^{-5}X^2$ $0.2838 + 0.0004X - 8\times10^{-7}X^2$
Ajayi et al.	$N(D) = \frac{N_T}{\sigma D\sqrt{2\pi}} \exp\left[-\frac{1}{2}\left\{\frac{\ln(D)-\mu}{\sigma}\right\}^2\right]$ $N_T(D) = 108R^{0.363}$ $\mu = -0.195 + 0.1999\ln(R)$ 2^{nd} *and* 3^{rd} *moment* $\sigma^2 = 0.137 - 0.013\ln(R)$ $\mu = -0.137 + 0.192\ln(R)$ 5^{th} *and* 6^{th} *moment* $\sigma^2 = 0.109 + 0.010\ln(R)$	$0mm/hr < R \le 20.0mm/hr$ $0.0971 - 0.0003X + 1x10^{-5}X^2$ $20.0mm/hr < R \le 250mm/hr$ $0.0948 + 0.00004X - 8x10^{-8}X^2$ $0mm/hr < R \le 20.0mm/hr$ $0.0947 - 0.0001X + 0.0947X^2$ $20.0mm/hr < R \le 250mm/hr$ $0.2739 + 0.0007X - 3x10^{-6}X^2$

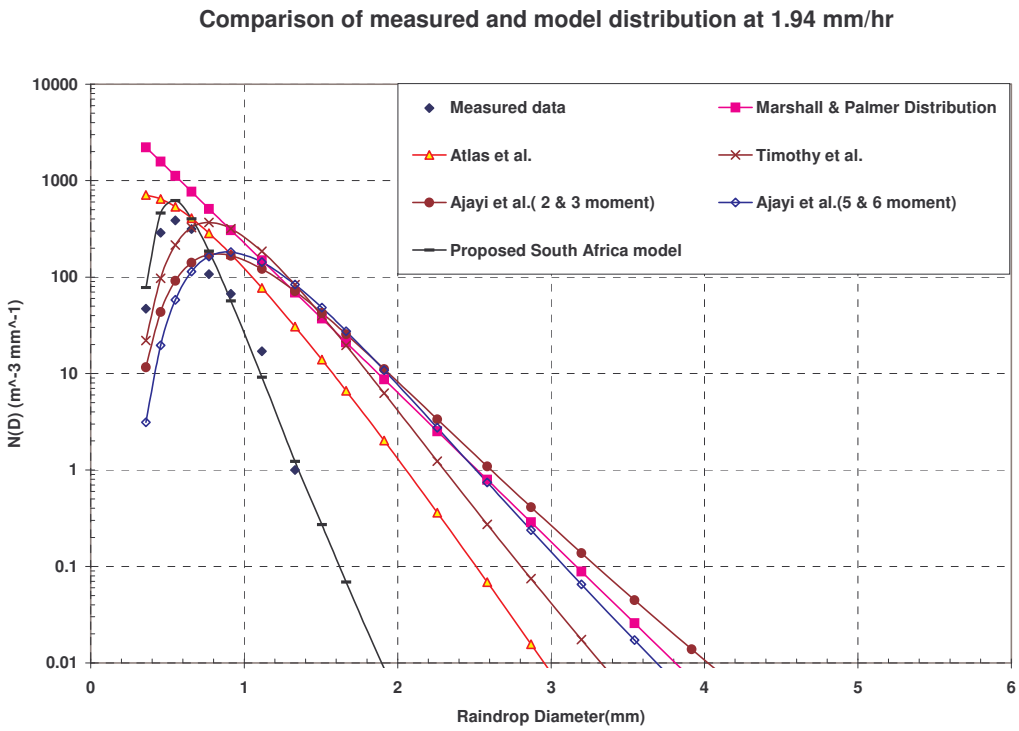

Figure 5.11a: Comparison of measured, proposed and other existing models of N (D) at R=1.94 mm/hr

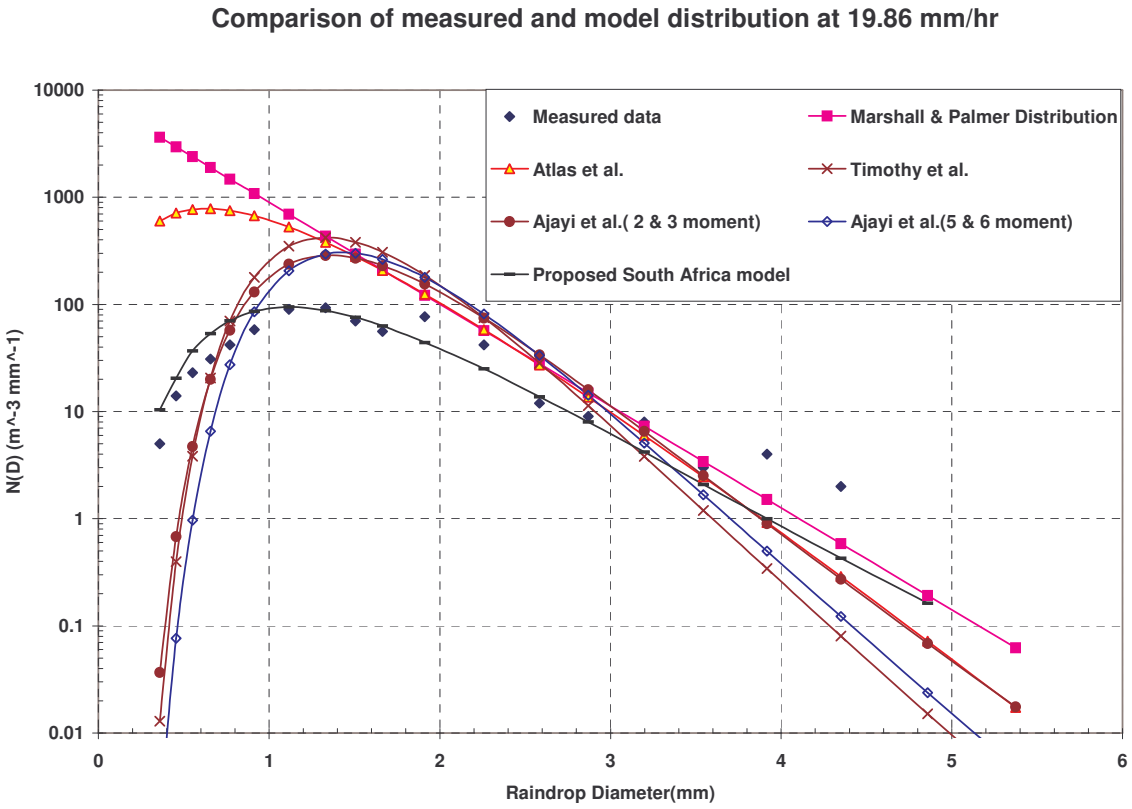

Figure 5.11b: Comparison of measured, proposed and other existing models of N (D) at R=19.86 mm/hr

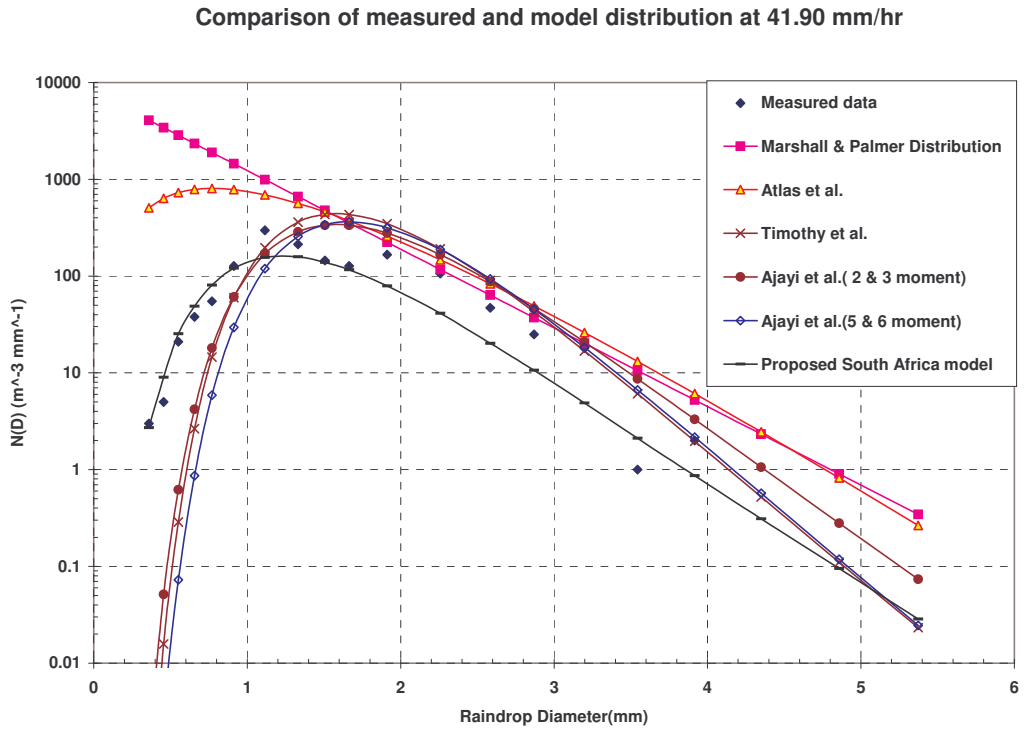

Figure 5.12a: Comparison of measured, proposed and other existing models of N (D) at R=41.90 mm/hr

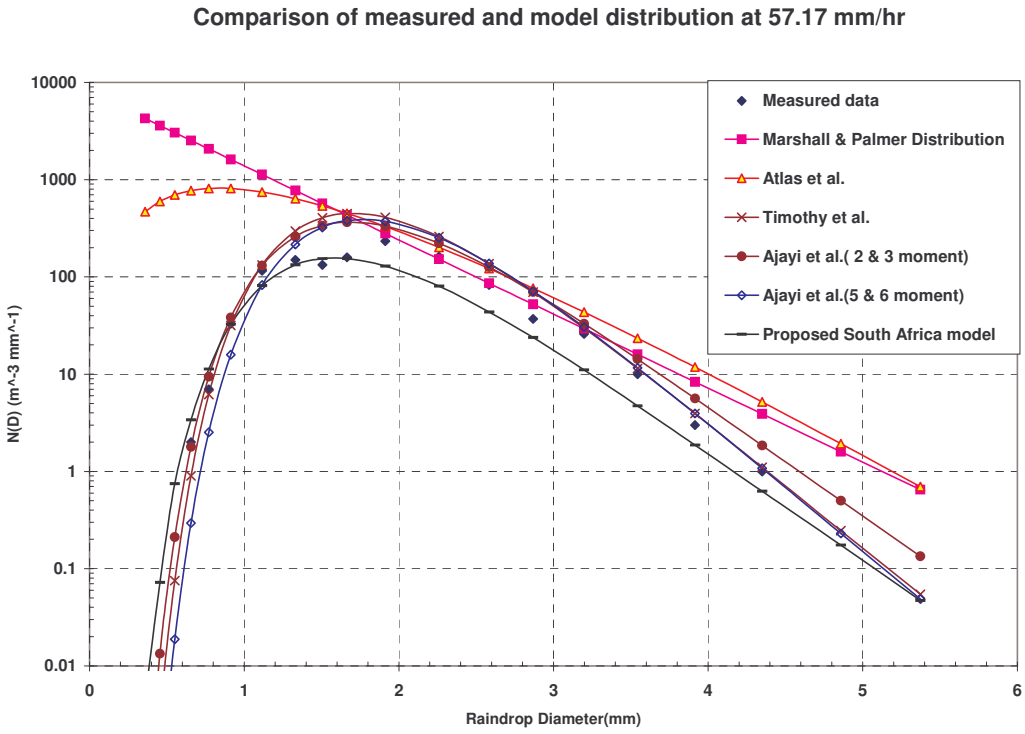

Figure 5.12b: Comparison of measured, proposed and other existing models of N (D) at R=57.17 mm/hr

Chapter Six

Conclusions and Recommendations for Future Work

6.0 Introduction

Because of the often severe tropospheric propagation conditions existing in many regions of the world at low latitudes and the resulting constraints on terrestrial and satellite communications systems operating in the microwave and millimetre-wave bands, there is a particular need for accurate propagation predictions. Overprediction of a propagation effect can result in costly overdesign of a system. On the other hand, underprediction can result in a system that is unreliable. Because of the high temperatures and frequently resulting high humidities in low-latitude regions of the world, severe propagation effects can sometimes occur in both clear-air and precipitation conditions.

Global ITU-R radioclimatic models of point rain-rate distributions within discrete rain zones have been available for prediction of annual cumulative distributions of rain attenuation on terrestrial and earth-space line-of-sight links since the early 1970's. Such models have also been used for prediction of interference due to rain scatter into terrestrial and earth-space systems sharing the same frequencies since the early 1970's. Distributions of rain attenuation have been used indirectly to predict cumulative distributions of crosspolarization discrimination (XPD) due to rain since the late 1970's.

The work of Crane (1980) has considerably influenced the zonal models of the ITU-R, and the Crane models have been used extensively in the United States, although to a lesser extent in other parts of the world. The work of Segal (Segal 1986) has also considerably influenced the ITU-R zonal models, and provided a systematic approach for obtaining a specified number of rain zones in countries such as Canada that have sufficiently large data bases of short-integration-time data. One of the values of the zonal approach is that it allows spectrum regulators to perform system calculations for a small number of somewhat representative situations. Because of the discrete nature of the zonal

approach and its inherent lack of precision to some degree, however, various other attempts have been made to predict point rain-rate distributions, or statistics on such distributions, at specific points within a region. Such approaches have normally used measured rain-rate distributions for as many locations in a region as possible, and then fitted contour maps for particular parameters of the distribution. Perhaps the first successful approach of this type was that of Segal for Canada (Segal B, 1986), which employed contour maps of two parameters of the rain rate distribution, based on data for 47 locations within Canada and adjacent regions of the United States. Watson *et al.* (1982) later mapped rain rates exceeded for 0.1% and 0.01% of an average year based on data for 400 locations within Europe. Moupfouma (1987) developed two more general global models using two parameters, one of which was conveniently the rain rate exceeded for 0.01% of the time.

Another attempt to avoid the zonal approach was made by Rice and Holmberg (1973), who developed a model employing three basic long-term parameters: the average annual rainfall (mm), the ratio of thunderstorm rain to total rain, and the average annual number of days with rainfall of 0.25 mm or more. The ITU-R (and its predecessor, the CCIR) has provided a global contour map of the rain rate exceeded for 0.01% of the year since 1982 ITU-R P.837-1 (1994), although it was derived in part from use of the zonal model, at least at the early stages. The accuracy of the global map of the ITU-R has of course always been quite variable because of the lack of data for several regions of world including Africa. This study therefore partly attempts to address this challenge.

6.1 Conclusions

Based on the work covered in chapters three, four and five, we state the following conclusions:

6.1.1 Chapter 3 – Rain Rate Integration Time Conversion Modelling

In this Chapter, a review of models used to convert rain rate from any integration time to the required one-minute equivalent were applied, covering the classification of the

conversion models into the three categories of physical, analytical and empirical models. A proposed hybrid method for the conversion of five-minute integration time to one-minute equivalent was discussed as well as comparison of the proposed model with two suggested global models.

In the proposed hybrid method, the strength of each category of model classes were combined to produced a hybrid model. The selected model consists of regional parameters in order to characterize the rain rate pattern for a defined area. The resulting one-minute cumulative distribution of rain rate is fitted with polynomial, power, linear and logarithm fits of distributions. The performances of these fits were optimized using standard deviation and root-mean square of absolute relative error at the control site of Durban. The optimizations were carried out over the equiprobable approach and conversion factor approach. The results show that the equiprobable approach gives better results than the conversion factor approach. In addition, the second order polynomial fit performed relative better than its counterparts. The evidence of good performance by the second order polynomial fit makes it a good candidate for conversion of rain rate from five-minute to equivalent one-minute in South Africa and the surrounding Islands. The South African region was subsequently classified into 12 sub-climatic zones using the Köppen climatic classification. The coefficients of polynomial, power, linear and logarithm fits were given for each of the classes with their square correlation coefficients. Finally, based on the work in this chapter, the polynomial fit of second order is adopted for South Africa and the two surrounding Islands.

6.1.2 Chapter 4 – Rain Rate Modelling

In this Chapter, the most widely used rain rate probability distributions were investigated using the maximum likelihood estimator to optimize the distributions. It was found that most of the studied areas were best defined by the Gamma distribution model, followed by Weibull distribution model, while the lognormal distribution did well at only a few sites. For the 21 stations, the Gamma model had an average χ^2 statistic of 10.8, followed by the Weibull model with an average of 19.85. The rest of the models gave an average

χ^2 statistic of above 55, which is too close to the threshold 63.7 for 40 degrees of freedom. The average root mean square percentage also gives credence to the fact that the Gamma model is the most appropriate to describe most sites in South Africa and surrounding islands. The proposed model will thus serve as a good tool for system designers because it is easy to use when rainfall distribution is needed for any site, and its parameters are easily understood.

The study proposes new rainfall climatic zones based on the ITU-R and the Crane rain climatic zone designations. It is found in several sites that the ITU-R model over-estimated, while in many others the ITU-R model under-estimated, rainfall rate values at defined probabilities of exceedence. It is observed that the widest percentage of differences between ITU-R P.837-1 and P.837-5 was 66.67% for Marion Island, and the least percentage was 13.63% observed in Beaufort and Cape Point. Crane rain climatic zone designations matches in some sites as noted in Pretoria, Tshipise, Cape Town, Beaufort, Klerksdorp and Upington.

Rain contour maps have been identified as desirable tools for the objective of providing system designers, site engineers and network planners with estimated fade margins due to rain attenuation. The two plotted contour maps were tailored to satisfy accepted rainfall climatic zones defined by the ITU-R and Crane maps which are available in most radio planning tools. In this research, the contour map was developed using advanced Geographic Information Systems (GIS) tools with the adoption of IDW estimator to provide the contour map for rainfall rate at 0.01% of exceedence.

6.1.3 Chapter 5 – Rain Dropsize Distribution Modelling

The purpose of this chapter was to model the characteristics of raindrop size distribution for the Southern Africa region. The importance of DSD modelling arises from the need to employ Mie scattering theory and appropriate, region-dependent DSD's (not just the Laws and Parsons (LP) drop size distribution) to obtain plots of specific attenuation γ (dB/km) against frequency for varying rain rate. The raindrop size distribution spectra showed that the major part of the drop density falls within the 0.3 mm and 4.0 mm

diameter range. Using the maximum likelihood regression method on the collected data, the three-parameter lognormal distributions are estimated for two rain rate regimes. The technique employed gives proper description of the DSD distribution curves very well even at lower rain rates. In this study, it was confirmed that Marshall and Palmer and other considered DSD models are not adequate to describe raindrop size distributions in the Southern Africa region. A simple lognormal distribution model is thus developed to describe the raindrop distribution for Durban using two rain rate regimes. Based on the comparisons carried out, it was found that the proposed model performs better than its counterparts, though at higher rain rates, the distribution patterns of Timothy *et al*. (2002) and Ajayi *et al*. (1985) seem to give similar shapes of distribution.

6.2 Recommendations for Future Work

6.2.1 Measurement Campaign

The need for proper estimation of rain rate and microphysics of rain requires equipment that will be capable of measuring spatial and real time rain events at optimal resolutions. In this thesis, the work done has been limited to measurements using the rain gauge and the distrometer. The information on water phase and drop size distribution gained through this is used to study the precipitation process and improve other measurement methods, such as weather radar or satellite estimates. The Micro Rain Radar (MRR) is a vertically pointing radar that measures the backscatter and fall velocity of precipitation particles in several heights. Its features include:

- Vertical profiles of rain rate, LWC and drop size distribution
- No influence of wind, sea spray or surroundings, no evaporation errors
- No maintenance, long term unattended operation
- The large sampling volume allows a very high time resolution
- Averaging interval adjustable within 10 s to 3600 s

The other set of equipment that will improve the research campaign is the introduction of network of rain gauges, as well as inclusion of video distrometers to sample raindrops at lower diameters.

6.2.2 Modelling and Simulation

There is need to further broaden the work done in this region by investigating the possibility of modelling raindrop size distribution using different estimator methods such as the Kernel estimator, Method of Moments, and statistical distributions methods such Weibull and Gamma. In addition, improvements must be made in terms of dropsize classifications using rain type and diameter classes. The variability characteristic of raindrop size distribution can also be evaluated using different classification methods such as rain rate regime, diameter classes, and type of rain such as drizzle, shower, widespread and thunderstorm classification.

6.2.3 Applications

Based on the results obtained from this work, the results can be extended to cover various research topics like the ones listed below:

- Effects of rain rate and microphysical characteristics in both satellite and terrestrial links.
- Comparative studies of depolarization of X, Ku, K, Ka, V, and W-bands satellite signal in the presence of rain.
- Evaluation of raindrop size distribution using different estimator methods for Southern Africa.
- Parameterization of raindrop size distribution using different dropsize classifications.
- Prediction of depolarization using T-matrix and Mie-scattering extinctions for Southern Africa.
- Prediction of rain backscattering effects at frequency ranges between 1-78 GHz.
- Development of different techniques to mitigate against signal loss due to rain at frequencies above 10 GHz.

References

Abraham, F.F. (1970): 'Functional dependence of drag coefficient of a sphere on Reynolds Number,' P*hys. Fluids 13, 2194-2195.*

Adimula I.A and Ajayi G.O. (1996): 'Variation in raindrop size distribution and specific attenuation due to rain in Nigeria,' Ann. Telecom, Vol.51, No. 1-2, pp.87-93.

Ajayi G.O and Ofoche, E. (1984): 'Some Tropical Rainfall Rate Characteristics at Ile-Ife for Microwave and Millimetre wave Applications,' *Journal of Climate and Applied Meteorology*, Vol. 23, No. 4, pp.562-567, April.

Ajayi G.O, Feng S., Radicella S.M. and Reddy, B.M. (1996): 'Handbook on Radiopropagation Related to Satellite Communications in Tropical and Subtropical Countries,' *ICTP*, Trieste, Italy.

Ajayi G.O and R.L Olsen (1985): 'Modelling of a raindrop size distribution for microwave and millimetre wave applications,' *Radio Science*, Vol. 20, No. 2, pp. 193-202.

Ajayi, G.O. and Adimula, I.A. (1996): 'Variations in Raindrop Size Distribution and Specific Attenuation due to Rain in Nigeria,' *Ann. Telecommunica*., 51(1-2), 87-93.

Ajewole, M.O, Kolawole, L.B and Ajayi, G.O (1999): 'Theoretical study of the effect of different types of tropical rainfall on microwave and millimeter-wave propagation,' *Radio Science,* Vol. 34, No 5, pp.1103-1124.

Ajewole, M.O, Kolawole, L.B and Ajayi, G.O (1999): 'Theoretical study of the effect of different types of tropical rainfall on microwave and millimeter-wave propagation,' *Radio Science,* Vol. 34, No 5, pp.1103-1124.

Atlas, D. and Ulbrich, C.W. (1977): 'Path- and aero-integrated rainfall measurements by microwave attenuation in the 1-3-cm band,' *Journal of Applied Meteorology*, 16, 1322-1331.

Atlas, D., Srivastava, R.C. and Sekhon, R.S. (1973): 'Doppler radar characteristics of precipitation at vertical incidence,' *Rev. Geophys. Space phys*., 11, 1-35.

Barclay, P.A., Bennett, J.A. and Botton, R.C. (1978) 'Properties of rain for microwave propagation studies,' Rep.MEE78-1, pp.35-68, Electrical Engineering Department, Monash University, Melbourne, August.

Beard, K.V. (1976): 'Terminal velocity and shape of cloud and precipitation drops aloft,' *Journal of the Atmospheric Sciences*, 33, 851-864.

Best, A.C. (1950): 'Empirical formulae for the terminal velocity of water drops falling through the atmosphere,' *Quart. J.R. Met.Soc*., 76, 302-311.

Brussard, G. (1976): 'A meteorological model for rain induced cross polarization,' *IEEE Trans. A-P*, Vol.AP-24, pp.5-11.

Burgueno, A.M., Puigcever, M. and Vilar, E. (1988): 'Influence of Rain gauge Integration Time on the Rain Rate Statistics Used in Microwave Communication,' *Ann. Telecomm*., Vol.43, No. 9-10, pp.522-527.

Capsoni, C. and Luini, L. (2008b): '1-min Rain Rate Statistics Predictions From 1-hour rain rate Statistics Measurements,' *IEEE Trans. Antennas and Propagation*, Vol.56, No. 3, March.

Capsoni, C., Emiliani, L.D and Luini, L. (2008a): 'Extension of ITU-R Method for Conversion of Rain Rate Statistics from various Integration times to One minute,' *Electronics Letters* , Vol. 44, No. 8, April.

Capsoni, C., Fedi, F., Magistroni, C., Paraboni, A. and Pawlina, A. (1987): 'Data and Theory for a New Model of the Horizontal Structures of Rain Cells for Propagation Applications', *Radio Science*, Vol. 22, No. 3, pp.1726-1733, May.

Chebil, J. and Rahman, T.A. (1999): 'Rain Rate Statistical Conversion for the Prediction of Rain Attenuation in Malaysia,' *Electronic Letters*, Vol.35, no. 12, pp.1019-1021.

Chi-Huei Tseng, Kun-Shan Chen, Chih-Yuan Chu, (2005): "Variability Analysis of Ka Band Rain Attenuation in Taiwan," Progress in Electromagnetics Symposium 2005, Hangzhou, August 23-26, pp.1-2.

Cohen, A. C. and Whitten, B.J. (1980): 'Estimation in the three-parameter Lognormal Distribution,' *Journal of American Statistical Association*, Vol.75, N0370 pp399-404

Crane, R.K, (2003): 'A local model for the prediction of rain-rate statistics for Rain-Attenuation models,' *IEEE Transactions on Antennas and Propagation*, Vol.51, No 9, pp.2260-2273.

Crane, R.K. (1980): 'Prediction of Attenuation by Rain,' *IEEE Trans. Commun.*, COM-28(9), pp. 1717-1733.

Crane, R.K. (1996): Electromagnetic Wave Propagation through Rain, John Wiley & Sons, Canada.

Davies C.N (1945): Definitive Equations For the fluid resistance of spheres. *Proc. Phys .Soc. London, A57, pp 259-270.*

Deirmendjian, D. (1969): Electromagnetic scattering on spherical polydispersion. Elservier, New York.

Dutton, E.J. and Dougherty, H.T. (1979): 'Year-to-year variability of rainfall for microwave applications in the U.S.A.,' *IEEE Trans. Commun.*, COM-27(5), 829-832.

Dutton, E.J. and Dougherty, H.T. (1984): 'A second modelling approach to year-to-year rainfall variability in the U.S.A for Microwave/millimeter wave applications,' *IEEE Trans. Commun.*, COM-32(10), pp. 1145-1148.

Dutton, E.J., Dougherty, H.T. and Martin Jr, R.F. (1974): 'Prediction of European Rainfall and Link Performance Coefficients at 8 to 30 GHz,' NTIS Rep ACC-ACO-16-17.

Dutton, E.J., Dougherty, H.T., and Martin (jr), R.F. (1974a): 'Prediction of European Rainfall and link performance coefficients at 8 to 30 *GHz* ,' *Inst. Telecommun. Sci.*, U.S. Department of Commerce, Washington DC.

Dutton, E.J., Dougherty, H.T., and Martin (Jr), R.F. (1974b): 'Prediction of European Rainfall and Link Performance Coefficients at 8 to 30 GHz,' NTIS Rep ACC-ACO-16-17.

Eckhard, L., Werner, A.S. and Markus, A. (2001): 'Lognormal Distributions across the Sciences: Key and Clues,' *BioScience* , Vol. 51, No.5 (May).

Emiliani, L.D., Agudelo, J., Gutierrez, E., Restrepo, J. and Fradique-Mendez, C. (2004): 'Development of Rain-Attenuation and Rain-Rate Maps for Satellite

System Design in the Ku and Ka Bands in Colombia,' *IEEE Antennas and Propagation Magazine,* Vol.46, No.6 December, pp.54-68.

Emiliani, L.D., Luini, L. and Capsoni, C. (2008): 'Extension of ITU-R Method for Conversion of Rain Rate Statistics from Various Integration times to One minute,' *Electronics Letters*, Vol. 44 (8), April, pp. 557-558.

Emiliani, L.D., Luini, L., and Capsoni, C. (2009): 'Analysis and parameterization of Methodologies for the Conversion of Rain-Rate Cumulative Distributions from various integration times to One minute,' *IEEE Antennas and propagation Magazine*, Vol.51, No 3, pp.71-84, June.

Evans, M., Hastings, N. and Peacock, B. (1993): Statistical Distributions, 2nd Ed. John Wiley and Sons Inc, New York.

Fashuyi, M.O., Owolawi, P.A. and Afullo, T.J. (2006): 'Rainfall Rate Modelling for LOS Radio Systems in South Africa,' *South African Institute of Electrical Engineers Journal*, Vol. 97(1), March, pp74-81.

Fedi, F. (1979): 'Rainfall Characteristics Across Europe,' *Alta Fre.,* Vol. 48 (4), pp. 158-166.

Fedi, F. (1981): 'Prediction of Attenuation due to Rainfall on Terrestrial Links,' *Radio Science,* Vol. 16(5), pp.731-743.

Flavin, R.K. (1982): 'Rain Attenuation Considerations for Satellite paths in Australia,' *Australian Telecommunications Research*, Vol. 16, pp.11-24.

Foote, G.B. and Du Toit, P.S. (1969): 'Terminal velocity of raindrops aloft,' *Journal Applied Meteorology*, 8, 249-253.

Gunn, R. and Kinzer, G.D. (1949): 'The terminal velocity of fall for water droplets in stagnant air,' *Journal of Meteorology*, Vol. 6,243-248.

Hall, M.P.M and Barclay, L.W. (1989): 'Radiowave propagation,' Peter Peregrinus Limited, UK.

Hall, M.P.M (1991): 'Overview of radiowave propagation,' In *Radiowave propagation*, eds. Hall, M.P.M, and Barclay, L.W., Peter Peregrinus Limited, UK.

Huang, J.Y. (1990): 'An Index of Precipitation Probability for Dryness/Wetness Analysis - Gamma Distribution Probability Index (in Chinese),' *Meteorology Monthly Weather Review,* Vol. 16(9), pp. 8-12.

Ippolito, L.J. (1981): 'Radio Propagation for Space Communications Systems'. *Proceedings*, Institute of Electrical and Electronics Engineers Conference, Vol.17, pp. 929-945.

Ito, C. and .Hosoya, Y. (1999): 'Worldwide 1 min Rain Rate Distribution Prediction Method which uses Thunderstorm Ratio as Regional Climatic Parameter,' *Electronic Letters*, Vol.35, No.18, pp.1585-1587, September.

Ito, C. and Hosoya, Y. (2001): 'A Study on Lavergnat-Golé Conversion Method for different Integration time Rain Rates' (in Japanese), Technical Report of IEICE, Japan, A.P 2001-40.

Ito, C. and Hosoya, Y. (2000): 'A Worldwide Conversion Method for different Integration time rain rates by using M distribution and Thunderstorm Ratio,' International Symposium on Antennas and Propagation (ISAP 2000), RP-0058, pp.277-280.

Ito, C. and Hosoya, Y. (2006): 'Proposal of a Global Conversion Method for Different Integration Time Rain Rates by Using M-Distribution and Regional Climatic Parameters,' *Electronics and Communications in Japan*, Part1, Vol.89, No.4.

ITU-R P.837 (2001): 'Characteristics of Precipitation for Propagation Modelling, Recommendation ITU-R P.837-1,2, 3, 4, 5'. International Telecommunication Union, Geneva, Switzerland

ITU-R P.837 (2007): 'Characteristics of Precipitation for Propagation Modelling, Recommendation ITU-R P.837-5,' International Telecommunication Union, Geneva, Switzerland.

ITU-R P.837-1 (1994): 'Characteristics of precipitation for propagation modelling,' ITU R Rec.P.837-1, Geneva.

ITU-R P.837-2 (1999): 'Characteristics of precipitation for propagation modelling,' ITU-R Rec.P.837-2, Geneva.

ITU-R P.837-5 (2007): 'Characteristics of precipitation for propagation modeling,' ITU-R Rec.P.837-5, Geneva.

ITU-R Document 3J/29-E (2008): 'Review and Analysis paper is concerning the Conversion of Statistics from various integration times and Recommendation ITU-R P.837-5", International Telecommunication Union Radiocommunications Sector, Geneva, Working paper 3J.

Jiang, H., Sano, M., and Sekine, M. (1997): 'Weibull raindrop-size distribution and its application to rain attenuation,' *IEE Proc. Microwave Antennas Propagation*, Vol.144, No.3, June, pp. 197-200.

Joss, J. and Waldvogel, A. (1969): 'Raindrop size distribution and sampling size error,' *Journal of the Atmospheric Sciences*, Vol. 26, pp.566-569

Joss, J., Thams, J. C. and Waldvogel, A. (1967): 'The Variation of raindrop-size distribution at Locarno,' *Proceedings of International Conference on Cloud Physics*, pp. 369-373, 1967

Joo, H.L., Yang, S. K., Jong, H.K and Yong, S.C. (2002): 'Emperical Conversion process of Rain Rate Distribution for Various Integration Time,' *Proceedings of URSI Commission F Wave Propagation and Remote Sensing, Maastricht,* pp. 1450-1454.

Karasawa, Y., and Matsudo, T. (1990): 'A Prediction Method of One-minute Rain Rate Distributions in Japan,' *Trans. IEICE Japan*, Vol. J73-B-II, No.10, pp.518-527.

Karasawa, Y., and Matsudo, T. (1991): 'One-minute Rain Rate Distributions in Japan derived from AMeDAS One-hour Rain Rate Data,' *IEEE Trans. Geosci.Remote Sensing*, Vol.29, No.6, pp.890-898, November.

Komabayasi, M., Gonda, T., and Isono, K. (1964): 'Life times of water drops before breaking and size distribution of fragment droplets,' *J.Meteor.Soc. Japan,* Vol. 42,330-340.

Lavergnat, J., and Golé, P. (1998): 'A Stochastic Raindrop Time Distribution Model,' *AMS Journal of Applied Meteorology*, Vol. 37, No. 8, pp.805-818, August.

Laws, J. O. and D. A. Parsons (1943): 'The Relation of Raindrop-Size to Intensity,' Transactions *on Amer. Geophysics Union*, Vol. 24, pp. 452-460.

Lee, J.H., Kim, Y.S, Kim, J.H and Choi, Y.S. (2001): 'A conversion method of rain rate stastics from various integration time data,' *CLIMPARA,* Budapest, Hungary, pp.43-47.

Li, L., Zhu, Y. and Zhao, B. (1998): 'Rainfall Rate Distributions for China from Hourly Rain Gauge Data,' *Radio Science,* Vol. 33, No. 3 (May-June), pp. 553-564.

Lin, S.H. (1976): 'Rain-rate distributions and extreme value statistics,' *Bell System Technical Journal,* Vol. 55, pp. 1111-1124.

Lin, S.H. (1978): 'More on rain rate distributions and extreme value statistics,' *Bell System Technical Journal,* Vol. 57, pp. 1545-1568.

Maciel, L.R. and Assis, M.S. (1990): 'Tropical Rainfall Dropsize Distribution,' *International Journal of Satellite Communication*, Vol.8, pp.181-186.

Maitra, A., Marina, D., Sutapa, B., and Sen, A.K. (1995): 'Modelling of Raindrop Size Distribution from Measurements of Rain Rate and Attenuation at Millimeter and Optical Wavelengths at Calcutta, India,' *Proceedings of* 7th URSI Comm.F Open Symposium on Wave Propagation and Remote Sensing, Ahmedabad, Indian, pp. 50-53.

Manabe, T., Ihara. I., Awaka. J. and Furuhama. Y. (1987): 'The relationship of raindrop size distribution to attenuation experienced at 50, 80, 140 and 240 GHz,' *IEEE. Transactions on Antennas and Propagation*, Vol.35, pp.1326-1330.

Marshall, J. S. and Palmer, W. (1948): 'The distributions of raindrop with size,' *Journal of Meteorology*, 5**,** 165–166

Marshall, J. S. and Palmer, W. (1948): 'The distributions of raindrop with size,' *Journal of Meteorology*, 5**,** 165–166.

Massey, F.J. (1951): 'The Kolmogorov-Smirnov Test for Goodness-of-Fit,' *Journal of the American Statistical Association*, Vol.46, No.255 (Mar.1951), pp.68-78.

Matzler,C. (2002): 'Drop-size distributions and Mie computations for rain,' *IAP RES.Rep.No.2002-16*, Meteorology, Institute of Applied Physics, University of Bern.

Mitchell, D.L. (1996): 'Use of mass-and area-dimensional power laws for determining precipitation particle terminal velocities,' *Journal of Atmospheric Science*, 53, 1710-1723.

Moupfouma, F and Dereffye, J. (1982): 'Empirical model for Rainfall rate distribution,' *Electronics Letters*, Vol.18, No. 11, pp.460-461.

Moupfouma, F and Martin, L. (1993): 'Point Rainfall Rate Cumulative Distribution Function Valid at Various Locations,' *Electronics Letters*, Vol.29, No. 17, pp.1503-1505

Moupfouma, F. (1985): 'Model of rainfall-rate distribution for radio system design,' IEE Proceedings, Vol.132, Pt. H, No. 1, pp.460-461.

Moupfouma, F. (1987): 'More about rainfall rate and their prediction for radio system engineering,' IEE Proceedings, Vol.134, Pt. H, No. 6, pp.527-537.

Moupfouma, F. and Tiffon, J. (1982): 'Raindrop Size Distribution from Microwave Scattering Measurements in Equatorial and Tropical Climates,' *Electronic Letters*, Vol. 18, No.23, pp.1112-1113.

Moupfounma, F. and Martin, L. (1995): 'Modelling of the Rainfall Rate Cumulative Distribution for the Design of Satellite and Terrestrial Communication Systems,' *International Journal of Satellite Communication*s, Vol. 13(2), pp.105-115.

Mulangu, C.T., Owolawi, P.A. and Afullo, T.J.O. (2007): 'Rainfall Rate Distribution for LOS Radio System in Botswana,' In *Proceedings* of 10th Southern Africa Telecommunication, Networks and Application Conference (SATNAC), Mauritius, ISBN No. 978-0-620-39351-5, September.

Mulangu, C. T. and Afullo, T. J. (2009): 'Variability of the Propagation Coefficients Due to Rain for Microwave Links in Southern Africa,' *Radio Science*, Vol. 44 RS 3006.

Ong, J. and Zhu, C. (1997): 'Rain Rate Measurements by a Rain Gauge Network in Singapore,' *Electronics Letters*, Vol. 33, January, pp. 240-242.

Ong, J.T. and Zhu, C.N. (1997): 'Effects of Integration Time in Rain Rate Statistics for Singapore,' *Proceedings*, 10th International Conference on Antennas and Propagation, Conf.Pub.No.436, 1997, pp.14-17, April.

Owolawi P.A, Afullo, T.J. and Malinga, S. (2009): 'Effect of Rainfall Rate on Millimeter Wavelength Radio in Gough and Marion Island,' *PIERS 2009 Progress in Electromagnetic Research Symposium*, pp. 23-27, March, Beijing China.

Owolawi, P. A. (2006): 'Rain Rate and Rain Drop Size Distribution Models for Line-of-sight Millimetric Systems in South Africa,' MSc. Dissertation, University of KwaZulu-Natal, Durban, South Africa.

Owolawi, P. A. and Afullo, T. J. (2007a): 'Rainfall Rate Modelling and its Worst Month Statistics for Millimetric LOS links in South Africa,' *Radio Science*, Vol. 42.

Owolawi, P. A., Afullo, T. J. and Malinga, S. B. (2007b): 'Effect of Worst-month Distribution on Radio Link Design in South Africa,' *Eleventh URSI Commission F Triennial Open Symposium on Radio Wave Propagation and Remote Sensing*, 55-61, October, Rio de Janeiro, Brazil.

Paraboni A., Masini, G. and Riva, C. (1998): 'The Spatial Structure of Rain and its impact on the design of advance TLC Systems,' *Proceedings*, Fourth Ka Band Utilization Conference, 2-4, Venice, Italy, pp.167-172. November.

Pan, W., Leung, P., Huang, W and Wei Liu, W. (2005): 'On interval estimation of the coefficient of variation for three-parameter Weibull, lognormal and gamma distribution: A simulation-based approach,'*European Journa of Operational Research*, 164, pp.367-377.

Peel, M.C., Finlayson, B.L. and McMahon, T.A. (2007): 'Updated World Map of the Köppen-Geiger Climate Clasification,' *Hydrology and Earth Systems Science*, Vol. 11, No. 5, pp.1633-1644, October

Press, W.H., Flannery, B.P., Teukolsky, S.A and Vetterling, W.T. (1992): 'Kolmogorov-Smirnov Test,' In *Numerical Recipes in FORTRAN: The Art of Scientific Computing*, 2nd ed. Cambridge, England: Cambridge University Press, pp.617-620.

Pruppacher, H.R. and Beard, K.V. (1970): 'A wind tunnel investigation of the internal circulation and shape of water drops falling at terminal velocity in air,' *Quart. J.R.Met.Soc*., 96, pp.247-256

Pruppacher, H.R., and Pitter, R.L. (1971): 'A semi-empirical determination of the shape of cloud and rain drops,' *Journal of the Atmospheric Sciences*, 28, 86-94.

Reddy, B.M. (1982): International Centre for Theoretical Physics (ICTP) Autumn Course on Geomagnetism, the Ionosphere, and Magnetosphere. SMR/98-44. Trieste, Italy.

Rice, P. and Holmberg, N. (1973): 'Cumulative Time Statistics of Surface-Point Rainfall Rate,' *IEEE Transactions on Communications*, COM-21, October, pp.1772-1774.

Roger, R.R. and Yau, M.K. (1989): A short Course in Cloud Physics, Pergamon Press, 3rd edition, pp126.

SAC&W: http://www.infoplease.com/atlas/country/southafrica.html

Saunders, M.J. (1971): 'Cross polarization at 18 and 30 GHz due to rain,' *IEEE Trans.A-P*, Vol.AP-19, pp.273-277.

Seeber, R.J. (1995): An extreme value model of surface-point rain-rate distribution for the prediction of microwave rain attenuation in Southern Africa, M.Sc. Thesis, University of Pretoria.

Seeber, R.J. (1995): 'n Model vir die bepaling van die punt-reenintensitverdeling vir die voorspelling van mikrogolf-reenverswakking in suidelike Afrika,' *South African Institute of Electrical Engineers Journal*, June, pp. 67-75.

Segal, B. (1986): 'The Influence of Rain gauge Integration Time on Measured Rainfall-Intensity Distribution Functions,' *Journal of Atmospheric and Oceanic Technology*, Vol. 3, pp.662-671.

Sekhon, R.S. and Srivastava, R.C. (1971): '*Doppler radar observations of drop-size distribution in a thunderstorm, Journal of the Atmospheric Sciences*, 28, 983-994.

Sekine, M. and Lind, G. (1982): 'Rain attenuation of centimetre, millimetre and sub-millimetre radio waves,' *Proceedings of the 12th European Microwave conference*, Helsinki, Finland, pp.584-589.

Singh, M.S., Tanaka, K., Lida, M. (2007): 'Conversion of 60-, 30-, 10- and five-minute Rain Rates to one-minute Rates in Tropical Rain Rate Measurement,' *ETRI Journal*, Vol. 29,No. 4,August.

Spyros, L., Vasilio, K. and John, K. (1998): 'A Prediction Method for the Rain Attenuation Statistics based on the Weibull Distribution,' *Proceedings*, URSI Commission F Open Symposium on Climatic Parameters in Radiowave Propagation Prediction Ottawa, Canada, April, pp.73-76.

Suhaila, J. and Jemain, A.A. (2007): 'Fitting Daily Rainfall Amount in Malaysia using the Normal Transformer Distribution,' *Journal of Applied Science*, Vol. 7(14).

Tharek, A.R. and Din, J. (1992): 'Raindrop Size Distribution Measurements in Malaysia,' *Proceedings*, URSI Comm.F.Open Symposium on Wave Propagation and Remote Sensing, North Yorkshire, United Kingdom, p1.2.1-1.2.5.

Thom, H.C. (1958): 'A Note on the Gamma Distribution,' *Monthly Weather Review,* Vol. 86, pp.117-122.

Timothy, K.I., Ong, J.T and Choo, E.B.L (2002): 'Raindrop Size Distribution Using Method of moments for Terrestrial and Satellite Communication Applications in Singapore,' *IEEE Transactions on Antennas and Propagation*, Vol. 50, No. 10, 2002.pp.1420-1424.

Tyson P.D, R.A Preston-Whyte, R.E. Schulze (1976): The Climate of the Drakensberg, Natal Town and Regional Planning Commission, pp50-60.

Van Mook, F.J.R. (2002): Driving rain on building envelopes, PhD. Thesis, Building Physics and Systems, Technische Universiteit Eindhoven University Press, Eindhoven, The Netherlands.

Walack, C. (2007): Hand-book on Statistical Distributions for Experimentalists, Internal Report SUF-PFY/96-01. University of Stockholm.

Waldvogel, A (1974): 'The N_0 jump of raindrop spectra,' *Journal of the Atmospheric Sciences*, Vol.31, pp.1067-1078.

Watson, P.A., Gunes, M., Potter, B.A., Sathiaseelan, V. and Leitao, J. (1982): Development of a Climatic Map of Rainfall Attenuation for Europe, Final Report of ESA/ESTEC Contract No.4162/79/NL/DG/ (SC), Report 327.

Watson, P.A., Sathiaseelan, V. and Potter, B.A. (1981): Development of a Climatic Map of Rainfall Attenuation for Europe, Post Graduate School of Electrical and Electronic Engineering, University of Bradford, U.K, Rep. No.300, pp.134-136.

Wilks, D.S. (1989): 'Rainfall Intensity, the Weibull Distribution and Estimation of Daily Surface Runoff,' *Journal of Applied Meteorology*, Vol. 28, pp.52-58.

Wong, R.K.W. (1977): 'Weibull Distribution, Iterative Likelihood Techniques and Hydrometeorlogical Data,' *Journal of Applied Meteorology*, Vol. 16, pp.1360-1364.

World Meteorological Organization (1953): World Distribution of Thunderstorm days,' WMO/OMM, NO.21, TP.6, Geneva.

World Meteorological Organization (1962): 'World Meteorological Organization Climatological Normal (CLINO) for Climate and Climate Ship Stations for the period 1931-1960,' WMO/OMM, No.117, TP.52, Geneva.

Xiao, J.M., Cheng D.H., and Wang, L.J. (1987): 'Rain Rate Statistics and Analysis in Xian District (In Chinese),' *China Journal of Radio Science*, Vol. 2(1), pp39-48.

Xin, M.X. and Lin, H. (1988): 'On Statistical Characteristics of Rainfall and Forecasts Method on Microwave Terrestrial Links (in Chinese),' *Journal of China Institute of Communications*, Vol. 9(4), pp.51-57.

Appendix A

Theoretical Background of Probability Density of Rainfall Rate

In many design considerations at microwave and millimetric bands with signal transmission for which rainfall is a major impairment, it is more practical to express the likelihood of events in terms of their probability. Distributions such as Weibull, Lognormal and Gamma are the most commonly used to describe or quantify a random event such as rainfall occurrence. Spyros *et al* (1998) proposed a rainfall rate statistics model based on the Weibull distribution, and describes the probability density as:

$$f_R(r) = abr^{b-1}e^{-ar^b} \qquad (r > 0) \tag{A.1}$$

and as a result, the cumulative rainfall intensity distribution is given by:

$$P(R \geq r) = \int_r^{\infty} f_R(x)dx = e^{-ar^b} \qquad (r > 0) \tag{A.2}$$

where a and b are parameters dependent on the geographical characteristics of the location concerned.

Lognormal statistics distribution was explored by Fedi (1979, 1981) and Xin and Lin (1988) to describe rainfall rate distributions for their regions. In the work carried out by Xin and Lin (1988) for China, they assumed that the point rainfall rate distribution from a certain rain gauge is lognormal and its cumulative distribution function thus given as:

$$P(R \geq R_O) = \frac{1}{\sigma\sqrt{2\pi}} \int_{R_O}^{\infty} \frac{1}{t} e^{-\frac{(\ln t - m)^2}{2\sigma^2}} dt \tag{A.3}$$

where R is the rainfall rate in (mm/hr), R_o is the threshold exceeded by R, and the mean (m) and standard deviation (σ) are the lognormal fitting parameters. In a wider probability range, research found that the Gamma distribution better described rainfall events than other mentioned distributions. The work by Huang (1990) in China and Li *et al* (1998) confirmed the suitability of this type of distribution in modelling rainfall rate. Huang (Huang, 1990) assumed that the rainfall rate in a gauge is a random variable X, and X satisfies the Gamma distribution.

In Li *et al* (1998) the probability density function of Gamma distribution is:

$$f(x) = \frac{1}{\beta^{\alpha}\Gamma(\gamma)} x^{\alpha-1} e^{-x/\beta} \qquad (x > 0) \tag{A.4}$$

Where, $\beta(>0)$ and $\alpha(>0)$ are size and shape parameters respectively, and $\Gamma(\gamma)$ is the Gamma function given by:

$$\Gamma(\alpha) = \int_0^{\infty} y^{\alpha-1} e^{-y} dy \tag{A.5}$$

Bearing in mind the authors' previous approach to defining the three named rainfall rate distributions, the distribution probability density relations are redefined for South African and surrounding islands rainfall rate modelling and summarized as follows:

1. Weibull Distribution

There are two versions of this distribution, namely, the two-parameter Weibull and three-parameter Weibull distributions. The probability density function (pdf) is given by Evans *et al* (1993) as:

$$f(x) = \frac{\alpha}{\beta}\left(\frac{x-\gamma}{\beta}\right)^{\alpha-1} \exp\left(-\left(\frac{x-\gamma}{\beta}\right)^{\beta}\right) \quad \gamma \le x < +\infty \tag{A.6}$$

where $\alpha =$ shape parameter ($\alpha > 0$)

$\beta =$ scale parameter ($\beta > 0$)

$\gamma =$ location parameter ($\gamma \equiv 0$ yields the two-parameter Weibull distribution)

The method of maximum likelihood (MLE) is used to optimize the estimated Weibull distribution parameters. The details of the method are presented by Wong (1977). The MLE estimates parameters $\hat{\alpha}$ and $\hat{\beta}$ assumed solution at condition when:

$$\frac{\partial \ln L}{\partial \alpha} = 0 \tag{A.7}$$

$$\frac{\partial \ln L}{\partial \beta} = 0 \tag{A.8}$$

$$\ln L = N \ln \alpha - N\alpha \ln \beta + (\alpha - 1)\sum_{i=1}^{N} \ln x_i - \sum_{i=1}^{N}\left(\frac{x_i}{\beta}\right)^{\alpha} \tag{A.9}$$

N denotes sample size and the Newton- Raphson approximation method is used to solve simultaneous equations at the rth iterative by the expression:

$$\begin{aligned} \hat{\alpha}(r) &= \alpha(r-1) + h(r) \\ \hat{\beta}(r) &= \beta(r-1) + k(r) \end{aligned} \tag{A.10}$$

where $h(r)$ and $k(r)$ are the correction terms in the expression (Wong, 1977; Wilks, 1989):

$$\begin{bmatrix} h \\ \\ k \end{bmatrix} = \begin{bmatrix} \dfrac{\partial^2 \ln L}{\partial \alpha^2} & \dfrac{\partial^2 \ln L}{\partial \alpha \partial \beta} \\ \\ \dfrac{\partial^2 \ln L}{\partial \beta \partial \alpha} & \dfrac{\partial^2 \ln L}{\partial \beta^2} \end{bmatrix}^{-1} \begin{bmatrix} -\dfrac{\partial \ln L}{\partial \alpha} \\ \\ -\dfrac{\partial \ln L}{\partial \beta} \end{bmatrix} \tag{A.11}$$

The iteration is terminated at the point where the correction terms lies below 0.002.

2. The Lognormal Distribution

This distribution is based on the normal distribution with the random variable lognormally distributed provided the logarithm of the random variable is normally distributed. Lognormal distribution pdf is expressed by Evans *et al* (1993) and Walack (2007) as:

$$f(x) = \frac{\exp\left(-\frac{1}{2}\left(\frac{\ln x - \mu}{\sigma} \right)^2 \right)}{x\sigma\sqrt{2\pi}} \qquad 0 \le x < +\infty \tag{A.12}$$

where

$\sigma =$ scale parameter of the included normal distribution ($\sigma > 0$)

$\mu =$ location parameter of the included normal distribution.

Here, the maximum likelihood estimation for the two-parameter lognormal used is given by Eckhard *et al* (2001) and Suhaila and Jemain (2007) as:

$$\hat{\mu} = \exp\left(\frac{1}{n} \sum_{i=1}^{N} \log(x_i) \right) = \left(\prod_{i=1}^{N} x_i \right)^{\frac{1}{N}} \tag{A.13}$$

$$\hat{\sigma} = \exp\left| \left(\frac{1}{N-1} \sum_{i=1}^{N} \left[\log\left(\frac{x_i}{\hat{\mu}} \right) \right]^2 \right)^{\frac{1}{2}} \right| \tag{A.14}$$

3. Gamma Distribution

This distribution is defined in terms of a shape factor, scale factor, and location factor. Its two-parameter version is more commonly used in rainfall rate distribution model. The three-parameter Gamma distribution is also referred to as the Pearson Type III distribution. Evans *et al* (1993) and Walack (2007) give the probability density function for the three-parameter Gamma distribution as:

$$f(x) = \frac{(x-\gamma)^{\alpha-1}}{\beta^{\alpha}\Gamma(\alpha)} \exp\left(-(x-\gamma)/\beta\right) \qquad \gamma \le x < +\infty \tag{A.15}$$

Its cumulative distribution function is represented as:

$$F(x) = \frac{\Gamma(x-\gamma)/\beta(\alpha)}{\Gamma(\alpha)} \qquad \gamma \le x < +\infty \tag{A.16}$$

while for two-parameter Gamma distribution, the probability density function is expressed as:

$$f(x) = \frac{x^{\alpha-1}}{\beta^{\alpha}\Gamma(\alpha)} \exp\left(-x/\beta\right) \quad \gamma \le x < +\infty \tag{A.17}$$

and its cumulative distribution function is represented as:

$$F(x) = \frac{\Gamma_{x/\beta}\beta(\alpha)}{\Gamma(\alpha)} \qquad \gamma \le x < +\infty \tag{A.18}$$

The modelling of rainfall rate distribution for South Africa and surrounding islands involves fitting a gamma probability density function to a given frequency distribution of rainfall totals for a station using the Maximum Likelihood estimator. The alpha (α) and beta (β) parameters of the gamma probability density function are estimated for each

selected site with over ten years' rainfall data. Approximate maximum likelihood estimates, as suggested by Thom (1958) are used to optimally estimate α and β:

$$\hat{\alpha} = \frac{1}{4A}\left(1 + \sqrt{1 + \frac{4A}{3}}\right) \tag{A.19}$$

$$\hat{\beta} = (n\hat{\alpha}) / \sum_{j=1}^{n} x_j \tag{A.20}$$

$$A = \ln(\sum_{j=1}^{n} x_j / n) - \sum_{j=1}^{n} \ln(x_j / n) \tag{A.21}$$

Here $n =$ number of rainfall rate observations. In this study, two main statistical tests are used to optimize and test the proposed models such as root mean square (RMS) and chi-square test statistics.

Appendix B

Appendix B: shows critical values of the absolute difference between sample and theoretical cumulative distributions.

Table 1-A: Kolmogrov-Smirnov Test Table

(Source http://www.eridlc.com/onlinetextbook/index.cfm?fuseaction=textbook.appendix&FileName=Table7)

(If calculated ratio is greater than value shown, then reject the null hypothesis at the chosen level of confidence.)

SAMPLE SIZE (N)	LEVEL OF SIGNIFICANCE FOR D = MAXIMUM [$F_0(X)$ - $S_n(X)$]				
	.20	.15	.10	.05	.01
1	.900	.925	.950	.975	.995
2	.684	.726	.776	.842	.929
3	.565	.597	.642	.708	.828
4	.494	.525	.564	.624	.733
5	.446	.474	.510	.565	.669
6	.410	.436	.470	.521	.618
7	.381	.405	.438	.486	.577
8	.358	.381	.411	.457	.543
9	.339	.360	.388	.432	.514
10	.322	.342	.368	.410	.490
11	.307	.326	.352	.391	.468
12	.295	.313	.338	.375	.450
13	.284	.302	.325	.361	.433
14	.274	.292	.314	.349	.418
15	.266	.283	.304	.338	.404
16	.258	.274	.295	.328	.392
17	.250	.266	.286	.318	.381
18	.244	.259	.278	.309	.371
19	.237	.252	.272	.301	.363
20	.231	.246	.264	.294	.356
25	.210	.220	.240	.270	.320
30	.190	.200	.220	.240	.290
35	.180	.190	.210	.230	.270
OVER 35	$\frac{1.07}{\sqrt{N}}$	$\frac{1.14}{\sqrt{N}}$	$\frac{1.22}{\sqrt{N}}$	$\frac{1.36}{\sqrt{N}}$	$\frac{1.63}{\sqrt{N}}$